UNIVERSITY OF SOUTHAMPTON

IN-PLANE ADHESIVELY BONDED JOINTS IN SANDWICH STRUCTURES

by

Nicholas Hamish Cossich

Master of Philosophy

School of Engineering Sciences
Faculty of Engineering and Applied Sciences

June 2000

UNIVERSITY OF SOUTHAMPTON

ABSTRACT

FACULTY OF ENGINEERING AND APPLIED SCIENCE
DEPARTMENT OF SHIP SCIENCE

Master of Philosophy

IN-PLANE ADHESIVELY BONDED JOINTS
IN SANDWICH STRUCTURES

by Nicholas Cossich

This work is concerned with the mechanical behaviour of in-plane joints in sandwich structures under static flexural loads. The impetus behind research into these joints stems from the growing development in modular construction techniques that offer competitive global access to higher technology sandwich structures. Characterisation of flexural response is therefore important, as in most instances the primary role of a sandwich is to impart flexural rigidity. A test program involving several commonly used joining methods, including scarf, internal spline and external tape, coupled with flexible and inflexible adhesives were used to demonstrate the mode of failure, strength and stiffness of the joined sandwich. Adaptation of an existing strain measurement technique to the sandwich offers the ability to quantify the joint as a unit, allowing the engineer to conceptualise its performance as a weld. Analytical approaches, together with a numerical study, are used to provide more general comment on optimum in-plane scarf joint configurations. The results are discussed in light of practical ship and boat construction applications, but are directly relevant to large sandwich constructions in general.

TABLE OF CONTENTS

LIST OF TABLES

LIST OF FIGURES

ACKNOWLEDGEMENTS

CHAPTER 1

INTRODUCTION

Latest sandwich technology is often limited in use due to lack of skilled labour, and perceived risks associated with new techniques. The adage 'if it isn't broken don't fix it' sees many fabricators locked into the same 80's technology now used by competing low cost labour markets. A quotation taken from Olsson and Reichard (1989) concisely summarises a general industry requirement.

> *"One of the most pressing needs is the development of efficient, inexpensive methods of manufacturing sandwich constructions of consistently high quality. This area of research and development is perhaps the most critical to widespread acceptance and use of sandwich constructions."*

Modular sandwich construction can minimise or even eliminate these barriers, and offers the safeguard of known parameters. Using smaller teams or third party contractors, and with adaptation of production line methods, modules can be efficiently produced for rapid assembly.

Developable panel systems and moulded sections encompass the genre of a sandwich module, with each method having advantages and disadvantages depending on structure size, number, geometry etc. The key to these techniques is the joint, with knowledge of the most efficient method for load transmission and stiffness continuity crucial to any systems success. It is the in-plane joint that forms the focus of this study, as shell to shell connections rather than stiffener to shell connections are required to provide principal continuity when considered in a global sense.

Classification authorities furnish recommendations on particular joint geometry, but in many instances they are based on experience rather than systematic investigations. Whilst experience is invaluable, without a thorough understanding of the mechanisms that lead to a structurally effective joint, variations, novel designs and ultimately progression will be restrained.

The in-plane joint, as opposed to the out of plane joint e.g. tee-joint, has always been addressed as a method of repair rather than a primary process during manufacturing. Characteristation of the joint as a unit in typical sandwich structures can offer the engineer a method by which intricacies on a comparative micro-level are eliminated. These intricacies are still however very important when passing more general comment, and so a closer look at details using analytical and numerical methods will provide an understanding of the fundamentals.

1

Adhesively bonded joints and not mechanically fastened are considered due to the distinct advantage of surface fairness. Although it is possible to achieve surface fairness with mechanical fasteners e.g. countersinking, the thin skins that can be associated with a sandwich are prohibitive. It is therefore often physically impossible to afford a good connection, and for composite skins this problem is exacerbated even further due to bearing and notch sensitivity unless an adhesive is used.

The issue of surface fairness is not solely aesthetic and is necessary due either to hydro- or aerodynamic requirements. It is true that fairing compounds can be used to mask surface discontinuities, but their use comes at the expense of increased weight and cost.

The aim of this study is to examine the behaviour of sandwich structures with adhesively bonded in-plane connections under a flexural loading regime. A variety of joint configurations and material combinations are explored. The overall approach involves combining experimentation and theory – the latter being based on both closed form analytical models and finite element analysis. An underlying maritime theme with a practical inclination is used throughout investigation of the joints, although in reality the techniques described therein are not industry specific.

CHAPTER 2

LARGE SANDWICH STRUCTURES

Sandwich structures have been in existence for almost 150 years, however there does exist some conjecture as to whether this time period should be extended back to include DaVinci's era (Allen, 1969). Indeed, modern engineers have made continued improvements in analysis techniques since this time, both analytical and numerical, with a resulting proliferation in the number and variety of uses for sandwich structures.

The focus of this review is to evaluate materials and fabrication methods used in large sandwich structures. For one to draw a definitive line between small, medium and large is difficult, and this relation could also be considered industry dependent. A volumetric basis is a reasonable way of distinguishing perceived size, and so a component volume of greater than $70m^3$ shall be defined as large.

When considering these structures, an emphasis is placed on the current commercially used constituent materials and manufacturing techniques. The importance of emerging technology has not been forgotten, and is mentioned briefly in the hope that it does become economically viable in the near future, for industry as a whole.

2.1 Constituent Materials

2.1.1 Metal Skins

The use of thin metal faces, and in particular aluminium and steel, has the attraction in many instances of isotropic high modulus skins at relatively low cost. Certain stiffness critical applications make good use of these characteristics, with adequate surface preparation being of paramount importance. The capital to invest in suitable metal treatment facilities is high since the environment is very corrosive, and dip tanks or spray equipment need to accommodate several sheets for efficiency. The sheet can be provided by the manufacturer with conversion coatings, however there is a narrow window, around 24hrs, in which optimal adhesion can be achieved. An additional benefit of metal skins is their inherent fire retardancy, which has been put to good use in items such as doors in the Eurostar and floors in New York City Subway (Walton, 1997).

3

2.1.2 Timber Skins

Being a renewable resource, timber has obvious appeal. It has good fatigue resistance, and when used in the form of plywood, much improved stability. Plywood is quite versatile, with numerous stress grades offering features such as boil resistance and a certain degree of fire retardancy. Nearly all types are hot pressed using phenol based adhesives that allow high and low temperature performance without creep or embrittlement. It finds a particularly interesting use as the skins on the balsa cored insulating liner for a 1000ft LPG tanker (Wood & Wood Products, 1976).

2.1.3 Composite Skins

2.1.3.a Reinforcement

The continuing development of new fibres, such as those based on the Nobel Prize winning discovery of Fullerenes (C_{60}) by Curl *et al* (1996), offers the potential of sandwich structures larger than any in existence today. For the moment however, E-glass is the predominant reinforcement in terms of global consumption, but for specific applications s-glass, aramid, carbon, polyethylene, boron and many others have their places. The processed fibres themselves can also be sub-categorised to cover fibre surface treatment, roving/yarn diameter, weave/knit configuration, strength/modulus and quality, so possibilities are endless. A good example of this ability to tailor fabrics is shown by the use of a custom made $\pm 45°$ knitted carbon fabric for production of the Space Shuttle booster rockets (Johnston Industries, 1997).

2.1.3.b Phenolic Resins

Phenolic resins are 'old technology' dating to the early 1900's, however they have seen a resurgence due to very stringent fire requirements in many industries. In particular the aircraft, rail, and offshore marine sectors are driving new development in this area, as concerns over smoke emissions, toxicity and combustibility mount. Traditionally phenolics require heat curing cycles, and are very unpleasant to use, with acidic hardeners and evolution of water as a by-product during polymerisation. Recent progress in this field has resulted in room temperature cures, however many countries are deficient in this and other technology, due to shipping times equaling the current shelf lives. Poor mechanical properties of this matrix have restricted its use to areas where fire retardancy is the primary concern.

4

2.1.3.c Unsaturated Polyester Resins

Ortho- and isophthalic polyesters find their way into low-medium technology, cost driven products, and in most instances are very suitable for the application intended. These catalytic cured unsaturated polyesters are susceptible to osmosis if not used correctly, with warm humid conditions promoting this phenomenon. Undoubtedly the marine environment best fits this description, and a survey conducted by Strand (1990) in the United States, found it likely that one in four boats will suffer from osmotic blistering during its lifetime. Typically strain to failure of 1-2% are applicable to these systems, and they therefore could be considered brittle. Shrinkage during cure is also of concern, particularly in large structures, as dimensional changes up to 5% are common. Whilst this may be good for removing a part from a mould, it introduces another complexity when considering tolerances.

2.1.3.d Vinylester Resins

A different chemistry is seen in vinylester, although still a catalytic cured system. Better mechanical properties than polyesters are achieved, and strain to failure of 3.5-7% give vinylesters a wider appeal. The higher end of the elongation range is usually achieved through addition of modifiers such as carboxyl terminated butadiene nitrile (CTBN), with a dispersion of these minute suspended rubber particles acting as crack stoppers and preventing premature failure. The benefits of modification do however come at the cost of heat distortion temperature (HDT), which in the unmodified state is typically 100-120°C. Other appealing attributes of these resins are excellent corrosion resistance, reduced susceptibility to osmosis, and low viscosity.

2.1.3.e Epoxy Resins

Epoxy resins (EP) are more complex systems in that many varieties are available depending on the application. Stoichiometricly mixed two part, catalytic and single part systems cover the available mixing options, nevertheless the number of base resins, hardeners and modifiers allows a limitless range. Properties are therefore diverse, and as a guide, strain to failure of 7-10% can be achieved. HDT is wide and varied with two part amine and aramine hardened systems giving ranges of 45-75°C during room temperature cures, and the catalytic systems achieving 180°C and over with post-cures (Marshall, 1992). Recent concerns about the toxicity of the liquid hardeners has led to some being listed as suspected carcinogens.

2.1.3.f Other Matrices

Polyurethane and acrylic systems offer good potential in many applications, but have been limited by the need for yet more specialised knowledge by the fabricator. Polyurethane is particularly good for tooling production due to short cure times without exotherm, and low viscosity acrylics offer the ability to load high percentages of aluminium tri-hydrate (ATH) for fire susceptible products.

It is worth noting the use of thermoplastics such as polyether ether ketone (PEEK), polyether imide (PEI), polyether sulfone (PES) and polyphenylene sulfide (PPS) primarily in the aircraft industry. They are used to produce such items as the Airbus A300/600ST floors, where their ability to close sandwich panel edges is exploited (Offringa, 1996). These plastics have good mechanical properties, toughness and recyclability, but their use to date in other areas has been hampered by cost.

Thermoset polyimides, bismaleimides, ceramic and metal matrices are also important in specific applications, but can be considered specialised due to complex processing and raw material costs.

2.1.4 Core Materials & Configurations

2.1.4.a Foams

Polyvinylchloride (PVC), styreneacrylonitrile (SAN), polyurethane (PUR), polystyrene (PS), polymethacrylimide (PMI) and phenolic (PH) form the backbone of this class of cores for marine use. The aircraft industry includes several more, such as polyetherimide (PEI), that cater for their specific requirements, but volume consumption is low in comparison. In recent years there has been increased concern about cross-linked PVC and its propensity to out-gas. Whilst not a new problem, it has become more widespread due to increases in demand preventing relaxation or aging of the material prior to shipping. The result is cells pressurised with gases developed during the foaming process, migrating over time and eventually collecting in bubbles at the skin/core interface.

2.1.4.b Honeycomb

Phenolic impregnated aramid (Nomex®), kraft paper, aluminium and GRP are but a few of the options when considering honeycomb cores. In general one must be careful when using such cores in combination with skins prone to porosity, as there is the possibility of moisture being drawn

into cells through pressure differentials. Apart from the moisture having adverse effects on mechanical properties, the potential of this water to freeze and cause delamination is a major concern. Properties of the aramid and aluminium are excellent on a specific basis, and hence have seen acceptance in many areas including rail, aerospace and marine, where flooring systems are a popular use.

2.1.4.c Timber

Often overlooked, the most popular form is end grain balsa and plywood, although numerous timbers orientated in long grain are also used as core materials. Balsa is a 'natural honeycomb' having comparable properties in compression, tension and shear on a specific weight basis when compared to PVC foam and several aramid based honeycombs. It has however been impeded by a perception that moisture ingress will spread uncontrolled, and rot is commonplace. This is despite the fact that Boeing, McDonnell-Douglas, Lloyd's Register of Shipping and many other statutory authorities have given type approval based on the fact that these problems do not occur if used correctly. One of the biggest compliments to this core's ability, is its recent specification by General Motors in the floor pan of the latest Corvette (Jost, 1997).

2.1.4.d Corrugated Cores

Probably the most easily recognised in this category is fluted cardboard, but steel, aluminium and FRP are also commonly used in more demanding applications. Latest development in corrugated cores has centred on laser welding techniques for thin steel sections. Kattan (1996) notes the increasing use of these structures in US Naval ships, and believes that the high penetrative ability of the laser will provide the means by which it can be more widely implemented into merchant ship production. Whilst progress is being made with lasers, traditional welding, adhesives and mechanical fastening are still widely accepted in the aircraft, rail and civil sectors. Some of the most promising development has been provided for bridge construction using the patented Advanced Composite Construction System (ACCS). Consisting of hollow FRP blocks and planks that can be joined together using a key system, it saw use in building the United Kingdom's first composite road bridge (Maunsell, 1994).

2.1.4.e Other Cores and Configurations

Concrete filled tubular steel sees enduring use in offshore platform legs, and a similar technique has recently been developed for use as steel faced building panels (Wright and Evans, 1996). Using a slurry of concrete to form the core *insitu*, presents the possibility of smooth integration

into civil engineering programs, as it is very similar to current formworking practice. Outside of infrastructure projects however concrete has little impact due to weight considerations.

3D-space fabrics offer a one step process to sandwich fabrication. Impregnation of the woven fabric and subsequent gelation causes the fabric to rise, with the final configuration looking somewhat like a forest of scissor springs separating two skins. This product is used extensively in double walled pipe enabling gas leak detection, and as fire restricting partitions on oilrigs and ships. Pilot programs to evaluate its performance in others areas are also underway, but current thickness limitations and processing techniques make it a rather specialised material.

2.2 Manufacturing Processes

2.2.1 Wet Lay-Up

This method is characterised by the use of liquid resin systems applied by hand or using mechanised devices such as resin spraying equipment, power rollers, chopper guns or impregnation machines. The techniques are suited to small production runs and in particular large structures.

2.2.1.a Mould Construction

A female mould is often used where its cost can be amortised over several items. For small production runs, in low complexity parts, a melamine or medium density fibreboard (MDF) mould is constructed with timber or steel support frames. Melamine is the cheapest method, as the sheet surface already has a high gloss and is easily released when coated with wax or polyvinyl alcohol (PVA). It is limited in dimensional tolerance and surface finish, as the thin sheets must be joined and tortured to form the desired shape. MDF sheet, laminated for dimensional stability and subsequently sprayed with modified polyester, offers the advantage of being sandable and buffable. Typically 1000 or 2000 grit finishes are achievable with better dimensional tolerance than the melamine mould.

For more difficult compound curved sections, a plug can be constructed using the strip plank technique, from which a mould is taken. These methods usually involve timber strips being formed around a set of male plywood frames. The frames are cut by hand or using more advanced machining methods such as CNC routing, laser or water-jet, and spaced at predetermined intervals to ensure that the strips do not flex under their own weight and cause unfairness. Each strip is then fastened to the framework with a sheet-rock screw and edge-glued to the preceding one using a

microsphere and epoxy blend, similar in concept to building a brick wall. Upon laminating, final fairing and top-coating, as with the MDF, the plug is ready to take a moulding.

A more exacting tolerance is achieved using milled polystyrene blocks that can be joined together to form a plug of any size. Rough sizing of the block using a five axis router, is followed by a thick coating of an epoxy based primer, similar in technique to the polyester, but does not cause styrene attack. Once this coating is precision machined, a hard durable topcoat can be applied sanded and polished. A mould can then be taken from the plug, as with the strip planked method.

Split moulds are particularly useful for very large components, as consideration must be given to the amount of room and machinery necessary for part removal. The split mould has been used with success in sandwich mega-yachts up to 50m in length, with figure 2.1 showing the arrangement and removal technique.
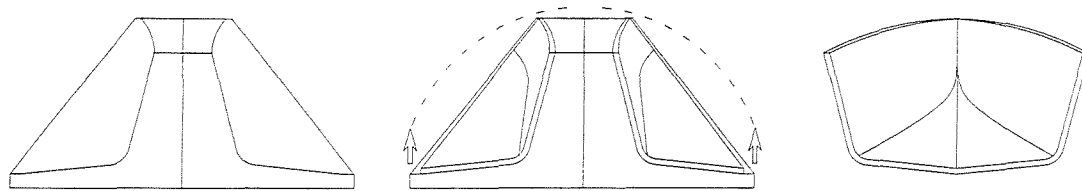
Figure 2.1 Split mould and removal technique.

2.2.1.b Lamination Process

In-mould wet lay-up processing with phenolic, vinylester and polyester consists of the application of a gelcoat or primer and subsequent backing with a gunned or hand applied tie-layer of chopped strand mat (CSM) as shown in figures 2.2.a-b. This provides a resin rich layer offering low porosity and reduced fabric print. Following fabric layers are then applied in turn and consolidated between each step to form the sandwich's outside skin in a female mould, or inside skin in a male mould. As it is likely that the total thickness of the skin will not be built up in one step, and plies allowed to cure, a method to ensure satisfactory interlaminar performance is necessary. Abrasion is a very effective technique and minimum surface finishes are normally 80 grit, however the best performance with vinylester and polyester was found by Bird and Allan (1981) to be a styrene wipe/immersion for 15min. This not only gives a better bond, but also results in a more cost-effective solution through reduced preparation times.
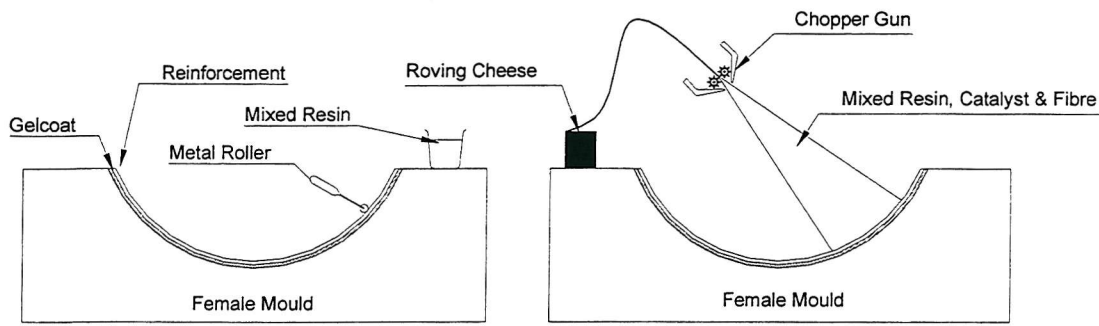
Figure 2.2.a Hand lay-up   Figure 2.2.b Chopper gun assisted lay-up

Hand lay-up of the reinforcement can be improved through the use of impregnation machines, with advantages such as higher fibre fraction, lower void content and higher impregnation rates. Many options exist in machine types, and it is possibly the first step a fabricator should take when modernising with a view toward increased efficiency. Figures 2.3.a-c show varying alternatives, with the novel vacuum assisted system worthy of consideration.
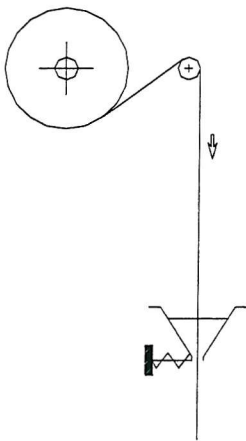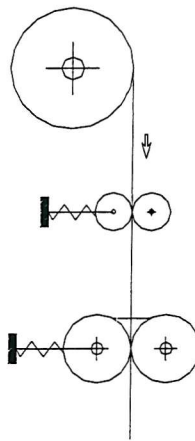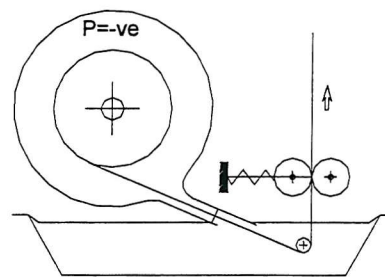
Figure 2.3.a Trough   Figure 2.3.b Roller   Figure 2.3.c Vacuum
(after Duckworth, 1997)   (after Raymer, 1991)   (after Vinogradov *et al*, 1995)

The second step of core to skin bonding is facilitated using the 'wet' or 'dry' method. The 'wet' method usually uses a CSM resin rich layer in which to bed the core either by hand or using a vacuum bag. The core can be configured in a multitude of ways, with choice being specific to the construction method and type of core used. Foam, as an example, can be used in plain sheet for flat or singularly curved areas, but grid-scored, in which small blocks of foam are supported on a scrim backing, is well suited to draping on compound sections. Once the resin has cured, the core is then sanded, shaped and vacuumed ready for a 'hot coat'. This coating is a thixotropic fast

curing resin used to seal the surface of the core and prevent any possible degradation due to prolonged styrene exposure. The second skin is now applied using the same technique as the first.

The 'dry' method differs slightly and involves the use of an adhesive or bedding compound applied to the cured skin. Again the core is placed by hand, vibrating roller or vacuum, and the adhesive allowed to cure prior to preparation and lamination of the second skin. Problems can occur with the grid scored material when the gaps between blocks are not totally filled with resin/adhesive. If a skin is penetrated during service, the component is very susceptible to water/moisture penetration. Without the slits filled, water can snake its way around the core, degrading its properties, penetrating the bondline, adding weight and even freezing, as was noted with honeycomb.

Epoxy lamination techniques are very similar to the other resins, with a few notable differences. Polyester gelcoats are seldom used due to strain incompatibility, and epoxy gelcoats are very susceptible to UV degradation. Post-painted parts are therefore common and are in most cases finished with two part polyurethane. For large structures where skins are laminated in several steps, peel-ply must be used. This is to prevent the contamination of the interlaminar bond with carbonised residue resulting from reaction of hardener with atmospheric moisture. Whilst the peel-plied finish may give satisfactory interlaminar adhesion, best performance is achieved through sanding, and is mandatory in fabrication of aircraft components (Anderson, 1997).

Long open time epoxy has given the additional benefit of co-curing in large structures. Open times of 24hrs or more are possible and allow inside skin, core and outside skin to be cured in one step. This procedure is always performed under vacuum and is very exacting, due to increased risk of over-bleeding and air entrapment.

Strip plank construction, as shown in figure 2.4, is identical to that described for plug manufacture, and is widely used to produce both small and large marine craft. Foam and longitudinally grained timber comprise the largest percentage of core utilised in this way, however honeycombs and directionally fragile cores are not excluded provided a suitable light fabric is pre-laminated to either side. Strip widths range from 30mm to limiting sheet dimensions and arespiled (tapered) at the ends to give a tight fit. There are many sectional variants including rectangular, tongue and groove, beveled and concave/convex, however it was shown by Robson (1984) that a V-joint configuration would provide a better quality bond and improved shock resistance.

11
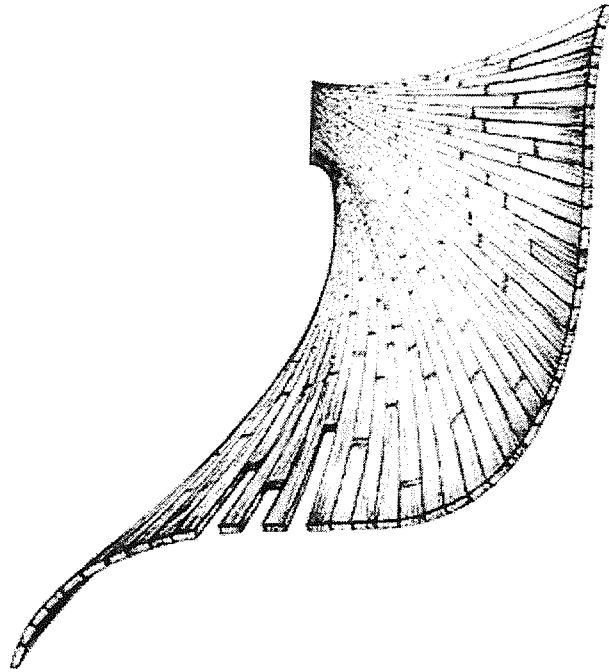
Figure 2.4 Strip plank construction.

Male planking is more attractive the larger a vessel becomes, as it requires the hull to be turned one less time and frame work is less expensive. A male construction jig is erected, and the hull stripped, laminated, faired and painted on the frames to achieve the final finished exterior surface. The hull need only be turned once in a cradle to allow installation of internals and superstructure and is the reason Sjogren et al (1984) working for the Swedish Navy, chose this method for construction of their 48m 'Landsort' mine counter measure vessel (MCMV).

2.2.2 Pre-Preg Lay-Up

A technological step forward from the wet methods, pre-pregs allow a much cleaner working environment and minimal exposure to hazardous volatiles. Any fabric can be supplied as a pre-preg, but light woven and uni-directional carbon constitutes the bulk of consumption. The production of uni-directional pre-preg ensures high fibre fraction, as tows are splayed before passing through epoxy, polyimide or bismaleimide resin impregnating equipment. This splaying of fibres eliminates resin pooling between fibre bundles, providing a more homogenous material, and preventing the need for weft binding threads.

Thermoset binding threads are however used in many instances where the pre-preg fabrics are to be split into tapes. Commonly called 'sticky string' they provide the fabricator with improved handling characteristics, as a selvedge is not required to hold a fabric's form.

2.2.2.a Mould Construction

Pre-preg lay-up methods involve the use of a mould that has a similar expansion coefficient to the cured part, particularly for high temperature cures of 350°F+. Steel and carbon moulds are therefore used extensively for aircraft components, where exacting tolerances are necessary. Low temperature curing pre-preg, around 80°C, is available for slightly less demanding applications such as yachts, and since the temperature gradient is not quite as severe, laminated plywood moulds are acceptable.

2.2.2.b Lamination Process

The technique of pre-preg construction is best shown diagrammatically in figure 2.5. The mould surface is prepared with wax, PVA or one of several proprietary polymer blends, prior to positioning of the first layer. Further layers are applied in turn and it is sometimes necessary to remove interlaminar air as an intermediary step by debulking. It may also be desirable to cure the skins separately at this stage, or alternatively a co-curing operation will require film adhesive if insufficient resin is available to afford a bond to the core. It is recommended that solid cores, and in particular foams, be presealed prior to positioning. This is to safe-guard against excess resin consumption, but also in some instances cross-linking being inhibited by migrating plasticisers at the core/laminate interface. The lamination procedure is then completed with film adhesive, required number of pre-preg plies, peel-ply, perforated release film, bleeder, release film, breather, caul plate, breather and finally vacuum bag. The completed assembly can now be placed in an oven or autoclave with the temperature curing profile highly regulated to ensure adequate flow and cross-linking of the resin.
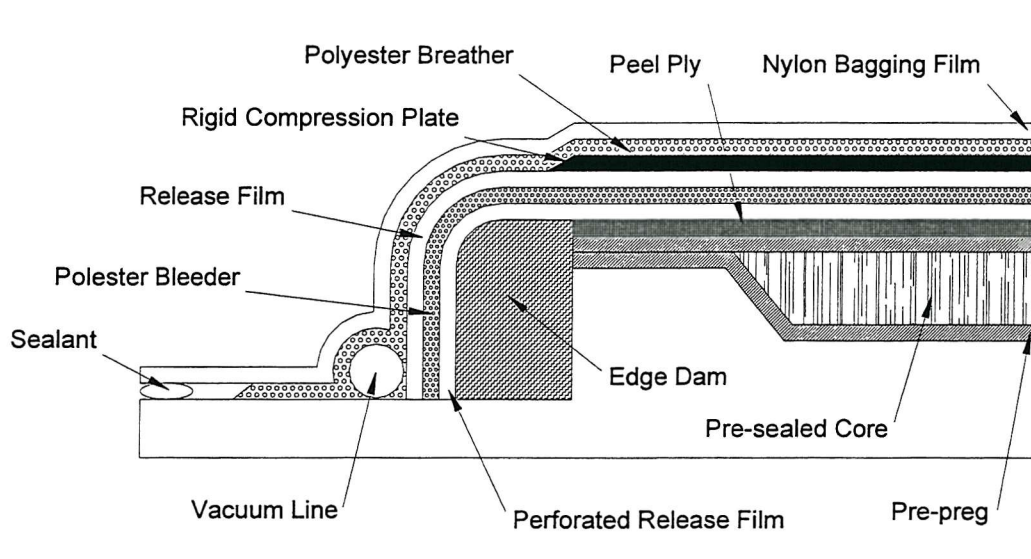
Figure 2.5 Schematic of pre-preg construction.

13

The autoclave is used extensively in aircraft operations to produce sandwich parts such as the Airbus A130 rudder, which comprises a mixture of ±45° carbon and 0°/90° E-glass pre-preg on a Nomex® core, giving optimum stiffness and strength. In contrast, low temperature oven cures have produced many of the worlds leading yachts, including the America's Cup winning 'Black Magic' from New Zealand. On a larger scale, a comprehensive study by Enlund (1995) showed the feasibility of producing the composite sandwich hulls and superstructure on a 150m catamaran ferry. FEA showed that it was necessary to use carbon fibre laminates in order to obtain adequate global stiffness, and cores of end grain balsa and aluminium honeycomb provided the local panel rigidity.

2.2.3 Secondary Bonding

Pre-cured composite skins, timber or metal can be post-bonded to cores using a variety of adhesives, including methacrylate, epoxy and polyurethane. The bonding process requires use of a vacuum, autoclave or hydraulic press to ensure skin to core contact and avoid possible delaminations. Thermoset liquid resins or film adhesives are most commonly used, with surface preparation still being of vital importance; even though some of the resins are less susceptible to contaminants than others.

Film adhesives have several advantages over liquid systems, which see them used widely in aircraft applications. They offer constant glue line thickness, and when processed at temperature do not flow excessively, only requiring a breather or silicon pressure cushion during consolidation. Honeycomb structures in particular benefit from their thixotropy, as this property allows the resin to form a perfect fillet on the cell wall.

Secondarily bonded metal skin, honeycomb and polyurethane cored panels are used extensively throughout the world to clad buildings, where low weight and optical flatness provide an architect with functional aesthetics. The Stockholm Globe Arena, clad with aluminium skinned honeycomb panels, is perhaps the epitome of this system (Karlsson and Åström, 1997).

Other large consumers of similar secondarily bonded panelling are the fast ferry and rail industries, where metal or phenolic skins provide the necessary fire restricting properties required under government regulations. Strict guidelines are set down for each industry; IMO Res. A653 for maritime structures and for rail, country dependent statutes based on rating basic performance indicators – smoke, combustibility, flame spread and radiance.

2.2.4 Resin Infusion

There are many techniques and trade names that revolve around the world of resin infusion e.g. Le Comte and Seemann Composites Injection Moulding Process (SCRIMP™). The basic principle however uses either closed mould injection or on larger components open mould vacuum assisted infusion, shown in figure 2.6. It is the open mould method that has been used widely in recent years with success, achieving fibre weight fractions of around 70% with consistency (Horsmon, 1994).
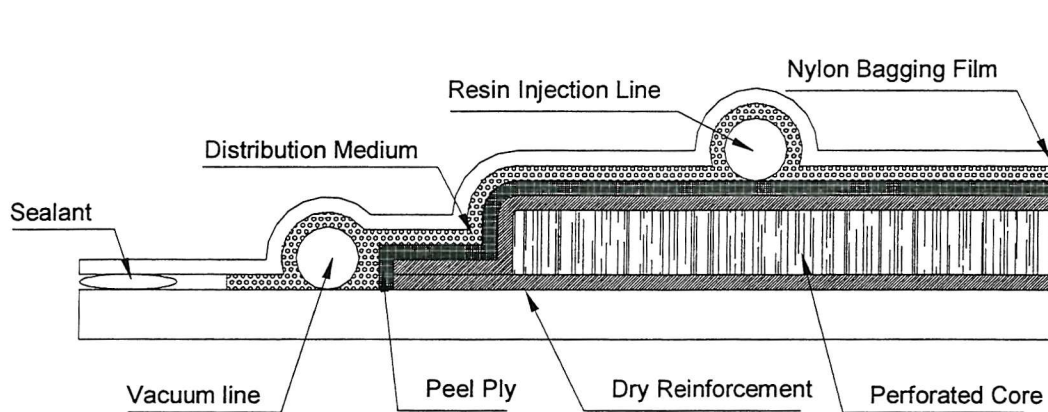
Figure 2.6 Schematic of resin infusion process (after Critchfield *et al*, 1994)

The manufacturing technique relies on a vacuum impervious mould into which dry reinforcement is placed. The actual placement of the cloth can be difficult, particularly on vertical surfaces, and so adhesive aerosols are used to hold it in position while the core, subsequent layers of fabric and peel ply are arranged on top. A distribution medium, network of infusion and vacuum lines, and finally the vacuum bag itself then cover this assembly. Upon pulling a vacuum, pre-mixed resin is allowed to be drawn into the part at various strategically placed reservoirs, with the vacuum lines and infusion points being turned on and off to keep the resin front moving and facilitate total impregnation.

The resin viscosity is one of the key aspects in the infusion process, as without a viscosity in the range of 100-300cps the process is just too slow, and reservoir exotherm becomes more likely. Consumables are obviously high, as the resin filled medium and lines must be discarded after each use. The appeal of this system is that it can be used to produce a large structure in one step with nearly all appropriate stiffening included. Several large structures have been built to date including a 28m yacht (Professional Boatbuilder, 1996), scaled 38m AMT US Marine landing craft (Critchfield *et al*, 1994), 22m landing craft (Le Comte, 1986) and a scaled midship section for 85m naval combatant (Nyguyen *et al*, 1997).

2.2.5. Filament Winding

Most often automated, filament winding is best suited to constant or linearly tapering sections as a mandrel is employed as a mould surface. It involves the placement of roving bands along predetermined optimum load paths, and can take several days to complete a large part. For this reason it is crucial that the resin resists any possible exotherm initiated cure and also has sufficient gel time to allow a primary bond between passes. Core placement techniques are as described for wet lay-up and excellent consolidation can often be achieved with the aid of shrink tape.

McLarty (1983) demonstrated, using a 1/48th scale model, that it is possible to construct large sandwich structures such as ships using modified filament winding methods, but its use in full scale production did pose some practical difficulties. More recently rail carriages have proven popular item with sandwich-winding technology (WiTEC) developed by Schindler Waggon (Huybrechts, 1998).

2.2.6. Other Methods

Karlsson and Åström (1997) describe the methods of continuous belt pressing, pultrusion and compression moulding. These are but a few more of the options successfully employed to produce large sandwich structures. Each requires large capital investment as the machines must be purpose built, but once operational they are well suited to high volume output. Inflexibility plagues such operations, as they cannot easily be adapted for different materials or prototype runs.

Bearing in mind geometrical limitations, any of the discussed materials and fabrication techniques can be used for large structures, provided suitable joining methods are utilised. It is these methods that hold the potential for increased acceptance and use of advanced sandwich structures.

2.3 Modular Construction

The concept of modular construction is not new, and some of the more optimised methods are seen in civil engineering projects. A building for example can be constructed using pre-fabricated sections giving numerous floor plan combinations and some degree of flexibility in catering for customer's tastes and site restrictions. This in turn enables modules to be produced using production line techniques, minimises the number of variables for the manufacturer, thereby reducing costs and increasing efficiency. Storch (1997) gives an excellent insight into these relationships using car industry manufacturing techniques as applied to shipbuilding.

It is these production line techniques that have spurred interest in modular sandwich construction of both small and large ships (Leake and Calkins, 1996). The reasons behind the desire for such a system are a direct result of increasing skilled labour costs, and a general industry need for accessibility to higher technology composite construction methods without the capital investment.

These increasing labour costs see a rising number of commercial projects going offshore to semi-skilled labour markets. Even if the vessel were for local capital investment in a skilled market, import tariff protection is not usually sufficient to offset the gains that can be made by building offshore. The use of these labour forces does however come at a cost, and can in some instances be characterised by long lead times and low quality, hence the niche builders of high performance yacht should remain safe from competition for years to come.

Globally the marine composite labour market could be broken up into skilled, semi-skilled and non-building regions. Table 2.1 shows a typical comparison of labour based on the author's experience, giving some idea as to the potential monetary savings offered by using a semi-skilled labour force.

Skilled	Rate ECU/hr	Semi-skilled	Rate ECU/hr
USA	34	China	7
EU	38	South Korea	13
Australia/NZ	30	Philippines	9
South Africa	17	Taiwan	13

Table 2.1 Typical regional labour rates for skilled and semi-skilled marine composite fabricators.

The advantage of modular construction is its provision of a more level playing field. It offers the ability for the skilled market to compete in their own region, as a direct result of significant reductions in assembly time. The semi-skilled market can also benefit from modules constructed in skilled regions, as it gives them access to higher technology composite materials that they can assemble with current abilities. Obviously this is a simplification of the economic impact, but the basic ideas can hopefully be grasped from this rationale.

There exists two prevailing trains of thought on the subject of modular construction, with each having its own merits and disadvantages. In fact, in some instances a combination of the two ideas

may prove an ideal solution to specific vessel geometry. It must not be forgotten however that the ability to effectively join components lies at the heart of either system's success.

2.3.1 Moulded

Any of the previously discussed manufacturing methods in earlier sections could be suitable for module production, depending on the variables imposed.

Advantages

(i)   Moulded surface finish.
(ii) Ability to produce complex curvatures.
(iii) Integral stiffening, recesses and edge closures can be included.

Disadvantages

(i)   Low flexibility in catering for alternative designs or changing sections.
(ii) Cost effective only in large production runs.
(iii) Voluminous for export projects.
(iv) Difficult to control dimensional tolerances.

Sections are produced either in turn or in separate production cells as blocks, being returned to a centre facility for final assembly. These block techniques offer the ability to introduce utilities such as plumbing, electrics etc. with increased access giving far more flexibility in time allotment to the project manager.

The practical use of moulded sandwich modules has developed in a wide and varied range of disciplines. Industry specific evaluations include cost effective housing by Woldesenbet and Vinson (1996), Chalmers' (1994) appraisal of large marine vessels, and a wellhead protection assessment (Brevik, 1996).

2.3.2 Panel Developed

Possibly one of the oldest forms of construction known to man, its origins can be traced back some 40,000 years to the *nganda* or aboriginal bark canoe. Flat sheet of any material can be singly curved into conically developed shapes i.e. Gaussian curvature is zero, and this method has been readily adopted by metal shipyards of the current day.

18

Metal shipyards have integrated many productivity and quality based improvements to panel forming methods over the past 35 years. Hooper (1986) and Lamb (1995) give a detailed history of numerically controlled cutting and lofting routines, to which the majority of advances can be attributed. Processing improvements also improved during this time, noticeably laser cutting and line heating for compound shell forms (Shin and Kim, 1997).

Use of developed composite sheet, and in particular sandwich has been limited to flat sections such as bulkheads and decks. Currently a few exceptions are gaining momentum, with an example modular hull kit shown in figure 2.7. Perhaps it is for aesthetic reasons, or maybe shipbuilders have not really considered the advantages associated with sandwich plate forming, but use in hulls and superstructures (Reichard and Neyhart, 1997) is seen only in a handful of cases.

Advantages

(i)   Cost effective regardless of component numbers.
(ii) Easily joined and aligned.
(iii) Excellent dimensional tolerances.
(iv) Optimal stacked volume for shipping.

Disadvantages

(i)   Limited to singly curved surfaces.
(ii) Exterior faces require fairing and post-painting.
(iii) Difficult to include inserts.
(iv) All sections require tabbing laminates; either pre-cured or wet.

An additional advantage of each system is the realistic possibility of implementing third party contractors to further reduce lead times and again reduce capital expenditure. This opens the doors for a traditionally metal shipyard to embrace advanced composite sandwich technology with reduced risk.

LIDGARD DESIGN - 12m POWER BOAT
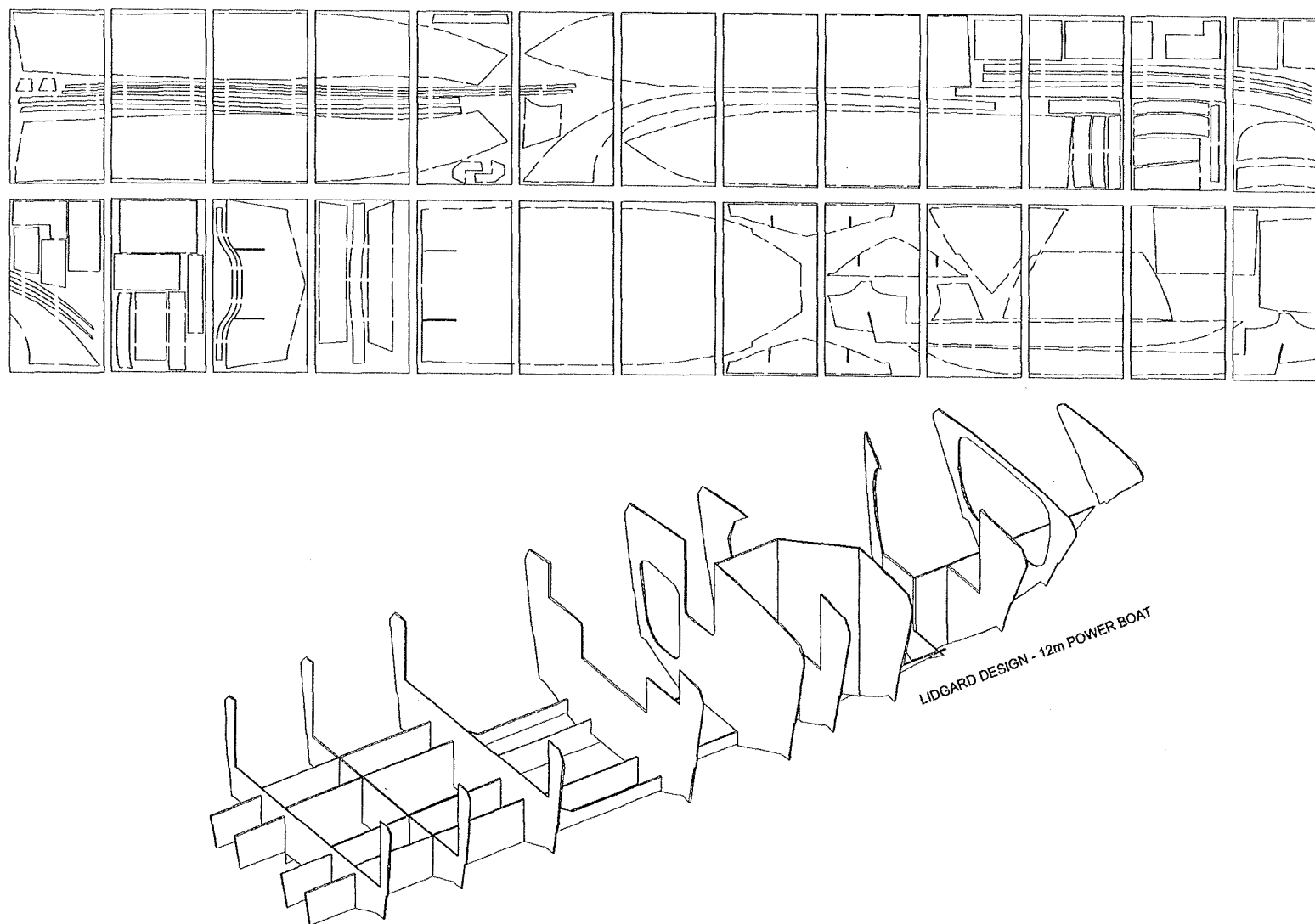
Figure 2.7 Assembled internal framing and CNC routed panel kit-set.

2.3.3 Typical Joints

Various joints currently used in a wide range of industrial disciplines for single skin and modular sandwich assembly are show below in figure 2.8. A discussion on the relative merits of each when used in single skin composite construction for an MCMV can be found in Dixon *et al* (1973) with joint specific analytical methods covered in the following chapter.
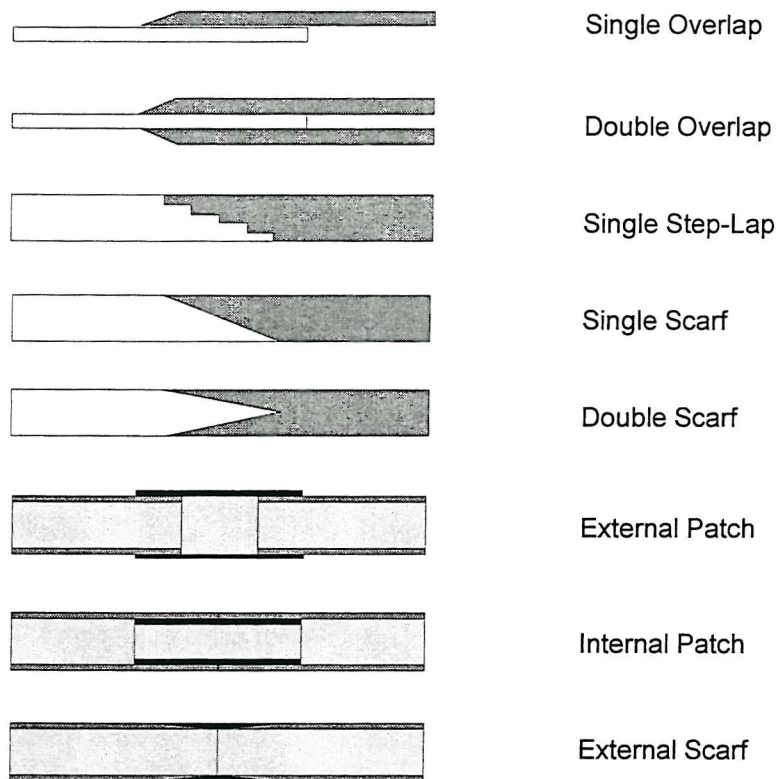
Figure 2.8 Typical adhesively bonded modular joining techniques.

CHAPTER 3

JOINING SYSTEMS

3.1 General

Undoubtedly one of the most important features of a modular system is the joining method. Niu (1990) suggests the six items that should be addressed during joint design as being

(a) The loads which must be transferred.

(b) The region within which it must be accomplished.

(c) The geometry of the members to be joined.

(d) The environment within which the joint must operate.

(e) The weight/cost efficiency of the joint.

(f) The reliability of the joint.

The last two items are part of an optimisation processes in which the basic components can be sub-categorised to accommodate further factors including availability, volume efficiency and production time.

Mechanical fastening, adhesive bonding and welding are the three choices when considering joining methods and a combination of these techniques is often used in fail safe designs, or for corrosion prevention. As composite structures, and in particular sandwich become more prevalent, there is a necessity to further investigate joint configurations, analysis options, and failure modes with a view to their practical and economic implications. Excellent reviews, although now dated, are provided by Godwin and Matthews (1980) and Matthews *et al* (1982), on joining of fibre-reinforced plastics.

Whilst it is recognised that mechanical fastening and more recently welding of composites, are valid methods of joining, the focus will be on adhesives. This restriction is imposed since mechanical fasteners are not usually the most suitable for the thin skins, as seen in sandwich structures. Similarly welding, requiring specialised equipment, in some instances could be considered a method of adhesive bonding.

Adhesively bonded joints have inherent stress concentrations as a result of maintaining strain compatibility, but with proper design should not reduce structural efficiency.

3.2 Lap Joints

The type and configuration of joints for adhesive bonding is limitless. Available analysis techniques play a vital part in constituent materials and fabricated geometry decisions, and it is important to understand the development and application of these principles. Use of the characteristic equation

$$\tau_{xy} = \frac{P}{bl} \qquad (3.1)$$

for calculation of average shear stress (τ_{xy}) over a given bonded area (bl) and under force (P), as specified in ASTM D1002 (1997), has long been the basis for many uninformed design calculations. Indeed, Adams (1986) comments on safety factors exceeding 10 often being incorporated into designs, and notes that they contain a large contribution towards ignorance.

Hart-Smith (1993) is another who is very concerned about propagation of incorrect design principles and devotes an entire paper to discussing the pitfalls of using data from tests such as ASTMD1002. He shows that the test results can only be applicable for the materials and overlap length being tested; there can be no reliable extrapolation of this data unless all components are fully scaled.

3.2.1 Theoretical Foundations

The earliest work on adhesive bonded joints, and in particular lap joints, has been attributed to Volkerson (1938), although in reality the analysis was for riveted plates. His work centered on a 'shear lag' model that neglected the effects of joint eccentricity, and considered only adhesive shear deformation and adherent elongation. Whilst this linear elastic analysis was simplified, and is more representative of a double lap joint, it formed the foundation for this area of study. According to Volkerson the shear stress distribution τ_{xy} in an adhesive layer can be described by

$$\tau_{xy} = \frac{P}{b}\sqrt{\frac{G_3}{t_3}\left[\frac{1}{E_1 t_1} + \frac{1}{E_2 t_2}\right]^{-1}}\left[-\frac{1}{E_2 t_2}\sinh(\lambda x) + \left(\frac{1}{E_1 t_1} + \frac{\cosh(\lambda l)}{E_2 t_2}\right)\frac{\cosh(\lambda x)}{\sinh(\lambda l)}\right] \qquad (3.2)$$

where

$$\lambda = \sqrt{\frac{G_3}{t_3}\left(\frac{1}{E_1 t_1} + \frac{1}{E_2 t_2}\right)} \qquad (3.3)$$

23

and E_1, E_2 are Young's modulus, t_1, t_2 thickness and v_1, v_2 Poisson's ratio for the respective adherents; E_3 the Young's modulus, G_3 shear modulus, t_3 thickness and v_3 Poisson's ratio of the adhesive; l lap joint length, b lap joint width and P applied load as shown schematically in figure 3.1. Volkerson may perhaps be the 'pioneer' of this field, but Goland and Reissner (1944) could also be considered in this light. Their analysis provides two theories, taking into account the bending moment and resultant joint rotation, neglected by Volkerson. The applied load was related to the resultant moment by a factor 'k', however their methods are still limited by the assumption that shear and peel are constant across the adhesive thickness.
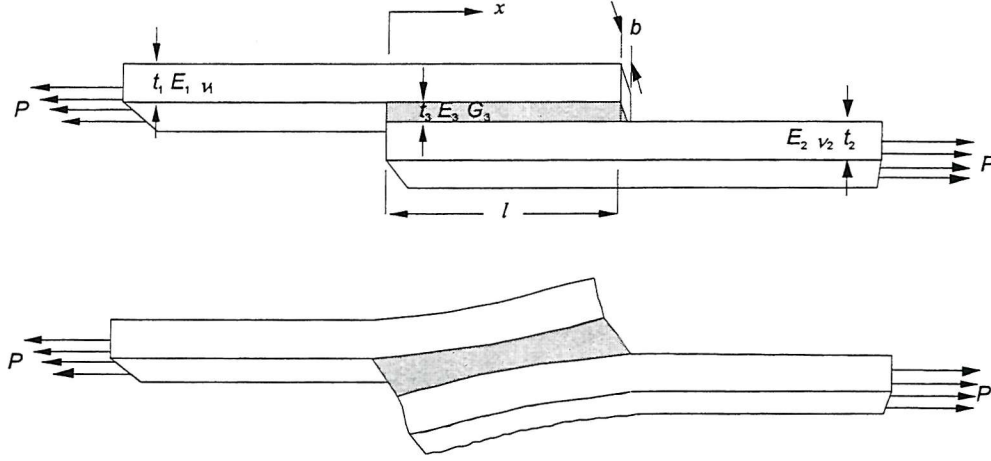
Figure 3.1 Joint rotation through eccentricity of load.

Goland and Resisner's first theoretical model centres on the adhesive having negligible thickness and moduli similar to the adherents eg. a wooden joint, whilst the more widely accepted second model which follows, allows for adhesive film flexibility and is more representative of a metal joint. Shear stress τ_{xy} and peel stress σ_y for $E_1=E_2=E$ and $t_1=t_2=t$ are expressed as

$$\tau_{xy} = \frac{Pt}{8c}\left[\frac{\beta c}{t}(1+3k)\frac{\cosh[\beta c/t]}{\sinh[\beta c/t]} + 3(1-k)\right] \tag{3.4}$$

$$\sigma_y = \frac{\sigma t^2}{c^2 R_3^{\ 3}}\left[\begin{array}{l}(R_2\lambda^2\,k/2 + \lambda k'\,\cosh(\lambda)\cos(\lambda))\cosh(\lambda x/c)\cos(\lambda x/c) \\ + (R_1\lambda^2\,k/2 + \lambda k'\,\sinh(\lambda)\sin(\lambda))\sinh(\lambda x/c)\sin(\lambda x/c)\end{array}\right] \tag{3.5}$$

where

24

$$\beta = \sqrt{\frac{8G_3 t}{E t_3}} \qquad\qquad \lambda = \frac{c}{t}\left(\frac{6E_3 t}{E t_3}\right)^{1/4}$$

$$\theta = l\sqrt{\frac{3P(1-v^2)}{bE t^3}} \qquad R_1 = \cosh(\lambda)\sin(\lambda) + \sinh(\lambda)\cos(\lambda)$$

$$R_2 = \sinh(\lambda)\cos(\lambda) - \cosh(\lambda)\sin(\lambda)$$

$$k = \left[1 + 2\sqrt{2}\,\tanh\!\left(\theta/2\sqrt{2}\right)\right]^{-1}$$

$$R_3 = \left(\sinh(2\lambda) + \sin(2\lambda)\right)/2$$

$$k' = k\frac{c}{t}\left(3(1-v^2)\frac{Pb}{Et}\right)^{1/2} \qquad c = \frac{l}{2}$$

Goland and Reissner's second theory is further restricted by imposing a validity range based on the following

$$\frac{tG_3}{t_3 G} < 0.1 \qquad \text{and} \qquad \frac{tE_3}{t_3 E} < 0.1 \tag{3.6}$$

This range was subsequently eliminated by Chen and Cheng (1983) using two-dimensional elasticity theory together with the variational theorem of complementary energy. They noted, as does Adams et al (1997), that many cases lie outside the limits stated above in (3.6), as adhesives are becoming increasingly a compromise between the so-called inflexible and flexible genre i.e. they exhibit elastic-plastic behaviour prior to failure.

One of the aims during the development of these closed form solutions for lap joints, was to satisfy the adhesive's stress free boundary condition, characterised by the law of complementary shears. Goland and Reissner, noted this anomaly in their work, and the first real attempt at satisfying the condition was made by Volkerson (1965). Unfortunately Adams et al (1997), notes that Peppiatt found numerous errors in Volkerson's paper and was therefore unable to obtain meaningful results.

Although his work is surprisingly rarely cited, Allmann (1977) derived a solution that satisfied the stress free boundary condition for a symmetrical lap joint. He notes that for non-identical adherents the solution gets unnecessarily complicated and therefore prefers approximate numerical techniques should this situation arise.

Aircraft bonded patch repairs often consider adhesive plasticity in wet/dry environments and hence Hart-Smith (1974) developed a simple equation to estimate the joint's load carrying capacity (P). Large safety factors are still required, but the basic equation is simply

$$P = 2\left(\eta \tau_{\mathrm{p}} (\tfrac{1}{2}\gamma_{\mathrm{e}} + \gamma_{\mathrm{p}}) Et\right)^{\frac{1}{2}} \qquad (3.7)$$

where τ_{p} is the effective yield stress of the adhesive, γ_{e} and γ_{p} are the elastic and plastic strain to failure assuming no elastic-plastic phase in the stress-strain profile, η the adhesive thickness, t patch thickness and E modulus.

Overlap length (l) still requires determination to ensure that the adhesive has sufficient area in the 'elastic trough' i.e. at maximum load potential creep is prevented by a given central area of adhesive under elastic conditions. Minimum design overlap can be given as

$$l = \left(\frac{P}{\tau_{\mathrm{p}}} + \frac{2}{\lambda} \right) \cdot \text{safety factor} \qquad (3.8)$$

where λ is given in equation (3.3), and E_3 is calculated as $\tau_{\mathrm{p}}/\gamma_{\mathrm{e}}$.

Edge effects can be further complicated by the presence of spew fillets, that occur when excessive resin is squeezed from the joint. Whilst in some instances a knife is used to clean the surface when the resin is 'green', Adams and Peppiatt (1974) have observed that it's presence is actually beneficial, reducing adhesive stresses by up to 30% when in triangular form. Practical tests by Adams and Davies (1996), evaluating a combination of fillet and adherent profiling shown in figure 3.2, have shown even more exceptional increases in load carrying capacity.
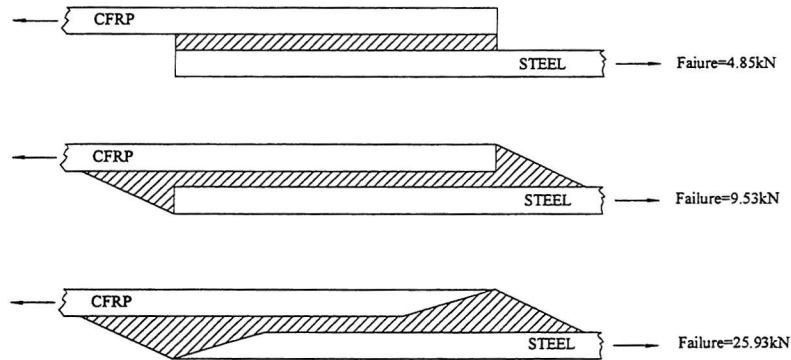
Figure 3.2 Adhesive and adherent profiling with associated failure load.

Adherent profiling to achieve a near uniform shear stress distribution is not a new concept, with a quadratic form first proposed by Adams *et al* (1973). The practical limitations are obvious,

26

however Hart-Smith (1981) also investigated the more concerning aspect of edge 'pinch off' under elastic-plastic adhesive conditions i.e. at the lap ends adhesive thickness is reduced. The problem is most pronounced where autoclave or vacuum pressure is used for joining components, and is not easily detected by NDT since the bond line is usually continuous. As the adhesive thickness reduction occurs at the most crucial location, i.e. in the vicinity of the free edge, a 50% decrease in adhesive thickness can result in a 50% increase in shear stresses.

3.2.2 Finite Element Methods

Whilst Hart-Smith prefers the continuum mechanics approach in analysis of bonded structures, Adams (1986) sees FEM as being the only accurate solution for determination of adhesive and adherent stress distributions. Adams' preference is particularly poignant since it is the only technique that can adequately account for adherent plasticity and the presence of spew fillets.

Early finite element analysis by Wooley and Carver (1971) used a program based on linear displacement functions within triangular elements. It gave excellent correlation with Goland and Reissner's work, but as Adams (1986) points out, made no allowance for adherent flexure.

More recent methods by Bezine et al. (1996), allow for material plasticity and adherent bending, and are a good compilation of various techniques previously employed by other authors, including Crocombe and Adams (1981), Lin and Lin (1993) and Tsai and Morton (1994). They show the presence of significant through thickness stresses, which are confirmed by use of a photoelastic model. The resultant effects of adherent beveling also substantiate the findings of Adams (1989), showing a somewhat linear reduction in peel stresses proportionate with bevel angle, and only appreciable reductions in shear stresses for included angles of the adherent less than 30 degrees at the adhesive interface.

Practical application of adhesive theory is invaluable as it demonstrates the true value of this type of research. A missile fin constructed using a metal hub and either of two alternate composite winglets in Boron/Epoxy (Br/Ep) and Boron/Aluminium (Br/Al) was analysed using FEM by Allred and Guess (1978). A subsequent validating test program showed that laminate transverse tensile failures dominated the Br/Ep, whilst conversely adhesive failure limited the Br/Al. An interesting development during this work was the implementation of through thickness bolts near the ends of the double lap, controlling peel and allowing a 25% increase in load carrying capacity of the Br/Ep laminate.

3.2.3 Through Thickness Stresses

Not to be confused with the across width or in-plane stresses, through thickness or out of plane stress is often the limiting case when considering bonded composites. Shenoi *et al* (1992) has observed the scarcity of reliable interlaminar tensile data, and commonly unidirectional transverse properties are used to model the limiting case. The failure sequence is particularly apparent in thick composite adherents as shown in figure 3.3.
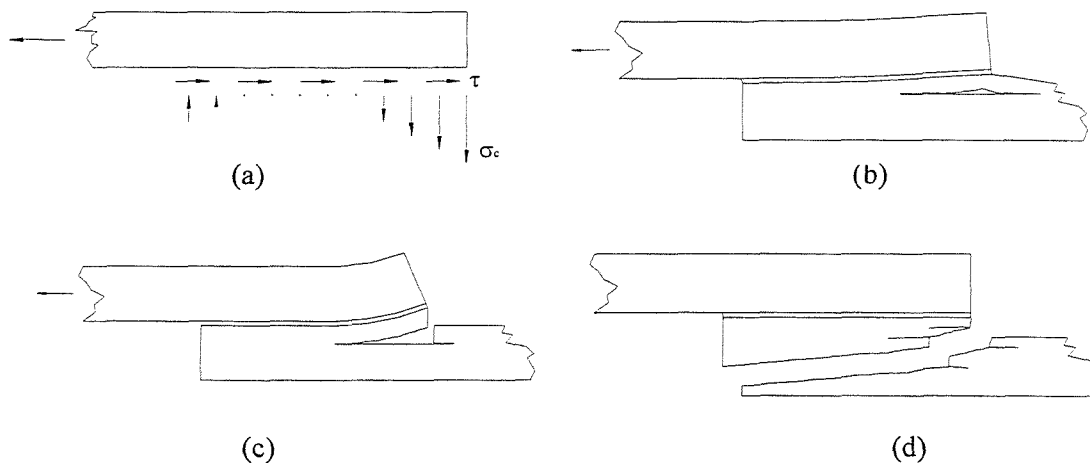
Figure 3.3 Demonstrating (a) peel and shear stress distribution and (b)-(d) failure sequence.

Unless moment restraints can be applied to the joint, Kinloch (1994) believes that the single lap should not be used as the basic configuration of a load-bearing composite connection.

3.3 Scarf and Stepped Lap Joints

The scarf joint and stepped lap have not received as much attention as their counterparts single and double lap joints, but hold special interest as the only joints that can offer continuity of thickness. Depending on aesthetical or various practical reasons, they may be more suitable or the only choice for a given set of circumstances. Hart-Smith (1974) describes the scarf joint as mathematically the most difficult to solve, due to the governing differential equations not possessing standard closed form integrals. In fact, the smooth scarf could be considered the limiting case of a stepped lap joint.

3.3.1 Theoretical Foundations

Early analysis of the scarf joint in tension by Lubkin (1956) showed that stresses were constant along the scarf joint provided the adherents have equivalent elastic properties. For non-identical adherents under plane stress, Lubkin was also able to determine the single scarf angle that provides homogenous elongation of the adhesive layer, given by

$$\alpha = \tan^{-1} \sqrt{\frac{E_2/E_1 - 1}{\nu_1 E_2/E_1 - \nu_2}} \tag{3.9}$$

where the plane strain problem is evaluated by substituting $E_x = \dfrac{E_x'}{\left(1-\nu_x'^2\right)}$ and $\nu_x = \dfrac{\nu_x'}{\left(1-\nu_x'\right)}$ with primes dropped.

Later work by Erdogan and Ratwani (1971) developed stress distributions for non-identical adherents using two-dimensional elasticity in both plane stress and strain, with a view to its application in bonding isotropic to orthotropic adherents. Reddy and Sinha (1975) extended their work to cover each adherent as orthotropic, and in Reddy and Sinha (1976) also included temperature effects. Their findings supported the theory that smoothly tapered joints are the most efficient at load transfer and also found that increasing adhesive thickness reduces shear strength, while increasing adherent modulus raised shear strength.

Chen and Cheng (1990), propose a different method of analysis for the scarf joint based on their previous techniques in Chen and Cheng (1983) cited above. They were able to show the existence of stress concentrations near the free edges and develop the following new criterion for Lubkin's single uniformly stressed adhesive angle α

$$\alpha = \tan^{-1} \sqrt{\frac{\nu_3 - (E_3/E_1)\nu_1}{1 - E_3/E_1}} \tag{3.10}$$

generally having no solutions unless

$$\left(\nu_3 - \frac{E_3}{E_1}\nu_1\right) \Big/ \left(1 - \frac{E_3}{E_1}\right) = \left(\nu_3 - \frac{E_3}{E_2}\nu_2\right) \Big/ \left(1 - \frac{E_3}{E_2}\right) > 0 \tag{3.11}$$

It should be mentioned that Thamm (1976) demonstrates that a fine tapered edge is required for the scarf in order for this joint to be structurally viable. Even an adherent taper to 10% of the

original thickness will result in a single lap joint proving more efficient at load transfer than the scarf. Whilst introducing increased difficulties in machining, it is not impossible to achieve adequate tapering, and particularly with composite adherents, stacking sequence plays a vital role in achieving the featheredge.

The scarf in pure bending is an interesting aberration in the history of joint analysis, as to date all resources have been focused on either tensile or compressive behaviour. Wah (1976) gives a brief and somewhat incomplete presentation of an approach using stress functions for determination of shear and tensile stresses developed under joint bending. It is this work that forms the focus of the next chapter, as it will be shown to have direct implications on sandwich structures and their flexural response.

3.3.2 Finite Element Methods

A limited amount of documented work has been published on scarf and stepped joints using FEA, and may be due to proprietary industry knowledge or the fact that analysis consumes considerable CPU time. Some of the earliest models were produced for use in flight vehicles by Barker and Hatt (1973), concentrating on bonding of unidirectional boron/epoxy (Br/Ep) to aluminium using the scarf and single step lap. Their work shows good correlation with the closed form solutions developed by Erdogan and Ratwani (1971), and demonstrates that the scarf is best suited to joining dissimilar materials.

The question does however arise: what happens to the stresses when the laminate has a multiple layer stacking sequence? Interlaminar stresses obviously develop, which in some ways could be considered analogous to transverse tensile stresses in lap joints.

Further expanding on the scarf joint, Johnson (1989) looks at the effects of ply stacking sequence on the stresses developed within the adhesive and adherents. The results show the adhesive interface shear stresses to oscillate about an average determined by Erdogan and Ratwani's solution. Similarly the longitudinal stresses developed in both the Br/Ep and aluminium show the same trend, with increasing ply numbers reducing the limits of the stress band and tending toward the exact homogeneous solution.

3.4 Failure Criterion

To date there has been no reliable and accurate adhesive failure criterion that can be applied to a wide range of situations. Adams et al (1997) suggest the use of upper bounds that have inherent

factors of safety, with others such as Clark and McGregor (1993) and Crocombe (1989) preferring an averaging range.

The application of failure or yield criterion can be looked at in two parts, the first is cohesive and the second adherent. It is assumed that the bond between the two adherents is sufficient that surface inconsistencies play little part in failure, otherwise much more complex probabilistic techniques must be used (Hart-Smith, 1981).

Cohesive failure, or yielding of the adhesive matrix should consider both tension and compression charactersitics of the polymer. Raghava *et al* (1973) proposed a modified von Mises criterion for adhesive yielding taking into consideration these differences and can be described as follows

$$(\sigma_1 - \sigma_2)^2 + (\sigma_2 - \sigma_3)^2 + (\sigma_3 - \sigma_1)^2 + 2(C - T)(\sigma_1 + \sigma_2 + \sigma_3) = 2CT \qquad (3.12)$$

where σ_1, σ_2 and σ_3 are the three principal stresses and C and T the absolute values of polymer compressive and tensile yield strength.

Jangblad *et al* (1988) showed that these methods, which are subject to ASTM standardisation for bulk adhesive property determination, show considerable scatter. An experimental method, based on butt and thick adherent lap joints, for adhesives used *in situ* was therefore developed to significantly reduce test sensitivity.

There are many difficulties associated with testing of adhesives, such as inevitable void formation and surface striations that can initiate premature failure. Many manufacturers of adhesives therefore neglect to perform compressive tests due to out of plane motion prevention necessitating bulky specimens. This added bulk tends to increase the potential of flaws. Vacuum techniques can be used for air bubble removal, but in many instances the required pressure falls below the vapour pressure of diluents used in formulation of adhesives and their subsequent boiling exacerbates the problem.

For this reason several studies on epoxies have been conducted in order to determine compressive to tensile strength ratios and eliminate the need for a full complement of mechanical properties. Sultan and McGarry (1970) found the C/T ratio to vary from 1.28 to 1.35 for epoxy, with a later study by Pick and Wronski (1975) narrowing this range to 1.33, which incidentally was the same as that found by Raghava *et al* for PVC.

In practice however Suzuki (1987) found that failure criteria is adhesive type dependent, with a maximum principal stress criterion suited to brittle adhesives and an unmodified Von Mises to ductile. Suzuki determined that the maximum stress predicted by finite element solutions did however overestimate the stress in a bonded joint, and hence introduced the idea of a boundary layer. The boundary layer can be considered analogous to the notch sensitivity of the adhesive and is shown in figure 3.4. Failure prediction is therefore based on the stress at a given distance from the free edge. A comparison of finite element and experimental results on bonded steel butt joints showed this value to be independent of adhesive thickness; giving a 0.02mm boundary layer for brittle adhesives and 0.2mm for ductile.
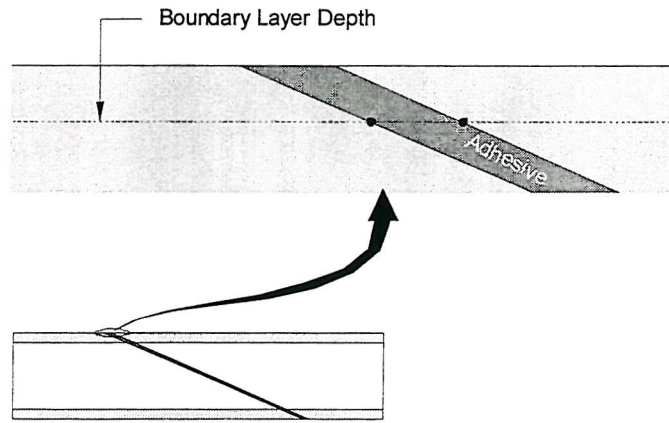
Figure 3.4 Boundary layer depth – as a concept for scarfed sandwich skin strength prediction.

A similar concept was introduced by Thomsen *et al* (1998) for failure prediction at ply drops, in laminated sandwich skins under tension. They introduced a characteristic length d^*, in essence a boundary layer, with failure prediction based on maximum principle stress. This failure criterion agrees with that determined by Suzuki, as laminating resins can normally be considered brittle. The characteristic length is determined by the following

$$d^* = \sqrt[4]{\alpha \frac{D_{11}^1}{\left(\frac{E_a}{t_a} \right)}}$$ (3.13)

where E_a is the bulk resin elastic modulus, t_a the adhesive interface thickness of the dropped ply, D_{11}^1 primary bending stiffness of the base laminate, and α a scaling factor determined from

$$\alpha = \frac{D_{11}^{tot}}{D_{11}^{tot} - D_{11}^1}$$

where D_{11}^{tot} is the combined flexural rigidity of the base laminate and dropped ply.

Adherent failure is normally far easier to determine with Von Mises criterion sufficing for metallic adherents. When using polymer matrix composites Adams (1986) suggests an essentially linear criterion, and Tong (1997) offers several proposals based on existing laminate failure theories (Nahas, 1986).

CHAPTER 4

METHODOLOGY

The concept of characterising a joint as a unit for sandwich construction offers immense potential provided the parent material being joined has guaranteed minimum mechanical properties. If this is achieved then the joint could be considered analogous to a weld in metal structures.

4.1 Experimental

Making a decision on the best materials to use for a joint analysis is important, as it reflects on the applicability of experimental results to real world structures. It is intended that a compilation of several prior and proposed experiments will offer the best step forward. Aspects to be considered include

(i)   Sandwich panel impact

(ii)   Laminate coupon tests

(iii)   In-plane joined sandwich

with each following on from the other. Impact will consider constituent materials in generic form i.e. reinforcement and resin. A fundamental approach to impact is necessary to give a basic view of the benefits associated with the constituent materials of a composite sandwich panel. Linked to the materials is the ever present question of cost. Financial considerations should never be forgotten, particularly in markets where material cost form a significant portion of final price, an example of which is the marine industry.

Laminate testing is a progression from impact evaluation, as mechanical properties are necessary for further analytical and numerical techniques. Together with material sourced from other literature this data was used for the description of various joints mechanical attributes.

Ultimately the goal is to characterise an in-plane sandwich joint. It is therefore necessary to select several joining methods and develop an experimental technique from which relevant information can be extracted. This information includes joint stiffness comparison, neutral axis movement relating to a failure progression, ultimate load carrying capacity, and finally the micro and macro morphology of failed regions.

It is expected that the scarf will form the basis of analytical and numerical methods as it has distinct advantages from a practical perspective, which are discussed in the next chapter.

4.2 Analytical

Choosing a closed form solution from which to estimate joint stresses can offer reduced complexity and rapid strength estimation when used as a design tool. Validity of assumptions and range of applicability must be given careful consideration, but it is always comforting when a realistic answer exists within the prescribed bounds.

Methods that can offer solutions to joint interface stress distributions were discussed earlier and it is Chen and Cheng (1990) together with Wah (1976) that will form the focus of the analytical investigation. It must be noted that their choice is based on the belief that a scarf joint will offer the most promise from a practical as well as mechanical stand point. Adaptation of lap joint theory to a scarf geometry is not dismissed however, as shallow angles tend toward pure shear in scarfs.

4.3 Numerical

Proprietary software such as Ansys, that package all the tools necessary for finite element solutions are invaluable. A linear elastic approach was used for a limited parametric study of scarf joints, as little work has been performed in this area. The progression will be from homogenous joints in tension, through flexure and finally application to a sandwich, with consideration given to plane stress as well as plane strain. From this position it will be possible for some general observations and recommendations to be passed, based on interfacial and internal stress distributions.

A further and final step is finite element results comparison with the chosen analytical and test models. This will provide an indication as to the validity of assumptions in each, and prove that one or both methods are suitable to joint stress prediction.

Each aspect and method of joint characteristation therefore ties into the next. This approach sees a logical progression from experimental, through analytical and finally finite element methods.

CHAPTER 5

EXPERIMENTAL PROGRAM

5.1 Preliminary Program

The requirement for an understanding of the basic constituent materials was important in test program design. Preliminary mechanical tests were carried out during the period 1995-97 at Queensland University of Technology and University of Southern Queensland to develop the foundation for panel joining principles. A parallel program in production methods was also run in-house at ATL Composites, to ascertain efficient and adaptable sandwich joining techniques, with an emphasis on marine vessels.

5.1.1 Impact Testing of Skin Laminates

The advantages and disadvantages of using particular types of resin, reinforcement and core, has been an endless concern for fabricators, with characteristics of each discussed in chapter 2. Their decisions are influenced by many factors including salesman, colleagues, industry standards and familiarity. This prompts the question, what is best? No easy answer exists, but some comparative tests show the distinct advantages of certain systems.

The impact testing of a sandwich enables a comparison to be made between different laminates on a given core. Should it be possible to decrease the skin thickness through equivalent impact resistance while still retaining the same flexural strength and stiffness of the comparative sandwich laminate, then substantial benefit can be gained by considering the resulting reduction in joint dimensions. Flexural property compensation for the thinner skin is possible by making a relatively small increase in core thickness. With this new sandwich laminate the thinner skin is directly responsible for shorter lap and scarf lengths, minimising intrusion into the sandwich structure and having associated benefits such as reduced machining, material and labour.

5.1.1.a Test Standards

A large number of impact apparatus exist, and are in continual development. The relationship between the tests and the physical structures actual service conditions is difficult if not impossible to predict and quantify. This has led to impact testing, in this study and in general, being a more qualitative exercise measuring the area of delamination, debond and fibre breakage, in order to establish a ranking of materials thought most suitable for the intended purpose.

Marine standards give guidelines to such tests, several of which are detailed in Appendix A, including American Bureau of Shipping: Tamura (1991), Australian Standards (1993), and Det Norske Veritas: Wiese *et al* (1998), although many other test standards pertaining to industry specific requirements are widely used.

An interesting point is that no reference to projectile 'bounce back' is mentioned in any standards. This 'bounce back' and subsequent hits are of extreme importance in a qualitative analysis since each specimen should be subjected to the same impact energy. The author has witnessed several instances where balsa and PVC foam has been compared without arresting the projectile after the first hit, under supervision of marine surveyors. This of course is detrimental to balsa core since the PVC foam can deform and absorb a large amount of energy, thereby greatly reducing the total impact energy associated with multiple hits from projectile bouncing.

5.1.1.b Experimental Program

A test program conducted by ATL Composites Pty Ltd, under contract CET3230/1(1995) and subsequent in-house programs, showed substantial dependence of delamination resistance on resin and reinforcement type. The tests involved changing resin systems, together with reinforcement type and weight, while leaving the core material as a fixed parameter.

Tests were performed under guidelines to DR 91044, a draft precursor to Australian Standards (1993). Incremental drop heights of 500 mm up to 2500 mm, using a 100 mm diameter round nose projectile with a mass of 15 kg, were documented.

5.1.1.c Experimental Results

Figure 5.1 details a representative crack and delamination profile for typical polyester, woven roving and CSM laminates at the final 2500 mm drop height, using the round nosed impactor.

■ Skin fracture ▨ Skin delamination

<u>Sandwich Laminate</u>

225g CSM (w_f=40%)
450g CSM
600g WR (w_f=50%)
450g CSM
6mm Al-600 Balsa Core
450g CSM
600g WR
450g CSM

Resin: Isophthalic Polyester
Fibre: E-glass

Total Mass = 8.76 kg/m^2
Reinforcement Mass = 3.23 kg/m^2

Top Face   Bottom Face
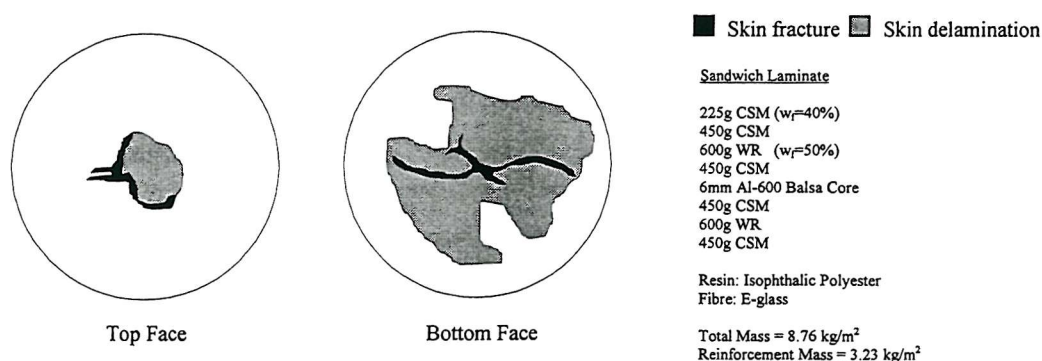
Figure 5.1 Fracture and delamination of a typical polyester laminate – 200 mm inclusion zone.

Similarly a representative lighter weight epoxy, stitched biaxial sandwich laminate delamination profile is shown in figure 5.2.

Skin delamination

Sandwich Laminate

600g Biaxial (0/90) (w_f=50%)
600g Biaxial (0/90)
6mm AL-600 Balsa Core
600g Biaxial (0/90)
400g Biaxial (0/90)

Resin: Epoxy RT Cure
Fibre: E-glass

Total Mass = 5.70 kg/m^2
Reinforcement Mass = 2.20 kg/m^2

Top Face   Bottom Face
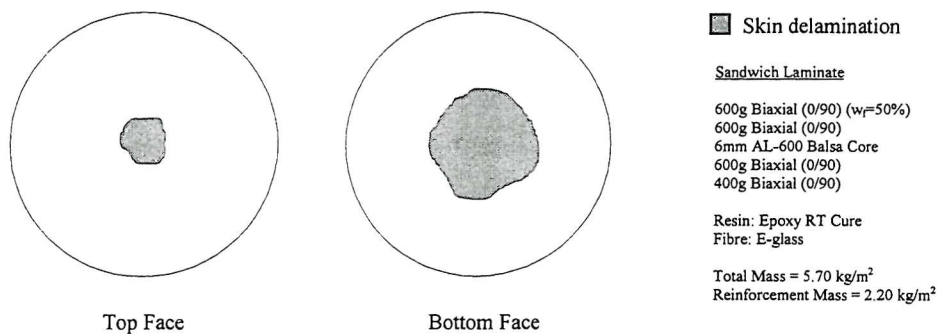
Figure 5.2 Delamination of a typical epoxy laminate – 200 mm diameter inclusion zone.

The preceding results are representative of typical sandwich panels used in small craft, but the delamination profiles can be considered representative of panels used in craft up to 100' in length. Testing at ATL Composites Pty Ltd has shown these results are the same for cores up to 40mm in thickness and skins to 2mm. Wiese *et al* (1998) have also demonstrated that core choice has a very small effect on impact resistance in terms of energy required for skin penetration.

5.1.1.d Cost Analysis

The cost implications were not forgotten during this exercise, since epoxy resin is almost three times the price of isophthalic polyester on a weight for weight basis. A simple cost analysis of the representative lay-ups in figures 5.1-2 is shown in table 5.1 overleaf, and demonstrates a move to a lighter and more durable panel has insignificant financial impact.

The polyester sandwich of table 5.1 was chosen as it is represents the majority of sandwich materials used for large volume production at the moment. It is recognised that material preferences are constantly changing, and the author does expect that in several years a transition from polyester to vinylester will be witnessed. The replacement of woven and chopped fibres with knitted materials has already commenced, but is still far from commonplace in a production environment.

Considerations such as cartage, import duty and sales tax/VAT which will effect this structure, are not included in table 5.1 so as to provide a realistic global view of net worth on an industrial usage scale.

Polyester Sandwich	Unit	ECU/unit	Epoxy Sandwich	Unit	ECU/unit
225g CSM[**]	m^2	0.91	600g Biaxial[***]	m^2	2.78
450g CSM[**]	m^2	1.39	600g Biaxial	m^2	2.78
600g WR[**]	m^2	2.91	6mm AL-600	m^2	11.21
450g CSM	m^2	1.39	600g Biaxial	m^2	2.78
6mm AL-600[§]	m^2	11.21	400g Biaxial[***]	m^2	2.69
450g CSM	m^2	1.39			
600g WR	m^2	2.91			
450g CSM	m^2	1.39			
6.9 kg Resin[†]	kg	2.10	2.8 kg Resin[‡]	kg	5.70
Total per m^2 of sandwich		37.99	Total per m^2 of sandwich		38.20

Sources: [**]ACI Fibreglass, Australia; [***]Johnston Industries, USA; [§]Baltek Corporation, USA; [†]Chemplex, USA; [‡]ATL Composites, Australia.

Table 5.1 Cost comparison of equivalent impact resistance, polyester and epoxy matrix sandwich.

5.1.1.e Conclusions

The tests resulted in the possibility of lighter and thinner laminates, with equivalent or better impact resistance to traditional polyester based laminates. A guideline was also determined for polyester based laminate reinforcement reductions when considering an epoxy resin matrix, and is shown in figure 5.3.

Figure 5.3 Polyester and epoxy resin; E-glass mass requirement for equal impact performance.

It must be emphasised that this is a fibre weight reduction, not laminate weight reduction, and as such will have the additional benefit of saving the associated resin weight. Such a guideline is important, since nearly all impact design recommendations for skin thickness determination are based on basic polyester laminates, making no quantitative allowance for 'tougher' resin systems. The one exception is the defunct American Bureau of Shipping (1994) guidelines for racing yacht

design. Appendix B describes the requirements of several widely used guides for marine code approval.

The cost analysis shows the competitiveness of an epoxy based laminate for sandwich construction, but it must be remembered that this is only a single aspect of the financial picture. Consumer perception and infrastructure, including equipment, staff training, health and safety are but a few other considerations that have associated costs, and often outweigh the benefits of just material cost and weight savings.

Nonetheless, from these encouraging results the focus for further investigation centred on thinner, lighter and more cost-effective sandwich laminates.

5.1.2 Tests on Scarf Joints in Skin Laminates

The ability to produce epoxy skins far thinner than their polyester counterparts allows the viable consideration of the scarf joining technique. The basis of this joint in sandwich would in principle be the same as a bonded single skin coupon, and as such this was the starting point.

5.1.2.a Coupon Tests

Two tensile test methods were considered, ASTM D638M (1996) and ASTM D3039M (1995). The specimen shape required under ASTM D638M was complicated, requiring necked samples similar to those used in metal coupon tests. ASTM D3039M provided a more suitable preparation technique where specimens maintained a rectangular section and had tapered tabs glued at either end to prevent jaw failure as detailed in figure 5.4.
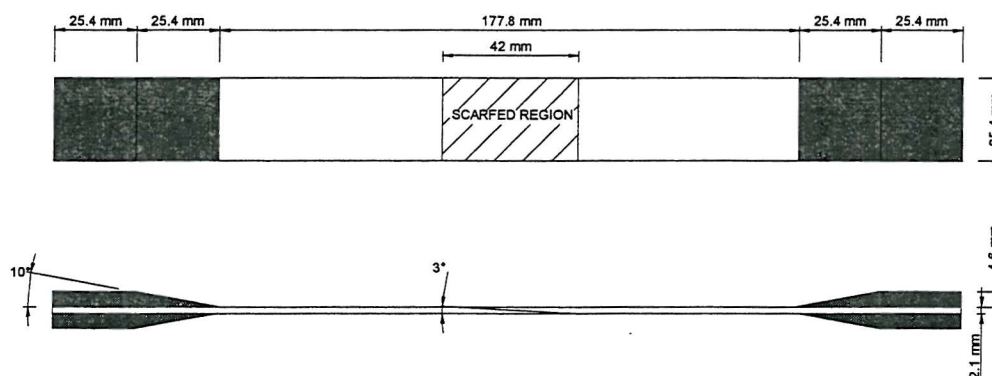
Figure 5.4 Scarfed laminate tensile test specimen.

5.1.2.b Coupon Manufacture

Control, together with scarfed samples of biaxial $[0°/90°]_{2s}$ and unidirectional $[0°]_2$ laminates, 500mm x 500mm, were produced for the tests using a custom manufactured hydraulic mini-press with thermochamber. The stacking sequence was chosen so as to eliminate any out of plane bending associated with unsymmetrical laminates. Fibre impregnation was provided by the traditional means of metal roller, with the application of a 50 g/m^2 peel ply on either side, prior to press consolidation. Pressure was maintained at 1.5 atmospheres, for an 8 hour cure cycle at 26°C.

A sheet of base material for tabs was also fabricated during the pressing procedure. Tab material was changed from that recommended by ASTM 3039M due to prior experiences showing a triaxial tab less likely to cause jaw or transition failure, irrespective of the laminate being tested.

Material Specification

E-glass: 600 g/m^2 biaxial $(0°/90°)$ 12k PPG input yarn.

750 g/m^2 unidirectional $(0°)$ 12k PPG input yarn with 25 g/m^2 Reemay polyester backing.

750 g/m^2 balanced triaxial* $(0°/\pm45°)$ 12k PPG input yarn.

Epoxy: ADR246 resin and ADH160 hardener - amine based 4:1 mix ratio by weight.

ADR60 resin and ADH60 hardener - thixotropic adhesive 2:1 mix ratio by volume.

*The triaxial fabric's 45 degree components are slightly misaligned (approximately 2-3 degrees) due to US patents held by Hexcel Corporation preventing these fabrics being produced in the US until 1999.

In order to obtain the required tab bevel, a diamond coated grinding disc was setup on a moving table, allowing a single pass cutting operation. During this procedure, the nylon peel ply was left on the laminate surface, as it tended to minimise any edge delamination and also prevented surface contamination prior to tab application. The same technique was also used for the scarf specimens, with an angle of 20:1 (2.9°) initially chosen due to its automatic satisfaction of all marine statutory requirements for composite repair methods.

Scarf bonding was achieved using the R60/H60 adhesive system, with the bonding area decontaminated by acetone and adhesive applied to both surfaces prior to joining. A bondline thickness of 0.20mm was attained through use of the mini-press, which provided constant pressure over the joint area.

41

The six base sheets were now ready for tab application. Peel ply was removed prior to sanding and subsequent bonding with R60/H60 gel adhesive, resulting in the formation of large coupons from which the tensile specimens could be taken. The samples were then docked from the sheets using a tungsten carbide tipped blade with a tooth spacing as used on aluminium. This type of blade provides a much cleaner edge than diamond coated blades, but has the disadvantage of needing frequent sharpening. The docking procedure produced the desired fine edge, but further sanding preparation using wet and dry paper was carried out to achieve a 1000-grit finish, thereby minimising the potential of fracture initiation due to edge delamination.

5.1.2.c Test Procedure

A total of 53 specimens were conditioned for 6 days at 22°C and tested at the University of Southern Queensland, during 1996 under the author's supervision. An Instron machine was used to carry out the tensile tests, at a load rate of 0.25 mm/min. Some slight modifications were necessary, after the serrated jaws continually slipped along the tab. These modifications involved placement of a swatch of 200-grit emery paper between the jaws and coupon, with the grit against the tab. Only the ultimate tensile strength was recorded as it reduced the time and expense involved in determining whether the scarf was a viable option.

5.1.2.d Results

A good performance from the scarf joint was achieved, considering that it was produced under less than perfect conditions. A summary of the results can be seen in table 5.2.

Specimen Set	No. Specimens	Failure Stress σ_{tav}	Standard Deviation	Failure Ratio Scarf/Control
Biaxial (0°) –S	7	298.6 MPa	12.73	0.803
Biaxial (0°) –C	7	371.9 MPa	15.17	
Biaxial (90°) –S	7	262.9 MPa	17.80	0.803
Biaxial (90°) –C	7	327.6 MPa	32.09	
Unidirectional (0°) –S	7	488.6 MPa	34.57	0.834
Unidirectional (0°) –C	9	585.6 MPa	18.70	
Unidirectional (90°) –C	9	23.0 MPa	3.01	**

** A scarf set (S) was not tested as theoretically there should be no difference between itself and the unscarfed control set (C).

Table 5.2 Failure stress of scarf and control tensile laminates.

5.1.2.e Discussion

All bonded scarf failures were cohesive in nature. The actual determination of the failure mode was difficult, as the adhesive used to bond the scarf together does not have constant thickness and has similar failure morphology to the laminate matrix. This thickness variation can be seen under a microscope and is due to the machining process removing resin from between single fibres and causing very small undulations on the bonding surface.

A sectional view of a typical laminate shows the presence of resin filled gaps between tows, locally increasing the apparent adhesive thickness. This increment in the adhesive thickness degrades the load carrying capacity of the bond. The 'pooled' resin contribution is therefore detrimental, and goes some way to explaining why the scarfed specimens only achieved 80-83% of the load carrying capacity of the control.

Elimination of the adhesive contribution between tows could provide a better model on which to base analysis, however it must be remembered that the final geometry of the consolidated tow will eventually govern this profile. The interface mismatch that is impossible to avoid, is therefore of little concern, as some part of each tow will lap the other and these gaps will always be present as shown in figure 5.5.
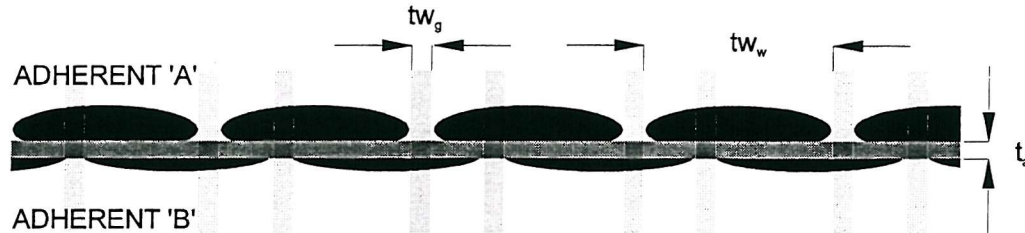
Figure 5.5 Unidirectional ply section at bonded scarf interface ($90°/0°/90°$ plies not shown).

Measurement of a typical 12k consolidated E-glass laminate gives the following cross-sectional parameters:

Tow thickness (tw_t)	300 μm
Tow width (tw_w)	2250 μm
Tow gap (tw_g)	375 μm
Adhesive thickness (t_a)	200 μm

By ignoring each small tow tip radii, a rectangular section can be used to approximate the tow width and thickness. This allows a simple calculation showing that the effective cross-section for load transmission will be reduced by the ratio

$$tw_g/tw_w = 0.167 \text{ or } 16.7\% \tag{5.1}$$

under the assumption that no load is transferred between tows along the adhesive interface. Comparison of this area reduction with the strength reduction of table 5.2 due to scarfing, shows remarkable agreement; 16.6% reduction for the unidirectional and 19.7% for the biaxial laminate.

The greater the tow weight, the more difficult such a comparison becomes, since its cross-section will tend away from a rectangular profile toward a much fuller ellipse. In this case allowance for adhesive thickness change based on the tow profile, as shown in figure 5.6, must also be considered. It can therefore be assumed that for increasing tow weight, a corresponding decrease in scarf strength will be observed under the same conditions.
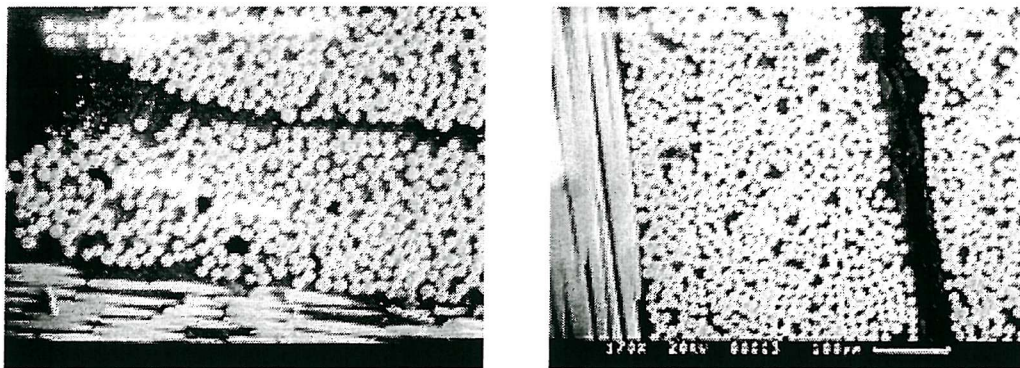
Figure 5.6 Test specimen - laminate cross sections demonstrating tow profile.

These fuller elliptical sections also exist in hand impregnated laminates where there is no pressure to flatten tows. An associated effect is that the tow gap is also larger since the bundle cannot be deformed to the same degree as a pressed or vacuum consolidated laminate. A good analogy is a rubber cylinder being squashed between two plates; its width increases corresponding to a tow gap reduction, and its section tends toward rectangular, reducing interface curvature and hence adhesive thickness.

Testing other lapped skin configurations was believed unnecessary, as available theory had shown its suitability to calculation of similar arrangements. The smoothly tapering scarf was however evaluated for this study, as prior published tests have only been conducted using metal and not laminated composite adherents.

5.2 Sandwich Program Design

5.2.1 Material Choice

Joining is obviously not limited to any specific material group. Certain adherent preparation techniques will change depending on the material, such as acid washing and priming of metal surfaces, compared with degreasing and abrasion of composites, but the basis of the system will remain the same. It was thought that composite laminates would form the limiting case when considering bonded joints, as there was the possibility of failure modes other than those guaranteed in homogenous isotropic skins such as metals. In essence there was some degree of uncertainty.

Laminate choice was representative of a small high-speed catamaran about 20m in length. Whilst the skins appear to be light for a vessel of this type, they are available because of the successful comparative impact studies produced against standard American Bureau of Shipping isopthalic polyester, woven roving and chopped strand mat laminates mentioned earlier.

The importance of stacking sequence was also earmarked at this stage, with a $(0/90)_3$ /core/ $(90/0)_2$ arrangement chosen for simplicity. While not the optimum stacking sequence for highest fibre fraction, it allows for reduced complexity in the analysis when considering future FEA and closed form solution comparisons. Knitted fabrics rather than woven fitted this criterion perfectly, as the effects of fibre kink could also be eliminated, particularly at a scarf interface. Figure 5.7 shows the method by which an increased fibre fraction is possible, through nesting of knitted plies.
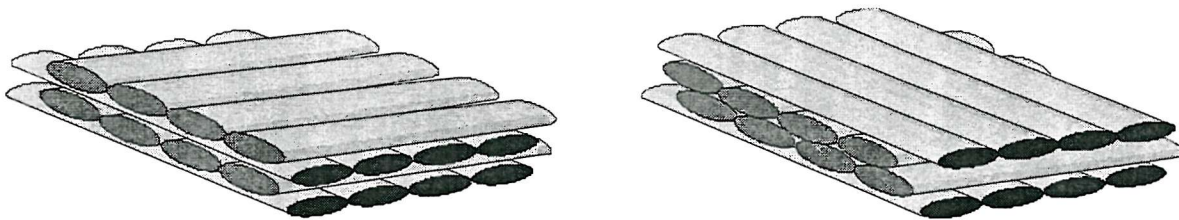
(a) Basic stacking sequence $[0^{\circ}/90^{\circ}/0^{\circ}/90^{\circ}]$.   (b) Optimum stacking sequence $[0^{\circ}/90^{\circ}/90^{\circ}/0^{\circ}]$.

Figure 5.7 Knitted biaxial - individual fibre bundle stacking (polyester knitting yarn not shown).

Availability limited the fabric choice to E-glass, as knitted carbon and aramid are normallycustom run materials, and almost exclusively produced on the $\pm 45^{\circ}$ bias.

The final consideration was a core, with balsa chosen due to high specific properties. Its compressive modulus and strength were important in minimising local stress and skin wrinkling under the supports, whilst a relatively high shear modulus limited core shear contribution to deflection. The added attraction of the core was its directional nature, with radial, tangential and longitudinal differences highlighting complexity.

The basic epoxy sandwich laminate configuration chosen was

$3 \times 600g/m^2$ knitted biaxial $(0°/90°)$ E-glass

60mm Non-segmented end grain balsa 150 kg/m^3

$2 \times 600g/m^2$ knitted biaxial $(0°/90°)$ E-glass

Base panel manufacturing was performed in Australia by ATL Composites Pty Ltd, using on-site epoxy impregnation machines and platen presses, ensuring high fibre fraction and consistent laminate thickness across the specimen range.

5.2.2 Joint Selection and Fabrication

In-plane joining of sandwich structures using adhesives can be achieved using many varied options, although most are a direct result of repair programs, and not primary structure design. Adapting some of these techniques offers several joint choices for consideration (figure 5.8).
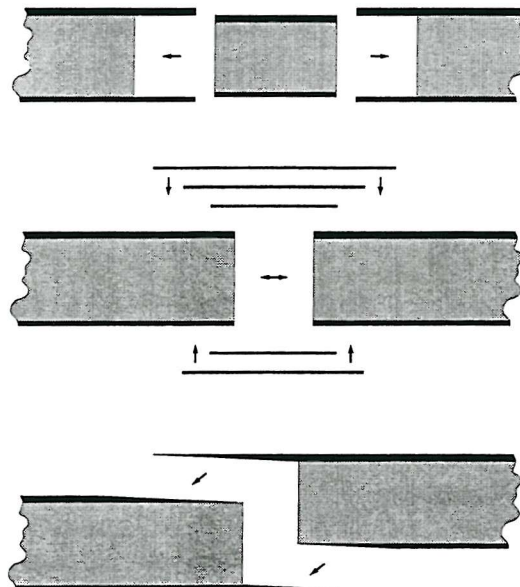
Figure 5.8 Joining techniques top to bottom: spline, external tape and Z-scarf.

5.2.2.a Tape or External Lap

Most commonly seen as a repair technique, and more often in combination with a tapered base laminate, it offers simple fabrication, but suffers disadvantages of surface unfairness and stiffness discontinuity. Laps are stepped to prevent stress concentrations at a single drop-off point, with a step length to ply thickness ratio of 20:1, commonly used as a rule of thumb in marine applications. Taping sequence is also important to minimise the number of edges exposed to potentially invasive environmental and mechanical forces. Laminations are therefore worked up from the smallest tape width, allowing subsequent layers to cover the preceding layer's edge.

5.2.2.b Scarf

While several configurations are possible, the Z-scarf design as developed at ATL Composites Pty Ltd offered ease of fabrication together with surface fairness, and possible stiffness continuity. Glue line thickness was easily metered using heated pressing devices, which also allow post-curing of the joint. The limitation of such scarfing systems is in the manufacturing process, where grinding or cutting the edge precludes aramids from the laminate.

An angle based on a 20:1 Z-scarf was chosen as giving the lowest practically achievable scarf angle; since cutting heads require custom manufacture, and grinding disks suffer from warping when the cutting depth becomes too great. This obviously has implications on thicker sandwich skins that has not been addressed fully during this phase of testing, but its importance is realised. Indeed, the thicker skins necessitate greater scarfing angles in order to keep joint dimensions within physically manageable limits and reduce material wastage. Hence, peel will become increasingly dominant as a thicker skin is used. A scarf angle of 10:1 was therefore included to evaluate performance at an increased scarf angle.

5.2.2.c Spline or Internal Lap

A form of tongue and groove, the spline offers a lap type configuration of the skin, with the spline itself being fabricated from a shell off-cut. Fabrication becomes increasingly difficult with rises in adhesive viscosity, as the hydraulic action prevents the parts from mating correctly. The protruding skins on the female joint are also pushed apart requiring external pressure to gauge glue line thickness accurately. As with the scarf, surface fairness is maintained, although local stiffness is increased. This stiffness increment can be minimised for specific applications. A beam for example could use a uni-directional spline laminate to transmit loads, and thus remove superfluous off angle fibres.

5.2.2.d Adhesives

Adhesive choice was important, but initially not a driving force behind the tests, as the actual concept and its potential, rather than specific constituents, was the focus of this evaluation. Two different adhesives, methacrylate and epoxy, were therefore chosen to represent a practical high and low limit of flexibility and ultimate elongation with properties detailed in table 5.3.

The epoxy system of choice was R60, a long open time two part epoxy adhesive, and untoughened since peel was not expected to feature significantly in these tests. The benefit of paste type systems is thixotropy, a gel like nature that does not come at the expense of increase viscosity. Practical concerns with mechanically mixed systems centre around the introduction of air bubbles into the mixture, but several options are available to minimise their presence including evacuated static dispensing equipment.

AO425 two-part methacrylate (ITW, 1997) is part of a new breed of hybrid adhesives and represents the upper viscosity range of these products having excellent gap filling properties. A short open time across the product line when compared with epoxy is a potential drawback, particularly where large surface areas must be bonded. Similar mixing problems are experienced, but again dispensing equipment is a solution.

	R60 (Epoxy)	AO425 (Methacrylate)
E (GPa)	2.015	1.000
v	0.368	0.34
Elongation*	8-12%	80-100%
Viscosity (cps)	20,000	100,000

*Variability due to temperature effects.

Table 5.3 Adhesive physical and mechanical characteristics.

5.2.3 Specimen and Fixture Characteristics

Many factors contributed to the final geometry of the test specimen and fixture (figure 5.9), with primary importance initially placed on the skin joint and its mechanism of failure. Specimens were therefore designed with the unbalanced laminates, to ensure selective skin failure.

The requirement for skin failure also necessitated an allowance for the comparison of joint performance under a reversed flexural load. The skin under consideration would therefore be under tension in one test and compression in another. This load reversal was thought important for several reasons:

(i) The core may dissipate stress concentrations in the joint differently.

(ii) Adhesive characteristics may change under reversal of load conditions.

(iii) Mode of failure may change.
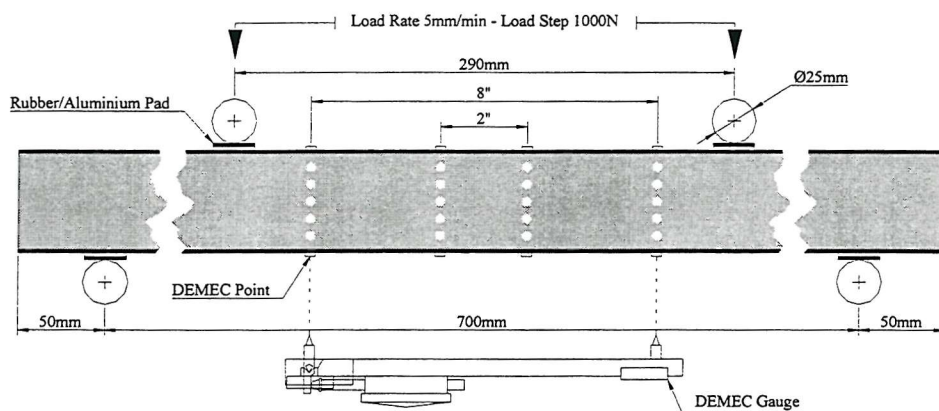
(iv) Tensile and compressive variations in laminate properties will be present.

Figure 5.9 Fixture arrangement including strain measurement locations (Demec points).

5.2.3.a Demec Gauge

Total joint strain in flexure, rather than local laminate strain, was measured by the use of aDemec (demountable mechanical) strain. The Demec gauge, developed in the early 1950's by the British Cement & Concrete Association, was chosen to measure these strains, as it offered the ability to cover large gauge lengths and thus encompass joint movement as a whole. Extensive testing was conducted during its development by Morice and Base (1953), who discuss potential pitfalls including aspects of gauge tilt and temperature effects during measurement. Further, more practical aspects of field use for concrete structures is covered by Base (1955), including rapid methods of point marker attachment.

Variable temperature ranges are an important consideration for field use. A gauge set therefore includes an Invar dummy bar for this purpose so that temperature corrections can be made for gauge dimensional changes over the measurement duration.

Imperial gauge lengths of 2" and 8", with accuracy of 0.0001" were selected, as measurement precision and effect of beam rotations and deflection were not initially apparent. Care was also necessary in designing a specimen with sufficient rigidity that only minor corrections need be made due to beam curvature.

5.2.3.b Measurement Error Estimation

The error is introduced due to the 1-D measurement, which can overlook the strain differential due to shape. Typical beam test data is listed in table 5.3 for error appraisal with a schematic of the deflected shape and calculation variables shown in figure 5.10.

Property	Value	Property	Value
E (skin modulus)	21.370 GPa	c (core thickness)	60 mm
G (core shear modulus)	159 MPa	d (sandwich thickness)	62.68 mm
L (beam length)	700 mm	a (support to load point)	205 mm
b (beam width)	120 mm	I (sandwich inertia)	289900 mm^4
L_{gauge} (gauge length)	203.2 mm	y_1 (thick skin moment arm)	25.34 mm
P (total applied load)	20000 N	y_2 (thin skin moment arm)	37.34 mm

Table 5.3. Representative four point sandwich specimen properties.
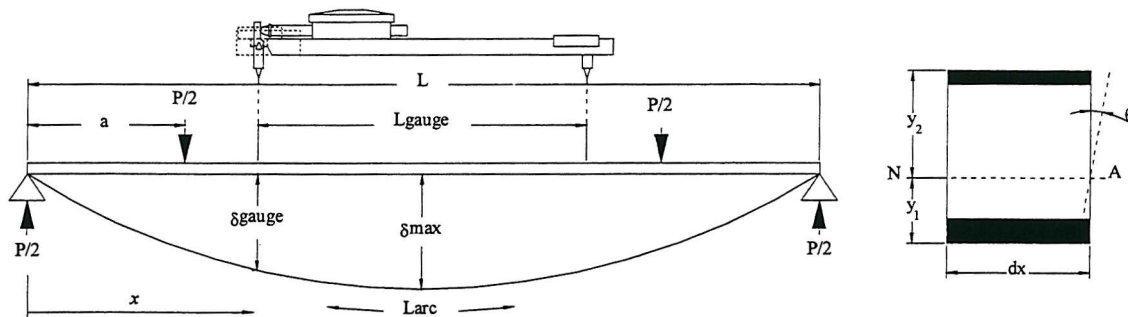
Figure 5.10 Beam elastic curve under variable four point loading including a typical element 'dx'.

Assuming the sandwich faces are thin and core flexural stiffness is negligible compared to the skins, deflection can be shown to be

$$\delta = \left[\frac{Pa^3}{12EI} \left[3\left(1+\frac{b}{a}\right)\frac{x}{a} - \left(\frac{x}{a}\right)^3 \right] + \frac{Px}{2GA} \right] \qquad 0 \le x \le a \qquad (5.2)$$

$$\delta = \left[\frac{Pa^3}{12EI} \left[3\left(1+\frac{b}{a}\right)\frac{x}{a} - \left(\frac{x}{a}\right)^3 + \left(\frac{x}{a}-1\right)^3 \right] + \frac{Pa}{2GA} \right] \qquad a \le x \le L\text{-}a \qquad (5.3)$$

$$\delta = \left[\frac{Pa^3}{12EI} \left[3\left(1+\frac{b}{a}\right)\frac{x}{a} - \left(\frac{x}{a}\right)^3 + \left(\frac{x}{a}-1\right)^3 + \left(\frac{x}{a}-\frac{b}{a}-1\right) \right] + \frac{P(L-x)}{2GA} \right] \qquad L\text{-}a \le x \le L \qquad (5.4)$$

where $A = bd^2/c$ (Plantema, 1966), and

δ_{max} occurs when $x = L/2$

The calculations differ slightly from those of ASTM C393 (1994), as the contribution of core shear to deflection is not limited to quarter point span positions.

When calculating the erroneous strain (ε_{err}) due to curvature it is assumed that the deflection profile can be described parabolically over the gauge length, although strictly speaking it is circular in form due to the constant moment.

$$\varepsilon_{err} = \frac{L_{arc} - L}{L} \qquad (5.5)$$

where

$$L_{arc} = \frac{1}{2}\sqrt{L^2 + 16(\Delta)^2} + \frac{L^2}{8\Delta}\ln\left(\frac{4\Delta + \sqrt{L^2 + 16\Delta}}{L}\right)$$

$$\Delta = \delta_{max} - \delta_{gauge}$$

Skin strain ($\varepsilon_{1,2}$) estimates based on plane rotation about the neutral axis i.e. $\theta = d\delta/dx$ give an indication as to the influence of ε_{err} associated with the gauge measurement.

$$\theta = \left[\frac{Pa^3}{12EI} \cdot \frac{3}{a} \left[\left(1+\frac{b}{a}\right) - \left(\frac{x}{a}\right)^2 + \left(\frac{x}{a}-1\right)^2 \right] \right] \qquad (5.6)$$

$$\varepsilon_{1,2} = \frac{2y_{1,2}\theta}{L_{gauge}} \qquad \text{since } \theta \text{ is small.} \qquad (5.7)$$

51

Substitution of table 5.3 variables into equations (5.2-7) yield the following strain and error curves (figures 5.11.a-c) as a function of load; both 8" and 2" gauge lengths yield the same results.

(a) Linear strain – thick skin (b) Erroneous strain (c) Comparative strain error
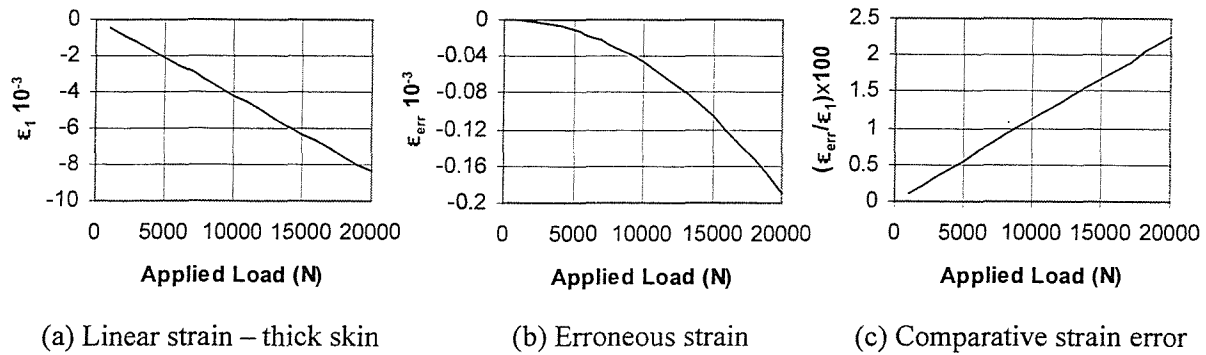
Figure 5.11 Theoretical strain calculations.

5.2.3.c Test Standards

Three point test arrangements such as those defined in ASTM C393 and ASTM D790 (1996) were not practical for experiments of this type, as loading point interference with the joint was inevitable. The joint could have been moved to one side of the central load. However as the section of interest would have been under a variable moment, the weakest link in the joint may not have failed first, or failed at a perceived artificially high load.

The solution to the problem was the four-point test, offering a constant bending moment over the section, and the added advantage of zero core shear in the joint. Loading point spans were the first dimensions to be fixed and are governed by the physical length of the 8" Demec gauge. From this, an iterative procedure was required to determine support span and specimen proportions, bearing in mind the following conditions:

(i)   Instron test bed dimensions

(ii) Core shear limit set at 60% of maximum

(iii) Requirement for skin failure

(iv) Optimum specimen nesting on base panels

(v)   Limited deflection

(vi) Sufficient width to negate any potential torsional effects

(vii) Sufficient overhang to minimise end effects

ASTM C373 was used as a basic guide to specimen and fixture parameters during this process, as it is the only internationally recognised test standard pertaining to flexural performance of

sandwich structures. Development of an ISO (International Standards Organisation) guide, as reported by Gower and Sims (1997), will in the future offer an alternative. However the only current difference between the proposed ISO standard and ASTM C373 is an increase in the number of differing support spans. This specimen increment is required for determination of skin and core modulus from the plots of $1/L^2$ vs. D/P^3L and L^2 vs. D/PL as discussed by Allen (1969).

5.2.3.d Test Sample Summary

The specimen codes of figure 5.12 are used for sample designation, describing the joint type, adhesives and load directions. A basic sandwich laminate was chosen as described in 5.2.1, incorporating readily available composite materials, with general specimen dimensions listed in table 5.3.
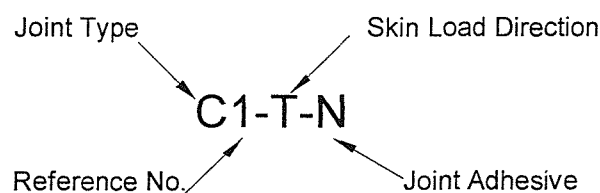
Figure 5.12 Test specimen reference coding.

Joint types as shown in figure 5.8 have the following designations in the specimen code; (C) control (no joint in specimen); (T) external tape joint; (S) scarf joint; (SP) spline joint. Joint geometry as used in the experimental investigation is defined for each in figures 5.13.a-d.
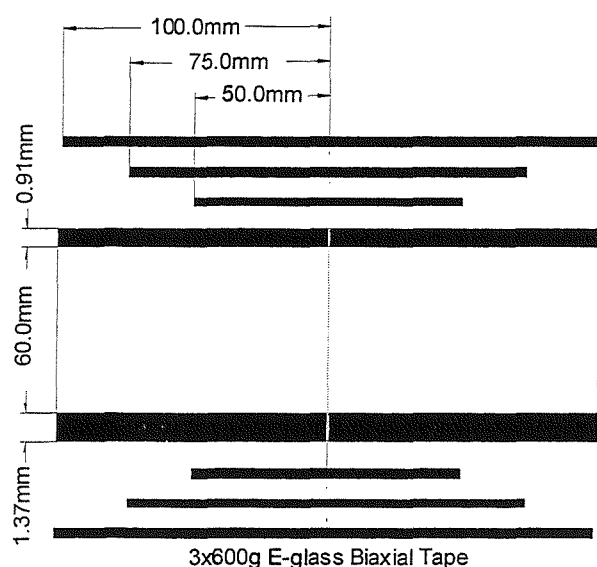
Figure 5.13.a External Tape Joint   Figure 5.13.b Scarf Joint 20:1 Angle
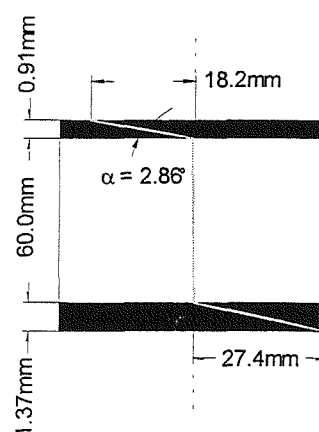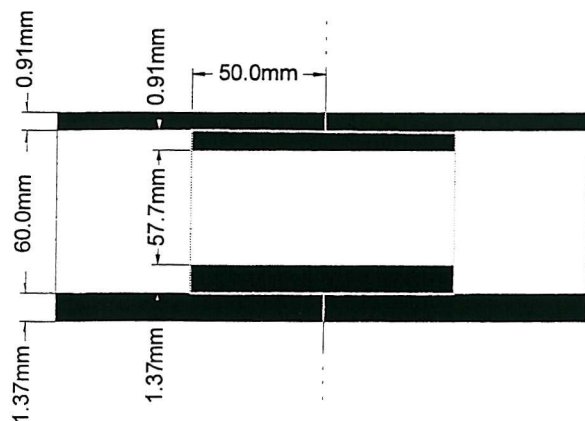
Figure 5.13.c Internal Spline Joint   Figure 5.13.d Scarf Joint 10:1 Angle
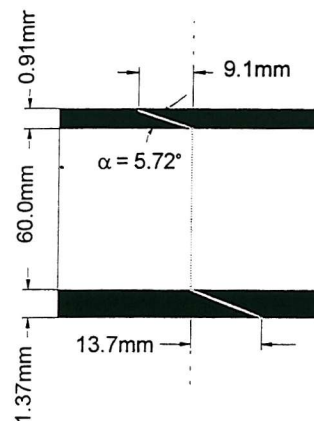
Skin load direction refers to the stress state under which the thinnest skin of the sandwich is placed; (T) Tension; (C) Compression. Figures 5.14.a-b demonstrate this schematically.
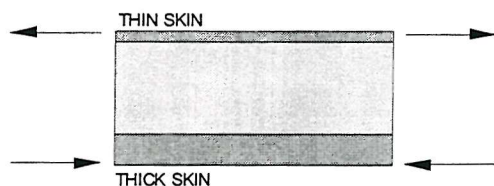
Figure 5.14.a Thin skin tension loading.   Figure 5.14.b Thin skin compression loading.
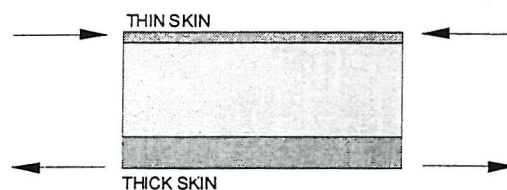
The joint adhesive was controlled to 0.2mm for both types of adhesives which were designated by (N) no adhesive; (EP) epoxy; (MA) methacrylate. Both adhesives were applied to each bonding surface prior to joining, including any core to core butt interfaces. Thickness control was achieved using a variety of methods, but the most successful was feeler gauges at panel edges. These areas of the panel were subsequently machined and discarded due to the presence of voids.

Another commonly available method is based on the use of glass bubbles with a 0.2mm mesh size. The material can be post mixed into the resin system and under pressure in the joint resin flows allow the rigid beads to provide a minimum adhesive film build. The author discarded this process, as previous experience had shown their presence to degrade mechanical properties significantly.

Failure mechanisms were either core, skin, adhesive or cohesive. Instances existed where it was not easily determined whether the skins themselves failed in interlaminar shear (substrate failure), or a cohesive failure was initiated. This was due to the adhesive and matrix being the same colour.

It was difficult to visualise fractures in the adhesive and so a separate light source to the microscope was used and positioned so that it refracted on fissure planes. This was a very time consuming process and often required a second filtered light source for photography.

Failure was usually restricted to the joint areas. Modes of failure are therefore only described rather than located, as they are easily referenced by the skin load direction for the thinnest laminate. The quantitative value for failure load is a total applied through the four point test fixture, and can easily be resolved into the various reactions if desired for other calculations.

5.3 Results

Testing involved more than 3000 manual readings taken over 30 specimens. Load was ramped in 1000 N steps at 5mm/min to allow for fixture stabilisation prior to measurement. Failure load and modes are listed in tables 5.5-9 following, with specimen macro and micro-morphology documented in Appendix C.

Stainless steel point markers, used for gauge readings, were applied using a quick setting epoxy adhesive to both core and outer skin. No correction was necessary for marker thickness since the conical locating holes are drilled to leave only a very thin membrane between adhesive and point.

A comparison of theoretical strain with experimental results in Appendix D was possible by using equation (5.7) under linear elastic assumptions. Similarly for load deflection, equation (5.3) can be compared against the experimental mid-span displacement in figures D.6.1-5. The figures of Appendix D demonstrate that the theoretical model is valid for strain rates up to 50% of failure load in the continuous and epoxy bonded scarf specimens, however those specimens joined with methacrylate cannot be modelled in this manner as they exhibit a distinct non-linear behaviour.

It should be noted that erroneous strain associated with curvature was not the only source of measurement error. Operator parallax when reading a dial gauge, loading roller friction not fully representing a simple support, roller slippage and resultant change in load span, specimen creep under constant load during readings and load increment through gauge application can also contribute to result inaccuracies. Material property variation from sample to sample is discussed in the following sections, and would undoubtedly be the largest contributor to any of the small deviations between experimental and theoretical results. The presence of these possible sources of error was however believed insignificant even when considering that each could be cumulative.

5.3.1 Control Specimens

Tensile specimens did not achieve the desired skin failure. Rather core shear failure dominated, with 1.36 MPa average shear stress over the three specimens, compared with an average published value of 2.98 MPa (Baltek, 1991). A more detailed discussion as to the reasons behind this occurrence is found in Appendix E.

Failure of the compression specimens did occur as expected between the two load points, and gave an average laminate compressive strength of 202 MPa. It was apparent from visual inspection of the failed specimens that there was a slight misalignment of weft fibres during the manufacturing process, measuring approximately $3°$.

Skin strain and beam deflection to failure showed linear behaviour. Due to the Demec gauge requiring manual placement for readings, it is feasible that just prior to failure some non-linearity could be encountered and not recorded. To eliminate this uncertainty, the results were compared with load versus cross-head movement plots on the Instron machine, and found to be equivalent.

Specimen	Failure Load	Failure Mode
C1-T-N (Tension)	18.65 kN	Core Shear
C2-T-N (Tension)	20.40 kN	Core Shear
C4-T-N (Tension)	19.80 kN	Core Shear
C5-C-N (Compression)	16.70 kN	Skin Compression
C6-C-N (Compression)	18.60 kN	Skin Compression
C7-C-N (Compression)	16.80 kN	Skin Compression
C8-C-N (Compression)	17.10 kN	Skin Compression

Table 5.5 Failure load and modes of control sandwich specimens.

5.3.2 Tape joint

Core failures occurred at an average shear stress of 1.15 MPa, well below even the 60% design allowance. In each case, core shear failure initiated at the lowest density balsa blocks within the constant shear regions of the beam i.e. between the outer most simple support and the load point inboard of this position.

The single compressive failure occurred outside the joint, just to one side of the load application point. Failure initiated as skin compression, which then allowed interlaminar separation and ultimately skin buckling.

As with the control specimens, strain and deflection showed linear behaviour under incremental loading. Some anomalies were experienced with the 8" strain gauge readings, showing localised increases in tensile strain, and corresponding decreases in compressive strain (figures D.3.1-2). This was due to tensile face slippage over the support rollers occurring at a single instant in time, countering the accumulated effects of roller friction, and therefore noticeably affecting such a large gauge length. One observes that no such aberration is present for the smaller 2" gauge length.

Specimen	Failure Load	Failure Mode
T1-T-EP (Tension)	19.10 kN	Core Shear
T2-T-EP (Tension)	13.30 kN	Core Shear
T3-T-EP (Tension)	15.00 kN	Core Shear
T4-T-EP (Tension)	19.15 kN	Core Shear
T5-C-EP (Compression)	15.90 kN	Core Shear
T6-C-EP (Compression)	16.00 kN	Skin Compression
T7-C-EP (Compression)	17.40 kN	Core Shear

Table 5.6 Failure loads and modes of tape joints.

5.3.3 Scarf Joint (methacrylate)

Non-linear behaviour was present in tests on all methacrylate joints, with the greatest scarf angles showing the highest prevalence for this type of response. Figures D.2.1-4 demonstrate the capacity of the Demec gauge to capture the movement and ultimately show the nature of a high elongation adhesive.

Failure of tensile specimens, even with some creep relief prior to failure, was sudden and catastrophic in nature. The separation of the joint and subsequent cleavage of the core meant only the compressive skin remained intact. Conversely, compressive failure was restrained, with joint failure followed by crushing of the core. This mechanism was of interest, as in some specimens it showed the capability of resisting loads as high as 3.00 kN (figure 5.15).
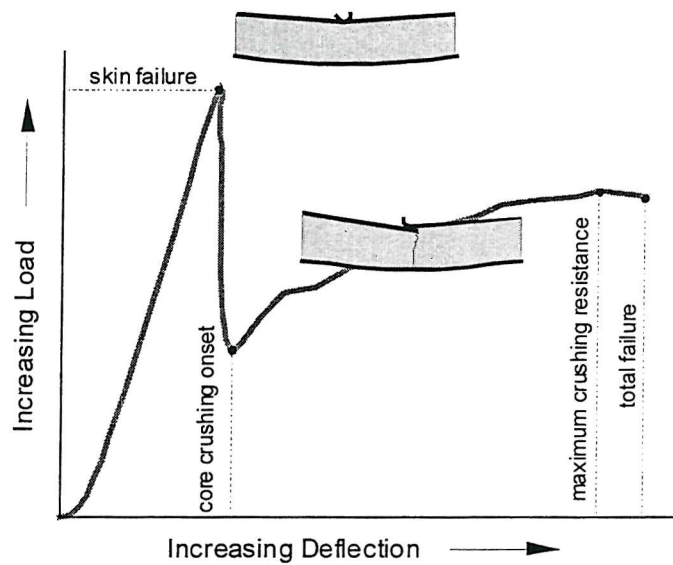
Figure 5.15 Balsa core crushing resistance under compressive skin failure.

Specimen	Scarf Angle	Failure Load	Failure Mode
S1-T-MA (Tension)	20:1	7.15 kN	Cohesive
S2-T-MA (Tension)	20:1	7.00 kN	Cohesive
S3-T-MA (Tension)	20:1	8.05 kN	Cohesive
S6-C-MA (Compression)	20:1	8.05 kN	Cohesive
S4-T-MA (Tension)	10:1	5.70 kN	Cohesive*
S5-C-MA (Compression)	10:1	5.00 kN	Cohesive*
S7-C-MA (Compression)	10:1	4.00 kN	Cohesive*

* Some failure indistinctness between adhesive and the actual laminate matrix was evident and therefore may potentially include a substrate component.

Table 5.7 Failure loads and modes of scarf joints using methacrylate adhesive

5.3.4 Scarf Joint (epoxy)

The modes of failure varied, however the tensile specimens demonstrated the potential of the scarf when used with a suitable adhesive. Shear failure between warp tows of E-glass initiated failures

on tensile skins, with the weft tows offering little load resistance and allowing interlaminar crack propagation. These cracks after travelling short distances then promoted tensile failure between 90° tows, usually at a void formed between fibre bundles.

Fibre 'pinging' was prevalent prior to explosive tensile failures. It offered some acoustical warning, but on several specimens stopped readings prematurely. The load versus strain diagrams do not therefore represent strain at failure.

Similar joint behaviour to the methacrylate adhesive was experienced, but on a different scale. Figures D.4.1-4 show the development of joint strain, and figure D.6.4 the load deflection profile.

Specimen	Scarf Angle	Failure Load	Failure Mode
S2-T-EP (Tension)	20:1	13.05 kN	Substrate/Cohesive
S3-T-EP (Tension)	20:1	13.00 kN	Substrate/Cohesive
S5-C-EP (Compression)	20:1	12.90 kN	Core Shear
S7-C-EP (Compression)	20:1	13.10 kN	Skin compression
S1-T-EP (Tension)	10:1	8.10 kN	Substrate/Cohesive
S4-T-EP (Tension)	10:1	5.05 kN	Substrate/Cohesive
S6-C-EP (Compression)	10:1	9.10 kN	Scarf Compression

Table 5.8 Failure loads and modes of scarf joints using epoxy adhesive.

5.3.5 Spline Joint (epoxy)

A small sample size was tested due to the complexity in making specimens. The spline's close proximity to the neutral axis offers reduced localised stiffness when compared with the tape, but as can be seen in figure D.6.5, does not show the same degree of stiffness continuity when compared to the control specimen as the scarf joint (figure D.6.4).

The glue lines failed in shear, as the specimens were designed for limited deflection, and therefore allowed only minimal peel forces to develop. Figure C.5 shows the 45° fractures in the adhesive, confirming this mode of failure.

Specimen	Failure Load	Failure Mode
SP1-T-N (Tension)	16.80 kN	Adhesive/Cohesive
SP2-C-N (Compression)	17.80 kN	Adhesive/Cohesive

Table 5.9 Failure loads and modes of spline joints using epoxy adhesive.

5.4 Discussion

The Demec gauge has the ability to measure joint strain, but is limited by the inability to provide continuous reading. These tests demonstrate adequate detail for materials having a relatively linear stress versus strain behaviour. Nevertheless for those materials that exhibit yielding e.g. metals, care would be necessary in determining the load steps at which readings were taken. Consideration must also be given to the manual nature of locating the gauge and force associated with this process. Unless a compensation method can be developed, strain in flexible specimens cannot be determined using a sprung mechanism, as in the Demec gauge.

In principle the stainless point markers could be attached permanently to a marine or other vessel so that the through life performance of a joint, or any other component could be cheaply and effectively monitored with little expertise required from the operator.

The scarf angle on experimental specimens was kept to a minimum in order that maximum strength is achieved and there is enough area over which flaws can be accommodated. It is likely that at low scarf angles the adhesive interface shear stress can be approximated by Volkerson's shear lag theory. This is possible in the sandwich since local skin bending effects are insignificant, and bending induced by asymmetry in the lay-up will be restrained by the core.

Introduction of a boundary layer as described by Suzuki (1987), offers the potential to predict failure. Assuming that the adhesive is ductile, then Von Mises yield stress (σ_y) under pure shear (τ_{xy}) in a two-dimensional system can be reduced to

$$\sigma_y = \sqrt{3\tau_{xy}^2} \qquad (5.8)$$

Bulk adhesive tensile yield strength (σ_a) is 45 MPa for the epoxy and 24 MPa for the methacrylate with other mechanical properties found in table 6.2.

From the failure loads of tables 5.7-8 it is possible to estimate the tensile or compressive force in the sandwich skin due to bending based on the extreme fibre maximum stress using

$$\sigma = \frac{My}{I}$$ (5.9)

and in pure tension or compression

$$\sigma = \frac{P}{A}$$ (5.10)

Assuming thin skins allows substitution of σ in equations (5.9-10) giving the failure load as

$$P = A\frac{My}{I}$$ (5.11)

where

σ - failure stress A - cross sectional area of skin considered

P - failure load M - maximum moment based on the failure load

I - sandwich second moment of area y - distance from sandwich NA to extreme fibre

Calculation can therefore proceed according to Volkerson equation (3.2) through substitution of variable P above. Selecting a boundary layer depth of 0.055mm results in two characteristic lengths (x^*). This is due to two scarf angles being present and can be calculated via

$$x^* = \frac{0.055}{\sin \alpha}$$ (5.12)

where x^* is substituted for x in equation (3.2) allowing shear stress prediction. Figure 5.16 shows a typical shear profile for epoxy with the ultimate stress predicted by Volkerson being 51.4 MPa, and that found using the characteristic length substantially reduced to 27.1 MPa. It should also be remembered for this calculation that the scarf length (l) is dependent on angle.
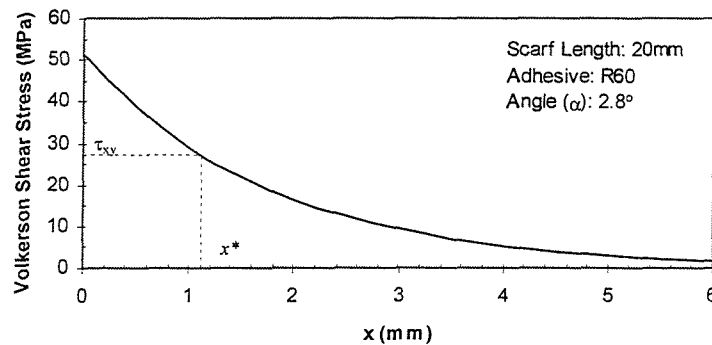

Figure 5.16 Modified shear stress prediction via use of characteristic length x^*.

61

Substitution of the predicted shear stress into equation (5.8) allows direct comparison with the quoted manufacturers tensile yield stress (σ_a) being listed in table 5.10.

Specimen	Failure Load (kN)	x^* (mm)	Predicted τ_{xy} (MPa)	Equiv. Stress σ_y (MPa)	Bulk Yield σ_a (MPa)	$1-\sigma_a/\sigma_y$ (%)
S1-T-MA	11.95	1.126	12.77	22.12	24.0	-7.8
S2-T-MA	11.70	1.126	12.51	21.66	24.0	-9.8
S3-T-MA	13.45	1.126	14.38	24.91	24.0	+3.8
S6-C-MA	13.45	1.126	14.38	24.91	24.0	+3.8
S4-T-MA	9.52	0.512	13.35	23.13	24.0	-3.6
S5-T-MA	8.35	0.512	11.71	20.29	24.0	-15.5
S7-C-MA	6.68	0.512	9.37	16.23	24.0	-32.4
S2-T-EP	21.81	1.126	27.22	47.14	45.0	+4.8
S3-T-EP	21.72	1.126	27.11	46.96	45.0	+4.4
S1-T-EP	13.53	0.512	23.47	40.65	45.0	-9.7
S4-T-EP	8.44	0.512	14.63	25.34	45.0	-43.7

Table 5.10 Comparison of predicted adhesive joint yield stress and bulk resin data.

The results are very good considering that joint failures occurred under both tension and compression loads. Furthermore, two differing scarf angles and adhesives show the insensitivity of choosing a 0.055mm boundary layer for these ductile adhesives. Inherent flaws due to poor specimen manufacture resulted in two anomalies at 32.4% and 43.7% deviation from bulk data.

The peak sandwich skin stress (σ_s) in either tension or compression, at which adhesive yield will occur, can now be estimated by the rearranging Volkerson's equation and substitution of equations (5.8-12) for the relevant variables.

$$\sigma_s = \sqrt{\frac{2E_s t_a \sigma_a^2}{3G_a t_s}} \left[\frac{\cosh(\lambda x^*)(1+\cosh(\lambda l))}{\sinh(\lambda l)} - \sinh(\lambda x^*) \right]^{-1} \qquad (5.13)$$

where

$$\lambda = \sqrt{\frac{2G_a}{E_s t_s t_a}} \qquad x^* = 0.055/\sin(\alpha) \qquad l = t_s/\sin(\alpha)$$

and

E_s – skin tensile or compressive modulus

G_a – adhesive shear modulus

t_s – skin thickness

t_a – adhesive thickness

σ_a – bulk tensile yield strength of adhesive

α – scarf angle

This semi-empirical approach should be suitable for scarfed sandwich skin laminates, provided the skins are thin and scarf angle is small. A more comprehensive study is however necessary so that this formula may be applied with confidence to laminates of varying ply orientation. While the theory does appear to be satisfactory for this particular set of experiments, a more comprehensive understanding of the scarf with varying laminate thickness and larger scarf angles is necessary to remove geometric limitations. Chapter 6 will therefore discuss two methods that can possibly cover the full spectrum of scarf parameters while still accurately predicting failure.

Figure 5.17.a overleaf shows from experimental results the tendency at increased loads for the neutral axis to shift towards the thicker skin due to adhesive shear deformation. Neutral axis position is determined by measuring the strain at various positions within the sandwich and extrapolating the through thickness position at which zero strain occurs for a given load. The neutral axis position (NA linear theory) determined from first moment of area and based on a homogenous sandwich beam, is also included as a baseline to show deviations from the assumption of linear elastic material properties. They are developed by averaging the experimental results for individual specimens, with a select set of readings shown in figures D.7.1-5. The neutral axis position occurs at a zero strain level, allowing through thickness motion to be tracked at varying load increments. Using the profiles described by these graphs, it is possible to model the joint as an individual element in closed form or finite element solutions.

Equivalent stiffness is also seen in the averaged experimental data for the scarf, with the spline and tape joins increasing in magnitude (figure 5.17.b overleaf). When used in practice the ability of the scarf to mimic the stiffness of an un-joined structure will have great benefit in reducing stress concentrations, and thereby increasing fatigue life.

Observation of adhesive fracture does not indicate whether the failed skin was under tension or compression, but does provide an accurate record as to the mode of failure. Fracture morphology is shown in figures C.1-7.
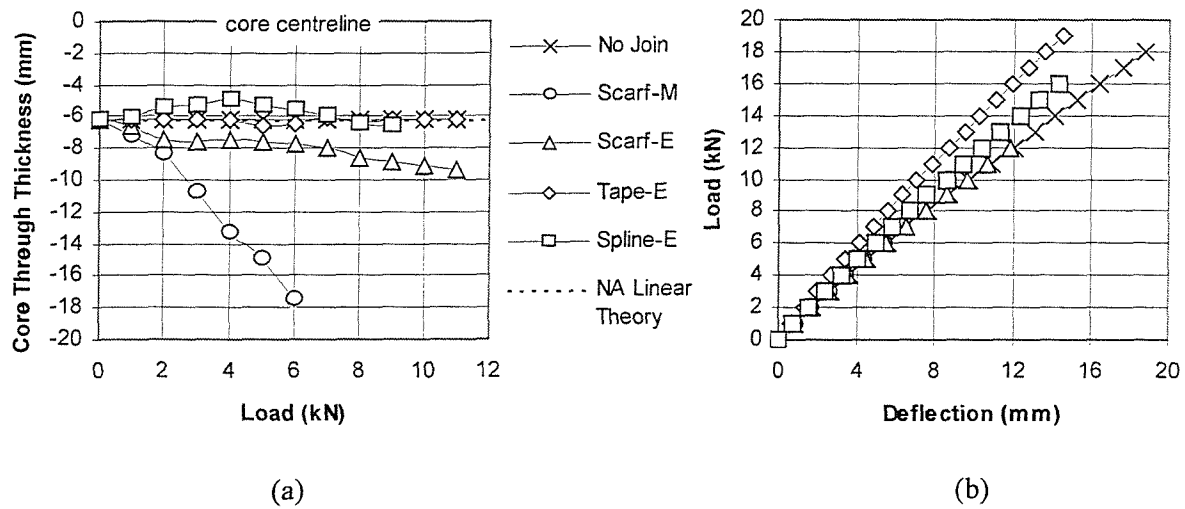
Figure 5.17 (a) Sandwich neutral axis movement; (b) Sandwich stiffness – centreline deflection.

Tensile joint failures were shown to be sudden and catastrophic in nature. It is therefore suggested that jointed structures be designed to initiate a compressive failure should a non-design load be encountered, with subsequent core crushing allowing an added degree of structural safety.

CHAPTER 6

APPLIED ANALYTICAL MODELS

In the majority of structural applications the sandwich has been designed to resist flexural loads, and transmit bending moments and shear forces. In order to characterise an in-plane sandwich joint, it is important to consider the limiting cases of such a system, and from this position propose models that can adequately reduce the number of variables and hence calculation time, whilst minimising any associated error. These limitations can be categorised into mechanical and dimensional with infinite combinations of each possible.

Considering isotropic skins and core, it is possible to look at several existing analytical models. Focus is placed on the scarf joint since it proved suitably adequate during the experimental program.

6.1 Chen and Cheng's Analytical Model

6.1.1 Problem Formulation

Neglecting the contribution of bending about its own axis, a sandwich skin can be considered under axial tension or compression only. The shear flow along the core skin interface is also neglected, but the probability of increased or decreased stress at the interface's meeting with the joint does require consideration when comparing analytical results with numerical methods.

The scarf joint under a purely axial load was discussed earlier in chapter 3. The advantages of Chen and Cheng's (1990) proposal were the inclusion of stress concentrations near the free edge that are not accommodated in any other analysis, and the ability to analyse any scarf angle from 0 to 90 degrees. It is somewhat surprising that this model is the latest development in scarf theory, as it only accommodates adherents and adhesive of differing linear elastic properties.

All early orthotropic theories pertaining to the scarf consider joining differing orthotropic adherents, but take no account of bundled fibres, stacking sequence or tip stress concentrations. The application of Chen and Cheng's theory to a given range of orthotropic adherents has potential, since the majority of cases involving modular construction will be joining 'like' orthotropic materials. Even with a varying laminate stacking sequence, each individual ply will meet the other at the adhesive interface and remain in plane. Thus, quasi-isotropy for the warp uni-

directional plies, whilst neglecting the transverse, may prove a suitable assumption. Due to joint geometry, an oblique rectlinear co-ordinate system was chosen, as shown in figure 6.1.
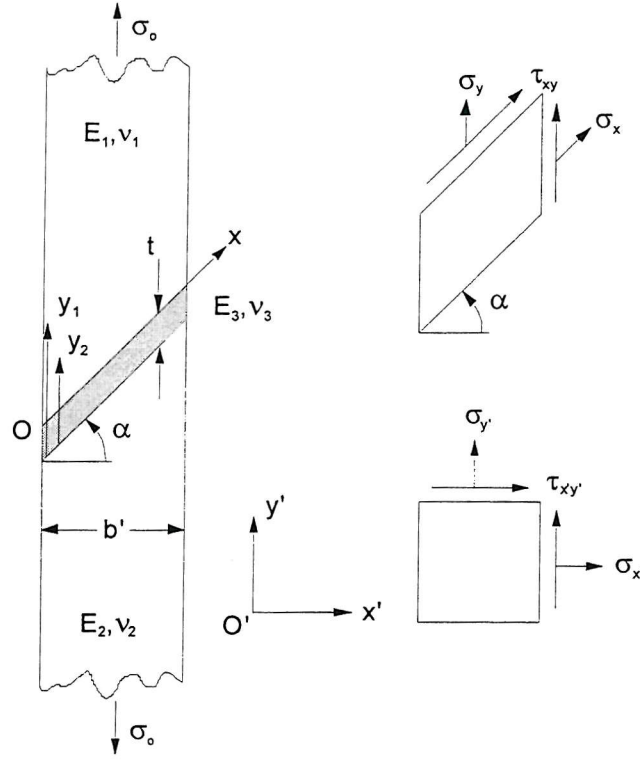

Figure 6.1 Joint stress sign convention and rectlinear co-ordinate system.

The stress distributions that were required for satisfaction of all equilibrium and limit state stresses under two-dimensional elastic plane stress used two approximations. The first was the application of Saint-Venant's principle to the stress decay from bonding surfaces, and the second was a linear stress distribution across the adhesive layer. The upper and lower stress components according to Chen and Cheng (1990) were expressed as follows, where $b = b'/\cos\alpha$

$$\sigma_{x1} = \sigma_1(x)e^{-\lambda_1(y_1/b)} \tag{6.1}$$

$$\sigma_{x2} = \sigma_2(x)e^{-\lambda_2(y_2/b)} \tag{6.2}$$

$$\tau_{xy1} = \frac{b}{\lambda_1}d\sigma_1(x)/dx \cdot e^{-\lambda_1(y_1/b)} \tag{6.3}$$

$$\sigma_{y1} = \left(\frac{b}{\lambda_1}\right)^2 d^2\sigma_1(x)/dx^2 \cdot e^{-\lambda_1(y_1/b)} + \sigma_0\cos\alpha \tag{6.4}$$

$$\tau_{xy2} = -\frac{b}{\lambda_2}d\sigma_2(x)/dx \cdot e^{\lambda_2(y_2/b)} \tag{6.5}$$

66

$$\sigma_{y2} = \left(\frac{b}{\lambda_2}\right)^2 d^2\sigma_2(x)/dx^2 \cdot e^{\lambda_2(y_2/b)} + \sigma_o \cos\alpha \qquad (6.6)$$

It was also necessary to satisfy the compatibility conditions, which allow the decay (λ_1 and λ_2) and stress ($\sigma_1(x)$ and $\sigma_2(x)$) coefficient determination, through use of the variational theorem of complementary energy developed by Washizu (1968). Application of this theory to the compatibility equations requires the energy (V) variation of the scarf system to be zero for any position within this system.

The equation to be minimised, in terms of the adherents and adhesive ($i=1,2,3$), is written as

$$V = \sum_{i=1}^{3} \frac{1}{2E_i} \int\int \left[\sigma_{x'i}^2 + \sigma_{y'i}^2 - 2v_i\sigma_{x'i}\sigma_{y'i} + 2(1+v_i)\tau_{x'y'i}\right] \cdot dx'i \cdot dy'i \qquad (6.7)$$

The actual determination of stress distribution relies on minimisation of the complementary energy function through simultaneous variation of the two decay coefficients ie. searching for level at which the energy variation disappears. Chen and Cheng proposed the use of a modified Newton method to find this level. The adaptation of the Newton method is a difficult task as differentiation, even using difference approximations, involves numerous back substitutions including internal matrix routines. In practice a direct search method can prove just as efficient provided suitable ranges are chosen. Appendix F details a typical MathCad Plus 6.0 program developed for stress determination, including the direct coefficient search. It is interesting to see how compact the solution can be made when optimally using a visual free-form interface for calculations. The looped routine writes each output variable to a matrix for internal graphing, or export to other packages as a data file.

The goal of Chen and Cheng's analysis was to determine the shear and normal stresses acting on the bonding surface. A transformation of the upper and lower stress components is required so as to achieve this desired output. Bondline shear (τ_t) and normal stresses (σ_n) that are normalised with respect to applied stress σ_0 can therefore be determined from the following:

$$\frac{\sigma_n}{\sigma_o} = \frac{\sigma_y \cos\alpha}{\sigma_o} \qquad (6.8)$$

$$\frac{\tau_t}{\sigma_o} = \frac{\tau_{xy} + \sigma_y \sin\alpha}{\sigma_o} \qquad (6.9)$$

and where a uniform stress level would be achieved when,

67

$$\frac{\sigma_n}{\sigma_0} = \cos \alpha \cdot \sin \alpha \qquad (6.10)$$

$$\frac{\tau_t}{\sigma_0} = \cos^2 \alpha \qquad (6.11)$$

6.1.2 Examples

The actual mechanics of Chen and Cheng's solution is best shown via example, using the arbitrary input parameters of table 6.1 for the program in Appendix F.

Upper Adherent	Lower Adherent	Adhesive
$E_1 = 30.0$ GPa	$E_2 = 7.50$ GPa	$E_3 = 1.50$ GPa
$v_1 = 0.25$	$v_2 = 0.25$	$v_3 = 0.25$
Scarf Angle	Adhesive Thickness	Adherent Thickness
$\alpha = 0$ (butt join)	$t = 0.2$ mm	$b' = 4.0$ mm

Table 6.1 Arbitrary material properties and geometric quantities.

Care must be taken in finding the minimum energy of all systems, as a typical contour map in figure 6.2, showing the energy variation for the given set of coefficients, demonstrates minimal surface undulation. Changing the input stress from the applied $\sigma_0 = 500$ MPa, only changes the magnitude of energy by $\Delta\sigma_0^2$, and not the actual demonstrated profile.

It should be noted that figure 6.2 does not actually show the desired zero value. The reason lies in the double integral of equation (6.7) leaving an integration constant equal to the minimum of the plot. Therefore to be strictly accurate, all contours should be increased in altitude by the lowest value, which is 297.5 in this case.

The resultant minimising decay coefficients are $\lambda_1 = 45.7$ and $\lambda_2 = 4.8$. It appears generally that accuracy equal to ±0.01 in the decay coefficient of equations (6.1) to (6.6) is required for solution convergence.
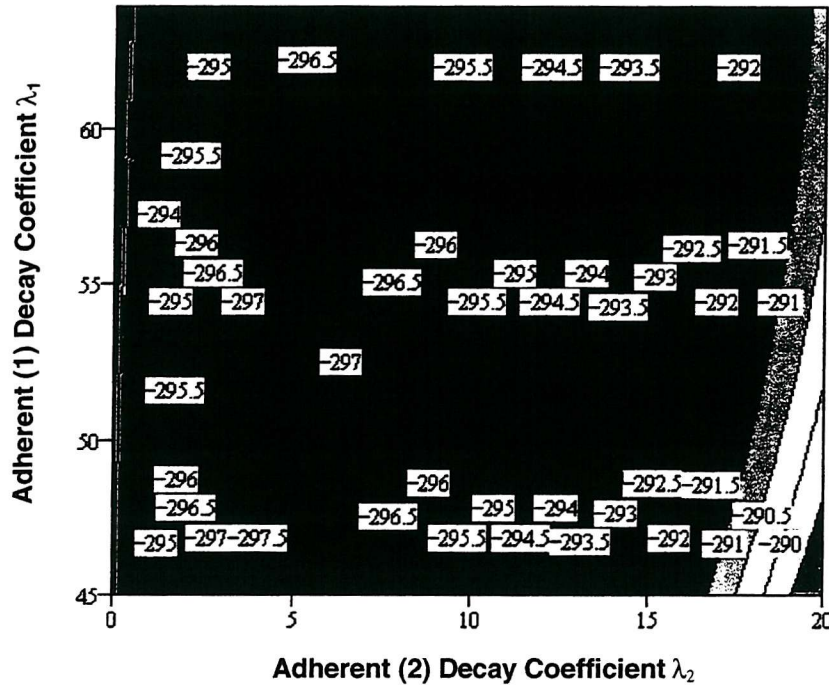
Figure 6.2 Contour plot of energy variation as a function of stress decay coefficients.

For the majority of cases to be analysed though, $\lambda_1 = \lambda_2$ since the adherents will be the same. This simplifies the decay coefficient determination immensely and allows two-dimensional plots of energy variation with much reduced calculation times.

The actual production of plots is very important, as numerical inaccuracies become immediately apparent as deviations from a smooth curve profile. Figures 6.3-4 demonstrate the emergence of such errors with only a 12.5% change in adherent thickness. Both adherents were modelled using the upper properties of table 6.1, with the other variables remaining the same.
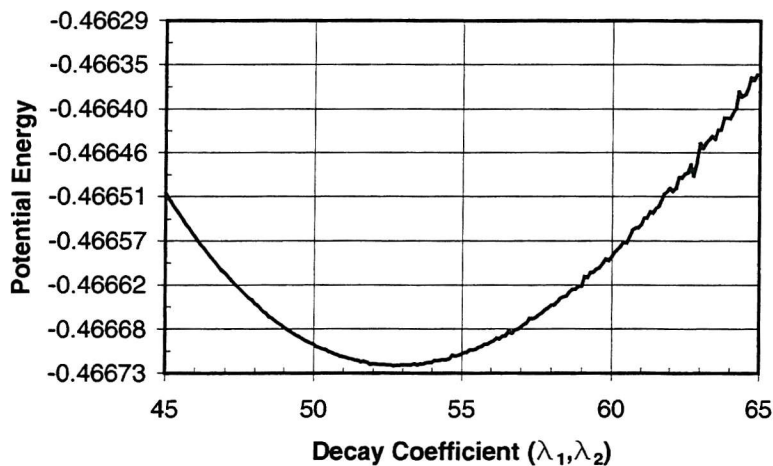

Figure 6.3 Decay coefficient versus potential energy for b'=3.5 mm.

69

-0.55400
-0.55408
-0.55416
-0.55424
-0.55432
-0.55440
-0.55448
-0.55456
-0.55464

Potential Energy

45   50   55   60   65

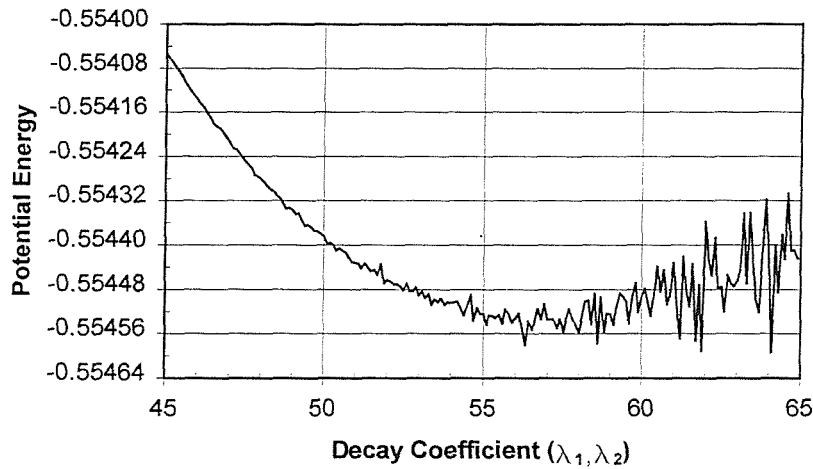Decay Coefficient (λ_1, λ_2)

Figure 6.4 Decay coefficient versus potential energy for b'=4.0 mm.

Figure 6.3 illustrates the ease with which the minimum energy, and hence decay coefficients can be found. It is also apparent that errors are increasing slowly as the decay coefficients become larger, noticeable by erratic movements away from the smooth curve. A small increase in the adherent thickness (b') is shown in figure 6.4 to have dramatic effects on the calculated potential energy. As the decay coefficient increases in magnitude, so does the erratic nature of the curve, which is due to loss of significance in the potential energy calculation.

As a means of setting a baseline for analysis two types of material were chosen and modelled under a given set of parameters: aircraft construction grade 7075-T6 aluminium plate, and ELT-600 E-glass/epoxy laminate used in the test program (table 6.2). Whilst the composite laminate is orthotropic in nature, the quasi-isotropy assumption requires a result comparison of actual shear modulus and that determined using $G=E/[2(1+\nu)]$.

	7075-T6*	ELT-600**	Adhesive†
E (GPa)	71.00	21.37	2.015
G (GPa)	26.60	3.020	0.736
ν	0.334	0.267	0.368

Source: *Niu (1990); **Appendix J; †ATL Composites.

Table 6.2. Adherent and adhesive mechanical properties.

Similar values to those used by Baylor and Sancaktar (1995) in their limited finite element study of joints in tension, were used for the following variables in table 6.3.

Scarf Angles	Adhesive Thickness	Adherent Thickness
$\alpha = 30, 45, 60, 75, 90°$	$t = 0.2$ mm	$d = 1,2,3,10,25.4$ mm

Table 6.3. Scarf joint geometry.

Decay coefficients are found in table G.1 for scarf angles from 30°-90° (butt join). It was found that constructing a plot of decay coefficient versus adherent thickness (figure G.1) gave linear trends for both types of material. This fact was exploited in narrowing the minimum energy search band, where extrapolation from the first three adherent thicknesses was possible.

From these decay coefficients normalised peel and shear stresses can be determined using equations (6.8-9). As each stress level asymptotes to that determined by equations (6.10-11) only tip profiles need be calculated i.e. normalised adherent positions (x/b) of 0-0.1 and 0.9-1.

6.1.3 Discussion

The analysis program was verified through substitution and comparison of parameters in Chen and Cheng (1990). From this position, the accuracy of the peel and shear stress output in figures G.2a-16b for both aluminium and composite adherents could be assured.

It is apparent from the profiles that increasing adherent thickness increases the maximum stresses. The composite shows marginally higher maximums, but the general trends are very similar. When considering the distance from the free edge that uniformity in stress begins, each adherent thickness shows a similar level at 1mm.

It is interesting to note that at angles greater than 45° for the aluminium and 60° for composite, the maximum stresses do not occur at the free edge, but rather a distance away. Whilst normalised shear is not zero, it must be remembered that the stress free boundary condition is still satisfied since peel and shear is shown relative to the scarf co-ordinate system. A scarf angle of 60° gives the most uniform stress profile, agreeing with that determined from equation (3.10), although the aluminium shows slightly less undulation.

The actual method of minimum energy determination is extremely important, and it is noted that Chen and Cheng have conveniently chosen examples for which such errors do not materialise near the minimum point. If a Newton or other unconstrained optimisation technique is used, there needs

71

to be limits set on the search range, as increasing decay coefficient increases the error, hence providing a false minimum. Even in figure 6.3, extending the plot beyond the maximum will result in a divergent solution for which no minimum can be found.

A combination of the chosen minimum search method and an internal scaling routine for exponential terms appears to provide the best solution in overcoming the difficulties associated with errors. It does still however rely on manual intervention to set a sliding multiplication scale that increases proportionately with error.

6.2 Wah's Analytical Model

6.2.1 Problem Formulation

The only paper pertaining to a joint under a pure bending moment was published more than twenty years ago. It has rarely been referenced and of those authors that have, no validity assessment has been made. Wah's (1976) model can potentially be applied to scarfed sandwich joint analysis by looking at either the core as an individual item under an imposed bending moment, or thick skins, where local bending becomes increasingly significant. Taking this hypothesis one-step further offers the possibility of a stress distribution based on through thickness limits or a boundary layer.

The basis of Wah's theory centres on using two known stress functions in two-dimensional elasticity. These stress functions result in opposing moments, simulated by a linearly varying and self equilibrating applied stress distribution, and a Fourier function in y and x, providing a solution to a rectangular section under prescribed conditions for all four sides, as discussed by Timeshenko and Goodier (1970).

Timeshenko and Goodier express their function relative to the rectangular sections mid-plane, as follows

$$\phi = A_i e^{-\gamma x/c}\left(\kappa \sin\frac{\gamma y}{c} + \frac{\gamma y}{c}\cos\frac{\gamma y}{c}\right) \tag{6.12}$$

however axis displacement is required when considering Wah's approach in order that transformation from rectangular to polar co-ordinates can be achieved. This transformation results in a less complex approach since only a single locating and differentiating variable need be changed when considering the interface stress rather than both x and y simultaneously. The co-ordinate system is shown in figure 6.5.
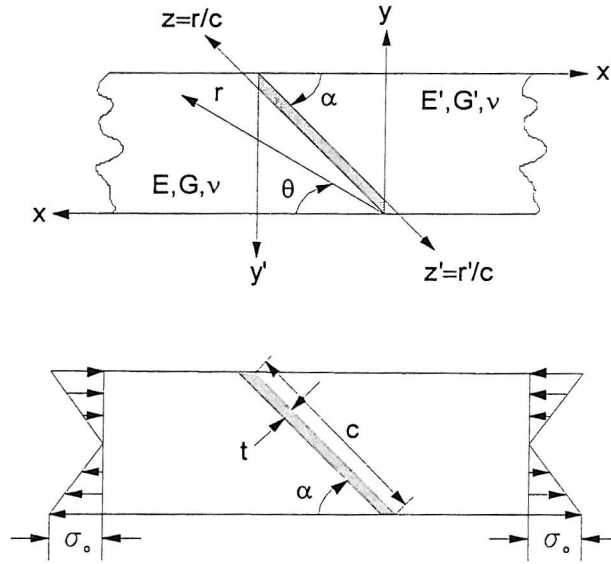
Figure 6.5 Scarf joint co-ordinate system and simulated moment stress profile.

The two components of the describing stress function

$$\phi = \phi_1 + \phi_2 \tag{6.13}$$

are written as

$$\phi_1 = \left(\sigma_o d^2 / 6\right)\left(3y^2 / d^2 - 2y^3 / d^3\right) \tag{6.14}$$

where

$$d = c \sin \alpha \tag{6.15}$$

and the biharmonic component

$$\phi_2 = A_i c^2 \exp\left(\frac{-2\gamma x}{c \sin \alpha}\right)\left\{\kappa \sin \gamma \left(\frac{2y}{c \sin \alpha} - 1\right) + \gamma \left(\frac{2y}{c \sin \alpha} - 1\right) \cos \gamma \left(\frac{2y}{c \sin \alpha} - 1\right)\right\} \tag{6.16}$$

As a self-equilibrating system is desired, taking a root of the following equation gives a zero resultant force and couple on any strip shown in figure 6.5, for which $x = $ constant in ϕ_2
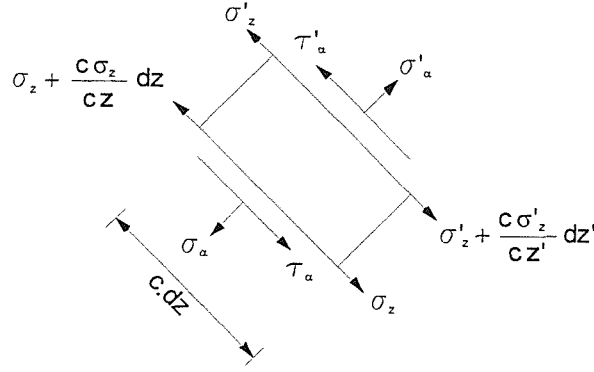
$$\sin 2\gamma - 2\gamma = 0 \tag{6.17}$$

73

Figure 6.6 Adhesive equilibrium conditions.

Roots can be determined using the Newton-Raphson technique, as it takes very few iterations. The importance of the initial guess should not be overlooked, and it was found that alternating unit increments in the real and imaginary components provided suitable preliminary estimates for at least the first ten solutions.

$$\gamma_{1,2,3,4,5} = 3.75\pm1.38i,\ 6.95\pm1.68i,\ 10.12\pm1.86i,\ 13.28\pm1.99i,\ 16.43\pm2.10i \tag{6.18}$$

An infinite number of roots can be determined but provide little increase in accuracy. The quantitatively larger roots can actually cause serious errors in numerical accuracy through significance loss. This propensity is due to the exponential term in ϕ_2 tending toward very low values, whilst the constant A_i tends to a similar positive power. Multiplication of the two must therefore be looked at closely, even when using double precision.

Wah's solution follows a co-ordinate transformation from rectangular (x,y) to polar (r,θ), so that the interface shear and normal stresses can be expressed in terms of z, where z is an ordinate normalised with respect to the scarf length and measured along the r-axis (figure 6.6).

The resulting equations for interface peel (σ_α) and shear (τ_α) stress determined from boundary conditions can be written as

$$\sigma_\alpha = 4A_i\left(\gamma^2/\sin^2\alpha\right)\begin{bmatrix}(\kappa+1)\sin\{\gamma(2z-1)-2\alpha\}+\\ \gamma(2z-1)\cos\{\gamma(2z-1)-2\alpha\}-\\ \sin\{\gamma(2z-1)\}\end{bmatrix}\cdot e^{-2\gamma z\cot\alpha}+\sigma_o\sin^2\alpha(1-2z) \tag{6.19}$$

74

$$\tau_\alpha = 4A_i\left(\gamma^2/\sin^2\alpha\right)\left[\begin{array}{l}(\kappa+1)\cos\{\gamma(2z-1)-2\alpha\}-\\ \gamma(2z-1)\sin\{\gamma(2z-1)-2\alpha\}\end{array}\right]\cdot e^{-2\gamma z\cot\alpha} + \sigma_o\sin\alpha\cos\alpha(2z-1) \qquad (6.20)$$

Further, more rigorous and tedious mathematics develops the base equilibrium equations from which the solution constant (A_i) and adhesive average axial stress (σ_z) can be determined (Appendix H). The constant A_i for each root is determined by using a linear least squares method i.e. solution of $[B][A]=[C]$. The actual calculation was not as simple as $[A]=[B]^{-1}[C]$, since each of these matrices included internal sub-matrix routines, and hence $[A]=[[B]^T[B]]^{-1}[B]^T[C]$ provides a workable alternative.

6.2.2 Examples

In order to ascertain glue line stresses in a sandwich at any arbitrary angle, it was important to initially consider solid adherent bonding. From this position it would be possible to evaluate potential boundary solutions that could be adapted to through-thickness stresses in sandwich joints.

As for the tensile model, determination of normalised peel and shear stresses was performed using the mechanical properties of table 6.2 and geometric parameters of table (6.4).

Scarf Angles	Adhesive Thickness	Adherent Thickness
$\alpha = 15, 30, 45, 60, 75, 90°$	t = 0.2 mm	d = 25.4 mm

Table 6.4. Scarf joint geometry in flexure.

A stress analysis for $0°$ was not included, since the $\sin\alpha$ components of the stress function result in a singularity. This is due to the compatibility equations no longer being satisfied when the adhesive position moves from one boundary to the other i.e. at $0°$ the glue line is along the centreline. It would therefore follow that a stress distribution based on a typical sandwich analysis, where the adhesive represents the core, would provide the most suitable solution.

6.2.3 Discussion

Figures I.1a-12b show the variation of stress at the adhesive interface in flexure. During the solution sequence it is obvious that the results are dimensional until normalised with respect to the

maximum stress (σ_o). Selecting suitable measurement units or associated factors can therefore be vitally important in overall solution stability. Unsuitable units may introduce unwanted complexities into the analysis including scale effects, and numerical inaccuracies through significance loss as mentioned earlier.

A look at the effect of units choice, or multiplication factor shows a seemingly random underlying perturbation at certain levels. Wah never discussed such problems, as perhaps it was not apparent during the very limited number of cases considered.

Multiplication scales of 10^{-10}, 10^{-2}, 1, 10^{2} and 10^{10} were applied systematically to the input variables for the normalised stress plots and zero scaling i.e. scale factor of 1, was considered to be designated by units of (MPa) and (mm). As an example, a 0.5mm thick adhesive would be input into the analysis as $0.5 \cdot 10^{-10}$, $0.5 \cdot 10^{-2}$ and so on for each variable. The applied moment must also be increased by a further power of 2, so that the applied stress profile remains constant.

A sample position was chosen at the mid-point of the adhesive line i.e. $z = 0.5$, as this showed the greatest degree of fluctuation in both types of joined adherent. The bonded aluminium shows incremental stress profile disturbances for multiplication levels decreasing from $4 \cdot 10^{3}$, and similarly the composite from $1 \cdot 10^{3}$. Logarithmic plots of the normalised stress against the multiple for each scarf angle are shown in figures I.13-17. During the factor decrement, normalised stress reaches a stable level at which point no further reduction in multiplication level changes the stress distribution. Whether this fluctuation is through solution instability due to the circular functions, or alternatively significance loss at the exponential term is unsure.

Wah found similar 'non-linearity' in the butt join, and slight disturbances at other angles. Inspecting this distribution even without an understanding of the solution mechanics casts some doubt on its accuracy. This doubt is caused by the theoretical maximum stress concentration occurring in the middle of the joint, whereas realistically one would expect tip concentrations working toward a more linear mid section profile.

From the limited number of cases analysed, which are far in excess of those covered by Wah, it appears that using a unit scaling of 10^{6} will provide an accurate joint stress profile for any scarf angle. Wah had previously limited the scope to large angles, most likely through the encounter of numerical inaccuracies. A close look at the contribution of ϕ_2 demonstrates little effect, and so the basic equation for interface stress distribution in the scarf joint could be written as

$$\sigma_\alpha = \sigma_i \sin^2 \alpha \qquad (6.21)$$

$$\tau_\alpha = \sigma_i \sin \alpha \cos \alpha \qquad (6.22)$$

where σ_i represents the stress at a given point through the thickness of the un-joined adherent being considered i.e. bending stress. Actual position in x is irrelevant since all positions are subject to pure bending and hence any scarf angle can be analysed, removing the limitation imposed by Wah which restricted the analysis to angles that are 'not too small'.

The hypothesis that the scarf jointed section, including that which is a laminate or sandwich, can have the bond interface stress profile approximated by the distribution in a continuous section, offers a far easier solution approach.

Variation of Poisson's ratio due to the assumption of quasi-isotropy for the composite adherent showed absolutely no variation in stress profile. This is not surprising since it is the ϕ_2 term that includes the Poisson ratio, and its contribution to the overall interface stress was shown to be negligible. Also the assumption of plane stress rather than plane strain helps in reducing the effects of Poisson ratio variation, particularly in the dominant ϕ_1 component of the stress function.

With the addition of both core and skin joints Wah's governing equations cannot realistically be used commercially unless simplified to that of (6.21-22).

6.3. Experimental Correlation and Discussion

Chen and Cheng's theory could not be used for joint failure stress estimation in the experimental program. This is due to problems arising in numerical significance, particularly at the low scarf angles (2.8° and 5.7°) used in the test specimens. The method is however included for discussion as it could form a valuable solution technique when a suitable algorithm is developed or applied to minimise the numerical inaccuracies. In its current form it provides a basis for theoretical comparison against larger scarf angles should they form part of a future test program. Further, it is possible for direct comparison against finite element methods.

Application of Wah's theory demonstrates that by developing a suitable failure criterion, the method could easily be adapted to scarf joint failure prediction. Estimation of extreme fibre stress due to bending in the scarf joints is calculated using elementary statics. This figure can be substituted for σ_i in (6.22), enabling adhesive shear stress calculation. Finally, failure stress (σ_y)

estimation using Von Mises yield criterion defined in (5.8) provides a preliminary prediction for comparison against quoted manufacturers bulk tensile yield stress (σ_a) in table 6.5. A similar procedure was used in chapter 5 for the modified Volkerson analysis.

Specimen	Failure Load (kN)	Skin Stress σ_i (MPa)	σ_y (MPa) Eq. (5.8)	$3\sigma_y$ (MPa)	Bulk Yield σ_a (MPa)	$1-\sigma_a/3\sigma_y$ (%)
S1-T-MA	11.95	94.40	8.20	24.61	24.0	+2.5
S2-T-MA	11.70	92.42	8.03	24.10	24.0	+0.4
S3-T-MA	13.45	106.28	9.24	27.71	24.0	+13.4
S6-C-MA	13.45	106.28	9.24	27.71	24.0	+13.4
S4-T-MA	9.52	75.25	13.02	39.05	24.0	+38.5
S5-T-MA	8.35	66.01	11.42	34.25	24.0	+30.0
S7-C-MA	6.68	52.81	9.13	27.40	24.0	+12.4
S2-T-EP	21.81	172.29	14.98	44.92	45.0	-0.2
S3-T-EP	21.72	171.63	14.92	44.75	45.0	-0.6
S1-T-EP	13.53	106.94	18.50	55.49	45.0	+18.9
S4-T-EP	8.44	66.67	9.13	34.59	45.0	-30.0

Table 6.5 Comparison of predicted adhesive joint yield stress and bulk resin data.

It is immediately apparent from table 6.4 that Von Mises yield stress (σ_y) prediction significantly underestimates the failure stress of the adhesive. By using a multiplication factor of 3 and applying to σ_y shows that $\sigma_y = 3\sqrt{3\tau_{xy}^2}$ may offer a better prediction, particularly for $2.8°$ scarf angles. The larger scarf of $5.7°$ does not support this figure, and it is therefore anticipated that with further testing a suitable linear modification related to scarf angle would be possible. In turn this would offer a far more flexible formula when considering scarf stresses and ultimately failure prediction.

CHAPTER 7

FINITE ELEMENT ANALYSIS

The finite element analysis enables a systematic approach to scarf joint investigation by varying material properties, scarf angles and through thickness elements to include core addition for sandwich analysis. This sequence is important, as no verification of either Cheng and Cheng or Wah's theory via this or any other method has been conducted.

Unfortunately the finite element analysis cannot be explicitly linked to the experimental results, due to the test scarf angle being only $2.86°$. Numerous model variations were trialled but resulted in no viable method for modelling tip stresses with scarf angles less than $15°$. Primary reasons centered around node and element structure limitations for aspect ratios of $20:1$.

Comparison with analytical models is still vitally important however as it offers an alternate means of method validation, together with the future possibility of test program verification at the scarf angles analysed by FEM (finite element methods). Conducting this numerical study while varying the adherent materials between aluminium and composite enables the minimal variation between the stress states to be demonstrated. Isotropy may therefore prove to be another simplification and result in reduced analysis times.

Ansys 5.3 running on a Unix platform was used for the majority of analysis, although preliminary modelling and analysis was performed with FEMAP 4.4 and Nastran 1.1 for Windows, in order to determine the optimum mesh configuration.

7.1 Problem Formulation

There are essentially two base conditions to be solved using finite element analysis. The first is a joint loaded in tension, and secondly the same joint under pure bending. Tension analysis is a necessary inclusion as the stress distribution around the tip may mimic that under bending.

Of particular interest in the analysis is the interface stress between adherent and adhesive, together with the internal stresses of the adhesive itself. It is expected that maximum stresses will be achieved on the boundary at the scarf tip, and so a strategy for solution convergence is of paramount importance.

7.1.1 h-Method

In order to obtain this convergence both the h-method and p-method were evaluated. Using the h-method or hierarchic method of finite element analysis, the base functions for each finite element are fixed and the dimensions of the largest element allowed to approach zero. In the majority of commercially available FEA software packages, the base functions are limited to linear or quadratic forms, and convergence achieved through mesh refinement.

7.1.2 p-Method

The effort in achieving a suitably refined mesh is rarely an easy task but the p-method, or polynomial method, offers far greater flexibility. A fixed finite element mesh can be used, with convergence achieved when the minimum number of polynomial base functions is allowed to approach infinity. The p-method represents the displacements within each element using these high-order polynomials, as opposed to the linear or quadratic functions used in conventional finite elements. A single geometric element can, therefore, represent a more complex state of deformation than a single, conventional finite element. A given set of convergence criteria are therefore chosen based on displacement, rotation, stress, strain or global energy, and successively higher-order polynomials used to satisfy this constraint.

The computational time required for successive increments in the polynomial sees the degree often being limited in commercial packages; eighth order in Ansys (1996) and ninth in Pro/Mechanica (1997). A combination of both the h- and p-methods is therefore beneficial, with Burnett (1987) showing in figure 7.1 that the unification can theoretically offer the fastest rate of convergence.
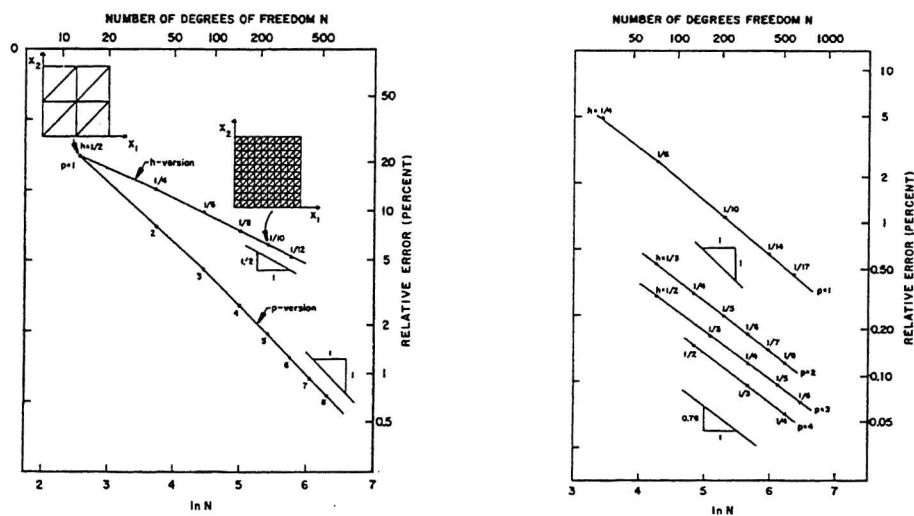
Figure 7.1 Typical comparison of h- and p-method rates of solution convergence (Burnett, 1987).

80

The finite element analysis was eventually restricted to the h-method due to the discovery of an arithmetic error in the path logic of Ansys 5.3 when using variable polynomial PLANE 145 super-elements. Further studies should not overlook the p-method as an efficient way of obtaining rapid convergence, with Ansys 5.4 Release 3 having rectified the detected bug (Cordani, 1998).

7.1.3 Homogenous Adherents

Homogenous models using properties in table 6.2 were developed in order to ascertain the interface and adhesive stress distribution. The orthotropic analysis was not based on a ply by ply model as it was expected that the stress undulations would decay rapidly from the free edge.

A representative adherent thickness of 25.4mm was chosen as it provided means by which a comparison with Baylor and Sancaktar (1995) could be achieved. This in itself posed problems as increased adherent thickness results in the tip stress variance moving closer to the free edge; when considered as a percentage of scarf length. The ultimate result is more elements in the finite element model to adequately capture this stress distribution.

Overall width was minimised to 80mm as successively varied models showed that the internal stress profile was not affected by the loaded free edges at this distance. Limiting the width was also important in reducing the number of elements, as Ansys nodal limitations restricted the degree of mesh refinement.

Angles were chosen from 30° through 90° (butt join) at 15° increments to demonstrate variations in stress at the adhesive interface and centreline. There are obviously infinite combinations of parameters that could be considered, however the study was limited to investigating the effect of scarf angular rotation on a 0.2mm adhesive thickness. For typical manually applied adhesives 0.2mm is a good average based on the author's experience, with support for this observation provided by aerospace film adhesive data (Ciba, 1996).

7.1.4 Sandwich Adherents

A plane stress and plane strain model based on the homogenous materials was modified to accommodate a core. It was not possible to produce the necessary mesh refinement for experimental comparison, as having a 60mm core and scarf angle at only 3° easily exceeded the nodal limitation, even on the coarsest model.

Representative sandwich structures that were both aluminium and composite skinned, using an isotropic SAN foam core (E = 500 MPa, ν = 0.3) provided a means by which general comment could be passed. Core to skin bond line was considered infinitely thin, however its presence and variability in manufactured components should not forgotten.

7.2 Modelling Procedure

7.2.1 Generation

PLANE 82, eight noded structural solid elements were used for adherents and adhesive. The benefit in using this element is its ability to represent either a plane stress or a plane strain problem. Such properties are important when considering the theoretical assumptions of plane stress in the analytical models and its relation to the more realistic representation of plane strain.

Nodal constraints were applied to the tensile model on one free edge restricting movement in the x-direction (figure 7.2). Rigid body motion was also prevented by restraining a single node at the midpoint of the restrained edge from displacement in the y-direction. An arbitrary tensile line load of 118.11 N/mm or a 3000 N total force over the 25.4mm edge length provided a realistic loading condition, although any magnitude of force could have been considered.

For the flexure case, edge restraint was provided by attaching rigid end beams to the section having stiffness some 100 times greater than that of the adherents (figure 7.2). This allowed transmission of the single node corner loads along the beam, simulating the required moment without undue element distortion. Single mid-side nodes on both edges were also constrained in x and y at the neutral axis position to enable rotation.

The most significant aspect of analysis was constructing the models for efficiency and nodal limitations. Three models were therefore required to characterise the tip stresses, using successive interpolated sub-models.

7.2.2 Submodelling

Also known as the cut-boundary or specified boundary displacement method, submodelling offers a unique method by which to obtain mesh refinement around a stress concentration. The refinement comes at a significantly reduced CPU time, since the whole model is not required to accommodate the refinement.
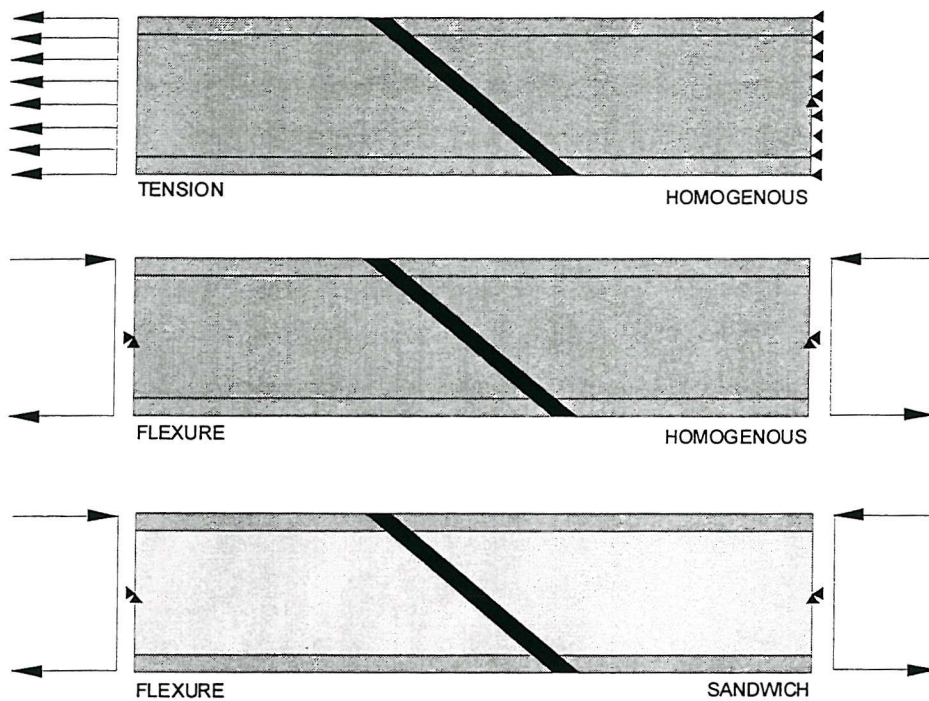
Figure 7.2. Tension and flexure model loading and boundary conditions.

The overall process involves creating a coarse global model of the joint, with a mesh density that characterises the majority of the structure. A sub-model can be created that effectively zooms in on the tip stress concentration, and whose boundary lies along an accurately displaced region in the coarse model i.e. some distance away from the concentration. A schematic of the actual process used is shown overleaf in figure (7.3).

The internal nodal displacements of the coarse model, along the boundary path of the submodel, are then determined. However, as the submodel has a refined mesh, a greater number of nodes exist along the boundary. Interpolated displacements based on the element shape function are therefore necessary to give a full description of the boundary conditions. There is no limit to the number of times the process can be carried out, but it is imperative that the boundary displacements be correctly defined.

7.2.3 Method Validation

Method validation is possibly the most important aspect of the finite element method, with some typical fundamental tests described by NAFEMS (1984) as being

GLOBAL MODEL

ELEMENTS: 2340
DOF: 14338

INTERPOLATED BOUNDARY

1ST INTERPOLATION

ELEMENTS: 1000
DOF: 5920

INTERPOLATED BOUNDARY

ADHESIVE

2ND INTERPOLATION

ELEMENTS: 1600
DOF: 9520
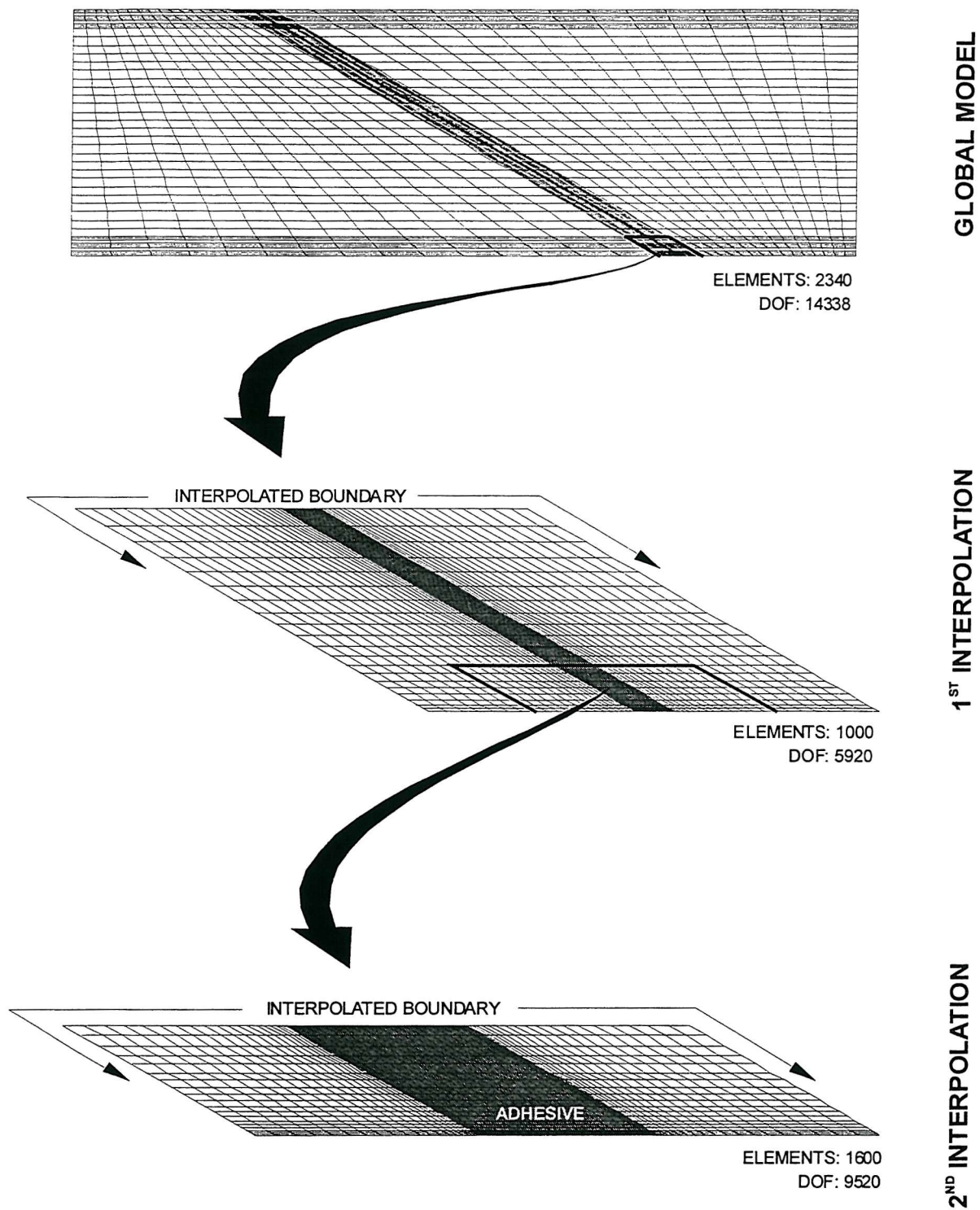
Figure 7.3 Typical mesh generation and biased submodelling regions (tension model).

84

(a) Invariance of element stiffness/flexibility matrices with choice of local reference axis.

(b) Absence of internal stress under rigid body motions.

(c) Freedom from spurious 'kinematic modes'.

(d) Convergence to exact solution in special cases.

(e) 'Patch test' for constant stress fields invariant with choice of local element boundaries.

Patch testing was found to be the easiest method of validation, with through thickness paths some distance from expected stress concentrations constructed. The required stress fields were known to be either constant in the case of tension, or varying linearly with applied bending moment. Non-averaged element stresses were interpolated along the paths, compared with the required solution, and found to be equivalent. Further verification in the case of applied bending moment was performed by differentiating along the path and checking for underlying perturbations; with none found. Confidence in the modelling procedure, element choice and boundary conditions was therefore gained.

Verification that the interpolated displacements on the submodel boundary accurately predict the stress field is achieved by a simple comparison of the sub- and global models. A ±2.5% difference in stress along the comparative boundaries was set as the limiting factor in order to minimise the number of successive model iterations. Figure 7.4 shows a typical difference distribution, with the scatter at one end due to the biased mesh profile of the submodel's interpolated displacement being created over an increasing number of nodes.
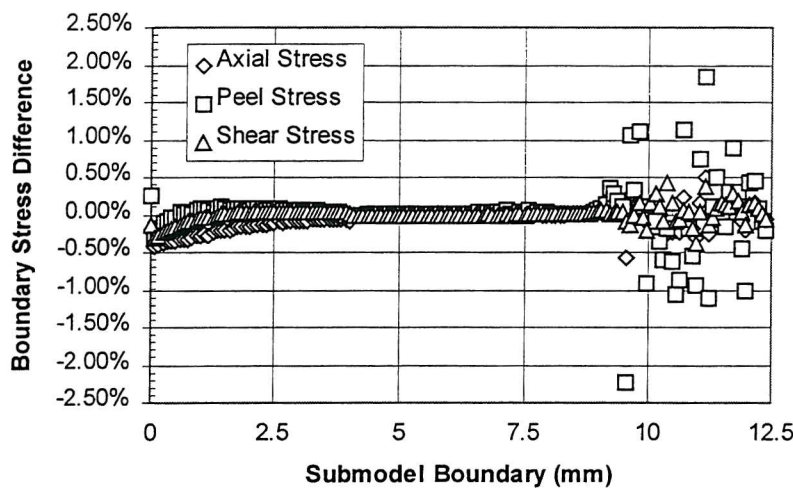
Figure 7.4 Sub- and global model boundary stress error due to displacement interpolation.

7.3 Results and Discussion

Models with varying scarf angle and adherents were analysed, enabling general comment to be passed on the stresses within a scarf joint, with representative global stress distributions for each case shown in figures M.1-3. Results for composite tension models are only included for a 60° scarf angle, as the variation between itself and aluminium is small and trends are similar. Interpolated element stress at the adhesive interface and centreline were extracted for comparison with available theory.

7.3.1 Homogenous Models in Tension

The homogenous tension models in figures K.1a-6b, suggest that Chen and Cheng's (1990) theoretical model does not accurately predict tip stress profiles. It is immediately apparent from the stress contour plots of figures M.4-5, that shear stress across the adhesive layer cannot be assumed linear. This is a fundamental assumption in Chen and Cheng's theory and can result in substantial variation from predictions using their formula.

Acute tip peel and shear stresses appear to be closely approximated by theory for angles of 30° and 45°, but at greater angles theory better approximates the adhesive centreline profile. Such variation is directly attributable to the non-linear stress distribution across the adhesive and sees load transmission, particularly at lesser angles, bypassing the obtuse scarf tip. Therefore at a 30° angle both peel and shear stress in this region are zero.

The butt join at 90°, whilst not agreeing with theory shows similar trends to early finite element models created by Anderson *et al* (1977) for poker chip tensile coupons. Therefore further doubt is cast on the validity of Chen and Cheng's basic assumptions.

When considering plane strain, a scaling of the plane stress case is seen. Whilst boundary conditions will still obviously be satisfied, an average positive or negative scaling effect of approximately 15% is seen for both aluminium and composite adherents.

A general evaluation of the results shows the minimum amount of tip fluctuation to occur at an angle of 60°, and is best shown by the Von Mises stress tip variance of figure K.12a.

This *optimum* angle of 60° has drawn little interest until now, although Zimmerman and Liu (1995) showed its presence in experimental tests. Baylor and Sancaktar's (1995) cruder finite

86

element analysis showed similar trend, but without investigation of these tip stresses failed to note its importance.

Tables 7.1-2 and figures 7.5-6 demonstrate the stress intensity factor associated with tip stresses at various scarf angles, and is compared against an existing finite element solution.
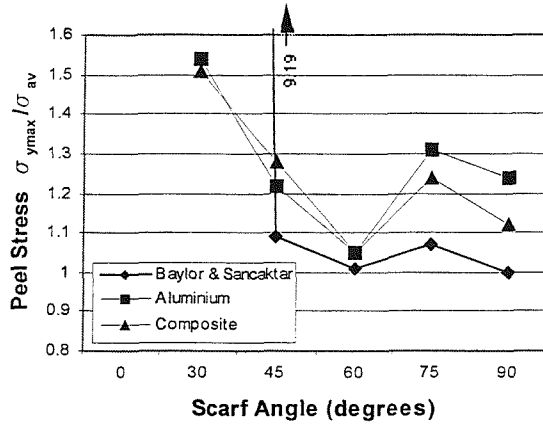
Fig. 7.5 Variation of peel stress with angle.
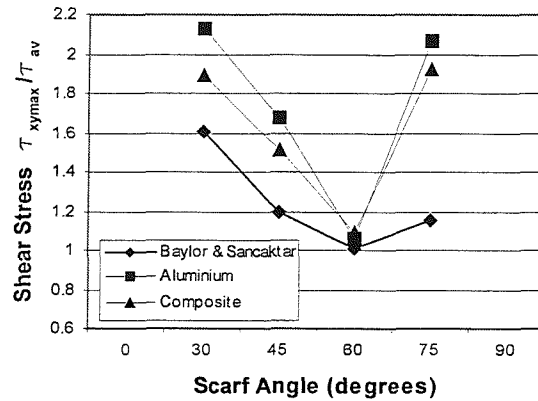
Fig. 7.6 Variation of shear stress with angle.

7.3.2 Homogenous Models in Flexure

Very similar trends to the tension model were experienced in the vicinity of the tip (figures K.7a-11b & M.6). The stresses were normalised with respect to the maximum extreme fibre i.e. free edge, and so in relative terms bending offers slightly lower peak magnitudes. This also supports the observation in chapter 6.1.3 that stress fluctuations are limited to a finite distance from the free edge. Considering the average tensile stress over a 1mm edge depth and accounting for the linear reduction due to the imposed bending moment, it is not surprising that the stresses are marginally lower than the tensile case.

Comparison with theory however does not show the same degree of continuity. The simplification of calculation to equations (6.21-22) may potentially offer an upper bound if the boundary layer concept is introduced as discussed in chapter 3.3, but only sees good agreement away from the free edge, and only for the limited number of models studied. The differences between plane stress and plane strain models are still significant, and showed the same scaling effects seen in the tension cases. Despite this fact, on a comparative level either can be used for analysing trends.

The angle of 60° appears again for the same reasons - very little fluctuation in stress. Table 7.3 shows the stress intensity variations associated with composite adherents.

87

Aluminium	Adhesive Length (mm)	Peel Stress			Shear Stress		
		σ_{av}/σ_o	$\sigma_{ymax}/\sigma_{av}$ (Baylor & Sancaktar)	$\sigma_{ymax}/\sigma_{av}$	τ_{xy}/σ_o	τ_{xymax}/τ_{xyav} (Baylor & Sancaktar)	τ_{xymax}/τ_{xyav}
30° Scarf	50.80	0.25	9.19	1.54 (A*)	0.43	1.61	2.13 (A)
45° Scarf	35.92	0.50	1.09	1.22 (A)	0.50	1.19	1.68 (A)
60° Scarf	29.33	0.75	1.01	1.05 (O*)	0.43	1.01	1.06 (O)
75° Scarf	26.30	0.93	1.07	1.31 (O)	0.25	1.15	2.07 (O)
90° Scarf (butt)	25.40	1.00	1.00	1.24 (O)	0.00	N.A.	N.A.

Table 7.1 Scarf angle effects on interfacial stress of 25.4mm thick aluminium adherents in tension including comparison with Baylor and Sancaktar (1995).

Composite	Adhesive Length (mm)	Peel Stress			Shear Stress		
		σ_{av}/σ_o	$\sigma_{ymax}/\sigma_{av}$	$\sigma_{ymax}/\sigma_{av}$ Al/Composite	τ_{xyav}/σ_o	τ_{xymax}/τ_{xyav}	τ_{xymax}/τ_{xyav} Al/Composite
30° Scarf	50.80	0.25	1.51 (O)	1.02	0.43	1.89 (A)	1.13
45° Scarf	35.92	0.50	1.28 (A)	0.95	0.50	1.51 (A)	1.11
60° Scarf	29.33	0.75	1.05 (O)	1.00	0.43	1.09 (O)	0.97
75° Scarf	26.30	0.93	1.24 (O)	1.06	0.25	1.92 (O)	1.08
90° Scarf (butt)	25.40	1.00	1.12 (A/O)	1.11	0.00	N.A.	N.A.

Table 7.2 Scarf angle effects on interfacial stress of 25.4mm thick composite adherents in tension.
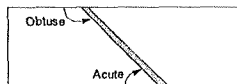
*Location of highest interface stress (A) – Acute tip (O) – Obtuse tip.

Composite	Adhesive Length (mm)	Peel Stress		Shear Stress	
		$\sigma_{imax} = \sigma_o \sin^2\alpha/\sigma_o$	$\sigma_{ymax}/\sigma_{imax}$	$\tau_{imax} = \sigma_o \cos\alpha \sin\alpha/\sigma_o$	τ_{xymax}/τ_{imax}
30° Scarf	50.80	0.25	1.25 (O)	0.43	1.73 (A)
45° Scarf	35.92	0.50	0.96 (A)	0.50	1.26 (A)
60° Scarf	29.33	0.75	0.93 (A)	0.43	0.85 (O)
75° Scarf	26.30	0.93	1.14 (A)	0.25	1.78 (O)
90° Scarf (butt)	25.40	1.00	1.24 (A/O)	0.00	N.A.

Table 7.3 Scarf angle effects on interfacial stress of 25.4mm thick composite adherents in flexure.

If Suzuki's 0.2mm boundary layer is introduced then figure K.12b can be used to determine failure, however applicability to these scarf angles and adherents requires further experimental validation.

7.3.3 Sandwich Models in Flexure

Since the sandwich analysis considers thin skins in bending, which essentially only have a small axial stress gradient, then it is not surprising that the finite element results for the skin material analysed separately as a solid adherent in axial tension, correlate well. A close look at figures K.13a-17b for aluminium skinned foam core sandwich, for which a typical Ansys input deck is detailed in Appendix L, and K.19a-23b with composite skins, see exactly the same profiles discovered earlier. Despite the scale accommodating a longer path length, it is apparent that tip stress fluctuations occur in the vicinity of the free edge and rapidly decay to the interior linear profile. The difference in this case is the subsequent reoccurrence of these fluctuations at the skin/core interface.

Although somewhat lower in magnitude, the sandwich skins stresses show a scaled down profile of the same skin if considered under pure axial tension. There are two primary explanations for this behaviour: the first is due to core presence and second from stress normalisation having been conducted relative to the extreme fibre stress some distance away from the adhesive interface, and not at the through thickness position being considered.

If a typical stress profile is followed for the acute tip distribution from the free edge, as expected the profile changes at the skin/core interface to the obtuse form. This form as mentioned previously is a scaled version of the free edge profile.

Transition through to the core sees a significant drop in the magnitude of the normalised stress due to strain compatibility. A closer look at the modelling is required in this region as it represents literally a point at which three materials meet i.e. skin, core and adhesive. Mesh density was increased and biased in this region so that a high density was achieved not only at the free surface, but also the skin/core interface and core/adhesive interface.

Figures K.18a-18e & K.24a-24e, are included to show how a boundary layer failure criterion might be employed using Von Mises or alternatively a principal stress. The 0.055mm boundary layer used in the modified Volkerson analysis of chapter 5, and 0.2mm used by Suzuki are included solely as a means of visualising their position relative to the tip variations.

The non-linear adhesive stress distributions are again discovered near the free edge and skin/core interface, but it is noticeable that it tends toward a linear profile at the skin's midpoint. Figures M.7a-8b demonstrate the complex stress state of a scarfed sandwich, in what is often thought a very simple joint. Orthotropy appears to have little effect on the resultant stress distributions at the adhesive interface, however minor differences are noticeable in the contours when considering points away from this area.

Another important aspect shown by the contours is the increment in magnitude of shear stress with scarf angle, showing that the smaller this angle becomes, the more significant its contribution. Conversely σ_y reduces and hence the peel contribution is less significant. Thus it is possible to establish clear links with shear lag theory for smaller scarf angles.

The general conclusion that can be made is tip stress variance occurs at a given distance from the free edge, regardless of whether the adherents are in tension or flexure. Similarly, extending this further allows the sandwich to be included showing the same observations hold true at the free edge and positions where there is significant differences in through thickness elastic modulus.

CHAPTER 8

GENERAL DISCUSSION

A three phased programme was developed in order to characterise in-plane joints in sandwich structures, in particular the scarf joint. Experimental, analytical and numerical investigations demonstrate that beneath this simple method of joining lies numerous complexities and uncertainties. The scarf can be difficult to machine, is mathematically the most difficult solve, and numerical analysis shows that tip stresses can be orders of magnitude greater than that applied.

8.1 Experimental Representation

Specimens used in the experimental programme were designed to minimise deflection and therefore reduce through thickness stress. The relationship between the four point specimen and a serviceable sandwich structure has some obvious deficiencies. This is not to say that the test programme is irrelevant, but consideration needs to be given to any limitations.

The specimens were designed to use a four point load fixture, however the majority of sandwich structures exist in panel form, where Poisson's ratio effects are magnified and load paths vary. Where edge compression or tension exists, the results should be valid as the skins are in pure tension or compression. Complexities arise when pressure loads are applied as the principal stress state is normally biaxial for two ply knitted reinforcements. The analysed transverse stress exists across the joint, but a longitudinal component that has not been addressed also results. It is however expected that this load transmitted along the length of the joint will have little effect on strength due to the fibres being continuous.

Coupled load conditions were eliminated during tests in order to isolate a pure bending moment. While this is not normally representative of a sandwich structure it allows an absolute maximum loading to be calculated since the presence of shear forces can reduce the scarf tip stresses. The numerical or analytical models can therefore be used for load estimation and suitable failure theory such as those proposed in chapters 5 and 6 applied confidently.

8.2 Modelling Uncertainties

Representation of the experimental procedure in the analytical and numerical studies saw several assumptions and restrictions. Quasi-isotropy, material and geometric linearity, together with a perfectly bonded and scarfed interface were the principal simplifications made to the analysis. In

reality the scarf has a blunt tip with the degree dependent on the machining method, together with a serrated interface on a micro level.

Assumption of material linearity appears to be suitable for the adherents and rigid adhesives such as epoxy, however non-linearity in high elongation adhesives such as the methacrylate was beyond the scope of this study. Geometric non-linearity was minimised through deflection restrictions, however its effects during the high loading of flexible sandwich structures should be recognised.

Inclusion of aluminium as a baseline showed that adherent modulus and Poisson's ratio affected joint stress distributions marginally. Its inclusion allowed comparison of theoretical models with existing results providing comfort in the accuracy of programs and modelling assumptions.

The relationship between the analytical and numerical studies as discussed in prior chapters was hampered by numerical tool restrictions. Experimental studies interacted with the analytical to provide semi-empirical models on which to base failure, while the analytical and numerical techniques demonstrated that stress profiles are accurately predicted away from the scarf tip. The numerical modelling in turn could therefore be related to testing through analytical verification, and more general predictions and recommendations made about angles other than those tested.

8.3 Failure Mode and Prediction

Experimental methods and post failure observation showed that adhesive failure modes could be precisely identified. Shear fracture patterns occurred almost precisely at a 45° angle, which was appropriate since analytical and numerical models showed that at decreasing scarf angles shear, as opposed to peel stresses, became increasingly significant.

The distinct lack of reliable failure criterion lead to proposals based on a boundary layer method and modified Von Mises criteria. Additional experimental projects would be desirable for alternative scarf angles and adhesives, so that the ranges of applicability can be further extended. The analytical and numerical models for angles up to and including the butt joint will then provide the basis from which any necessary modifications to failure prediction models can be achieved.

8.4 Production Implications

It was not only the quantitative results that have production implications, but also the practical factors noted during test specimen fabrication. Taped specimens are a multi step operation during which fibre fraction and hence mechanical properties can vary. Associated with this is surface

unfairness and stiffness discontinuity. Similarly the spline joint was a three component joint that was difficult to align. In fairness, problems such as alignment can be solved by location ridges, however the hydraulic action of fitting, which was particularly noticeable with high viscosity adhesives, gives a non-uniform bondline. This bondline thickness is extremely important, as increases result in decreased joint strengths.

Scarfing provided a viable option for construction based on a two piece joint, allowing stiffness continuity and surface fairness. The analytical and numerical studies demonstrated that an optimum 60° scarf angle does exist, which has significance for sandwich structures with thicker skins. The experimental programme however showed that decreasing the scarf angle improves the joint strength, which is contrary to the theoretical findings, but intuitively correct. It is therefore apparent that adhesive non-linearity is important, particularly during its plastic phase at the scarf tip.

When using liquid adhesives, it was found that heat distortion properties can be compromised without post cure, and so for scarf jointed panels a heated pneumatically operated press was developed by ATL Composites Pty Ltd. It offers the ability to post cure, and though use of pressure controls, gauge glue line thickness and ensure surface fairness, as seen in figure 8.1. Modular construction is therefore aided, allowing routed sandwich panel kits to be joined into infinite lengths. These infinite lengths do not come at the expense of freight costs either, as the panels and pressing mechanisms can be containerised and shipped worldwide for rapid assembly of conically developable structures, including some ships.
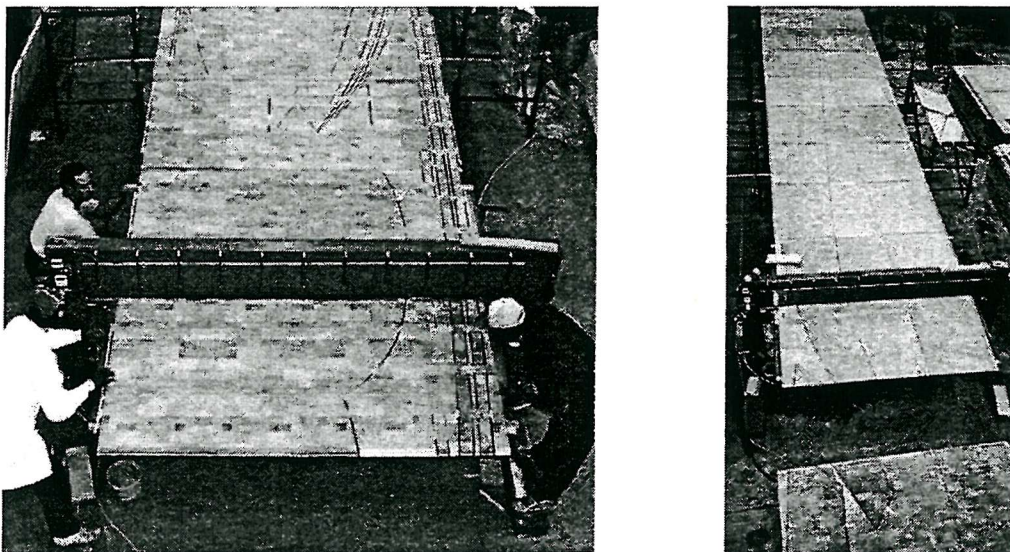
Figure 8.1 Scarfed and pre-routed sandwich panel assembly in heated pressing mechanism.

CHAPTER 9

RECOMMENDATIONS FOR FURTHER WORK

A considerable number of other facets could be investigated that are not limited exclusively to the sandwich joint.

One aspect that necessitates further study, is the effect of bundled fibres, rather than the evenly distributed pre-preg filaments on scarf interfacial strength. It is undoubtedly possible to develop an analytical model based on an elliptical (or otherwise) tow section, demonstrating a transient stress profile and resulting decreased joint efficiency. Consolidation pressure dependency could also be introduced as a variable showing the effect of increased fibre fraction, and hence flattened tow profile on scarf strength.

The composite laminates used in sandwich construction will often have thickness that cannot accommodate a 20:1 scarf angle as the amount of material to be removed can be excessive. Further tests on an increased number of scarf angles and fibre orientations is required to ascertain whether the 0.055mm boundary layer holds true for any angle. It is expected that at large angles the modified Volkerson approach will need to be changed to a Von Mises criterion based on equations (6.21-22) and may in fact tend toward the 0.2mm found by Suzuki.

The limitation of beam deflection in the experimental program does not in many instances represent a realistic structure. Experiments with reduced stiffness, increased deflection, and hence greater significance of peel may in fact degrade the joint strength further. In such a study the effectiveness of using a Demec gauge must be looked at carefully as increased beam curvature will most likely cause excessive error.

Creep, fatigue and impact will always have an important place in further studies as they hold the key to reduced (or increased) margins of safety. A long term study which includes environmental degradation effects, which are of particular importance in a marine environment, is necessary before a thorough understanding of the sandwich joint is gained. It is expected that increased joint strength may be initially gained due adhesive moisture absorption at the tip, thereby reducing the stress concentration.

A test program that has evolved from this study, but not included is currently being conducted on pre-stressed joints with curvature at the University of Southampton under Prof. R.A.Shenoi and the author's supervision. The importance of the pre-stressed joint is attributable to the force

necessary to form sandwich plating in panel developable structures. A post-buckled analysis with subsequent joint stress relief due to pressure loading can be used for strength analysis. A schematic of the test fixture and specimens is shown in figure 9.1.
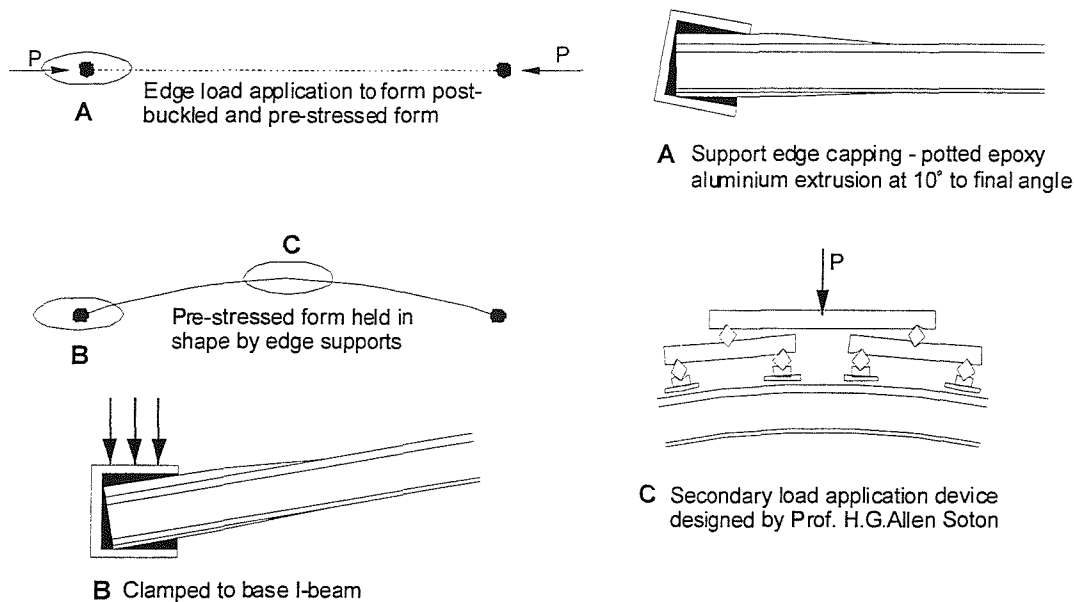
Figure 9.1 Post-buckled and pre-stressed beam including flexible load application device.

Actual performance of joined panels, as opposed to beams, is perhaps the final step in characterising the joint by experimental means as it represents closely the end use. A Gougeon Hydromat (Bertelsen *et al*, 1994) or similar panel pressure loading apparatus can be used to simulate out of plane loads experienced during service life and provide information on whether beam data is sufficiently accurate for design purposes.

Similarly the interaction and most favourable positioning of the joint in a structure i.e. in way of framing or at panel centreline, needs close scrutiny. Under prescribed loads it is feasible that increased fatigue lives and ultimate strength can be achieved with a correct joining arrangement.

Taking the interaction one step further, and considering panel construction techniques; analysis of stiffened flat panels to form complex curvatures rather than conically developed, and subsequent joining would be of immense benefit. Panels can be either edge or centreline stiffened to give biaxial curvature as either convex/convex or concave/convex and *vice versa*. Preliminary testing at ATL Composites Pty Ltd has shown great potential, although the amount of force required to form the desired shape for a given sandwich stiffness is considerable. Figure 9.2 shows the method by

which complex curvature can be achieved through local neutral axis movement of the sandwich at a stiffener.
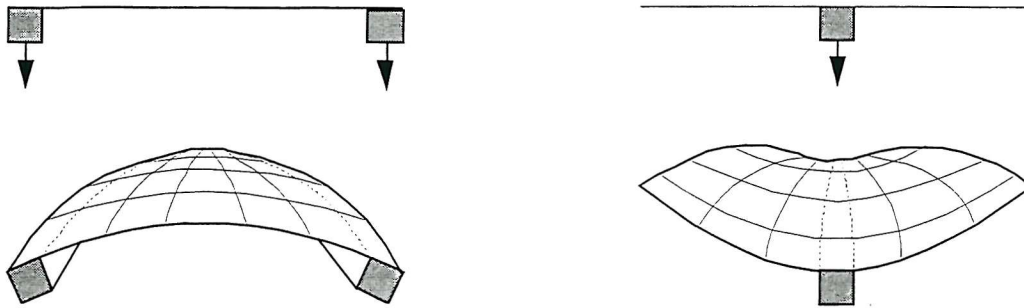
Figure 9.2 Complex curvature induced into stiffened flat panelling.

Finite element analysis that includes material non-linearity should provide a better understanding of tip stress profiles. The effect of voids and varying tip profiles must also be included to determine the magnitude of production variables on joint strength. Even a three dimensional study in panel configuration would be worthy of consideration, although the CPU time required may prove prohibitive.

Finally Chen and Cheng's analytical solution should be re-addressed based on the findings of the finite element analysis. With a non-linear profile of higher order polynomial form used for the adhesive shear stress variation, their method can more closely approximate the tip stress profile of the scarf joint and be readily adapted to methods of failure prediction.

CHAPTER 10

CONCLUSIONS

In-plane joints as applied to the sandwich can be characterised in numerous ways. This work has set out to establish suitable methods by which a greater understanding of joint mechanics can be achieved.

The Demec gauge proved satisfactory for joint strain measurements using stainless steel measurement markers attached to the skin and core of the sandwich. It is not imperative that markers be applied to the core since neutral axis position can be determined solely from skin markers, although to minimise erroneous measurements, core readings are invaluable.

The author sees potential field use for the Demec gauge, and not only with sandwich structures. As an example, permanent gauge markers can be applied to a ship's hull over joints or selected highly strained regions, and systematically measured at given time periods. Using these readings it would be possible to determine whether the study region is undergoing permanent deformation. Any associated creep may be due to adhesive deformation in the case of bonded structures, crack propagation in welded fabrications or more generally exceeding the elastic limit of the substrate. Invasive environments are of little consequence as locating holes can be filled with wax and cleared during measurement, ensuring the locating point is not affected by corrosion or foreign substance deposition.

The device has distinct advantages over resistance strain gauges, including ease of use and more importantly cost. Its ability to encompass large gauge regions means that deformation can occur at any position (or at all positions) within this region, whereas the resistance gauge is normally limited to smaller dimensions. Several improvements such as digital display and application force indicator would help minimise any errors and provide a more appealing industrial tool. The primary disadvantage is the gauge's inability to provide continuous reading.

A progression from materials choice, through impact and laminate coupon charaterisation provided a base from which an experimental focus could be placed on the sandwich joint as a quantifiable unit. Uncomplicated linear elastic beam theory for strain and deflection estimation showed good correlation with test results, although toward failure non-linear behaviour was apparent. The spline and tape joints showed no strength reduction, but a comprehensive comparison with the control and scarfed sandwich specimens was not possible due to consistent core shear failures. Stiffness continuity was therefore considered to be just as important, and it was

hypothesised that long term fatigue characteristics of a joint with stiffness discontinuities i.e. scarf and spline, would be detrimental to structural life. Aside from these aspects, surface fairness, ability to gauge glue line thickness accurately and ease of manufacture further endorsed the scarf joint as the most suitable method of in-plane joining for a sandwich.

The experience of consistent core shear failures during the experimental study of the tape and splined specimens had further implications. As a by-product of this study, a proposed extension of McGeorge and Hayman's (1998) semi-empirical model for balsa core shear strength, based on Feichtinger's (1992) density profiles was possible. Although not covering as wide a sample range as liked, the comparison with experimental data and third party investigations was excellent and should provide a basis from which further investigation is possible.

Modification of Volkerson's equation to give a semi-empirical approach to scarf failure prediction, showed good agreement with the author's experimental results. The modification of shear lag theory based on a boundary layer and Von Mises failure criterion to shear stress also saw support on a micro-level. Micrographs of cohesive failures demonstrated that shear dominates when deflection is limited. Mode II is a result of the sandwich skin essentially being supported by the core and restrained from peel stress development through excessive planar rotation.

Analytical and numerical studies centred on the scarf joint, as it had proven to be well suited to in-plane joining. A wide range of scarf angles needed to be considered, as the thicker a sandwich skin becomes the greater the necessity to increase scarf angle in order to keep material loss and machining costs to a minimum. Aluminium and composite adherents were chosen as basic adherent materials and by looking at the scarf in tension and flexure using these homogenous adherents, a basis for application to a sandwich joint could be founded.

The analytical modelling of the scarf joint in tension was performed using Chen and Cheng's (1990) theory, and provided the tip stress variance they had discussed. A computer program was developed for solving the equations, and it was found that extreme care was necessary in minimising errors. The scarf in pure bending saw application of Wah's (1976) procedure using stress functions that satisfied all boundary conditions. The solution was lengthy and showed the presence of geometric scale inconsistencies at varying multiplication levels. Although the exact reason for these discrepancies could not be pin-pointed, a multiplication level at which a stable solution is achieved was suggested. From this position a simple tensor rotation of applied stress could be used for calculation of adherent and adhesive interface stress profiles. Both models were based on the assumption of plane stress due to the increased complexities involved when considering plane strain.

A numerical study using finite element analysis allowed direct comparison with theory. Experimental results were not included since it was impractical to model a scarf angle of 3° in this manner. It was hoped that the comparison would allow validation of the analytical models so that a simple calculation could be performed in the future to estimate adhesive interface stress at any angle.

As the study progressed the analytical models showed considerable deviation from the finite element path results. The reasons were immediately apparent from stress contour plots. Chen and Cheng's assumption of linear stress distribution across the adhesive was invalid and Wah's theory had no means of accommodating scarf tip stresses. The results showed, as might be expected, that tension and flexural models in both homogenous and sandwich joints showed similar tip stress distributions. Internal stresses showed linear behaviour and agreed well with theory.

An optimum scarf angle of 60° showed the least amount of tip stress variation, and agrees exactly with that calculated using Chen and Cheng's simple formula. The practicality of joining thin skins at 60° is a major concern and in reality impossible to achieve unless the skins are thick. Furthermore adherent and adhesive plasticity would most probably result in stress variation being minimal, and the bonded area that can withstand creep whilst transmitting the load effectively will therefore be a more important consideration.

Again, discussion comes full circle to the practical application of a scarf joint which has been an underlying theme in this study. If the joint cannot be used commercially then it is of little use. Approximately nine planing marine vessels have been built to date using panel developed sandwich kit forms that are joined using the scarfing method described in this work. Overall length ranges from 24m down to 5m, with hard chined hull forms in both catamaran and mono configurations (Appendix N). The joints long-term performance has yet to be proven, but analogies could be drawn with first adhesively bonded aircraft fuselages that had no such history either. Based on this research it is hoped that further developments will be possible in fabrication techniques not only for marine vessels but large sandwich constructions in general.

This work has shown a logical progression in the characterisation of in-plane sandwich joints, and in particular the scarf, for use in modular construction. The research route began with investigation of suitable raw materials, proceeding through experimental programs and finally detailed the applicability of analytical and numerical methods, whilst at all times considering the underlying practical application.

Particularly in aerospace and marine applications where surface fairness is a primary concern, pre-determined joint strength reductions analogous to a weld can be designed into the structure. Ultimate strength, strain, stiffness and neutral axis movements were therefore determined during jointed beam tests, with results offering a mechanical description of the in-plane sandwich joint as a unit. Reductions are not always necessary however, as in many instances and especially with composites, excess load carrying material exists to counter impact damage. Flexural stiffness and its continuity in the structure therefore took precedence, with test results showing the scarf joint most suited to this role.

A simple and cost effective method for determining skin, core and overall joint strain in sandwich structures was adapted from existing tools, and shown to give excellent results. It was also demonstrated that Demec gauge measurements are less susceptible to global specimen movements, and require minimal correction when using a 2" rather than an 8" gauge length.

As a means of aiding design, Volkerson's shear lag model was modified using the concept of a boundary layer and Von Mise's yield criterion. This provided a semi-empirical method by which a scarfed sandwich skins ultimate load carrying capacity could be estimated using the bulk yield strength of an adhesive. For small scarf angles ($<10°$), good correlation with experimental results was achieved, and also showed prediction is insensitive to scarf angle and adhesive type. Support for using such a model was also gained on a microscopic level, where cohesive shear failures were apparent.

Adaptation of existing analytical methods to sandwich joint stress prediction offer potential but do require some principle assumptions to be readdressed. Their practical use should not however be dismissed, since the inclusion of suitable safety factors can provide an upper bound for design. Similarly in the numerical studies, more general observations were made. Most noticeable of these was the $60°$ scarf angle at which identical adherents have the least tip stress fluctuation. Further observations demonstrated almost identical fluctuations for the scarf joint whether in tension or flexure, solid or sandwich. This in turn suggests that variance is limited to a finite band from the free edge that is independent of adherent thickness.

The complexities involved with the characterisation of an in-plane sandwich joint are numerous. It is however hoped that the experimental methods, simple analysis tools and general observations described herein, will make it possible for more general access to higher technology sandwich fabrications.

REFERENCES

ADAMS, D.F. and Doner, D.R., (1967), Longitudinal Shear Loading of a Uni-directional Composite, *Journal of Composite Materials*, Vol. 1, No. 1, p. 4-17

ADAMS, R.D. and Davies, R., (1996), Strength of Joints Involving Composites, *Journal of Adhesion*, Vol. 59, p. 171-182

ADAMS, R.D. and Peppiatt, N.A., (1974), Stress Analysis of Adhesive-Bonded Lap Joints, *Journal of Strain Analysis*, Vol. 9, No. 3, p. 185-196

ADAMS, R.D., (1986), The Mechanics of Bonded Joints, *Structural Adhesives in Engineering*, Proceedings of the Institute of Mechanical Engineers, ISBN 0-85298-592-4, p. 17-24

ADAMS, R.D., (1989), Strength Predictions for Lap Joints, Especially with Composite Adherends: A Review, *Journal of Adhesion*, Vol. 30, p. 219-242

ADAMS, R.D., Chambers, S.H., Del Strother, P.J.A. and Peppiatt, N.A., (1973), Rubber Model for Adhesive Lap Joints, *Journal of Strain Analysis*, Vol. 8, No. 1, p. 52-57

ADAMS, R.D., Comyn, J. and Wake, W.C., (1997), *Structural Adhesive Joints in Engineering*, Chapman and Hall, ISBN 0-412-70920-1

ALLEN, H.G., (1969), *Analysis and Design of Structural Sandwich Panels*, Pergamon Press, ISBN 08-012869-8

ALLMAN, D.J., (1977), A Theory for Elastic Stresses in Adhesive Bonded Lap Joints, *Quarterly Journal of Mechanics and Applied Mathematics*, Vol. 30, No. 4, p. 415-436

ALLRED, R.E. and Guess, T.R., (1978), Efficiency of Double-Lapped Composite Joints in Bending, *Composites*, April, Vol. 9, No. 2, p. 112-118

AMERICAN BUREAU OF SHIPPING, (1994), Offshore Racing Yachts, *Guide for Building and Classing*, November, Section 7

AMERICAN BUREAU OF SHIPPING, (1997), High-Speed Craft, *Guide for Building and Classing*, February, Part 3, Section 9

ANDERSON, C.S., (1997), *Private Communication*, Structural Bonding Centre Quality Co-Ordinator, Boeing - ASTA Components

ANDERSON, G.P., Bennett, S.J. and DeVries, K.L., (1977), *Analysis and Testing of Adhesive Bonds*, Academic Press, ISBN 0-12-056550-1

ANSYS 5.3, (1996), *p-Method Structural Static Analysis*, Structural Analysis Guide, SAS IP Incorporated

ASTM C273, (1984), *Shear Test in Flatwise Plane of Flat Sandwich Constructions or Sandwich Cores*, American Society for Testing and Materials, Philadelphia

ASTM C393, (1994), *Flexural Properties of Sandwich Constructions*, American Society for Testing and Materials, Philadelphia

ASTM D1002, (1997), *Apparent Shear Strength of Single Lap Joint Adhesively Bonded Metal Specimens by Tension Loading (Metal to Metal)*, American Society for Testing and Materials, Philadelphia

ASTM D3039, (1995), *Tensile Properties of Polymer Matrix Composite Materials*, American Society for Testing and Materials, Philadelphia

ASTM D638, (1996), *Tensile Properties of Plastics*, American Society for Testing and Materials, Philadelphia

ASTM D790, (1996), *Flexural Properties of Unreinforced and Reinforced Plastics and Electrical Insulating Materials*, American Society for Testing and Materials, Philadelphia

ATL COMPOSITES, (1996), ADR240/ADH160 High Performance Laminating System, *Technical Specification Sheet 960801*, ATL Composites Pty Ltd, Australia

AUSTRALIAN STANDARDS, (1993), Fibre-reinforced plastics construction, *Boat and Ship Design and Construction*, Standards Australia, ISBN 0-7262-8138-7, Part 3, Section 3

BABUSKA, I. and Szabo, B., (1982), On the Rates of Convergence of the Finite Element Method, *International Journal for Numerical Methods in Engineering*, Vol. 18, p. 323-341

BALTEK, (1991), Why Baltek Core: The Properties of End-Grain Balsa Core, *Data File 159*, Baltek Corporation, USA

BARKER, R.M. and HATT, F., (1973), Analysis of Bonded Joints in Vehicular Structures, *AIAA Journal*, December, Vol. 11, No. 12, p. 1650-1654

BASE, G.D., (1955), Further Notes on the Demec, a Demountable Mechanical Strain Gauge for Concrete Structures, *Magazine of Concrete Research*, March, p. 35-38

BAYLOR, J.S. and Sancaktar, E., (1995), A Comparison of Adhesively Bonded Single Lap, Scarf and Butt Joints, Reliability, *Stress Analysis, and Failure Prevention Issues – Issues in Emerging Technologies and Materials*, ASME-DE, Vol. 87, p. 41-48

BERTLESEN, W.D., Rau, C.S. and Sikarskie, D.L., (1994), On the Development of a Two-Dimensional Test Fixture for Composite Panels, *Proceedings of the Fifth International Conference on Marine Applications of Composite Materials*, Melbourne, Florida, 18 April

BEZINE, G., Roy, A. and Vinet, A., (1996), Stress in Bonded Adherends for Single Lap Joints, *Journal of Ship Production*, August, Vol. 12, No. 3, p. 167-171

BIRD, J. and Allan, R.C., (1981), The Development of Improved FRP Laminates for Ship Hull Construction, *Composite Structures*, edited by Marshall, I.H., ISBN 0-85334-988-6, Chapter 14, p. 202-223

BREVIK, A.F., (1996), Sandwich Structures for Subsea Applications, *Sandwich Constructions 3*, Vol. 1, edited by Allen, H.G., ISBN 0-947817-81-6, p.27-36

BURNETT, D.S., (1987), *Finite Element Analysis*, AT&T Bell Laboratories, ISBN 0-201-108062

CET 3230/1, (1995), *Comparative Sandwich Impact Study*, Queensland University of Technology, August (Restricted)

CET 4149/1-5, (1995), *Composite Mechanical Properties*, Queensland University of Technology, December (Restricted)

CHALMERS, D.W., (1994), The Potential for the Use of Composite Materials in marine Structures, *Marine Structures*, Vol. 7, p. 441-456

CHEN, D. and Cheng, S., (1983), An Analysis of Adhesive Bonded Single-Lap Joints, *Journal of Applied Mechanics*, March, Vol. 105, p. 109-115

CHEN, D. and Cheng, S., (1990), Stress Distribution in Plane Scarf and Butt Joints, *Journal of Applied Mechanics*, March, Vol. 57, No. 1, p. 78-83

CIBA, (1996), *Redux Bonding Technical Manual*, Ciba-Geigy, Switzerland

CLARK, J.D. and McGregor, I.J., (1993), Ultimate Tensile Stress Over a Zone: A New Failure Criterion for Adhesive Joints, *Journal of Adhesion*, Vol.42, p. 227-245

CORDANI, L., (1998), *Private Communication*, Software Support Manager, IDAC Limited

CRITCHFIELD, M.O., Judy, T.D. and Kurzweil, A.D., (1994), Low-Cost Design and Fabrication of Composite Ship Structures, *Marine Structures*, Vol. 7, p. 475-494

CROCOMBE, A.D., (1989), Global Yielding as a Failure Criteria for Bonded Joints, *International Journal of Adhesion and Adhesives*, Vol. 9, No. 3, p. 145-153

CROCOMBE, A.D. and Adams, R.D., (1981), Peel Analysis Using the Finite Element Method, *Journal of Adhesion*, Vol. 12, p. 127-139

CURL, R.F., Kroto, H.W. and Smalley, R.E., (1996), Discovering the Fullerenes, *Nobel Lecture*, December

DET NORSKE VERITAS, (1991), Hull Structural Design, Fibre Composite and Sandwich Constructions, *Tentative Rules for Classification of High Speed and Light Craft*, July, Part 3, Chapter 4

DIXON, R.H., Ramsey, B.W. and Usher, P.J., (1973), Design and Build of the GRP Hull of HMS Wilton, *Proceedings of the Symposium on GRP Ship Construction*, London, 24 October, p. 1-32

DUCKWORTH, A., (1997), *Private Communication*, Technical Director, ATL Composites Pty Ltd, Australia

ENLUND, H., (1995), Developing a Composite Hull for a Large High Speed Catamaran, *11th Fast Ferry International Conference*, Hong Kong, 21-23 February

ERDOGAN, F. and Ratwani, M., (1971), Stress Distribution in Bonded Joints, *Journal of Composite Materials*, July, Vol. 5, No. 3, p. 378-393

FEICHTINGER, K.A., (1986), Properties of End Grain Balsa Core Material as a Function of Density, *International Conference Marine Applications of Composite Materials*, Florida, 24-26 March

FEICHTINGER, K.A., (1988), Test Methods and Performance of Structural Core Materials – I. Static Properties, *4th Annual ASM International/Engineering Society of Detroit – Advanced Composites Conference and Exposition*, USA, 13-15 September, p. 1-11

FEICHTINGER, K.A., (1990), Test Methods and Performance of Structural Core Materials – IIA. Strain Rate Dependence of Shear Properties, *5th Autumn INERN Conference*, Lorient, France, 16-17 October, p. 37-47

GODWIN, E.W. and Matthews, F.L., (1980), A Review of the Strength of Joints in Fibre-Reinforced Plastics - Part 1. Mechanically Fastened Joints, *Composites*, July, Vol. 11, No. 3, p. 155-160

GOLAND, M. and Reissner, E., (1944), The Stresses in Cemented Joints, *Journal of Applied Mechanics*, March, Vol. 11, p. 17-27

GOWER, M.R.L. and Sims, G.D., (1997), *An Evaluation of Test Methods for Composite Sandwich Laminates*, NPL Report CMMT(C)25, July

HALPIN, J.C. and Tsai, S.W., (1969), Effects of Environmental Factors on Composite Materials, *AFML-TR 67-423*, June

HART-SMITH, L.J., (1974), Analysis and Design of Advanced Composite Bonded Joints, *NASA CR-2218*, April

HART-SMITH, L.J., (1981), Further Developments in the Design and Analysis of Adhesive-Bonded Structural Joints, *Joining of Composite Materials,* ASTM STP 749, p. 3-31

HART-SMITH, L.J., (1993), The Bonded Lap-Shear Test Coupon - Useful for Quality Assurance but Dangerously Misleading for Design Data, *38th International SAMPE Symposium and Exhibition,* Anaheim, 10-13 May

HOOPER, H., (1986), The Nesting and Marking of Ship Parts Cut from Steel Plate, *Journal of Ship Production,* February, Vol. 2, No. 1, p. 8-17

HORSMON, A.W., (1994), Composites for Large Ships, *Journal of Ship Production,* November, Vol. 10, No. 4, p. 274-280

HUYBRECHTS, D., (1998), Dimensioning of Wound Sandwich Tramway Carriage, *Fourth International Conference on Sandwich Construction,* Stockholm, Sweden, 9-11 June, Vol. 1, p. 111-122

ITW, (1997), AO425 Methacrylate Adhesive, *Technical Data Sheet,* ITW Plexus, USA

JANGBLAD, D., Gradin, P. and Stenström, T., (1988), Determination and Verification of Elastic Parameters for Adhesives, *Adhesively Bonded Joints: Testing Analysis and Design,* ASTM STP 981, p. 54-68

JOHNSON, C.L., (1989), Effect of Ply Stacking Sequence on Stress in a Scarf Joint, *AIAA Journal,* January, Vol. 27, No. 1, p. 79-86

JOHNSTON INDUSTRIES, (1997), *Product List and Handbook,* Johnston Industries, USA

JOST, K., (1997), Fifth Generation Corvette, *Automotive Engineering,* January, Vol. 105, No. 1, p. 67-71

KARLSSON, K.F. and Åström, B.T., (1997), Manufacturing and Applications of Structural Sandwich Components, *Composites - Pt. A: Applied Science and Manufacturing,* Vol. 28, No. 2, p. 97-111

KATTAN, M.R., (1996), Steel Sandwich Construction for Ships – a Reality, *Sandwich Constructions 3,* Vol. 1, edited by Allen, H.G., ISBN 0-947817-81-6, p. 399-410

KINLOCH, A.J., (1994), *Adhesion and Adhesives: Science and Technology*, Chapman and Hall, ISBN 0-412-27440-X

LAMB, T., (1995), Shell Development Computer Aided Lofting – Is There a Problem or Not, *Journal of Ship Production*, February, Vol. 11, No. 1, p. 34-46

LEAKE, J.M. and Calkins, D.E., (1996), Small Ship Producibility, *Journal of Ship Production*, May, Vol. 12, No. 2, p. 126-140

LE COMTE, (1986), Injection Moulding for Large Craft, *Ship and Boat International*, January /February, p. 43-44

LIN, C. and Lin, Y., (1993), A Finite Element Model of Single-Lap Adhesive Joints, *International Journal of Solids and Structures*, Vol. 30, No. 12, p. 1679-1692

LLOYD'S REGISTER, (1996), Hull Construction in Composite, *Rules and Regulations for the Classification of Special Service Craft*, Vol. 6, Part 8, Chapter 3

LUBKIN, J.L., (1957), A Theory of Adhesive Scarf Joints, *Journal of Applied Mechanics*, June, Vol. 24, No. 2, p. 255-260

MATTHEWS, F.L., Kilty, P.F. and Godwin, E.W., (1982), A Review of the Strength of Joints in Fibre-Reinforced Plastics – Part 2. Adhesively Bonded Joints, *Composites*, January, Vol. 13, No. 1, p. 29-37

MAUNSELL, (1994), *Advanced Composite Construction System*. Designer Composites Technology Limited, UK

McGEORGE, D. and Hayman, B., (1998), Shear Strength of Balsa-Cored Sandwich Panels, *Fourth International Conference on Sandwich Construction*, Stockholm, Sweden, 9-11 June, Vol. 2, p. 545-556

McLARTY, J.L., (1983), Demonstration of the Feasibility of Filament Winding Large Ship Hulls, *Materials & Processes - 28th National SAMPE Symposium*, Anaheim, 12-14 April

MORICE, P.B. and Base, G.D., (1953), The Design and Use of a Demountable Mechanical Strain Gauge for Concrete Structures, *Magazine of Concrete Research*, August, p. 37-42

NAFEMS, (1984), *Guidelines to Finite Element Practice,* National Agency for Finite Element Methods and Standards, Department of Trade and Industry UK, ISBN 0-903640-16-3

NAHAS, M.N., (1986), Survey of Failure and Post-Failure Theories of Laminated Fibre-Reinforced Composites, *Journal of Composites Technology and Research,* Vol. 8, No. 4, p 138-153

NGUYEN, L.B., Juska, T. and Mayes, J.S., (1997), Evaluation of low Cost Manufacturing Technologies for Large Scale Composite Ship Structures, *Proceedings of the 38th AIAA /ASME /ASCE /AHS /ASC Structures, Structural Dynamics and Materials Conference,* Vol. 2, p. 992-1001

NIELSEN, L.E., (1970), Generalized Equation for the Elastic Moduli of Composite Materials, *Journal of Applied Physics,* Vol. 41, No. 11, p. 4626-4627

NIELSEN, L.E., (1974), *Mechanical Properties of Polymers and Composites: Volume 2,* Marcel Dekker Inc., ISBN 0-8247-6208-8

NIU, M.C.Y., (1990), *Airframe Structural Design,* Conmilit Press Ltd., ISBN 962-7128-04-X

OFFRINGA, A.R., (1996), Thermoplastic Composites Rapid Processing Applications, *Composites - Pt. A: Applied Science and Manufacturing,* Vol. 27A, No. 4

OLSSON, K.A. and Reichard, R.P., (1989), Preface, *First International Conference on Sandwich Construction,* Stockholm, Sweden, 19-21 June, ISBN 0-947817-37-9

PHILLIPS, H.J., (1997), *Assessment of Damage Tolerance Levels in FRP Ship Structures,* Ph.D. Thesis, Department of Ship Science, University of Southampton

PRO/MECHANCIA 18.0, (1997), *Geometric Elements and the p-Method,* Getting Started with Structure, On-line Manuals, Parametric Technology Corporation

PROFESSIONAL BOATBUILDER, (1996), Resin Infusion/SCRIMP Applications, *Professional Boatbuilder,* No. 31

RAGHAVA, R., Caddell, R.M. and Yeh, G.S.Y., (1973), The Macroscopic Yield Behaviour of Polymers, *Journal of Materials Science,* Vol. 8, p. 225-232

RAYMER, J.F., (1991), Large-Scale Processing Machinery for Fabrication of Composite Hulls and Superstructure, *Journal of Ship Production*, November, Vol. 7, No. 4, p. 220-226

REDDY, M.N. and Sinha, P.K., (1975), Stresses in Adhesive Bonded Joints for Composites, *Fibre Science and Technology*, Vol. 8, p. 33-47

REICHARD, R.P. and Neyhart, T.L., (1997), Development of a Composite Superstructure System: A Joint US Government/Industry Project, *Fast '97*, Sydney, Australia, July, p. 591-597

ROBSON, B.L., (1984), The RAN GRP Minehunter - A Status Report, *International Symposium on Mine Warfare Vessels and Systems*, London, 12-15 June, Vol. 1

SHENOI, R.A. and Hawkins, G.L., (1992), Influence of Material and Geometry Variations on the Behaviour of Bonded Tee Connections in FRP Ships, *Composites*, September, Vol. 23, No. 5, p. 335-345

SHENOI, R.A. and Wellicome, J.F., (1993), Appendix: Mechanical Properties of Composite Materials' Constituents, *Composite Materials in Maritime Structures*, Volume 1 Fundamental Aspects, edited by Shenoi, R.A. and Wellicome, J.F., Cambridge University Press, ISBN 0-521-45153-1

SHENOI, R.A., (1993), An Engineering Approach to the Prediction of Elastic Properties of a Laminate, *Composite Materials in Maritime Structures*, Volume 1 Fundamental Aspects, edited by Shenoi, R.A. and Wellicome, J.F., Cambridge University Press, ISBN 0-521-45153-1

SHIN, J.G. and Kim, W.D., (1997), Kinematic Analysis of the Process Planning for Compounding Ship Hull Plates, *Journal of Ship Production*, February, Vol. 13, No. 1, p. 28-35

SINHA, P.K. and Reddy, M.N., (1976), Thermal Analysis of Composite Bonded Joints, *Fibre Science and Technology*, Vol. 9, p. 153-159

SJÖGREN, J., Celsing, C.G., Olsson, K.A., Levander, C.G. and Hellbratt, S.E., (1984), Swedish Development of MCMV-Hull Design and Production, *International Symposium on Mine Warfare Vessels and Systems*, London, 12-15 June, Vol. 1

STORCH, R., (1997), Build Strategy and Design for Production, *IMDC '97*, Delft, April, p. 18-22

STRAND, R., (1990), Blisters Under the Microscope, *Practical Sailor*, May, p. 8-10

SULTAN, J.N. and McGarry, F.J., (1973), Polymer Engineering Science, Vol. 13, p. 29-

SUZUKI, Y., (1987), Adhesive Tensile Strengths of Scarf and Butt Joints of Steel Plates, *JSME International Journal*, Vol. 30, No. 265, p. 1042-1051

TAMURA, K., (1991), *Private Communication*, Chief Surveyor Pacific Division, American Bureau of Shipping

THAMM, F., (1976), Stress Distribution in Lap Joints with Partially Thinned Adherends, *Journal of Adhesion*, Vol. 7, p. 301-309

THOMSEN, O.T., Frostig, Y. and Mortensen, F., (1998), Delamination Failure at Ply Drops in CFRP/Sandwich Panels Loaded in Tension, *Fourth International Conference on Sandwich Construction*, Stockholm, Sweden, 9-11 June, Vol. 2, p. 829-840

TIMOSHENKO, S.P. and Goodier, J.N., (1970), *Theory of Elasticity*, McGraw-Hill, ISBN 0-070-85805-5

TONG, L., (1997), An Assessment of Failure Criteria to Predict the Strength of Adhesively Bonded Composite Double Lap Joints, *Journal of Reinforced Plastics and Composites*, Vol. 16, No. 8, p. 698-713

TSAI, M.Y. and Morton, J., (1994), Three-Dimensional Deformations in a Single-Lap Joint, *Journal of Strain Analysis*, Vol. 29, No. 1, p. 137-145

VINOGRADOV, V.M., Golovkin, G.S., Gorokhovich, A.I., Grechishkin, V.A. and Tikhonov, A.I., (1995), Technology for Prepreg Production of Semifinished Products of Polymeric Composite Materials, *Composite Manufacturing Technology*, edited by Bratukhin, A.G. and Bogolyubov, V.S., Chapman and Hall, ISBN 0-412-58250-3, Chapter 2, p. 29-124

VOLKERSON, O., (1938), Die Nietkraftverteilung in Zugbeanspruchten Nietverbindungen mit Konstanten Laschenquerschnitten, *Luftfahrtforschung*, Vol. 15, p. 41-47

VOLKERSON, O., (1965), Recherches sur la Théorie des Assemblages Colles, *Construction Métallique*, Vol. 4, p. 3-13

WAH, T., (1976), The Adhesive Scarf Joint in Pure Bending, *International Journal of Mechanical Science,* May, Vol. 18, No. 5, p. 223-228

WALTON, K., (1997), *Private Communication,* Technical Director, Baltek Corporation, USA

WASHIZU, K., (1968), *Variational Methods in Elasticity and Plasticity,* Pergamon Press, ISBN 0-08017653-4

WIESE, M., Echtermeyer, A. and Hayman, B., (1998), Evaluation of Oblique Impact Damage on Sandwich Panels with PVC and Balsa Core Materials, *Fourth International Conference on Sandwich Construction,* Stockholm, Sweden, 9-11 June, Vol. 2, p. 807-818

WOLDESENBET, E. and Vinson, J.R., (1996), Sandwich Composite Structure for Low Cost and Emergency Housing, *Sandwich Constructions 3,* Vol. 1, edited by Allen, H.G., ISBN 0-947817-81-6, p.61-70

WOOD & WOOD PRODUCTS, (1976), Wood Defies Minus 260 Temperatures, *Wood and Wood Products,* November, Vol. 81, No. 11, p. 37-38

WOOLEY, G.R. and Carver, D.R., (1971), Stress Concentration Factors for Bonded Lap Joints, *Journal of Aircraft,* October, Vol. 8, No. 10, p. 817-820

WRIGHT, H.D. and Evans, H.R., (1996), Profiled Steel Concrete Elements for Use in Wall Construction, *Sandwich Constructions 3,* Vol. 1, edited by Allen, H.G., ISBN 0-947817-81-6, p.91-100

WRONSKI, A.S. and Pick, M.J., (1977), Pyramidal Yield Criteria for Epoxides, *Journal of Materials Science,* Vol. 12, p. 28-34

ZIMMERMAN, K. and Liu, D., (1995), Geometrical Parameters in Composite Repair, *Journal of Composite Materials,* Vol. 29, No. 11, p. 1473-1487

APPENDIX A

Marine Impact Test Equipment

AS4132.3 (1996)

APPARATUS The following apparatus is required

(a) *Impactor* A mild steel projectile with a mass of 15 kg.
(b) *Drop Tube* A smooth-bore tube manufactured from any suitable material, fixed in a vertical plane above the panel frame. The length of the drop tube shall be not less than 3m and the maximum clearance between the impactor and the side of the tube shall be not more than 5mm.
(c) *Panel Frame* A mild steel frame for holding the test panel with an unsupported area of 500mm by 500mm. The test panel shall be clamped to the frame on opposite sides.

PROCEDURE The procedure shall be as follows

(a) Clamp the test panel on the panel frame.
(b) Drop the impactor onto the test panel from a height of 500mm.
(c) Inspect the test panel for rupture or damage.
(d) If rupture has not occured repeat steps (a)-(c) with the drop height of the impactor being increased by increments of 500mm until rupture occurs.
(e) Measure the length of the cracks in the skin and observe the extent of skin delamination at rupture.
(f) Repeat steps (a)-(e) for the other test panels selected for comparison.

3m
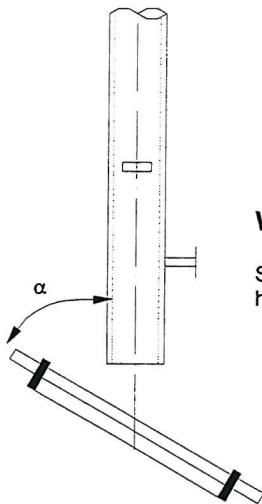
Weise, Echtermeyer and Hayman (1998)

Similar procedure to AS4132.3 however increased drop height, impact angle and projectile weight are variable.

α
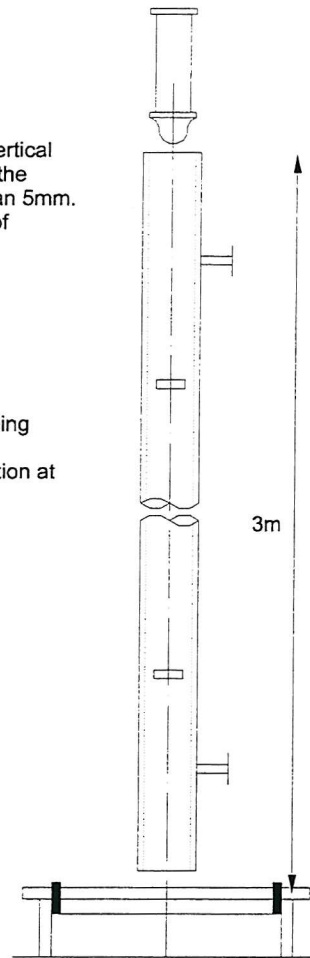
Tamura (1991)

APPARATUS The following apparatus is required

(a) *Impactor* A spherical steel ball with a mass of 8 kg (dia 125mm).
(b) *Drop Tube* PVC pipe (inner diameter >125mm).
(c) *Specimen* 300mm x 100mm x t (shell plating)
(d) *Support* Two pieces of round steel bar

PROCEDURE The procedure shall be as follows

(a) Arrange steel bar on 250mm centres.
(b) Drop steel ball onto specimen from 3,4,6 and 8ft at midspan.
(c) Observe tearing and delamination
(d) Impact load is to be absorbed at 3ft without tearing or delamination.
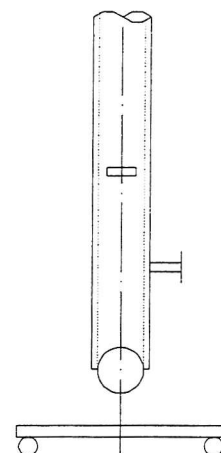
APPENDIX B

Marine Code Approval Minimum Skin Thickness Requirements

Lloyds Register (1996)– Special Service Craft

2.4.1 The Rule minium skin thicknesses are to be corrected for craft type irrespective of the reinforcement being used, the corrected minimum skin thickness of side, bottom, transom, wet-deck, vehicle deck and weather decks is to be determined from:

$t_{min} = 2\omega$ (mm)

ω = Service type correction factor given in table

Service type notation	ω
Cargo	1.1
Passenger	1.0
Patrol	1.0
Pilot	1.1
Yacht	1.0
Workboat	1.2

3.7.6 Multi-Hull Craft - In no case are the minimum thicknesses of reinforcement which form the skins of a sandwich laminate to be taken as less than 4 mm and 3mm for the outer and inner skins respectively.

7.3.6 Mono-Hull Craft - In no case is the minimum thickness of reinforcement which forms the skin of a sandwich laminate to be taken as less than 2 mm.

American Bureau of Shipping (1994) – Offshore Racing Yachts

7.2e The weight of reinforcement in the outer skin of shell plating sandwich laminates is not to be less than given in table (c).

W_s = minimum required weight of reinforcement
L = craft length between perpendiculars in m, not to be taken less than 9.5 m

Laminate	Fibre g/m^2
E-glass reinforcement with polyester or vinylester	$W_s = 105L+138$
S or R-Glass reinforcement with epoxy or vinylester	$W_s = 90.2L+125$
Kevlar reinforcement with epoxy or vinylester	$W_s = 59.0L+80.2$
HS carbon fibre with epoxy or vinylester	$W_s = 73.8L+100$

Australian Standard (1993) – Boat & Ship Design and Construction

4.4 To allow for adequate puncture and impact resistance, the mass of reinforcement in the outer skin of the sandwich laminate shall be greater than the minimum thickness given by:

$W_s = 22L_{wl} + 1340$ (g/m^2)   Hull bottom shell and topsides
$W_s = 22L_{wl} + 1040$ (g/m^2)   Weather and freeboard decks and superstructure
$W_s = 22L_{wl} + 390$ (g/m^2)   Other structural components

W_s = minimum mass of reinforcement for e-glass fibre
L_{wl} = craft waterline length in m

The minimum thickness of the inner skin of a sandwich laminate should not be less than 80 percent of the outer skin thickness.

Det Norske Veritas (1991) – High Speed and Light Craft

A203 The thickness of skin laminates on structural sandwich panels are in general not to be less than:

$$t = \frac{t_o + kL}{\sqrt{f}} \quad (mm)$$

$$f = \frac{\sigma_{nu}}{160}$$

σ_{nu} = ultimate tensile stress in N/mm^2

L = length of craft between perpendiculars in m

Structural member	t_o		k
	A	B	
Hull bottom below deepest WL	1.5	1.0	0.09
Hull side and transom above deepest WL	1.5	1.0	0.09
Stem and keel to 0.01 from centreline	5.0	4.0	0.09
Weather deck not intended for cargo	1.5	1.0	0.05
Cargo deck	2.5	1.0	0.05
Accommodation deck	1.5	1.0	0.03
Structural/watertight bulkheads	1.5	1.0	0.03
Superstructures and deckhouses	1.5	1.0	0.03
Tank bulkheads	2.0	1.5	0.05

A - Exposed
B - Protected

American Bureau of Shipping (1997) – High Speed Craft

3.4e After all other requirements are met, the skin thicknesses of laminates complying with basic laminate requirements are in general to be not less than given by the following equations.

$t_{os} = 0.35k_3(C_1+0.26L)$ (mm)
$t_{is} = 0.25k_3(C_1+0.26L)$ (mm)

t_{os} = thickness of outer skin
t_{is} = thickness of inner skin
k_3, C_1 = factors for service and location
L   = craft length between perpendiculars in m

	C_1 mm	k_3	
		Bottom Shell	Side Shell & Deck
Unrestricted Ocean Service	3.2	1.1	1.0
Restricted Ocean Service	5.7	1.2	1.0

APPENDIX C

Micro- and Macro Morphology
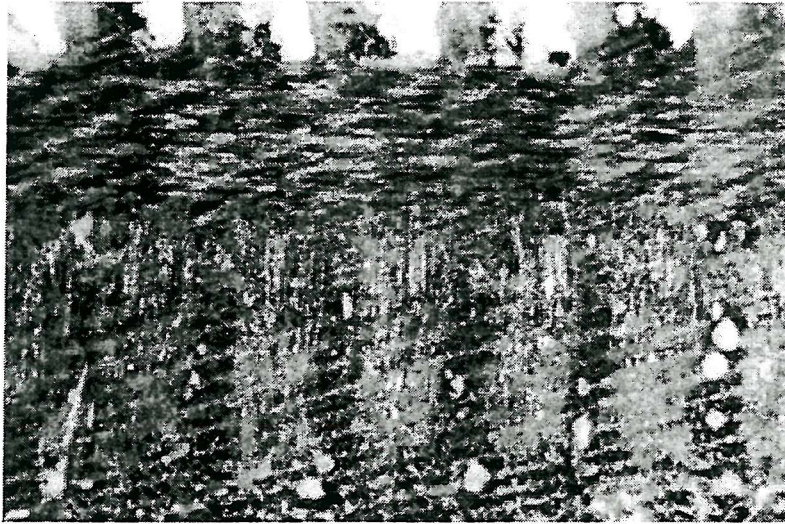
Fig. C.1 Scarfed laminate surface prior to bonding.
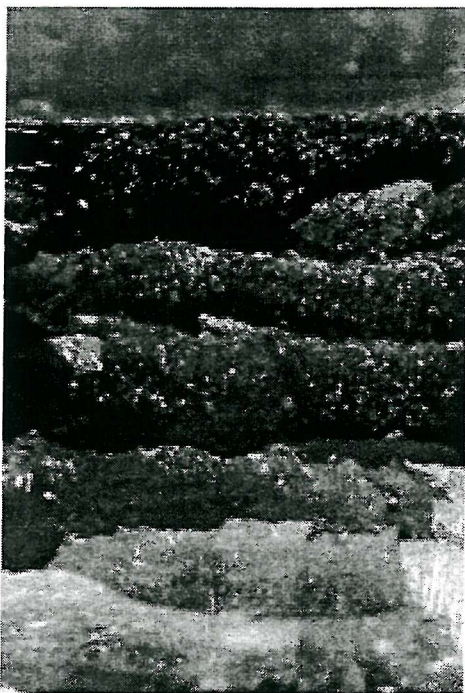
Fig. C.2 Epoxy shear fracture showing defined ridge pattern in scarf joint.

Fig. C.3 Methacrylate shear failure with plastic tearing in scarf joint.
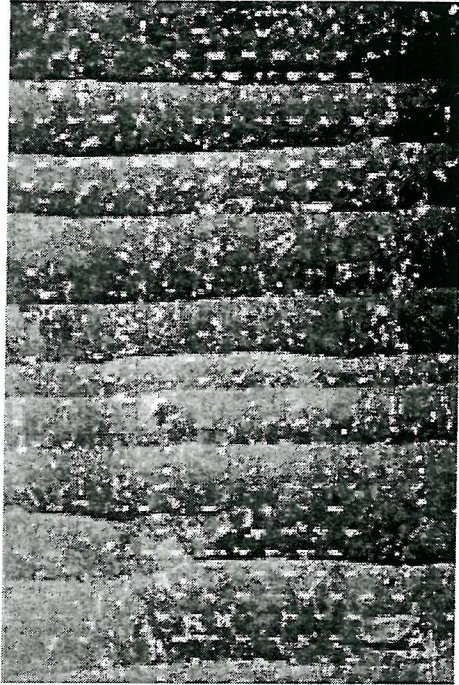
Fig. C.4 Epoxy shear ridges in spline joint.
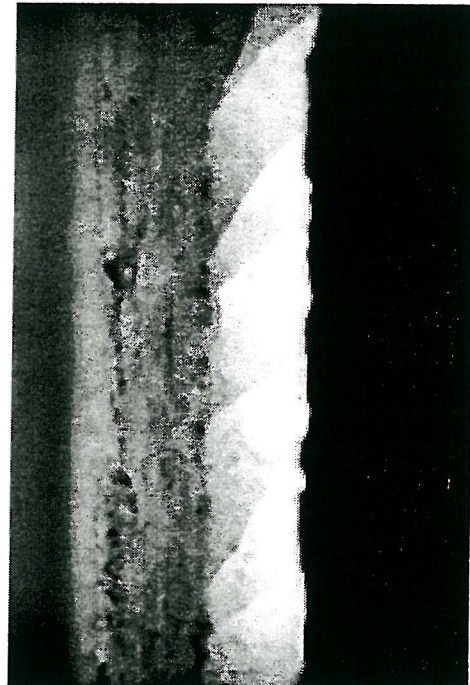
Fig. C.5 Sectional view through bondline post-failure showing 45° shear fractures.
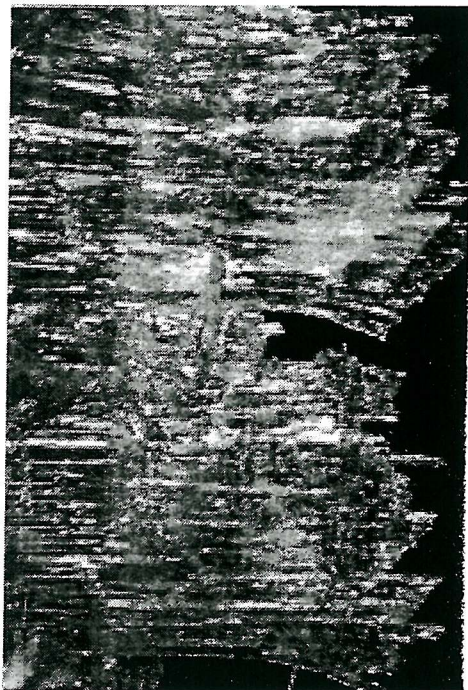
Fig. C.6 Scarfed tows demonstrating layering and tip fineness.
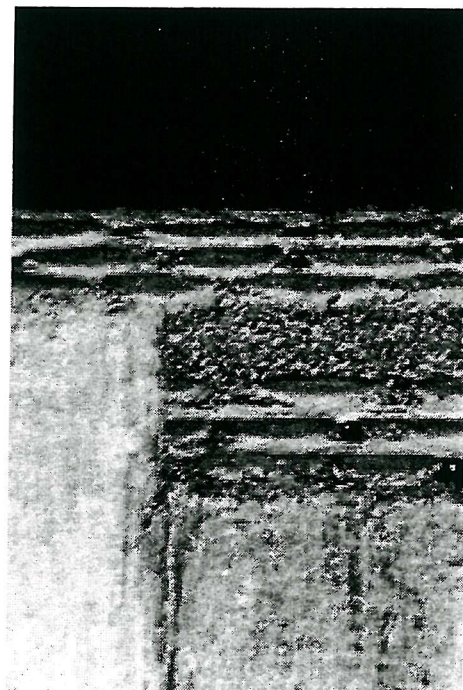
Fig. C.7 Internal spline sectional view with thick adhesive layer.

116
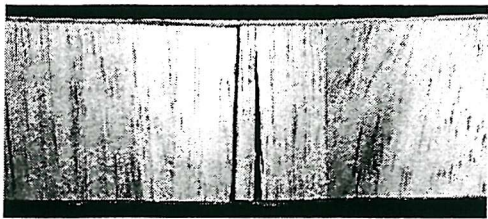
Fig. C.8 Scarf (methacrylate) tension failure.
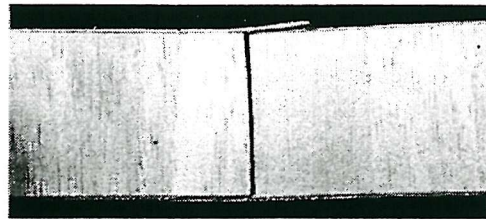
Fig. C.9 Scarf (methacrylate) compressive failure.
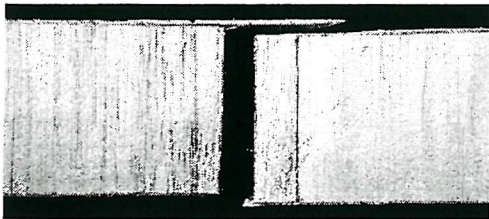
Fig. C.10 Scarf (epoxy) tension failure.
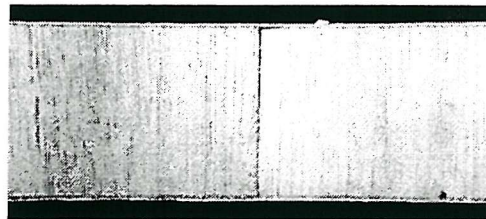
Fig. C.11 Scarf (epoxy) compressive failure.
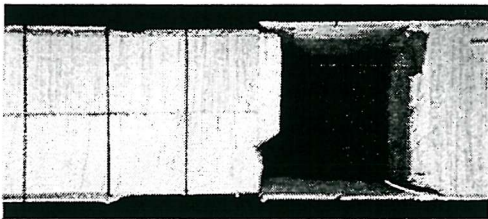
Fig. C.12 Spline (epoxy) tension failure.
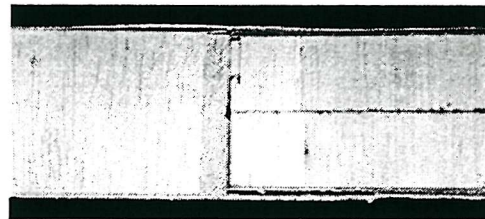
Fig. C.13 Spline (epoxy) core shear failure.
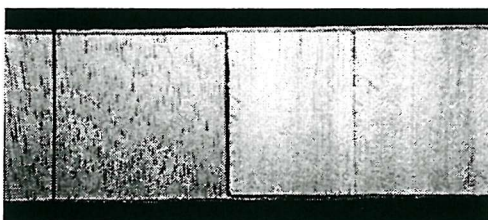
Fig. C.14 Tape core shear failure.
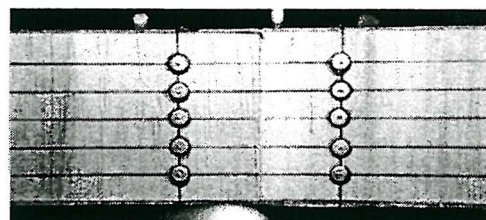
Fig. C.15 Core strain measurement Demec points.
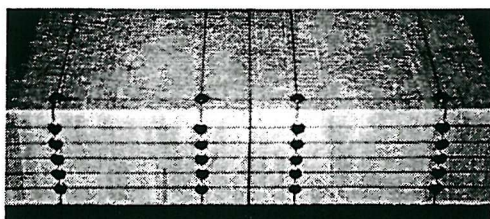
Fig. C.16 Core and skin Demec points.

Fig. C.17 Demec gauge.

117
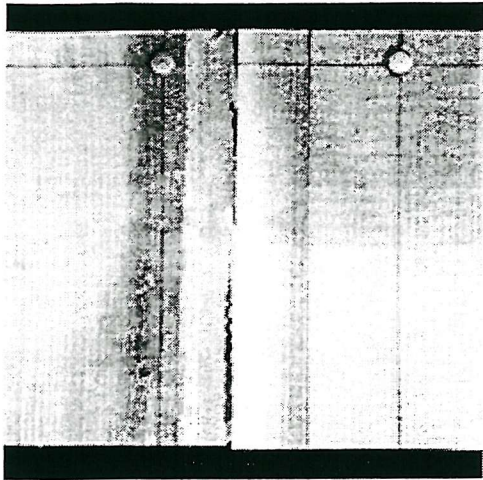
Fig. C.18 Scarf (methacrylate) tension failure.
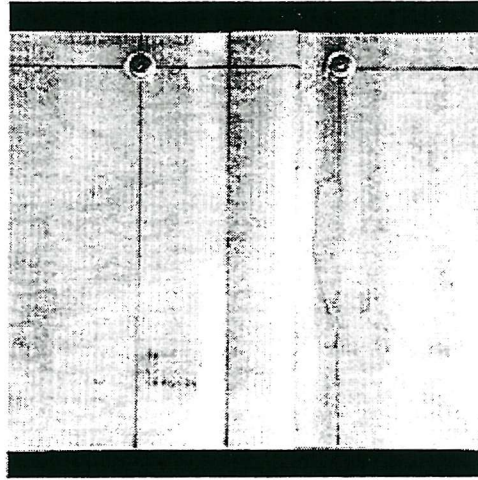
Fig. C.19 Scarf (methacrylate) compressive failure.
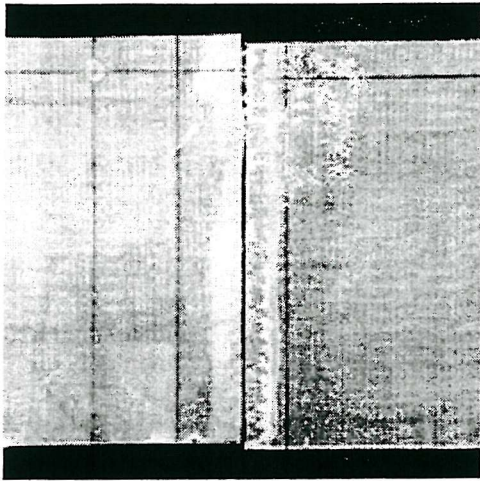
Fig. C.20 Scarf (epoxy) tension failure.
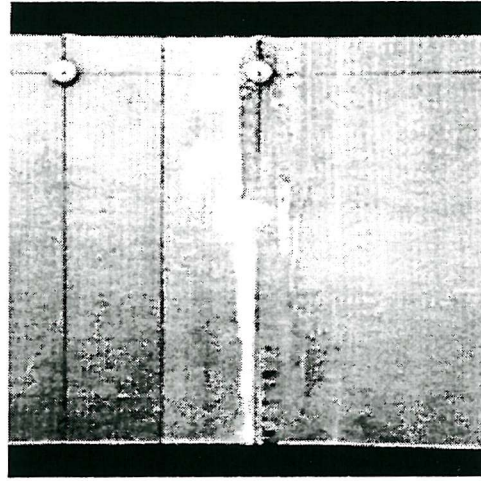
Fig. C.21 Scarf (epoxy) compressive failure.
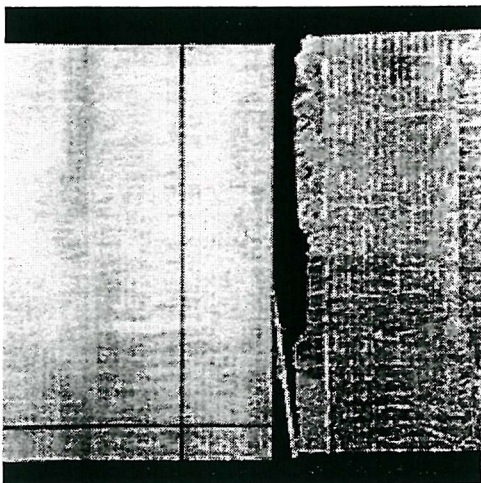
Fig. C.22 Spline (epoxy) tension failure.

Fig. C.23 Spline (epoxy) compressive failure.

118
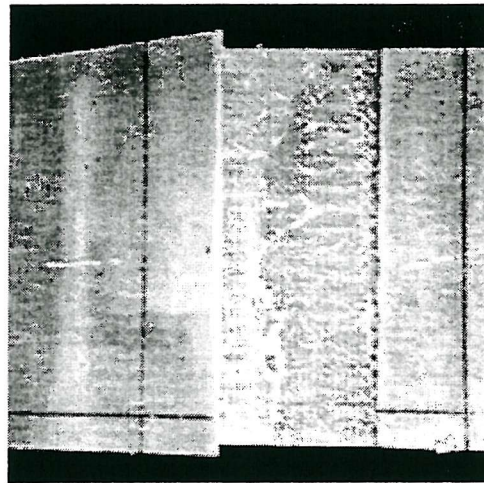
APPENDIX D

Experimental Strain and Deflection Readings
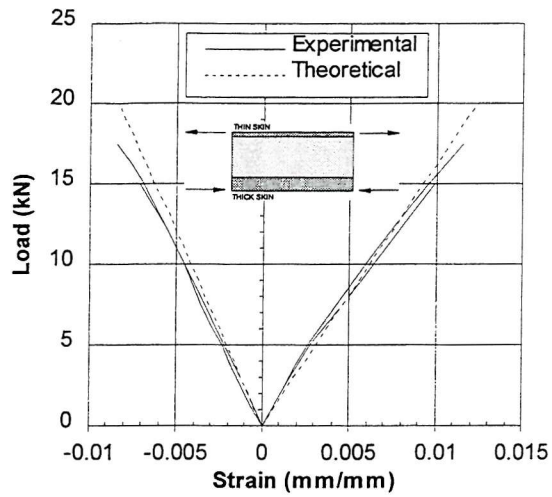
Fig. D.1.1 Continuous tensile 8" gauge
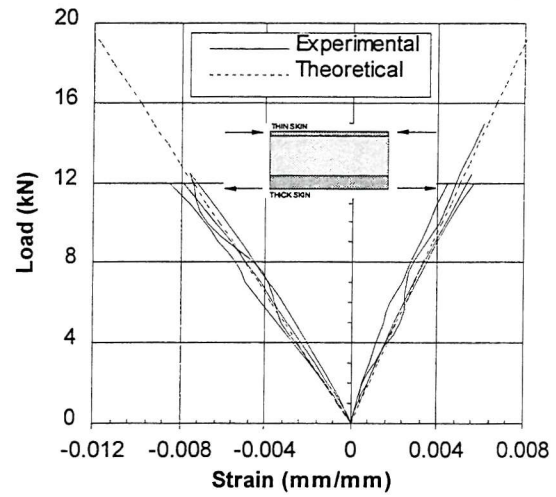
Fig. D.1.2 Continuous compression 8" gauge
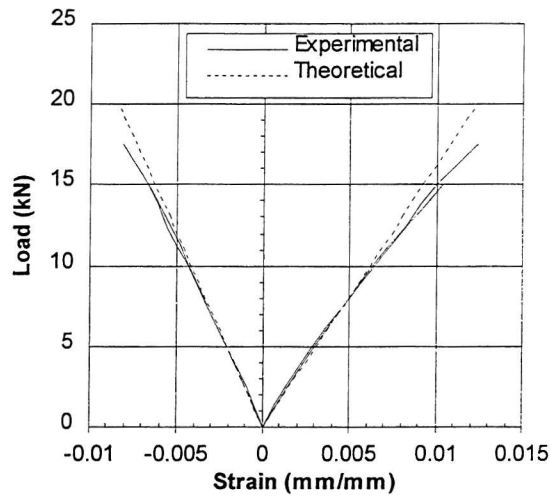
Fig. D.1.3 Continuous tensile 2" gauge
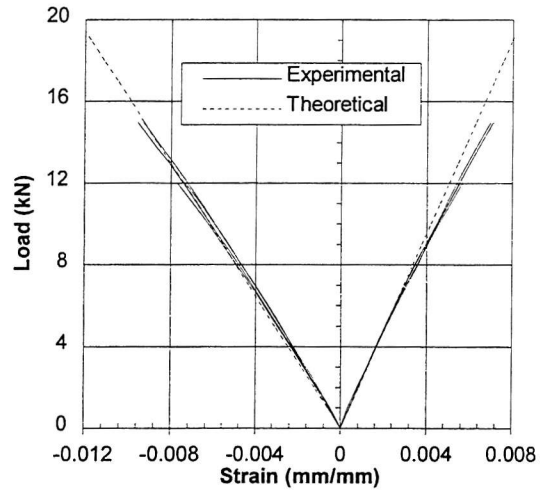
Fig. D.1.4 Continuous compression 2" gauge
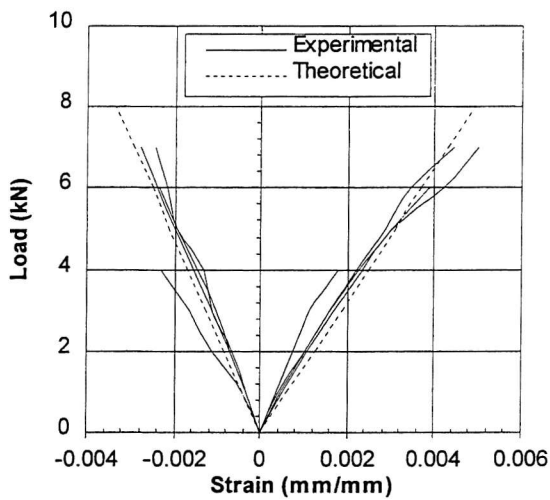
Fig. D.2.1 Scarf (M) tension 8" gauge
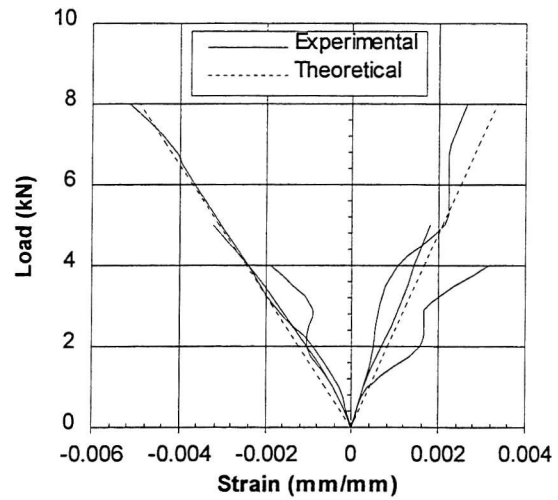
Fig. D.2.2 Scarf (M) compression 8" gauge
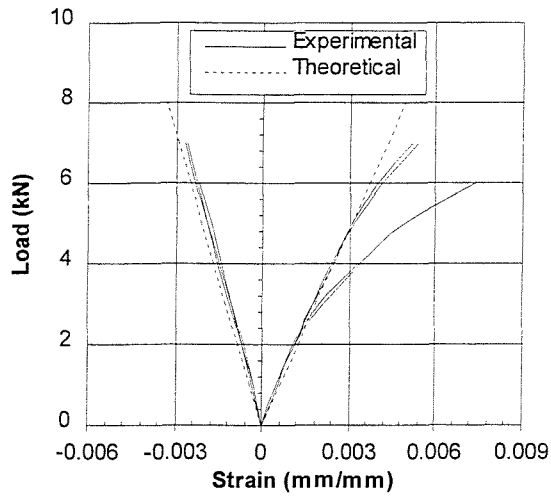
Fig. D.2.3 Scarf (M) tension 2" gauge
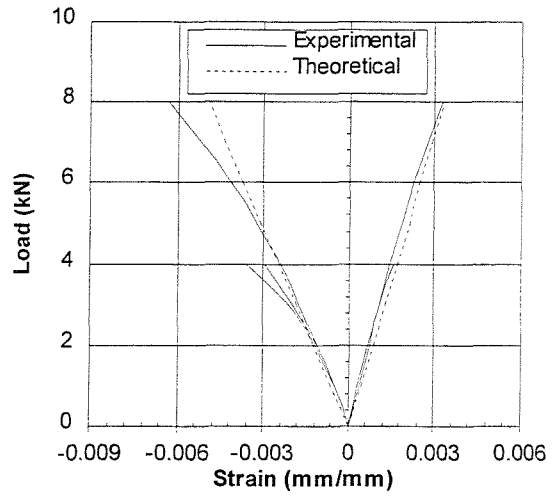
Fig. D.2.4 Scarf (M) compression 2" gauge
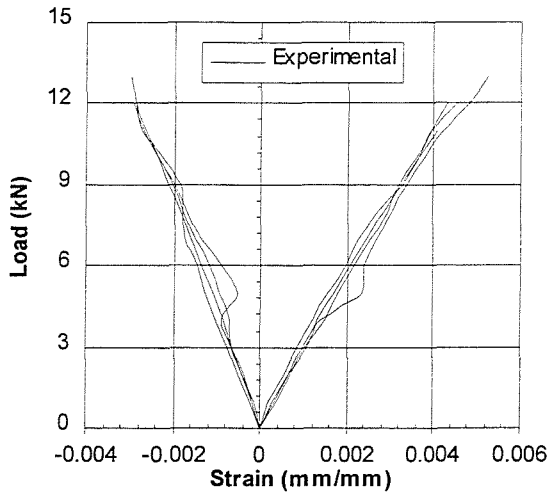
Fig. D.3.1 Tape (E) tension 8" gauge
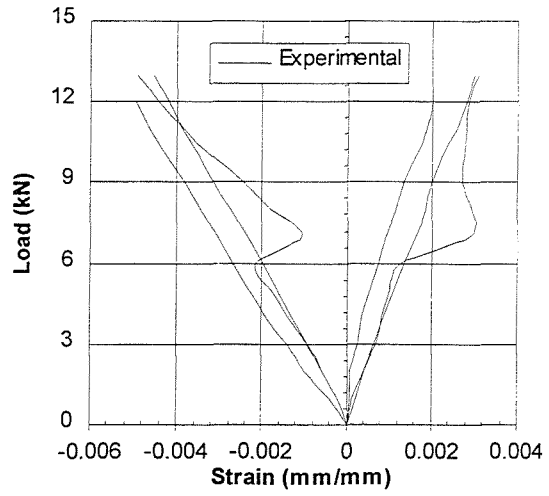
Fig. D.3.2 Tape (E) compression 8" gauge
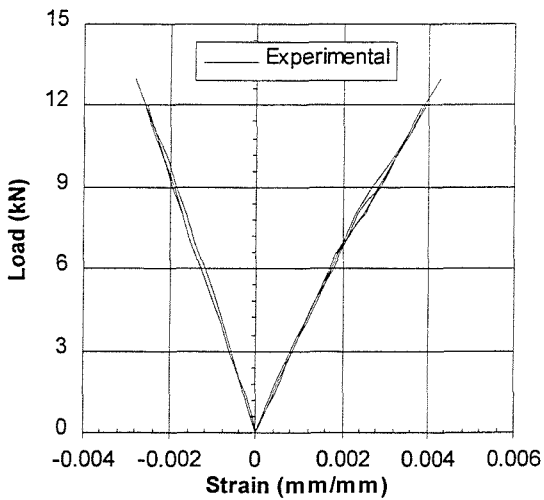
Fig. D.3.3 Tape (E) tension 2" gauge
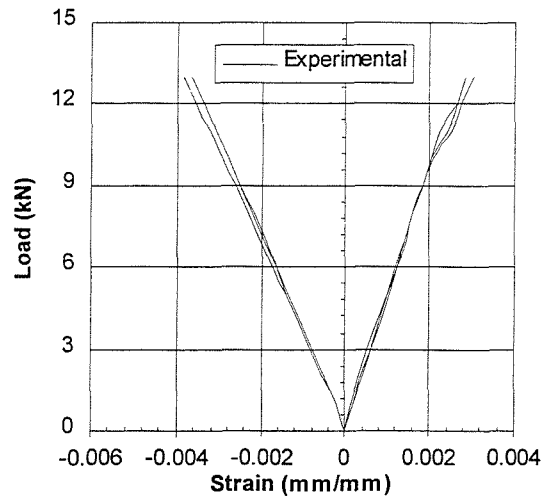
Fig. D.3.4 Tape (E) compression 2" gauge

121
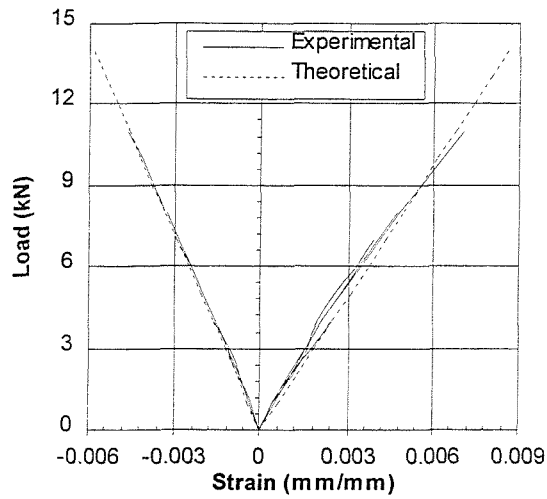
Fig. D.4.1 Scarf (E) tension 8" gauge
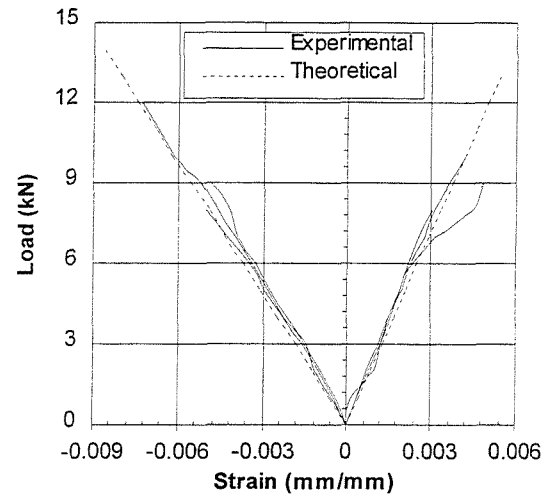
Fig. D.4.2 Scarf (E) compression 8" gauge
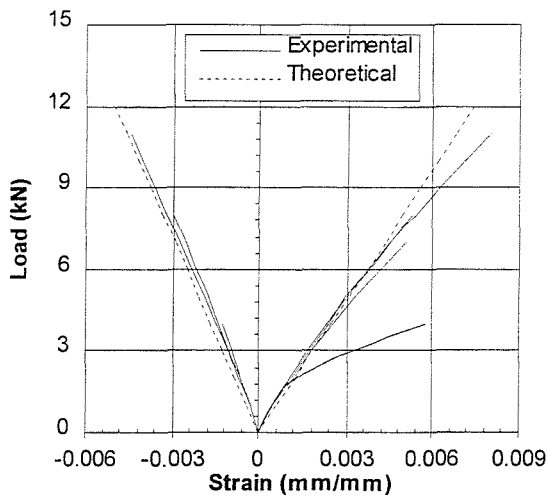
Fig. D.4.3 Scarf (E) tension 2" gauge
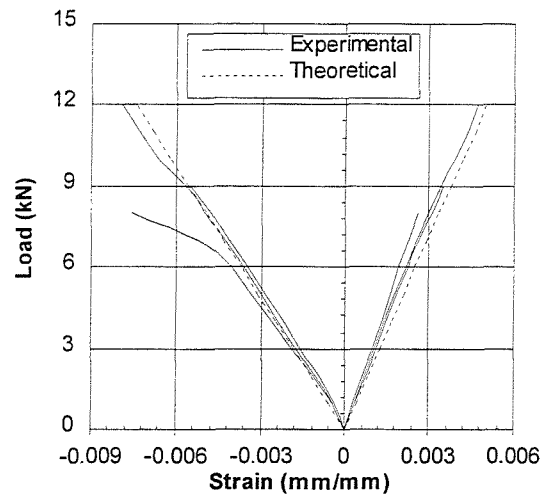
Fig. D.4.4 Scarf (E) compression 2" gauge
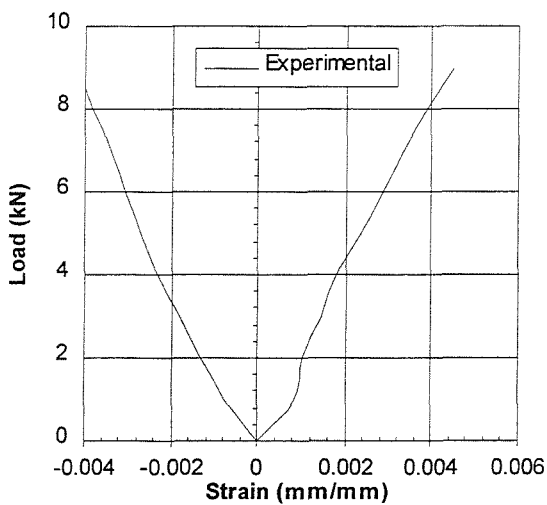
Fig. D.5.1 Spline (E) tension 8" gauge
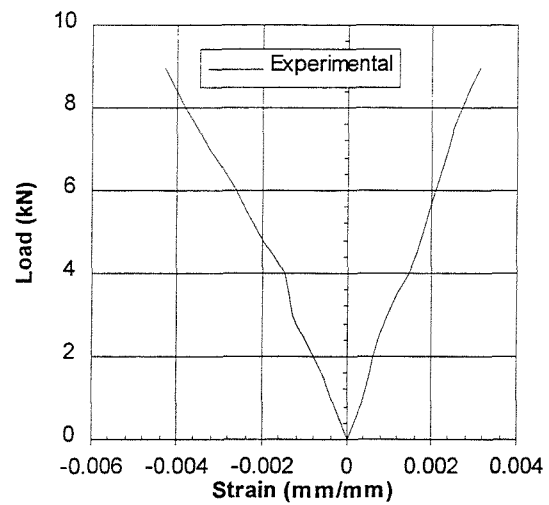
Fig. D.5.2 Spline (E) compression 8" gauge
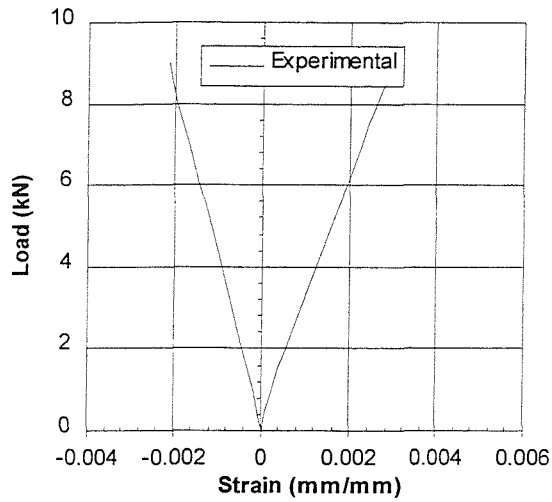
Fig. D.5.3 Spline (E) tension 2" gauge
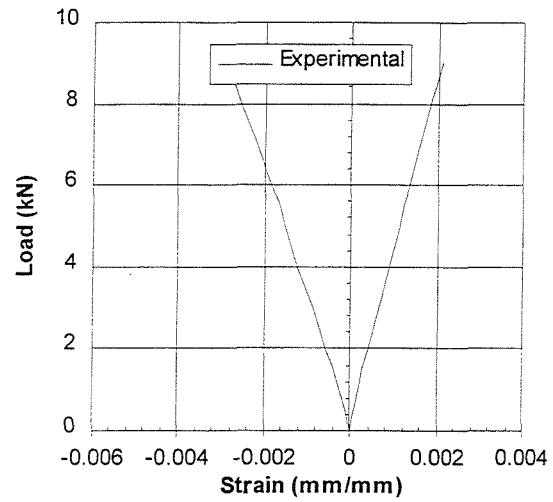
Fig. D.5.4 Spline (E) compression 2" gauge
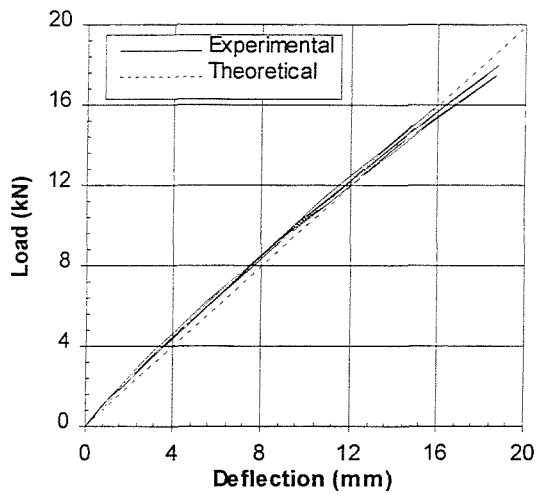
Fig. D.6.1 Continuous beam stiffness
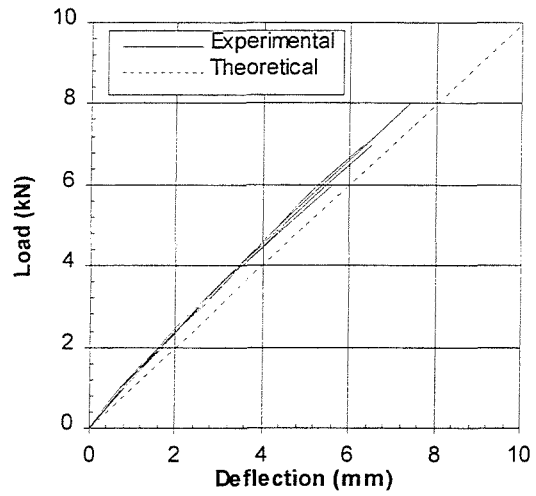
Fig. D.6.2 Scarf (E) beam stiffness
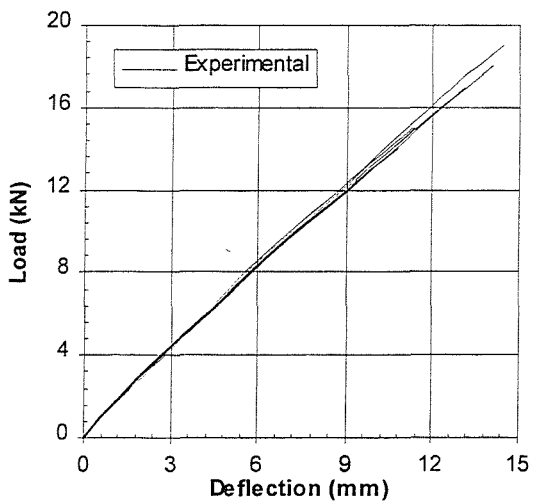
Fig. D.6.3 Tape (E) beam stiffness
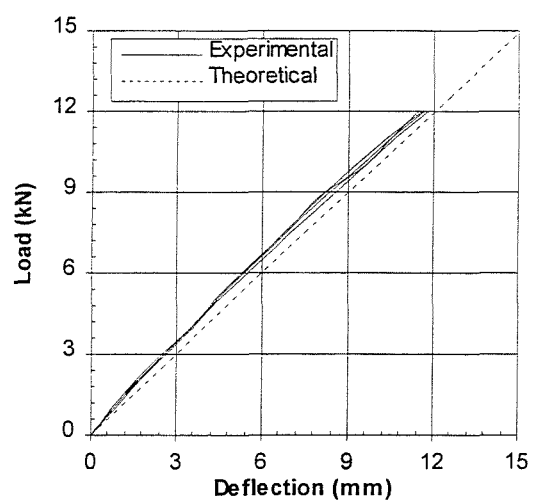
Fig. D.6.4 Scarf (E) beam stiffness

123
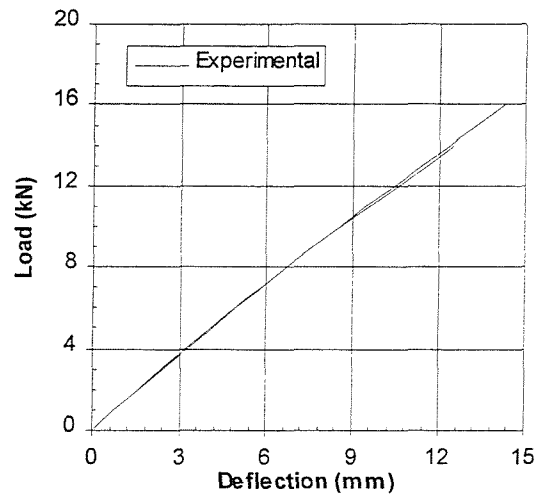
Fig. D.6.5 Spline (E) beam stiffness

The following graphs are representative of through-thickness strains measured from Demec points attached to the core material. The x-axis represents the core proper; zero denoting the core centreline and the negative value of −30 representing the core/thick skin interface. Similarly +30 represents the core/thin skin interface. Experimental determination of the neutral axis is performed by measuring the x-value assoociated with zero strain at each load increment.
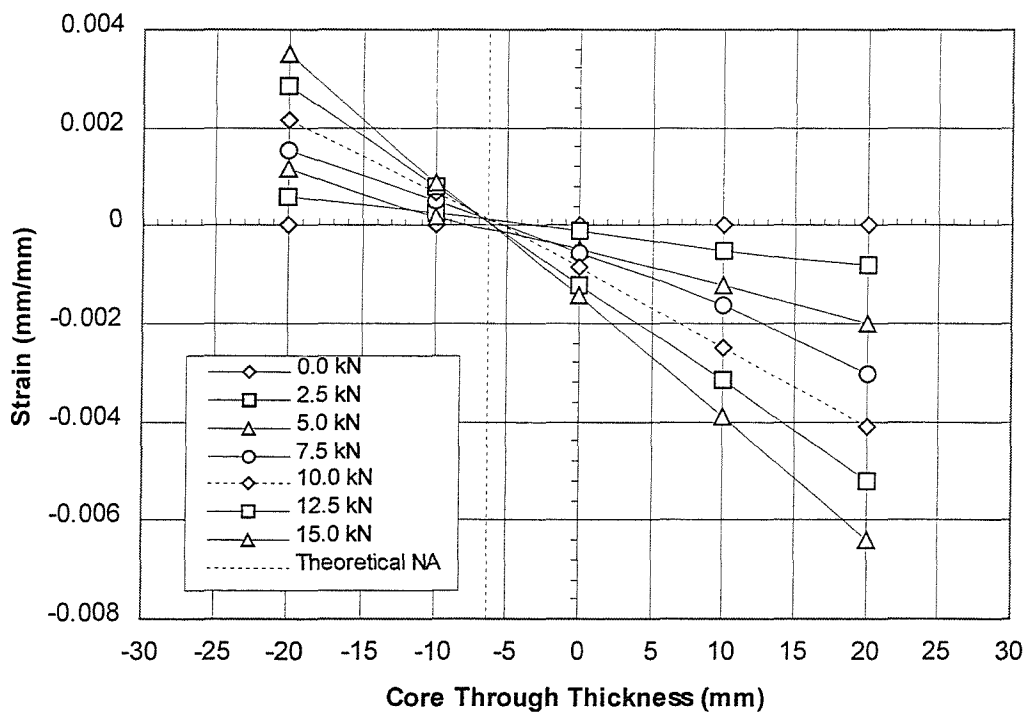
Figure D.7.1 Control specimen axial core strain associated with incremental load.

124
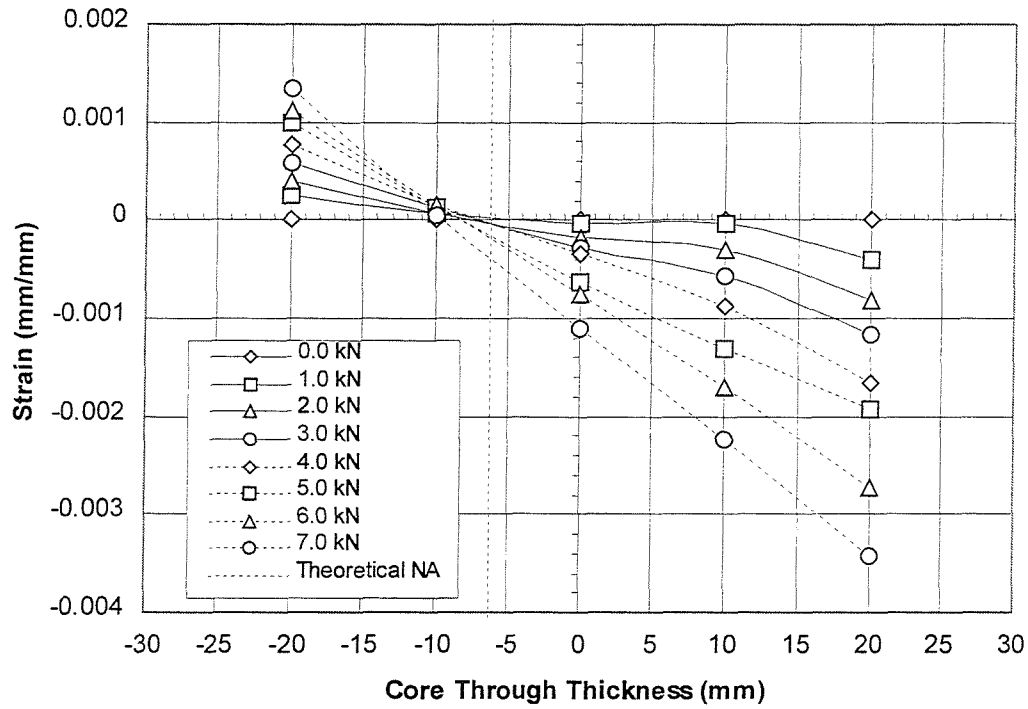
Figure D.7.2 Scarf (methacrylate) specimen axial core strain associated with incremental load.
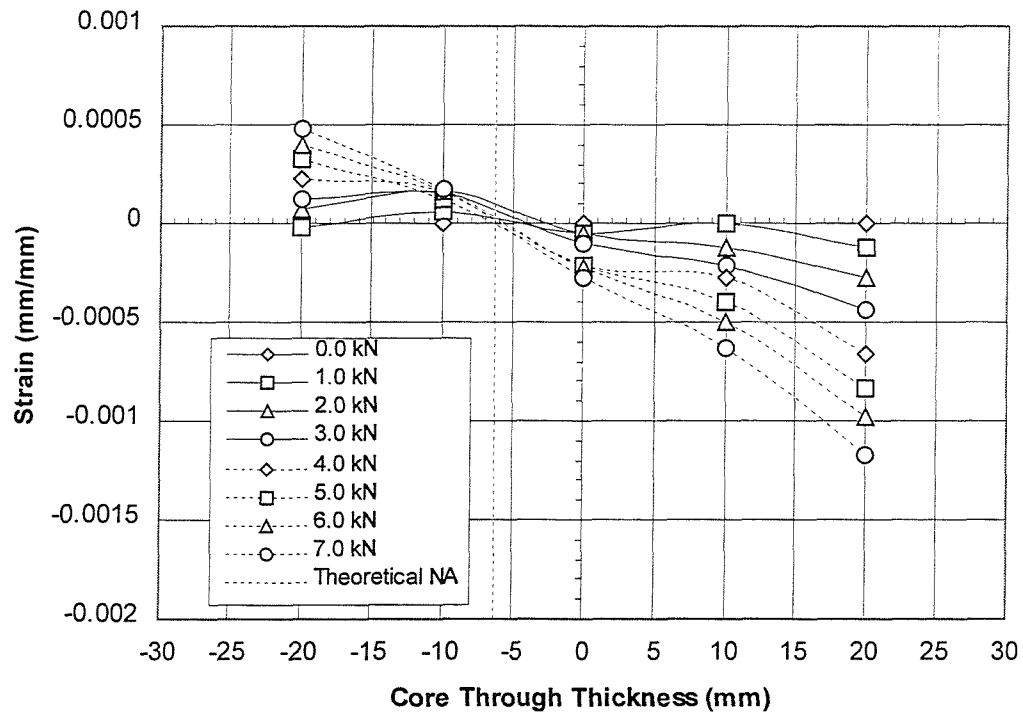
Figure D.7.3 External tape (epoxy) axial core strain associated with incremental load.

125
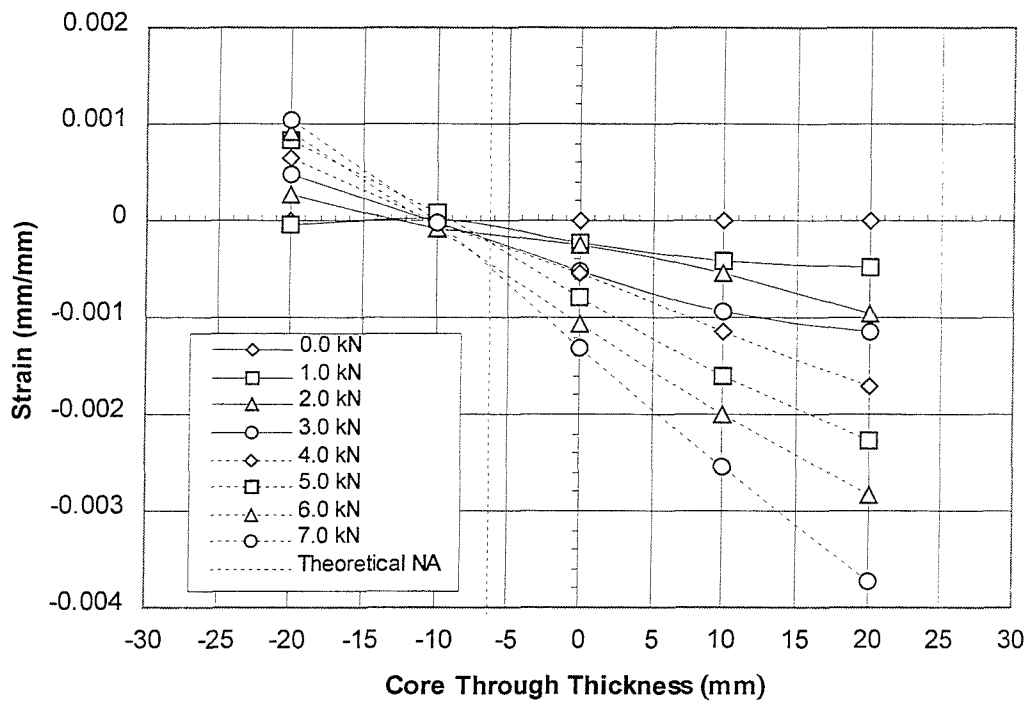
Figure D.7.4 Scarf (epoxy) axial core strain associated with incremental load.
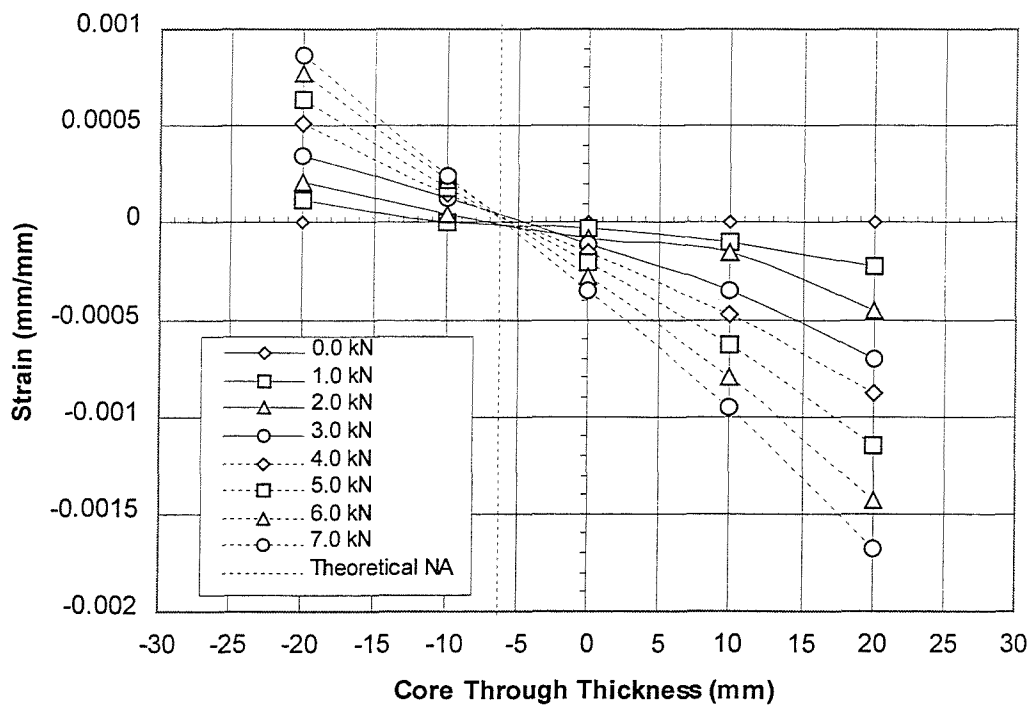
Figure D.7.5 Spline (epoxy) specimen axial core strain associated with incremental load.

APPENDIX E

Balsa Core Shear Strength

As was discussed earlier, the specimens were designed in such a way as to initiate skin, rather than core failure. For ten specimens, core shear failure initiated at loads far below that expected.

It has been documented in numerous tests by Feichtinger (1990) and Baltek (1991), that 150 kg/m^3 end-grain balsa's average shear strength is approximately 2.98 MPa. However, as can be seen from the experimental results in table E.1, the shear strength ranged from only 30-48% of this value.

Whilst these values are substantially lower than expected, some relationship with the block density was thought possible, as it was noticed that the core shear fractures were occurring in differing density balsa.

The balsa sheet is made from a select density range and averages to 150 kg/m^3, including the adhesive between blocks. Measuring the individual block range showed that a distribution from 100-200 kg/m^3 was possible.

Segments were therefore cut from the region where the shear fracture occurred, taking care not to include blocks outside this region, and the resulting distribution compared against the shear strength. The density can therefore be directly compared against the core shear strength.

Specimen	Core Shear Strength (MPa)	Density (kg/m^3)	Specimen	Core Shear Stress (MPa)	Density (kg/m^3)
C1-T-N	1.30	185	T3-T-EP	1.04	127
C2-T-N	1.42	198	T4-T-EP	1.33	179
C4-T-N	1.38	185	T5-C-EP	1.10	130
T1-T-EP	1.33	175	T7-C-EP	1.21	153
T2-T-EP	0.92	112	S5-C-EP	0.90	103

Table E.1 Experimental core shear strength and associated density.

A similar comparison of balsa shear strength, modulus and core density was first performed by Feichtinger (1986), using methods as described by ASTM C273 (1984). Two differing sets of specimens were created in order to characterise both radial and tangential growth ring orientations. This was important since balsa is a natural timber and after ripping to size, both types of end-grain patterns will exist.

From these experimental results Feichtinger proposed the following power-law and exponential descriptions of the shear strength (τ) and modulus (G) dependency on core density (ρ).

Radial growth ring orientation.

$$\tau_{LR} = 0.02081\rho^{0.9972} \tag{E.1}$$

$$G_{LR} = 72.69e^{5.953.10^{-3}\rho} \tag{E.2}$$

Tangential growth ring orientation.

$$\tau_{LT} = 0.01186\rho^{1.090} \tag{E.3}$$

$$G_{LT} = 43.66e^{7.772.10^{-3}\rho} \tag{E.4}$$

These models provided a confidence interval of greater than 99%, and were subsequently modified, allowing a single analytical model for the random growth ring orientation in the final manufactured balsa panel.

Random growth ring orientation.

$$\tau_{L} = 0.01616\rho^{1.038} \tag{E.5}$$

$$G_{L} = 54.68e^{7.023.10^{-3}\rho} \tag{E.6}$$

Still these models did not agree with the test results, implying that there existed core thickness dependency in some form.

McGeorge and Hayman (1998) had experienced similar core thickness dependency in a series of four point and panel tests, and hypothesised that bending superimposed on the shear load reduced the cores shear strength.

Their model is based on Weibull's theory (E.7) for brittle materials, showing failure stress $(\sigma_{1,2})$ dependence on loaded volume $(V_{1,2})$.

$$\frac{\sigma_1}{\sigma_2} = \left(\frac{V_2}{V_1}\right)^{\frac{1}{m}} \tag{E.7}$$

They consequently developed a reference case, determined from fitting the following correction factors and linear interaction term to experimental data.

$$f_c = \left(\frac{50}{c}\right)^{\frac{1}{3.7}} \tag{E.8}$$

$$f_i = \left(\frac{35200}{2L_b w}\right)^{\frac{1}{7.9}} \tag{E.9}$$

$$f_b = \frac{104}{27\frac{\varepsilon}{\gamma} + 87} \tag{E.10}$$

where,

$$\frac{\varepsilon}{\gamma} = \frac{L_b}{t} \frac{G_c}{E_f} \frac{c}{d} \tag{E.11}$$

Thus core correction factor, in-plane size effect and the interaction term accounting for bending gave the following model for 150 kg/m^3 balsa core shear strength.

$$\tau = 1.52 f_c f_i f_b \tag{E.12}$$

A comparison of results obtained by test fixture parameter substitution in (E.12) and the experimental data of table E.1, is shown in figure E.1. A definition of variables can be found in table E.4
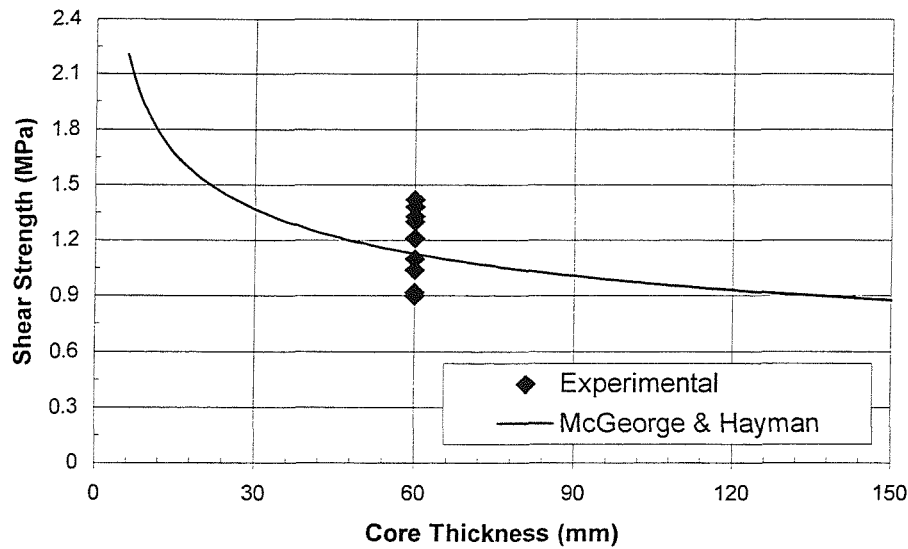
Figure E.1 Core thickness versus shear strength for nominally150 kg/m^3 balsa core.

The experimental results show reasonable correlation with (E.12), however there is still a large degree of spread. McGeorge and Hayman believed such spread to be inevitable, but is possibly attributable to block density variation in their measurements. The experimental data in figure E.1 is not for a single density as noted in table E.1, but technically is considered to be nominally 150 kg/m^3; the average of a glued 600mm x 1200mm x 1200mm block prior to machining.

If consideration is given to density variation, it is possible that substitution of Feichtinger's models for strength and modulus variation into (E.11) and (E.12), may yield a more accurate solution with less spread. Figure E.2 compares the resulting proposals with the experimental data.
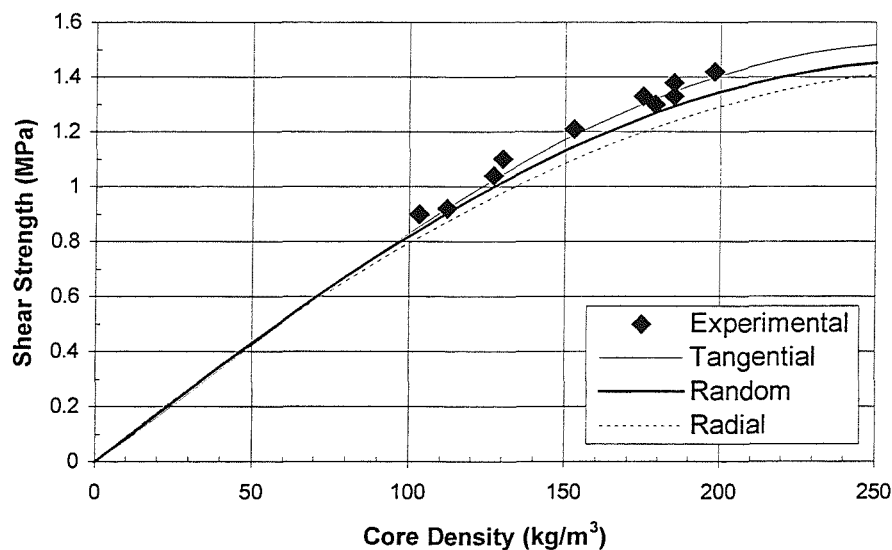
Figure E.2 Density versus shear strength for 60mm balsa core.

Excellent correlation with the tangential growth ring model is seen. The proposed semi-empirical model for balsa shear strength variation at any density can therefore be written as

$$\tau = \frac{1.52}{2.793} \cdot \left(\frac{50}{c}\right)^{1/3.7} \left(\frac{35200}{2L_b w}\right)^{1/7.9} 104 \cdot \left[27 \cdot \left(\frac{L_b}{t} \, \frac{43.66 \cdot e^{7.772.10^{-3}\rho}}{E_f} \, \frac{c}{d}\right) + 87\right]^{-1} 0.01186\rho^{1.090} \qquad (E.13)$$

Using this equation it is possible to produce three-dimensional design curves, or alternatively a contour plot as shown in figure E.3, for the parameters of table E.2.

Experimental Fixture – GRP skins

Width (w)	120 mm	Skin thickness (t)	1.2 mm	Skin NA distance (d)	61.2 mm
Modulus (E_f)	17500 MPa	Quarter span (L_b)	205 mm	Core thickness (c)*	60 mm

*Shown as ordinate variable in figure E.3.

Table E.2 Experimental constraints of four point bend tests with GRP skins.
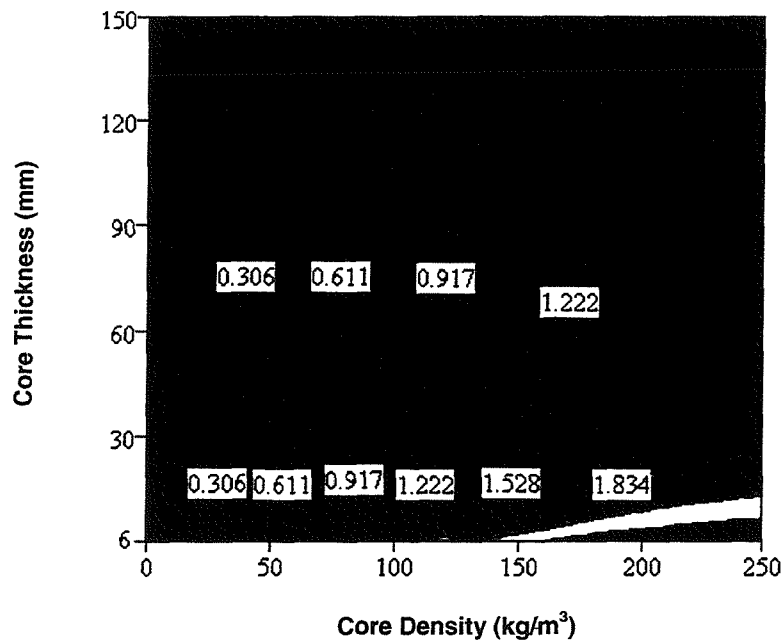
Figure E.3 Contour plot of shear strength (MPa) variation as a function of density and thickness.

Further credence for (E.13) is obtained through a comparison against aluminium skinned four point test results by Feichtinger (1990). Table E.3 compares the proposed semi-empirical model and experimental data, with the fixture parameters listed in table E.2, and permutations shown graphically in figure E.4.

Core Density	112 kg/m^3	170 kg/m^3
Experimental shear strength (Feichtinger)	2.03 MPa	3.34 MPa
Semi-empirical model (E.13)	2.04 MPa	3.16 MPa

Table E.3 Shear strength comparison of Feichtinger's test results with proposed model.

Experimental Fixture (Feichtinger) – 2024-T3 aluminium skins					
Width (w)	76 mm	Skin thickness (t)	1.5 mm	Skin NA distance (d)	14.2 mm
Modulus (E_f)	72400 MPa	Quarter span (L_b)	114.2 mm	Core thickness (c)*	12.7 mm

*Shown as ordinate variable in figure E.4.

Table E.4 Experimental constraints of Feichtinger's four point bend tests with aluminium skins.
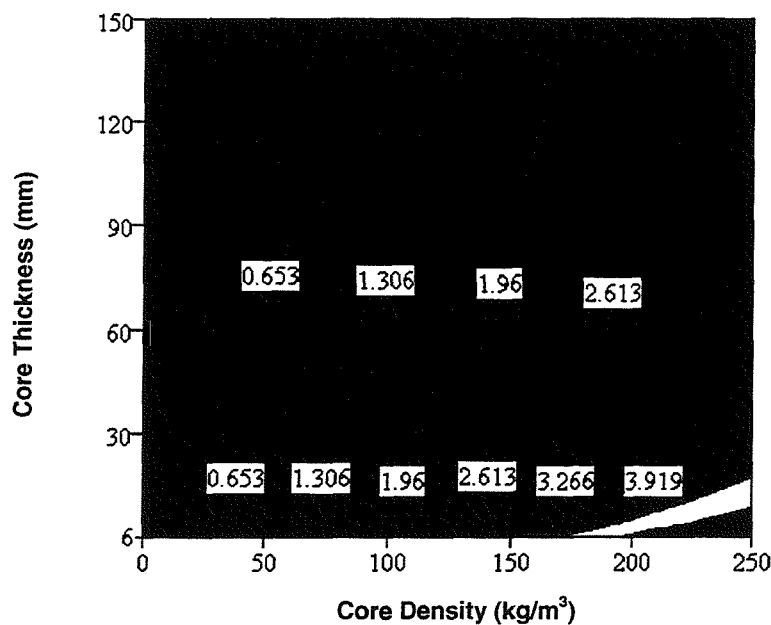
Figure E.4 Contour plot of shear strength (MPa) variation as a function of density and thickness.

The increase in skin stiffness and hence reduction of bending contribution to core stress allowed higher ultimate 'shear stresses' to be achieved. Excellent correlation with Feichtinger's results is seen in table E.4, despite the fact that all variables in (E.13) were changed.

It should be noted that McGeorge and Hayman's determination of the factors in (E.8-10) may have been changed had they corrected for the density of balsa surrounding the failure zone.

Another important point is that the contour plots are produced for a variable shear volume. The calculations are based on a combined bending and shear failure of the core, however during calculation, and particularly for thinner cores, a check must be made for skin failure.

Practical considerations must also be included in such observations, with the thinnest commercially available core being 6mm. It is interesting to note the reason behind this thickness limitation is balsa's 'brittle' nature causing block cleavage when passed through a thickness sander. Calculating the shear strength for this lower bound on core thickness using (E.13), a value of 2.28 MPa is obtained. This is of interest since the superimposed bending contribution at failure is obviously still significant when compared with the pure shear failure stress of 2.98 MPa discussed earlier.

APPENDIX F

Chen and Cheng – MathCad Plus 6.0 Program

Material Properties

$E1 := 71000$	Elastic Modulus Adherent 1
$E2 := 71000$	Elastic Modulus Adherent 2
$E3 := 2015$	Elastic Modulus Adhesive
$v1 := 0.334$	Poisson's Ratio Adherent 1
$v2 := 0.334$	Poisson's Raito Adherent 2
$v3 := 0.368$	Poisson's Ratio Adhesive

Geometric Properties

$\alpha := 0$	Scarf angle

$t := \dfrac{0.2}{\cos(\alpha)}$	Adhesive thickness parallel to load direction

$bdash := 10$	Adherent thickness perpendicular to load direction

$b := \dfrac{bdash}{\cos(\alpha)}$	Scarf interface length

$\sigma o := 200$	Applied stress

$\lambda 1 \equiv 93.24$	Stress decay coefficient

$\lambda 2 \equiv \lambda 1$	Equivalent coefficients Adherent 2 = 1

$\beta := \left[\dfrac{t}{2}\cdot\left(\dfrac{b}{\lambda 1}\right) + \left(\dfrac{b}{\lambda 1}\right)^2\right]\cdot\left[\dfrac{t}{2}\cdot\left(\dfrac{b}{\lambda 2}\right) + \left(\dfrac{b}{\lambda 2}\right)^2\right]^{-1}$	Stress constraint conditions

$A1 := \dfrac{1}{\cos(\alpha)^2}\cdot\left[\left(\dfrac{E3}{E1}\right)\cdot\dfrac{1}{2\cdot\lambda 1^5} + \left(\dfrac{E3}{E2}\right)\cdot\dfrac{\beta^2}{2\cdot\lambda 2^5} + \dfrac{1}{3}\left(\dfrac{\beta}{\lambda 2}\right)^2\cdot\left(\dfrac{t}{b}\right)^3 + \dfrac{1}{20}\left(\dfrac{t}{b}\right)^3\cdot\left(\dfrac{1}{\lambda 1} + \dfrac{\beta}{\lambda 2}\right)^2 \dots \right.$ $\left. + \left(\dfrac{t}{b}\right)\cdot\dfrac{\beta^2}{\lambda 2^4} - \dfrac{1}{4}\left(\dfrac{t}{b}\right)^3\cdot\dfrac{\beta}{\lambda 2}\cdot\left(\dfrac{1}{\lambda 1} + \dfrac{\beta}{\lambda 2}\right) + \left(\dfrac{t}{b}\right)^2\cdot\dfrac{\beta^2}{\lambda 2^3} - \dfrac{1}{3}\left(\dfrac{t}{b}\right)^2\cdot\dfrac{\beta}{\lambda 2^2}\cdot\left(\dfrac{1}{\lambda 1} + \dfrac{\beta}{\lambda 2}\right)\right]$	Energy function coefficient

$A2 := \left(\dfrac{E3}{E1}\right)\cdot\dfrac{1+v1}{\lambda 1^3} + \left(\dfrac{E3}{E2}\right)\cdot\dfrac{(1+v2)\cdot\beta^2}{\lambda 2^3} + \left(\dfrac{t}{b}\right)\cdot\dfrac{2\cdot(1+v3)\cdot\beta^2}{\lambda 2^2} - \left(\dfrac{t}{b}\right)\cdot\dfrac{2\cdot(1+v3)\cdot\beta}{\lambda 2}\cdot\left(\dfrac{1}{\lambda 1} + \dfrac{\beta}{\lambda 2}\right) \dots$ $+ \dfrac{2}{3}\cdot\left(\dfrac{t}{b}\right)\cdot(1+v3)\cdot\left(\dfrac{1}{\lambda 1} + \dfrac{\beta}{\lambda 2}\right)^2 + \left(\tan(\alpha)^2 - v3\right)\cdot\left(\dfrac{t}{b}\right)\cdot\left(\dfrac{1}{\lambda 1} + \dfrac{\beta}{\lambda 2}\right)\cdot\dfrac{\beta}{\lambda 2} \dots$ $+ -\dfrac{1}{3}\cdot\left(\tan(\alpha)^2 - v3\right)\cdot\left(\dfrac{t}{b}\right)\cdot\left(\dfrac{1}{\lambda 1} + \dfrac{\beta}{\lambda 2}\right)^2 - \left(\dfrac{E3}{E1}\right)\cdot\dfrac{\tan(\alpha)^2 - v1}{\lambda 1^3} - \left(\dfrac{E3}{E2}\right)\cdot\dfrac{\tan(\alpha)^2 - v2}{\lambda 2^3}\cdot\beta^2 \dots$ $+ 2\cdot\left(\tan(\alpha)^2 - v3\right)\cdot\left(\dfrac{1}{\lambda 1} + \dfrac{\beta}{\lambda 2}\right)\cdot\dfrac{\beta}{\lambda 2^2}$	Energy function coefficient

134

$A2 := \left(\dfrac{E3}{E1}\right) \cdot \dfrac{1+v1}{\lambda1^3} + \left(\dfrac{E3}{E2}\right) \cdot \dfrac{(1+v2)\cdot\beta^2}{\lambda2^3} + \left(\dfrac{t}{b}\right) \cdot \dfrac{2\cdot(1+v3)\cdot\beta^2}{\lambda2^2} - \left(\dfrac{t}{b}\right) \cdot \dfrac{2\cdot(1+v3)\cdot\beta}{\lambda2} \cdot \left(\dfrac{1}{\lambda1}+\dfrac{\beta}{\lambda2}\right) \dots$ $+ \dfrac{2}{3} \cdot \left(\dfrac{t}{b}\right) \cdot (1+v3) \cdot \left(\dfrac{1}{\lambda1}+\dfrac{\beta}{\lambda2}\right)^2 + \left(\tan(\alpha)^2 - v3\right) \cdot \left(\dfrac{t}{b}\right) \cdot \left(\dfrac{1}{\lambda1}+\dfrac{\beta}{\lambda2}\right) \cdot \dfrac{\beta}{\lambda2} \dots$ $+ -\dfrac{1}{3} \cdot \left(\tan(\alpha)^2 - v3\right) \cdot \left(\dfrac{t}{b}\right) \cdot \left(\dfrac{1}{\lambda1}+\dfrac{\beta}{\lambda2}\right)^2 - \left(\dfrac{E3}{E1}\right) \cdot \dfrac{\tan(\alpha)^2-v1}{\lambda1^3} - \left(\dfrac{E3}{E2}\right) \cdot \dfrac{\tan(\alpha)^2-v2}{\lambda2^3} \cdot \beta^2 \dots$ $+ 2 \cdot \left(\tan(\alpha)^2 - v3\right) \cdot \left(\dfrac{1}{\lambda1}+\dfrac{\beta}{\lambda2}\right) \cdot \dfrac{\beta}{\lambda2^2}$	Energy function coefficient
$A3 := \dfrac{1}{\cos(\alpha)^2} \cdot \left[\dfrac{E3}{E1} \cdot \dfrac{1}{2\cdot\lambda1} + \dfrac{E3}{E2} \cdot \dfrac{\beta^2}{2\cdot\lambda2} + \left(\dfrac{b}{t}\right) \cdot \left(\dfrac{1}{\lambda1}+\dfrac{\beta}{\lambda2}\right)^2 \right]$	Energy function coefficient
$A4 := \dfrac{\sigma o}{E3} \cdot \cos(\alpha) \cdot \left[\left(\dfrac{E3}{E1}\right) \cdot \dfrac{\tan(\alpha)^2-v1}{\lambda1} + \beta \cdot \left(\dfrac{E3}{E2}\right) \cdot \dfrac{\tan(\alpha)^2-v2}{\lambda2} - \left(\tan(\alpha)^2-v3\right) \cdot \left(\dfrac{1}{\lambda1}+\dfrac{\beta}{\lambda2}\right) \right]$	Energy function coefficient
$A1\cdot\gamma^4 - A2\cdot\gamma^2 + A3$	Minimisation of g
$\gamma := \begin{bmatrix} \dfrac{1}{2}\cdot\sqrt{2}\cdot\dfrac{\sqrt{A2+\sqrt{A2^2-4\cdot A1\cdot A3}}}{\sqrt{A1}} \\ \dfrac{1}{2}\cdot\sqrt{2}\cdot\dfrac{\sqrt{A2-\sqrt{A2^2-4\cdot A1\cdot A3}}}{\sqrt{A1}} \end{bmatrix}$	Quartic solution
$\gamma_0 = 58.78$	Solution roots (±)
$\gamma_1 = 58.78$	Solution roots (±)

Simultaneous Solutions for Determination of Coefficients

$k1 + k2 + k3 + k4 = \dfrac{A4}{A3}$	Boundary condition A
$k1\cdot\exp(\gamma_0\cdot1) + k2\cdot\exp(\gamma_1\cdot1) + k3\cdot\exp(-\gamma_0\cdot1) + k4\cdot\exp(-\gamma_1\cdot1) = \dfrac{A4}{A3}$	Boundary condition B
$k1\cdot\gamma_0 + k2\cdot\gamma_1 + k3\cdot-\gamma_0 + k4\cdot-\gamma_1 = 0$	Boundary condition C
$k1\cdot\gamma_0\cdot\exp(\gamma_0\cdot1) + k2\cdot\gamma_1\cdot\exp(\gamma_1\cdot1) + k3\cdot-\gamma_0\cdot\exp(-\gamma_0\cdot1) + k4\cdot-\gamma_1\cdot\exp(-\gamma_1\cdot1) = 0$	Boundary condition D
$A := \begin{bmatrix} 1 & 1 & 1 & 1 \\ \exp(\gamma_0\cdot1) & \exp(\gamma_1\cdot1) & \exp(-\gamma_0\cdot1) & \exp(-\gamma_1\cdot1) \\ \gamma_0 & \gamma_1 & -\gamma_0 & -\gamma_1 \\ \gamma_0\cdot\exp(\gamma_0\cdot1) & \gamma_1\cdot\exp(\gamma_1\cdot1) & -\gamma_0\cdot\exp(-\gamma_0\cdot1) & -\gamma_1\cdot\exp(-\gamma_1\cdot1) \end{bmatrix}$	Coefficient matrix

135

$B := \begin{bmatrix} \dfrac{A4}{A3} \\ \dfrac{A4}{A3} \\ 0 \\ 0 \end{bmatrix}$	Result matrix

$k := A^{-1} \cdot B$	Matrix coefficient solution

Base function determination

$\sigma 1(x) := \left(k_0 \cdot \exp\left(\gamma_0 \cdot \dfrac{x}{b} \right) + k_1 \cdot \exp\left(\gamma_1 \cdot \dfrac{x}{b} \right) + k_2 \cdot \exp\left(-\gamma_0 \cdot \dfrac{x}{b} \right) + k_3 \cdot \exp\left(-\gamma_1 \cdot \dfrac{x}{b} \right) - \dfrac{A4}{A3} \right) \cdot E3$	Base function

$\sigma d1(x) := \left(k_0 \cdot \dfrac{\gamma_0}{b} \cdot \exp\left(\gamma_0 \cdot \dfrac{x}{b} \right) + k_1 \cdot \dfrac{\gamma_1}{b} \cdot \exp\left(\gamma_1 \cdot \dfrac{x}{b} \right) - k_2 \cdot \dfrac{\gamma_0}{b} \cdot \exp\left(-\gamma_0 \cdot \dfrac{x}{b} \right) - k_3 \cdot \dfrac{\gamma_1}{b} \cdot \exp\left(-\gamma_1 \cdot \dfrac{x}{b} \right) \right) \cdot E3$	First derivative

$\sigma dd1(x) := \left[k_0 \cdot \dfrac{(\gamma_0)^2}{b^2} \cdot \exp\left(\gamma_0 \cdot \dfrac{x}{b} \right) + k_1 \cdot \dfrac{(\gamma_1)^2}{b^2} \cdot \exp\left(\gamma_1 \cdot \dfrac{x}{b} \right) + k_2 \cdot \dfrac{(\gamma_0)^2}{b^2} \cdot \exp\left(-\gamma_0 \cdot \dfrac{x}{b} \right) + k_3 \cdot \dfrac{(\gamma_1)^2}{b^2} \cdot \exp\left(-\gamma_1 \cdot \dfrac{x}{b} \right) \right] \cdot E3$	Second derivative

Adherent and adhesive stress profiles

$x := 0, 0.01 .. b$	Scarf solution steps – 0.01 mm increments

$\sigma x1(x,y) := \sigma 1(x) \cdot \exp\left(-\lambda 1 \cdot \dfrac{y}{b} \right)$	Adherent 1 stress profile – parallel to scarf inclination

$\sigma 2(x) := \beta \cdot \sigma 1(x)$	Adherent interaction equation

$\sigma x2(x,y) := \sigma 2(x) \cdot \exp\left(-\lambda 2 \cdot \dfrac{y}{b} \right)$	Adherent 2 stress profile – parallel to scarf inclination

$\sigma y1(x,y) := \left(\dfrac{b}{\lambda 1} \right)^2 \cdot \sigma dd1(x) \cdot \exp\left[-\lambda 1 \cdot \left(\dfrac{y}{b} \right) \right] + \sigma o \cdot \cos(\alpha)$	Adherent 1 stress profile

$\sigma dd2(x) := \beta \cdot \sigma dd1(x)$	Adherent interaction equation

$\sigma y2(x,y) := \left(\dfrac{b}{\lambda 1} \right)^2 \cdot \sigma dd2(x) \cdot \exp\left[-\lambda 1 \cdot \left(\dfrac{y}{b} \right) \right] + \sigma o \cdot \cos(\alpha)$	Adherent 2 stress profile

$\tau xy1(x,y) := \dfrac{b}{\lambda 1} \cdot \sigma d1(x) \cdot \exp\left[-\lambda 1 \cdot \left(\dfrac{y}{b} \right) \right]$	Adherent 1 rectlinear shear stress (no physical meaning)

$\sigma d2(x) := \beta \cdot \sigma d1(x)$	Adherent interaction equation

$\tau xy2(x,y) := \dfrac{b}{\lambda 2} \cdot \sigma d2(x) \cdot \exp\left[-\lambda 1 \cdot \left(\dfrac{y}{b} \right) \right]$	Adherent 2 rectlinear shear stress

136

$\sigma x3(x,y) := -\dfrac{1}{t}\left[\left(\dfrac{b}{\lambda 1}\right)\cdot\sigma 1(x) + \left(\dfrac{b}{\lambda 2}\right)\cdot\sigma 2(x)\right]$	Adhesive stress profile

$\sigma y3(x,y) := y\cdot\left(\dfrac{b}{\lambda 2}\right)\cdot\sigma dd2(x) - \dfrac{y^2}{2\cdot t}\cdot\left[\left(\dfrac{b}{\lambda 1}\right)\cdot\sigma dd1(x) + \dfrac{b}{\lambda 2}\cdot\sigma dd2(x)\right] + \left(\dfrac{b}{\lambda 2}\right)^2\cdot\sigma dd2(x) + \sigma o\cdot\cos(\alpha)$	Adhesive stress profile

$\tau xy3(x,y) := -\left(\dfrac{b}{\lambda 2}\right)\cdot\sigma d2(x) + \dfrac{y}{t}\cdot\left[\left(\dfrac{b}{\lambda 1}\right)\cdot\sigma d1(x) + \left(\dfrac{b}{\lambda 2}\right)\cdot\sigma d2(x)\right]$	Adhesive rectlinear shear

Normalised peel stresses

$\sigma y0(x,y) := \dfrac{\sigma y1(x,y)\cdot\cos(\alpha)}{\sigma o}$	Adherent 1 (y=0 at interface)

$\sigma y00(x,y) := \dfrac{\sigma y2(x,y)\cdot\cos(\alpha)}{\sigma o}$	Adherent 2 (y=0 at interface)

$\sigma y000(x,y) := \dfrac{\sigma y3(x,y)\cdot\cos(\alpha)}{\sigma o}$	Adhesive (y=t/2 at centre)

Normalised shear stresses

$\tau xy0(x,y) := \dfrac{\tau xy1(x,y) + \sigma y1(x,y)\cdot\sin(\alpha)}{\sigma o}$	Adherent 1 (y=0 at interface)

$\tau xy00(x,y) := \dfrac{\tau xy2(x,y) + \sigma y2(x,y)\cdot\sin(\alpha)}{\sigma o}$	Adherent 2 (y=0 at interface)

$\tau xy000(x,y) := \dfrac{\tau xy3(x,y) + \sigma y3(x,y)\cdot\sin(\alpha)}{\sigma o}$	Adhesive (y=t/2 at centre)

Data written to output file

Ref. Chen and Cheng (1990) for further specific detail.

Decay coefficient and energy direct search program for minimum determination overleaf.

137

$$S(\text{mesh}, \lambda 1) := \begin{array}{|l}
\text{count} \leftarrow 0 \\
\text{for } j \in 1 .. \text{mesh} \\
\quad \begin{array}{|l}
\beta \leftarrow \left[\dfrac{t}{2} \cdot \left(\dfrac{b}{\lambda 1} \right) + \left(\dfrac{b}{\lambda 1} \right)^2 \right] \cdot \left[\dfrac{t}{2} \cdot \left(\dfrac{b}{\lambda 1} \right) + \left(\dfrac{b}{\lambda 1} \right)^2 \right]^{-1} \\[4mm]
A1 \leftarrow \dfrac{1}{\cos(\alpha)^2} \cdot \left[\left(\dfrac{E3}{E1} \right) \cdot \dfrac{1}{2 \cdot \lambda 1^5} + \left(\dfrac{E3}{E2} \right) \cdot \dfrac{\beta^2}{2 \cdot \lambda 1^5} + \dfrac{1}{3} \cdot \left(\dfrac{\beta}{\lambda 1} \right)^2 \cdot \left(\dfrac{t}{b} \right)^3 + \dfrac{1}{20} \cdot \left(\dfrac{t}{b} \right)^3 \cdot \left(\dfrac{1}{\lambda 1} + \dfrac{\beta}{\lambda 1} \right)^2 \cdots \right. \\
\qquad \left. + \left(\dfrac{t}{b} \right) \cdot \dfrac{\beta^2}{\lambda 1^4} - \dfrac{1}{4} \cdot \left(\dfrac{t}{b} \right)^3 \cdot \dfrac{\beta}{\lambda 1} \cdot \left(\dfrac{1}{\lambda 1} + \dfrac{\beta}{\lambda 1} \right) + \left(\dfrac{t}{b} \right)^2 \cdot \dfrac{\beta^2}{\lambda 1^3} - \dfrac{1}{3} \cdot \left(\dfrac{t}{b} \right)^2 \cdot \dfrac{\beta}{\lambda 1^2} \cdot \left(\dfrac{1}{\lambda 1} + \dfrac{\beta}{\lambda 1} \right) \right] \\[4mm]
A2 \leftarrow \left(\dfrac{E3}{E1} \right) \dfrac{1+v1}{\lambda 1^3} + \left(\dfrac{E3}{E2} \right) \cdot \dfrac{(1+v2) \cdot \beta^2}{\lambda 1^3} + \left(\dfrac{t}{b} \right) \cdot \dfrac{2 \cdot (1+v3) \cdot \beta^2}{\lambda 1^2} - \left(\dfrac{t}{b} \right) \cdot \dfrac{2 \cdot (1+v3) \cdot \beta}{\lambda 1} \cdot \left(\dfrac{1}{\lambda 1} + \dfrac{\beta}{\lambda 1} \right) \cdots \\
\qquad + \dfrac{2}{3} \cdot \left(\dfrac{t}{b} \right) \cdot (1+v3) \cdot \left(\dfrac{1}{\lambda 1} + \dfrac{\beta}{\lambda 1} \right)^2 + \left(\tan(\alpha)^2 - v3 \right) \cdot \left(\dfrac{t}{b} \right) \cdot \left(\dfrac{1}{\lambda 1} + \dfrac{\beta}{\lambda 1} \right) \cdot \dfrac{\beta}{\lambda 1} \cdots \\
\qquad + -\dfrac{1}{3} \cdot \left(\tan(\alpha)^2 - v3 \right) \cdot \left(\dfrac{t}{b} \right) \cdot \left(\dfrac{1}{\lambda 1} + \dfrac{\beta}{\lambda 1} \right)^2 - \left(\dfrac{E3}{E1} \right) \cdot \dfrac{\tan(\alpha)^2 - v1}{\lambda 1^3} - \left(\dfrac{E3}{E2} \right) \cdot \dfrac{\tan(\alpha)^2 - v2}{\lambda 1^3} \cdot \beta^2 \cdots \\
\qquad + 2 \cdot \left(\tan(\alpha)^2 - v3 \right) \cdot \left(\dfrac{1}{\lambda 1} + \dfrac{\beta}{\lambda 1} \right) \cdot \dfrac{\beta}{\lambda 1^2} \\[4mm]
A3 \leftarrow \dfrac{1}{\cos(\alpha)^2} \cdot \left[\dfrac{E3}{E1} \dfrac{1}{2 \cdot \lambda 1} + \dfrac{E3}{E2} \dfrac{\beta^2}{2 \cdot \lambda 1} + \left(\dfrac{b}{t} \right) \cdot \left(\dfrac{1}{\lambda 1} + \dfrac{\beta}{\lambda 1} \right)^2 \right] \\[4mm]
A4 \leftarrow \dfrac{\sigma o}{E3} \cdot \cos(\alpha) \cdot \left[\left(\dfrac{E3}{E1} \right) \cdot \dfrac{\tan(\alpha)^2 - v1}{\lambda 1} + \beta \cdot \left(\dfrac{E3}{E2} \right) \cdot \dfrac{\tan(\alpha)^2 - v2}{\lambda 1} - \left(\tan(\alpha)^2 - v3 \right) \cdot \left(\dfrac{1}{\lambda 1} + \dfrac{\beta}{\lambda 1} \right) \right] \\[4mm]
\gamma_0 \leftarrow \dfrac{1}{2} \cdot \sqrt{2} \cdot \dfrac{\sqrt{A2 + \sqrt{A2^2 - 4 \cdot A1 \cdot A3}}}{\sqrt{A1}} \\[4mm]
\gamma_1 \leftarrow \dfrac{1}{2} \cdot \sqrt{2} \cdot \dfrac{\sqrt{A2 - \sqrt{A2^2 - 4 \cdot A1 \cdot A3}}}{\sqrt{A1}} \\[4mm]
A \leftarrow \begin{bmatrix} 1 & 1 & 1 & 1 \\ \exp(\gamma_0 \cdot 1) & \exp(\gamma_1 \cdot 1) & \exp(-\gamma_0 \cdot 1) & \exp(-\gamma_1 \cdot 1) \\ \gamma_0 & \gamma_1 & -\gamma_0 & -\gamma_1 \\ \gamma_0 \cdot \exp(\gamma_0 \cdot 1) & \gamma_1 \cdot \exp(\gamma_1 \cdot 1) & -\gamma_0 \cdot \exp(-\gamma_0 \cdot 1) & -\gamma_1 \cdot \exp(-\gamma_1 \cdot 1) \end{bmatrix} \\[6mm]
B \leftarrow \begin{bmatrix} \dfrac{A4}{A3} \\ \dfrac{A4}{A3} \\ 0 \\ 0 \end{bmatrix} \\[6mm]
k \leftarrow A^{-1} \cdot B \\[3mm]
V \leftarrow \dfrac{1}{2} \cdot E3 \cdot b^2 \cdot \cos(\alpha) \cdot \displaystyle\int_0^1 A4 \cdot \left(k_0 \cdot \exp(\gamma_0 \cdot \xi) + k_1 \cdot \exp(\gamma_1 \cdot \xi) + k_2 \cdot \exp(-\gamma_0 \cdot \xi) + k_3 \cdot \exp(-\gamma_1 \cdot \xi) - \dfrac{A4}{A3} \right) d\xi \\[3mm]
c^{\langle \text{count} \rangle} \leftarrow \begin{pmatrix} V \\ \lambda 1 \end{pmatrix} \\[3mm]
\lambda 1 \leftarrow \lambda 1 + 1 \\
\text{count} \leftarrow \text{count} + 1
\end{array} \\
c^T
\end{array}$$

APPENDIX G

Scarf – Tension Decay Coefficients & Stress Profiles

Scarf Angle	Adherent Thickness				
	1mm	2mm	3mm	10mm	25.4mm
30°	52.00/28.39	62.00/32.51	72.00/36.90	143.79/65.47	301.50/128.90
45°	46.50/26.13	55.80/30.16	65.10/34.00	130.20/62.54	273.46/122.20
60°	40.20/23.50	48.70/27.30	56.40/30.90	112.53/55.50	235.56/110.02
75°	34.90/21.08	42.60/24.89	49.60/28.32	99.12/52.25	207.88/105.10
90° (Butt)	32.70/20.20	40.20/24.00	46.70/27.30	93.31/51.25	195.66/104.10

Table G.1. Aluminium/Quasi-isotropic composite adherent decay coefficients.
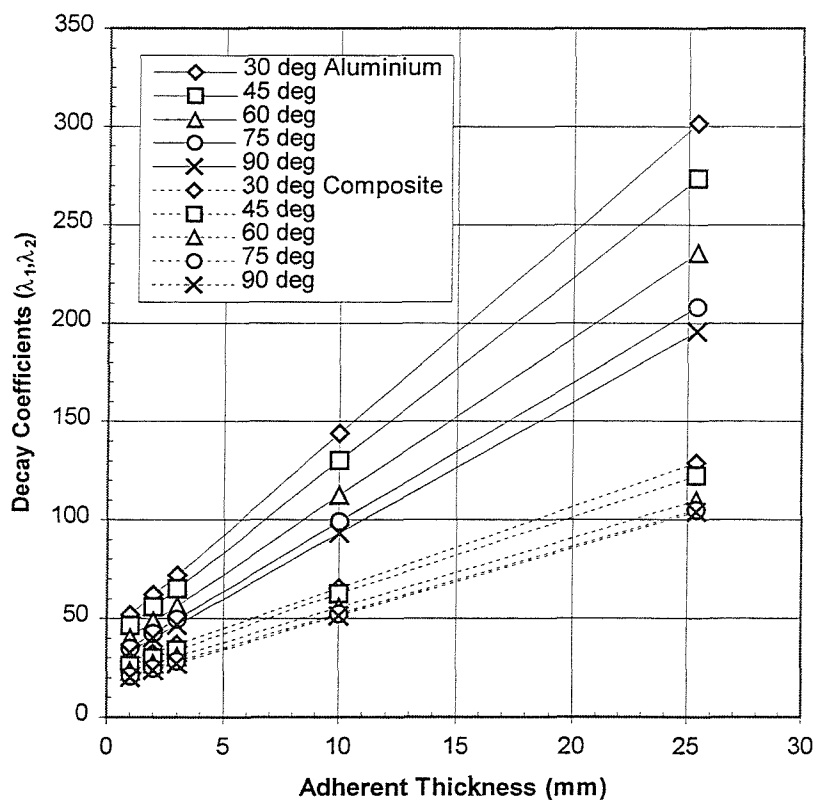
Figure G.1 Aluminium and composite decay coefficient variation.

Figures G.2.a-16.b overleaf demonstrate the normalised tip stress profiles for the scarf joint based on the decay coefficients of table G.1.
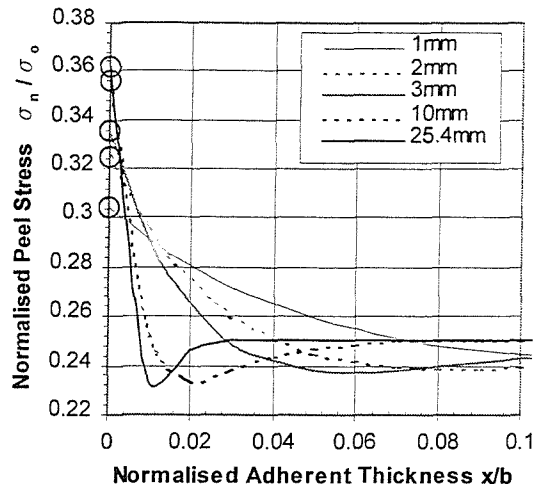
Fig. G.2a Aluminium 30° scarf
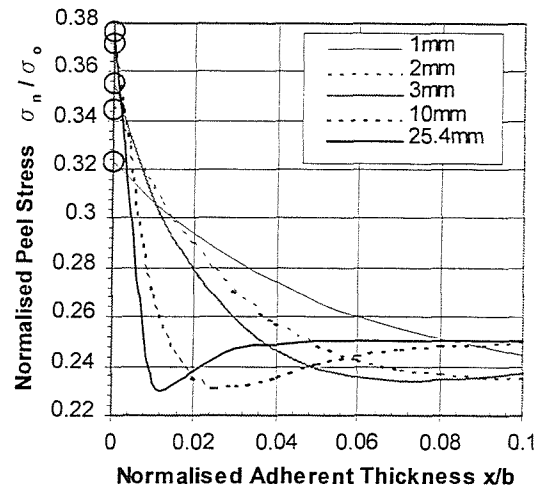
Fig. G.2b Composite 30° scarf
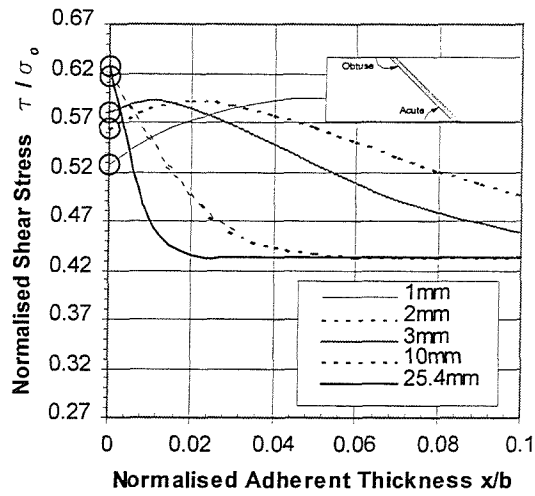
Fig. G.3a Aluminium 30° scarf – acute tip
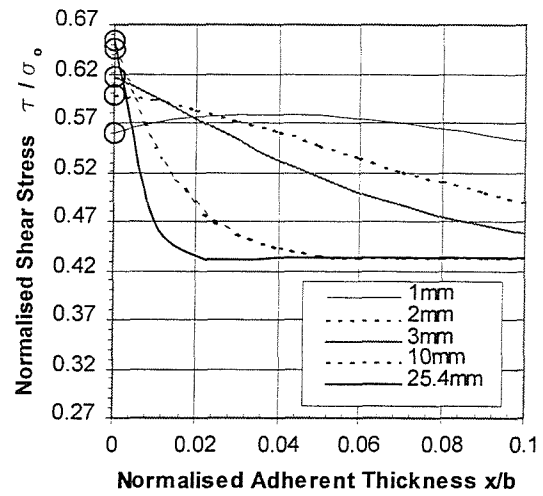
Fig. G.3b Composite 30° scarf – acute tip
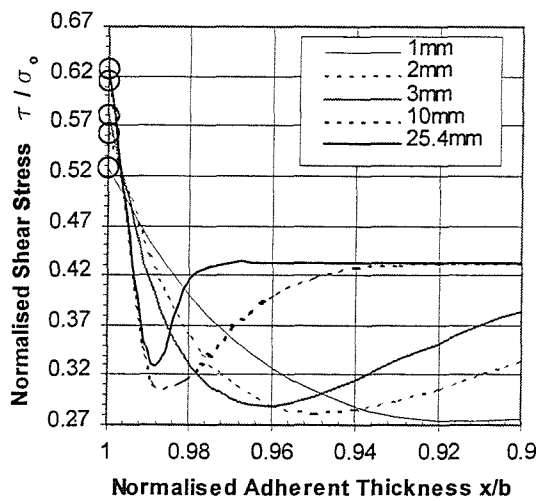
Fig. G.4a Aluminium 30° scarf – obtuse tip
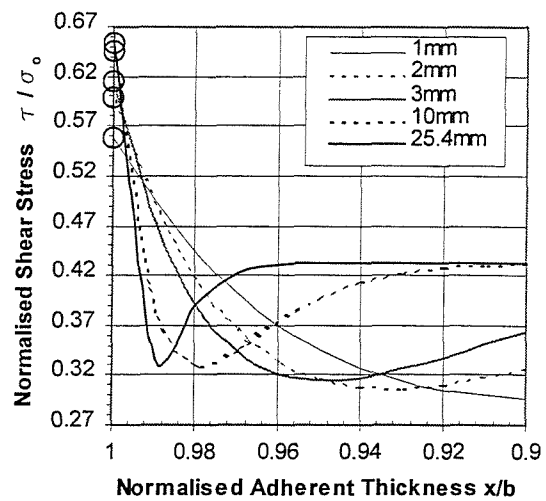
Fig. G.4b Composite 30° scarf – obtuse tip

140
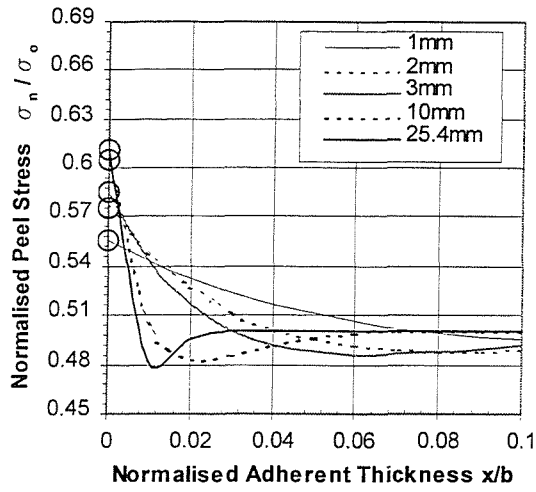
Fig. G.5a Aluminium 45° scarf
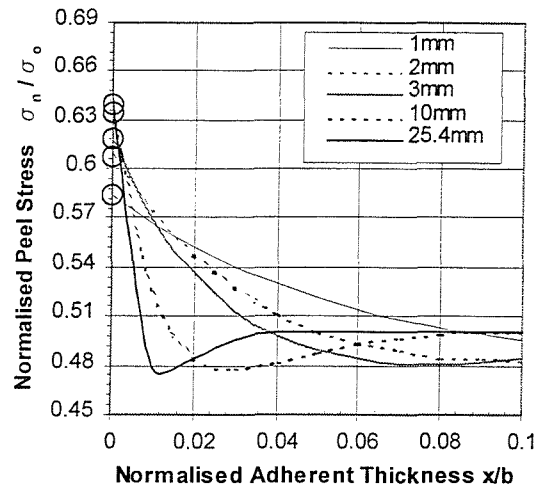
Fig. G.5b Composite 45° scarf
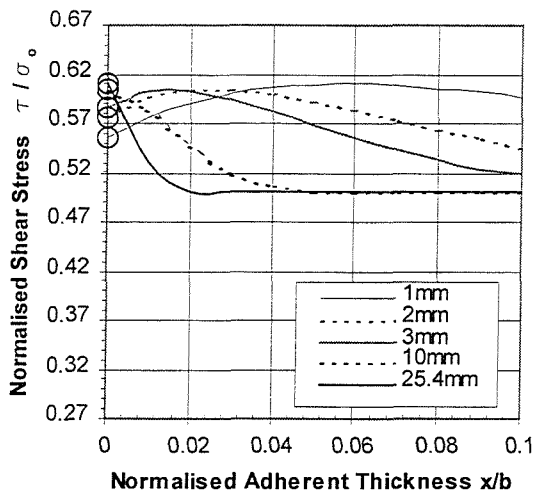
Fig. G.6a Aluminium 45° scarf – acute tip
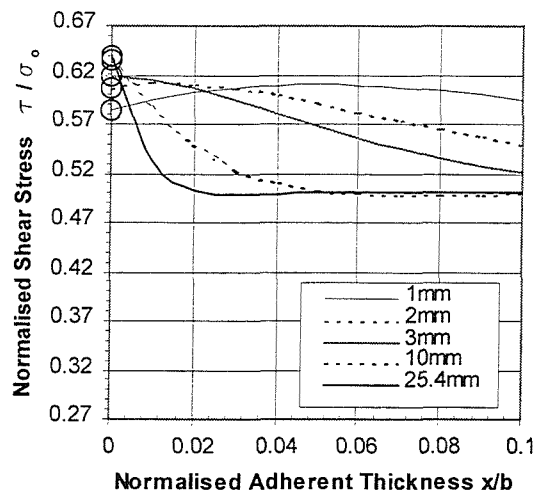
Fig. G.6b Composite 45° scarf – acute tip
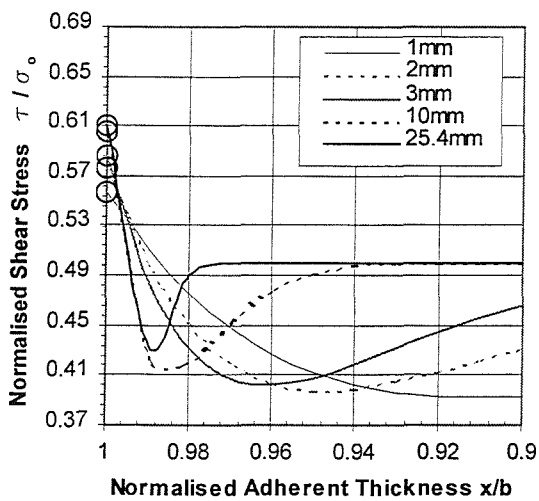
Fig. G.7a Aluminium 45° scarf – obtuse tip
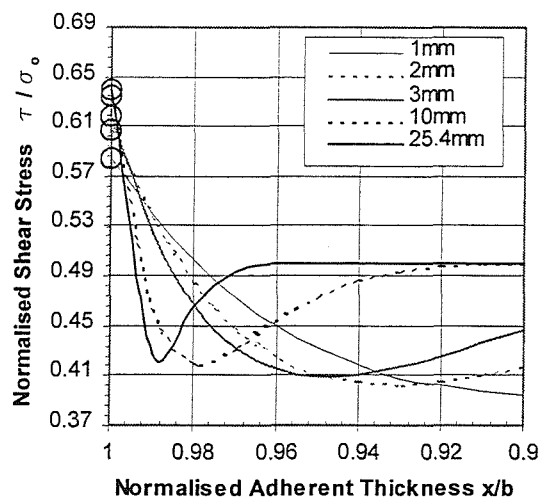
Fig. G.7b Composite 45° scarf – obtuse tip

141
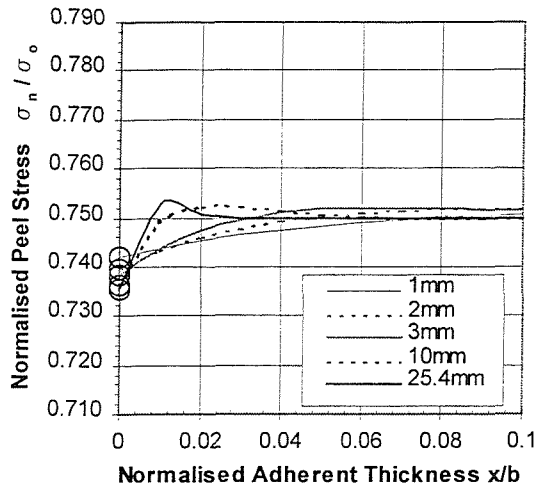
Fig. G.8a Aluminium 60° scarf
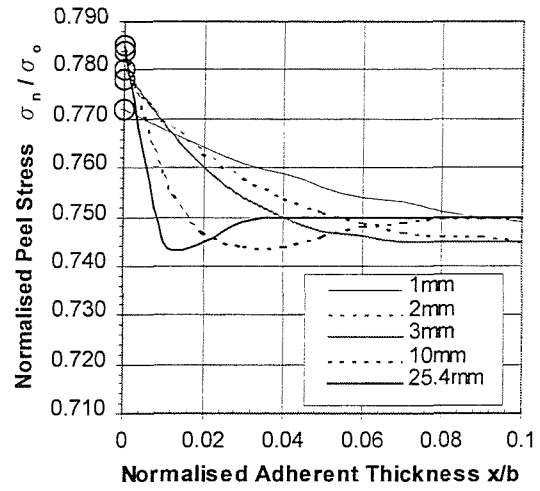
Fig. G.8b. Composite 60° scarf
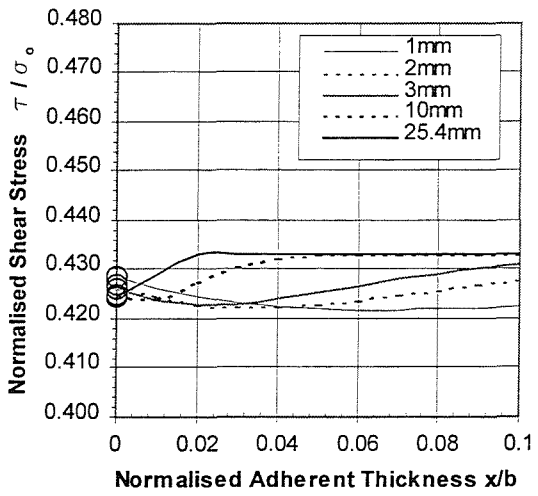
Fig. G.9a Aluminium 60° scarf – acute tip
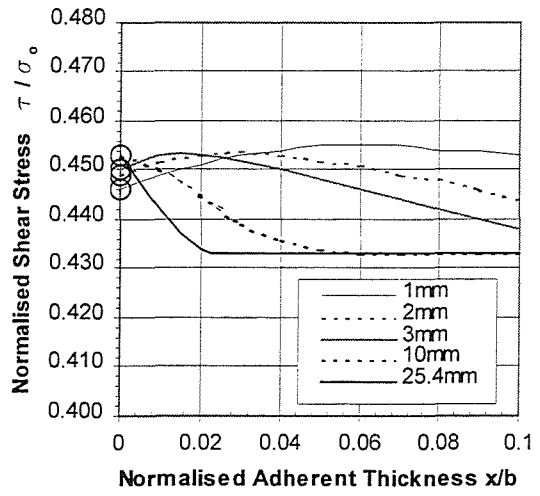
Fig. G.9b Composite 60° scarf – acute tip
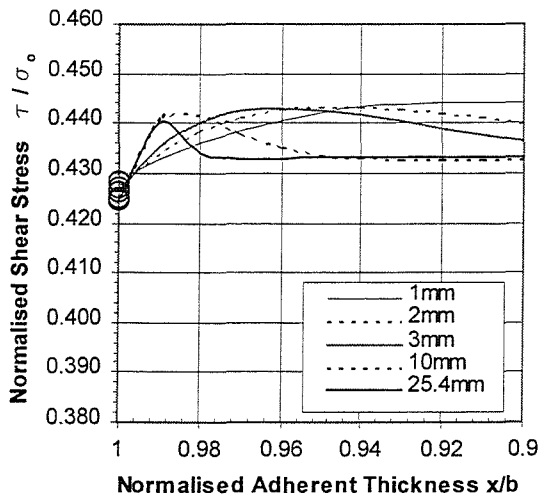
Fig. G.10a Aluminium 60° scarf – obtuse tip
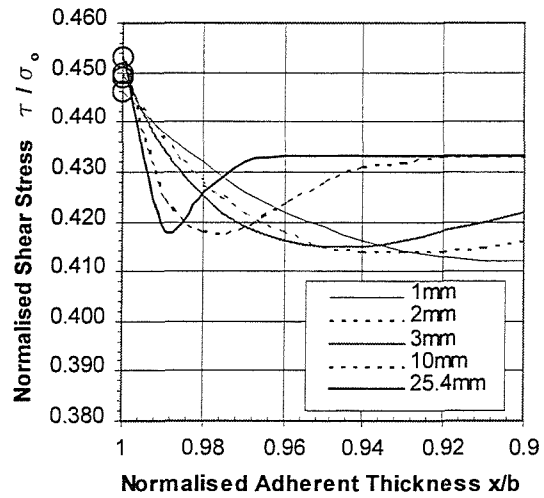
Fig. G.10b Composite 60° scarf – obtuse tip
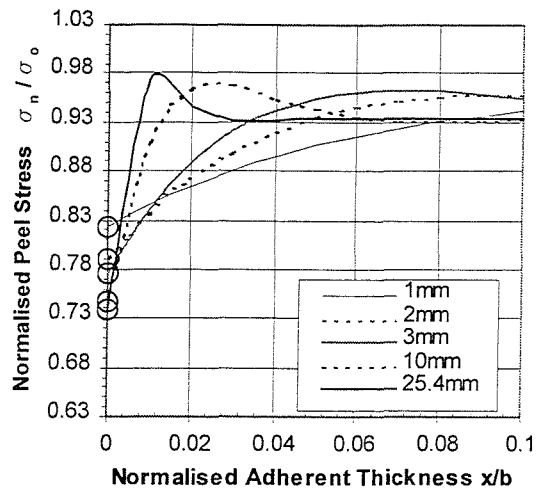
Fig. G.11a Aluminium 75° scarf
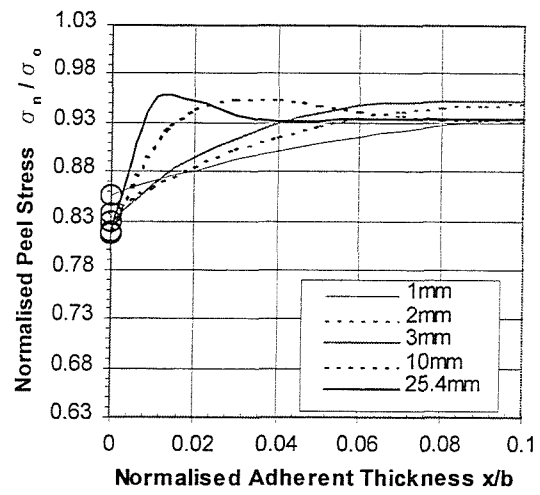
Fig. G.11b Composite 75° scarf
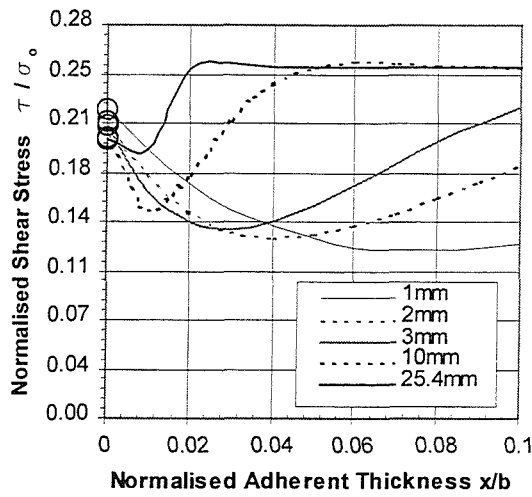
Fig. G.12a Aluminum 75° scarf – acute tip
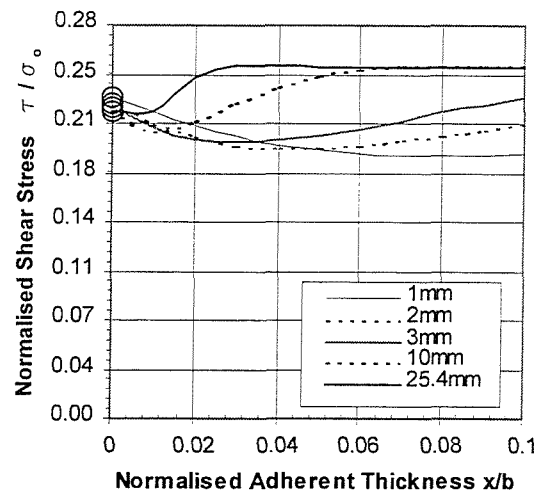
Fig. G.12b Composite 75° scarf – acute tip
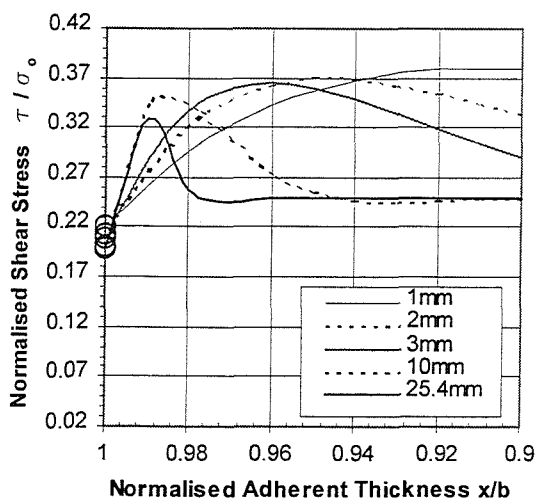
Fig. G.13a Aluminium 75° scarf – obtuse tip
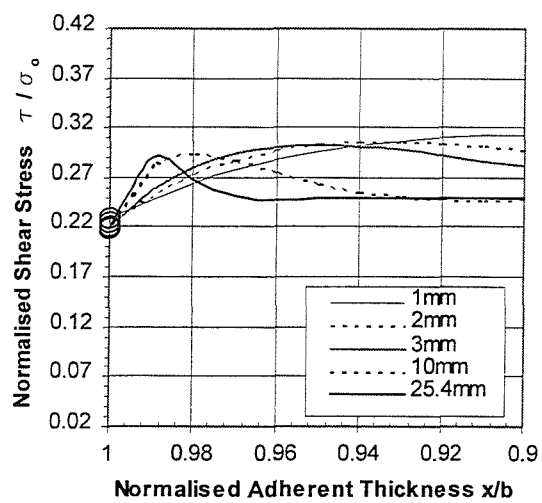
Fig. G.13b Composite 75° scarf – obtuse tip

143
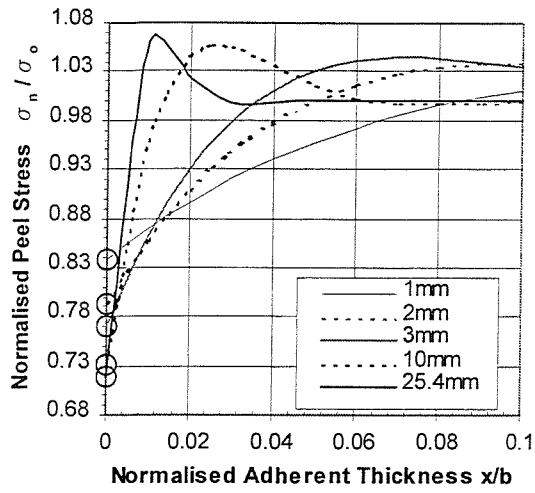
Fig. G.14a Aluminium 90° (butt) scarf
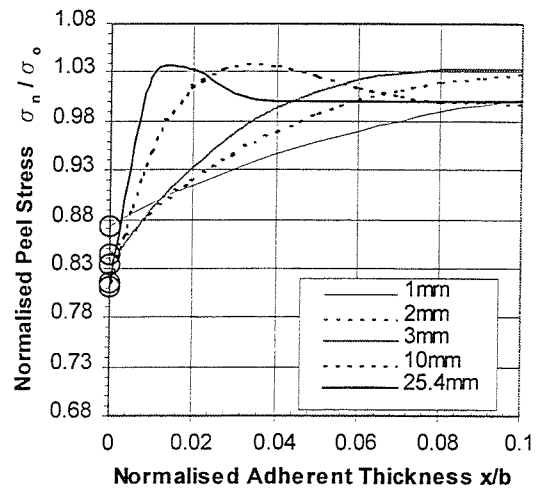
Fig. G.14b Composite 90° (butt) scarf
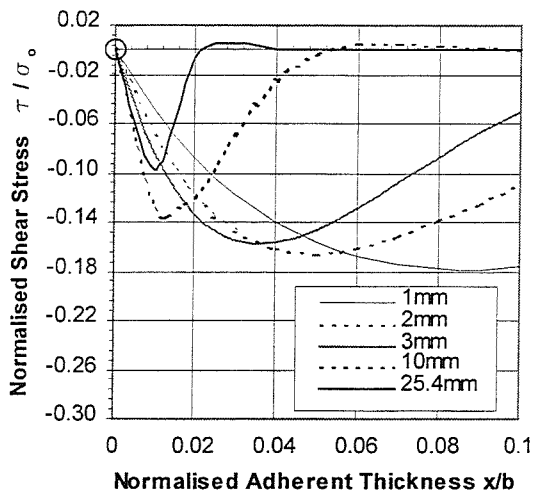
Fig. G.15a Aluminium 90° (butt) scarf – acute tip
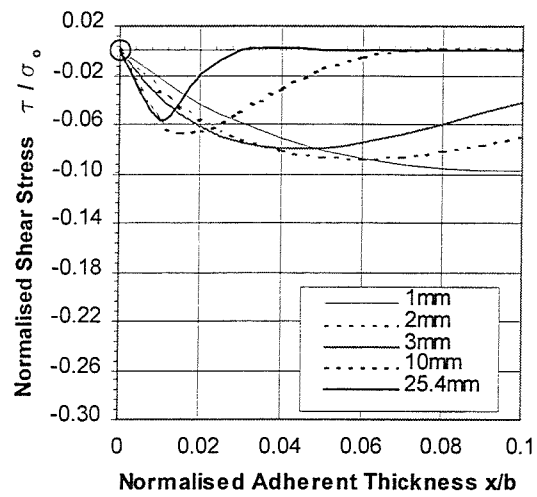
Fig. G.15b Composite 90° (butt) scarf – acute tip
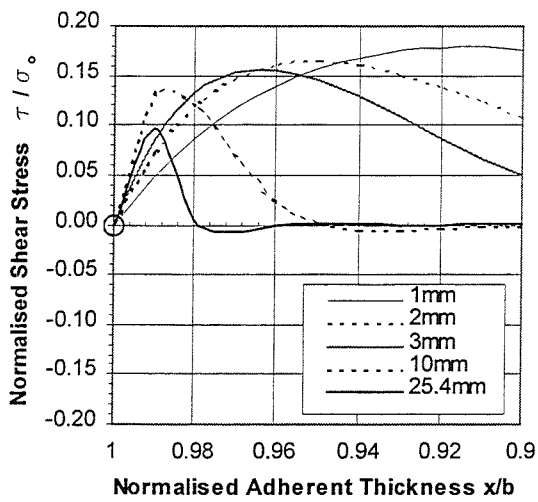
Fig. G.16a Aluminium 90° (butt) scarf – obtuse tip
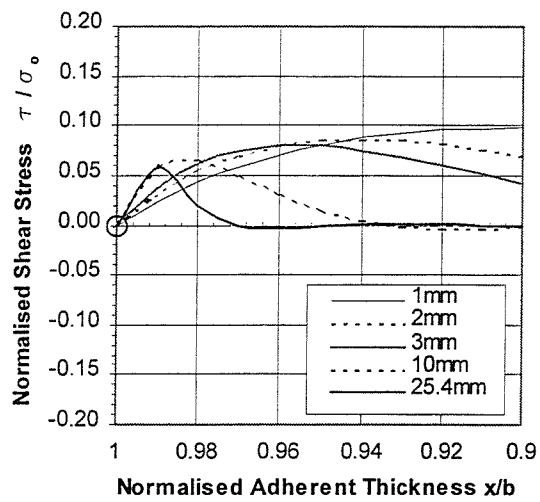
Fig. G.16b Composite 90° (butt) – obtuse tip

144

APPENDIX H

Wah – MathCad Plus 6.0 Program

Material Properties

$E := 26000 \cdot 10^6$	Elastic Modulus Adherent A
$E1 := 26000 \cdot 10^6$	Elastic Modulus Adherent B
$Ec := 250 \cdot 10^6$	Elastic Modulus Adhesive
$v := 0.3$	Poisson's Ratio Adherent A
$v1 := 0.3$	Poisson's Ratio Adherent B
$vc := 0.25$	Poisson's Ratio Adhesive

$G := \dfrac{E}{2 \cdot (1 + v)}$	Shear Modulus Adherent A

$G1 := \dfrac{E1}{2 \cdot (1 + v1)}$	Shear Modulus Adherent B

$Gc := \dfrac{Ec}{2 \cdot (1 + vc)}$	Shear Modulus Adhesive

$\mu := \dfrac{G}{G1}$	Adherent Shear Modulus Ratio

Geometric Properties

$t := 0.5 \cdot 10^6$	Adhesive thickness – normal to scarf inclination
$\alpha := \dfrac{\pi}{2}$	Scarf angle
$c := 500 \cdot 10^6$	Scarf interface length

Load Application

$Mo := 21505 \cdot 10^{12}$	Applied end moment

$\sigma o := \dfrac{6 \cdot Mo}{c^2 \cdot \sin(\alpha)^2}$	Resultant maximum free edge stress

Coefficients

$\lambda 1 := \dfrac{G \cdot t}{Gc \cdot c}$	$\lambda 2 := \dfrac{G \cdot t}{Ec \cdot c}$	$\lambda 3 := \dfrac{t \cdot vc}{2 \cdot c}$	$\lambda 4 := \dfrac{\lambda 3}{\lambda 2 \cdot vc^2}$	$\lambda 5 := \dfrac{\lambda 3}{vc}$	$COF := \dfrac{\lambda 3}{2 \cdot vc \cdot \lambda 2}$

Stress function roots - first ten

$\gamma_0 := 3.7487812975 + 1.3843394253i$	$\gamma_1 := 3.7487812975 - 1.3843394253i$
$\gamma_2 := 6.9499801296 + 1.6761052368i$	$\gamma_3 := 6.9499801296 - 1.6761052368i$
$\gamma_4 := 10.1192555197 + 1.858384346i$	$\gamma_5 := 10.1192555197 - 1.858384346i$
$\gamma_6 := 13.2772736552 + 1.9915708557i$	$\gamma_7 := 13.2772736552 - 1.9915708557i$
$\gamma_8 := 16.429868459 + 2.0966259523i$	$\gamma_9 := 16.429868459 - 2.0966259523i$

145

Solution terms

$$H_x := e^{\left(-2 \cdot \gamma_x \cdot z \cdot \cot(\alpha)\right)}$$

$$F1_x := \sin\left[\gamma_x \cdot (2 \cdot z - 1) - \alpha\right]$$

$$F2_x := \cos\left[\gamma_x \cdot (2 \cdot z - 1) - \alpha\right]$$

$$F3_x := \gamma_x \cdot (2 \cdot z - 1) \cdot \sin\left[\gamma_x \cdot (2 \cdot z - 1) - \alpha\right]$$

$$F4_x := \gamma_x \cdot (2 \cdot z - 1) \cdot \cos\left[\gamma_x \cdot (2 \cdot z - 1) - \alpha\right]$$

$$X1(\gamma, z) := \left((-\gamma \cdot \cot(\gamma) + 1) \cdot \sin(\gamma \cdot (2 \cdot z - 1) - 2 \cdot \alpha) + \gamma \cdot (2 \cdot z - 1) \cdot \cos(\gamma \cdot (2 \cdot z - 1) - 2 \cdot \alpha) - \sin(\gamma \cdot (2 \cdot z - 1))\right) \cdot e^{(-2 \cdot \gamma \cdot z \cdot \cot(\alpha))}$$

$$X2(\gamma, z) := \left((-\gamma \cdot \cot(\gamma) + 1) \cdot \cos(\gamma \cdot (2 \cdot z - 1) - 2 \cdot \alpha) - \gamma \cdot (2 \cdot z - 1) \cdot \sin(\gamma \cdot (2 \cdot z - 1) - 2 \cdot \alpha)\right) \cdot e^{(-2 \cdot \gamma \cdot z \cdot \cot(\alpha))}$$

$$X3(\gamma) := \left[\begin{array}{l} -\left(-\gamma_x \cdot \cot\left(\gamma_x\right) + 1\right) \cdot \cos\left[\gamma_x \cdot (2 \cdot z - 1) - \alpha\right] + \gamma_x \cdot (2 \cdot z - 1) \cdot \sin\left[\gamma_x \cdot (2 \cdot z - 1) - \alpha\right] \dots \\ + \dfrac{1-\nu}{1+\nu} \cdot \cos\left[\gamma_x \cdot (2 \cdot z - 1) + \alpha\right] + \cos\left[\gamma_x \cdot (2 \cdot z - 1)\right] \cdot \cos(\alpha) \end{array}\right] e^{\left(-2 \cdot \gamma_x \cdot z \cdot \cot(\alpha)\right)}$$

$$X4(\gamma) := \left[\begin{array}{l} \left(-\gamma_x \cdot \cot\left(\gamma_x\right) + 1\right) \cdot \sin\left[\gamma_x \cdot (2 \cdot z - 1) - \alpha\right] + \gamma_x \cdot (2 \cdot z - 1) \cdot \cos\left[\gamma_x \cdot (2 \cdot z - 1) - \alpha\right] \dots \\ + \dfrac{1-\nu}{1+\nu} \cdot \sin\left[\gamma_x \cdot (2 \cdot z - 1) + \alpha\right] + \cos\left[\gamma_x \cdot (2 \cdot z - 1)\right] \cdot \sin(\alpha) \end{array}\right] e^{\left(-2 \cdot \gamma_x \cdot z \cdot \cot(\alpha)\right)}$$

$$DX1(z, \nu, \gamma) := \left[\begin{array}{l} -\left(-\gamma_x \cdot \cot\left(\gamma_x\right) + 1\right) \cdot \cot(\alpha) \cdot \sin\left[\gamma_x \cdot (2 \cdot z - 1) - 2 \cdot \alpha\right] \dots \\ + \left(-\gamma_x \cdot \cot\left(\gamma_x\right) + 2\right) \cdot \cos\left[\gamma_x \cdot (2 \cdot z - 1) - 2 \cdot \alpha\right] \dots \\ + -\left[\gamma_x \cdot (2 \cdot z - 1) \cdot \sin\left[\gamma_x \cdot (2 \cdot z - 1) - 2 \cdot \alpha\right]\right] \dots \\ + -\cot(\alpha) \cdot \left[\gamma_x \cdot (2 \cdot z - 1) \cdot \cos\left[\gamma_x \cdot (2 \cdot z - 1) - 2 \cdot \alpha\right]\right] - \cos\left[\gamma_x \cdot (2 \cdot z - 1) - 2 \cdot \alpha\right] \dots \\ + \cot(\alpha) \cdot \sin\left[\gamma_x \cdot (2 \cdot z - 1)\right] \end{array}\right] \cdot e^{\left(-2 \cdot \gamma_x \cdot z \cdot \cot(\alpha)\right)}$$

$$DX2(z, \nu, \gamma) := \left[\begin{array}{l} -\left(-\gamma_x \cdot \cot\left(\gamma_x\right) + 2\right) \cdot \sin\left[\gamma_x \cdot (2 \cdot z - 1) - 2 \cdot \alpha\right] \dots \\ + -\left(-\gamma_x \cdot \cot\left(\gamma_x\right) + 1\right) \cdot \cot(\alpha) \cdot \cos\left[\gamma_x \cdot (2 \cdot z - 1) - 2 \cdot \alpha\right] \dots \\ + \cot(\alpha) \cdot \left[\gamma_x \cdot (2 \cdot z - 1) \cdot \sin\left[\gamma_x \cdot (2 \cdot z - 1) - 2 \cdot \alpha\right]\right] - \gamma_x \cdot (2 \cdot z - 1) \cdot \cos\left[\gamma_x \cdot (2 \cdot z - 1) - 2 \cdot \alpha\right] \end{array}\right] \cdot e^{\left(-2 \cdot \gamma_x \cdot z \cdot \cot(\alpha)\right)}$$

$$DX3(z, \nu, \gamma) := \left[\begin{array}{l} \left[\left(-\gamma_x \cdot \cot\left(\gamma_x\right) + 2\right) \cdot \sin\left[\gamma_x \cdot (2 \cdot z - 1) - \alpha\right] + \left(-\gamma_x \cdot \cot\left(\gamma_x\right) + 1\right) \cdot \cot(\alpha) \cdot \cos\left[\gamma_x \cdot (2 \cdot z - 1) - \alpha\right]\right] \dots \\ + -\cot(\alpha) \cdot \left[\gamma_x \cdot (2 \cdot z - 1)\right] \dots \\ + \gamma_x \cdot (2 \cdot z - 1) - \dfrac{1-\nu}{1+\nu} \cdot \left[\sin\left[\gamma_x \cdot (2 \cdot z - 1) + \alpha\right] + \cot(\alpha) \cdot \cos\left[\gamma_x \cdot (2 \cdot z - 1) + \alpha\right]\right] \dots \\ + -\left[\sin\left[\gamma_x \cdot (2 \cdot z - 1)\right] + \cot(\alpha) \cdot \cos\left[\gamma_x \cdot (2 \cdot z - 1)\right]\right] \cdot \cos(\alpha) \end{array}\right] \cdot e^{\left(-2 \cdot \gamma_x \cdot z \cdot \cot(\alpha)\right)}$$

$$DX4(z, \nu, \gamma) := \left[\begin{array}{l} -\left(-\gamma_x \cdot \cot\left(\gamma_x\right) + 1\right) \cdot \cot(\alpha) \cdot \sin\left[\gamma_x \cdot (2 \cdot z - 1) - \alpha\right] + \left(-\gamma_x \cdot \cot\left(\gamma_x\right) + 2\right) \cdot \cos\left[\gamma_x \cdot (2 \cdot z - 1) - \alpha\right] \dots \\ + -\gamma_x \cdot (2 \cdot z - 1) \cdot \sin\left[\gamma_x \cdot (2 \cdot z - 1) - \alpha\right] - \cot(\alpha) \cdot \sin\left[\gamma_x \cdot (2 \cdot z - 1) - \alpha\right] \dots \\ + \dfrac{1-\nu}{1+\nu} \cdot \left[\cos\left[\gamma_x \cdot (2 \cdot z - 1) + \alpha\right] - \cot(\alpha) \cdot \sin\left[\gamma_x \cdot (2 \cdot z - 1) + \alpha\right]\right] \dots \\ + -\left[\sin\left[\gamma_x \cdot (2 \cdot z - 1)\right] + \cot(\alpha) \cdot \cos\left[\gamma_x \cdot (2 \cdot z - 1)\right]\right] \cdot \sin(\alpha) \end{array}\right] \cdot e^{\left(-2 \cdot \gamma_x \cdot z \cdot \cot(\alpha)\right)}$$

$$DDX1(z, \nu, \gamma) := \left[\begin{array}{l} \left[\left(-\gamma_x \cdot \cot\left(\gamma_x\right) + 1\right) \cdot \cot(\alpha)^2 - \gamma_x \cdot \cot\left(\gamma_x\right) - 3\right] \cdot \sin\left[\gamma_x \cdot (2 \cdot z - 1) - 2 \cdot \alpha\right] \dots \\ + -2 \cdot \left(-\gamma_x \cdot \cot\left(\gamma_x\right) + 2\right) \cdot \cot(\alpha) \cdot \cos\left[\gamma_x \cdot (2 \cdot z - 1) - 2 \cdot \alpha\right] \dots \\ + 2 \cdot \cot(\alpha) \cdot \left[\gamma_x \cdot (2 \cdot z - 1) \cdot \sin\left[\gamma_x \cdot (2 \cdot z - 1) - 2 \cdot \alpha\right]\right] \dots \\ + \left(\cot(\alpha)^2 - 1\right) \cdot \left[\gamma_x \cdot (2 \cdot z - 1) \cdot \cos\left[\gamma_x \cdot (2 \cdot z - 1) - 2 \cdot \alpha\right]\right] - \left(\cot(\alpha)^2 - 1\right) \cdot \sin\left[\gamma_x \cdot (2 \cdot z - 1)\right] \dots \\ + 2 \cdot \cot(\alpha) \cdot \cos\left[\gamma_x \cdot (2 \cdot z - 1)\right] \end{array}\right] \cdot e^{\left(-2 \cdot \gamma_x \cdot z \cdot \cot(\alpha)\right)}$$

146

$$DDX3(z,v,\gamma) := \left[\begin{array}{l} -2 \cdot \left(-\gamma_x \cdot \cot(\gamma_x) + 2 \right) \cdot \cot(\alpha) \cdot \sin\left[\gamma_x \cdot (2 \cdot z - 1) - \alpha \right] \ldots \\ + \left[\left(-\gamma_x \cdot \cot(\gamma_x) + 1 \right) \cdot \cot(\alpha)^2 - \gamma_x \cdot \cot(\gamma_x) - 3 \right] \cdot \cos\left[\gamma_x \cdot (2 \cdot z - 1) - \alpha \right] \ldots \\ + \left(\cot(\alpha)^2 - 1 \right) \cdot \left[\gamma_x \cdot (2 \cdot z - 1) \cdot \sin\left[\gamma_x \cdot (2 \cdot z - 1) - \alpha \right] \right] \ldots \\ + -2 \cdot \cot(\alpha) \cdot \left[\gamma_x \cdot (2 \cdot z - 1) \cdot \cos\left[\gamma_x \cdot (2 \cdot z - 1) - \alpha \right] \right] \ldots \\ + \dfrac{1-v}{1+v} \cdot \left[\left(\cot(\alpha)^2 - 1 \right) \cdot \cos\left[\gamma_x \cdot (2 \cdot z - 1) + \alpha \right] + 2 \cdot \cot(\alpha) \cdot \sin\left[\gamma_x \cdot (2 \cdot z - 1) + \alpha \right] \right] \ldots \\ + \cos(\alpha) \cdot \left[\left(\cot(\alpha)^2 - 1 \right) \cdot \cos\left[\gamma_x \cdot (2 \cdot z - 1) \right] + 2 \cdot \cot(\alpha) \cdot \sin\left[\gamma_x \cdot (2 \cdot z - 1) \right] \right] \end{array} \right] \cdot e^{\left(-2 \cdot \gamma_x \cdot z \cdot \cot(\alpha) \right)}$$

$$DDX4(z,v,\gamma) := \left[\begin{array}{l} \left[\left(-\gamma_x \cdot \cot(\gamma_x) + 1 \right) \cdot \cot(\alpha)^2 - \gamma_x \cdot \cot(\gamma_x) - 3 \right] \cdot \sin\left[\gamma_x \cdot (2 \cdot z - 1) - \alpha \right] \ldots \\ + 2 \cdot \left(-\gamma_x \cdot \cot(\gamma_x) + 2 \right) \cdot \cot(\alpha) \cdot \cos\left[\gamma_x \cdot (2 \cdot z - 1) - \alpha \right] \ldots \\ + 2 \cdot \cot(\alpha) \cdot \left[\gamma_x \cdot (2 \cdot z - 1) \cdot \sin\left[\gamma_x \cdot (2 \cdot z - 1) - \alpha \right] \right] \ldots \\ + \left(\cot(\alpha)^2 - 1 \right) \cdot \left[\gamma_x \cdot (2 \cdot z - 1) \cdot \cos\left[\gamma_x \cdot (2 \cdot z - 1) - \alpha \right] \right] \ldots \\ + \dfrac{1-v}{1+v} \cdot \left[\left(\cot(\alpha)^2 - 1 \right) \cdot \sin\left[\gamma_x \cdot (2 \cdot z - 1) - \alpha \right] - 2 \cdot \cot(\alpha) \cdot \cos\left[\gamma_x \cdot (2 \cdot z - 1) + \alpha \right] \right] \ldots \\ + \sin(\alpha) \cdot \left[\left(\cot(\alpha)^2 - 1 \right) \cdot \cos\left[\gamma_x \cdot (2 \cdot z - 1) \right] + 2 \cdot \cot(\alpha) \cdot \sin\left[\gamma_x \cdot (2 \cdot z - 1) \right] \right] \end{array} \right] \cdot e^{\left(-2 \cdot \gamma_x \cdot z \cdot \cot(\alpha) \right)}$$

$$DDDX4(z,v,\gamma) := \left[\begin{array}{l} \cot(\alpha) \cdot \left[-\gamma_x \cdot \cot(\gamma_x) \cdot \left(3 - \cot(\alpha)^2 \right) + 9 - \cot(\alpha)^2 \right] \cdot \sin\left[\gamma_x \cdot (2 \cdot z - 1) - \alpha \right] \ldots \\ + \left[-\gamma_x \cdot \cot(\gamma_x) \cdot \left(3 \cdot \cot(\alpha)^2 - 1 \right) + 6 \cdot \cot(\alpha)^2 - 4 \right] \cdot \cos\left[\gamma_x \cdot (2 \cdot z - 1) - \alpha \right] \ldots \\ + \left(1 - 3 \cdot \cot(\alpha)^2 \right) \cdot \left[\gamma_x \cdot (2 \cdot z - 1) \cdot \sin\left[\gamma_x \cdot (2 \cdot z - 1) - \alpha \right] \right] \ldots \\ + \cot(\alpha) \cdot \left(3 - \cot(\alpha)^2 \right) \cdot \left[\gamma_x \cdot (2 \cdot z - 1) \cdot \cos\left[\gamma_x \cdot (2 \cdot z - 1) - \alpha \right] \right] \ldots \\ + \dfrac{1-v}{(1+v)} \cdot \left[\cot(\alpha) \cdot \left(3 - \cot(\alpha)^2 \right) \cdot \sin\left[\gamma_x \cdot (2 \cdot z - 1) + \alpha \right] + \left(3 \cdot \cot(\alpha)^2 - 1 \right) \cdot \cos\left[\gamma_x \cdot (2 \cdot z - 1) + \alpha \right] \right] \ldots \\ + \sin(\alpha) \cdot \left[\left(1 - 3 \cdot \cot(\alpha)^2 \right) \cdot \sin\left[\gamma_x \cdot (2 \cdot z - 1) \right] + \cot(\alpha) \cdot \left(3 - \cot(\alpha)^2 \right) \cdot \cos\left[\gamma_x \cdot (2 \cdot z - 1) \right] \right] \end{array} \right] \cdot e^{\left(-2 \cdot \gamma_x \cdot z \cdot \cot(\alpha) \right)}$$

Parameters for simultaneous solution of $A1_x$ for Adherent A

$$Q1_x := \left(\gamma_x \right)^3 \cdot DX2(z,v,\gamma)$$

$$Q2_x := \left(\gamma_x \right)^3 \cdot \left(\sin(\alpha) \cdot \lambda 4 \cdot t \cdot DDX4(z,v,\gamma) + DX1(z,v,\gamma) \right)$$

$$Q3_x := \left(\gamma_x \right)^2 \cdot \left(t \cdot DX4(z,v,\gamma) + 2 \cdot \gamma_x \cdot \lambda 1 \cdot \dfrac{DX2(z,v,\gamma)}{\sin(\alpha)} - 2 \cdot t \cdot \gamma_x \cdot \lambda 5 \cdot DDX3(z,v,\gamma) \right)$$

$$Q4_x := \left(\gamma_x \right)^3 \cdot \left[t \cdot \sin(\alpha) \cdot DDX3(z,v,\gamma) + 2 \cdot \gamma_x \cdot \lambda 2 \cdot \left(1 - vc^2 \right) \cdot DDX1(z,v,\gamma) - 2 \cdot t \cdot \gamma_x \cdot \lambda 3 \cdot \sin(\alpha) \cdot DDDX4(z,v,\gamma) \right]$$

Parameters for simultaneous solution of $A11_x$ for Adherent B

$$Q11_x := \left(\gamma_x \right)^3 \cdot DX2(1-z,v1,\gamma)$$

$$Q22_x := \left(\gamma_x \right)^3 \cdot \left(\sin(\alpha) \cdot \lambda 4 \cdot t \cdot DDX4(1-z,v1,\gamma) + DX1(1-z,v1,\gamma) \right)$$

$$Q33_x := \left(\gamma_x \right)^2 \cdot \left(t \cdot DX4(1-z,v1,\gamma) + 2 \cdot \gamma_x \cdot \lambda 1 \cdot \dfrac{DX2(1-z,v1,\gamma)}{\sin(\alpha)} - 2 \cdot \gamma_x \cdot \lambda 5 \cdot t \cdot DDX3(1-z,v1,\gamma) \right)$$

$$Q44_x := \left(\gamma_x \right)^3 \cdot \left[t \cdot \sin(\alpha) \cdot DDX3(1-z,v1,\gamma) + 2 \cdot \gamma_x \cdot \lambda 2 \cdot \left(1 - vc^2 \right) \cdot DDX1(1-z,v1,\gamma) - 2 \cdot t \cdot \gamma_x \cdot \lambda 3 \cdot \sin(\alpha) \cdot DDDX4(1-z,v1,\gamma) \right]$$

147

Stress function constant determination via least squares method

$$A_x := \begin{bmatrix} Q1_x & Q11_x \\ Q2_x & Q22_x \\ Q3_x & -Q33_x \\ Q4_x & Q44_x \end{bmatrix}$$

$s := \sin(\alpha)^2 + \dfrac{1}{(1+v)}$	$s1 := \sin(\alpha)^2 + \dfrac{1}{(1+v1)}$

$$\begin{pmatrix} A1_x \\ A11_x \end{pmatrix} := \left(A_x{}^T A_x \right)^{-1} \cdot A_x{}^T \cdot \begin{bmatrix} 0 \\ -0.5 \cdot \lambda 4 \cdot \infty \cdot \sin(\alpha)^2 \cdot (s - \mu \cdot s1) \\ \infty \cdot \left[0.25 \cdot (1 - 2 \cdot z) \cdot \sin(\alpha) \cdot (s - \mu \cdot s1) + 0.5 \cdot \lambda 5 \cdot \cos(\alpha) \cdot (s + \mu \cdot s1) - \lambda 1 \cdot \sin(\alpha)^2 \cdot \cos(\alpha) \right] \\ -0.125 \cdot \infty \cdot \sin(2 \cdot \alpha) \cdot (s - \mu \cdot s1) \end{bmatrix}$$

Adherent interface stress

$\sigma y0_x := 4 \cdot A1_x \cdot \left[\dfrac{\left(\gamma_x \right)^2}{\sin(\alpha)^2} \right] \cdot X1\left(\gamma_x, z \right) + \infty \cdot \sin(\alpha)^2 \cdot (1 - 2 \cdot z)$	Peel stress – Adherent A

$\tau xy0_x := 4 \cdot A1_x \cdot \left[\dfrac{\left(\gamma_x \right)^2}{\sin(\alpha)^2} \right] \cdot X2\left(\gamma_x, z \right) + \infty \cdot \sin(\alpha) \cdot \cos(\alpha) \cdot (2 \cdot z - 1)$	Shear stress – Adherent A

$\sigma y00_x := 4 \cdot A1_x \cdot \left[\dfrac{\left(\gamma_x \right)^2}{\sin(\alpha)^2} \right] \cdot X1\left(\gamma_x, 1 - z \right) + \infty \cdot \sin(\alpha)^2 \cdot (1 - 2 \cdot (1 - z))$	Peel stress – Adherent B

$\tau xy00_x := 4 \cdot A1_x \cdot \left[\dfrac{\left(\gamma_x \right)^2}{\sin(\alpha)^2} \right] \cdot X2\left(\gamma_x, 1 - z \right) + \infty \cdot \sin(\alpha) \cdot \cos(\alpha) \cdot (2 \cdot (1 - z) - 1)$	Shear stress – Adherent B

$\sigma z_x := COF \cdot 4 \cdot \left(\gamma_x \right)^2 \cdot \csc(\alpha) \cdot \left(A1_x \cdot DX4\left(z, v, \gamma_x \right) + A11_x \cdot \mu \cdot DX4\left(1 - z, v1, \gamma_x \right) \right) \dots$ $+ 0.5 \cdot vc \cdot \left(\sigma y0_x - \sigma y00_x \right) - \infty \cdot COF \cdot \left[\left(\sin(\alpha)^2 - \dfrac{1}{1+v} \right) + \mu \cdot \left(\sin(\alpha)^2 - \dfrac{1}{1+v1} \right) \right] \cdot (1 - 2 \cdot z)$	Interface axial stress

Data written to output file

148

APPENDIX I

Scarf in Flexure– Peel and Shear Stress Profiles

The following figures represent interface stress profiles according to theory developed by Wah. The legends refer to the power of 10 that geometric parameters are raised. Figures I.13-17 show typical stress variance at the centreline, tending toward an asymptote of 0 as expected.
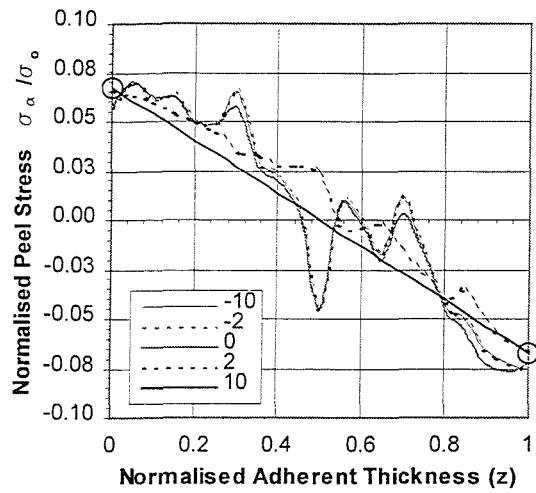
Fig. I.1a Aluminium 15° scarf
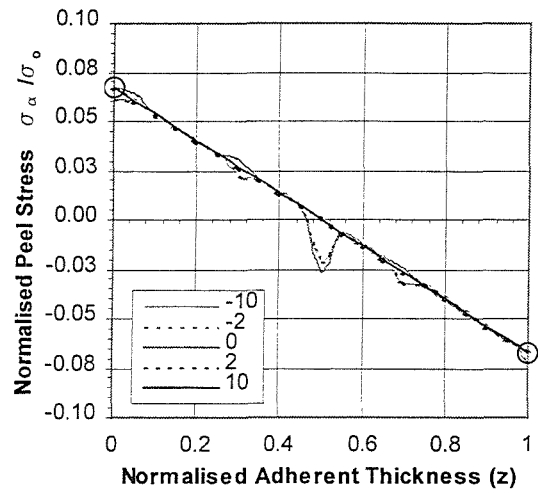
Fig. I.1b Composite 15° scarf
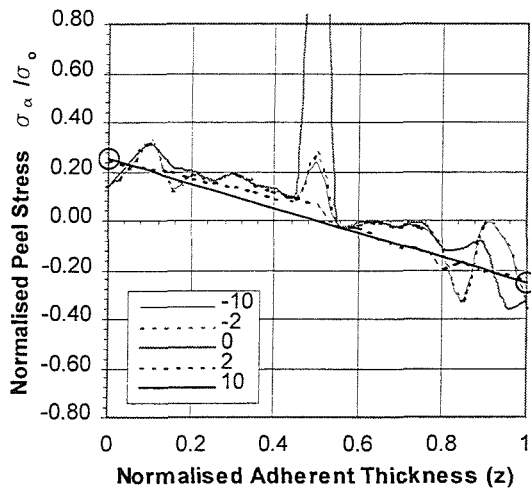
Fig. I.2a Aluminium 30° scarf
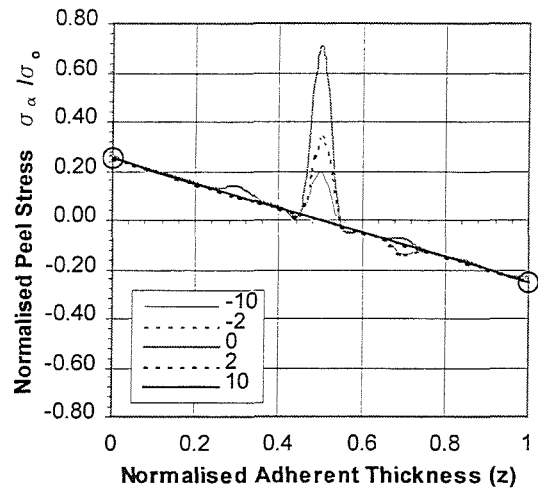
Fig. I.2b Composite 30° scarf
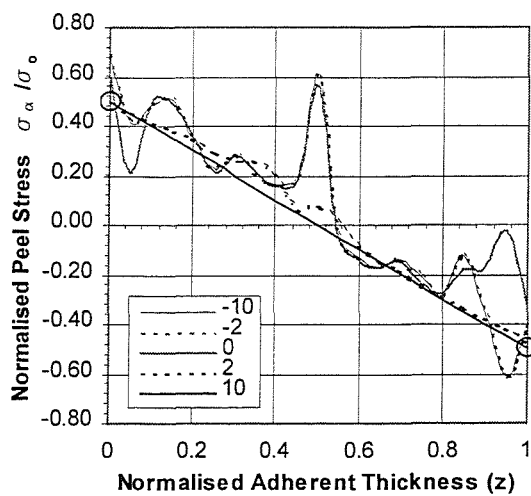
Fig. I.3a Aluminium 45° scarf
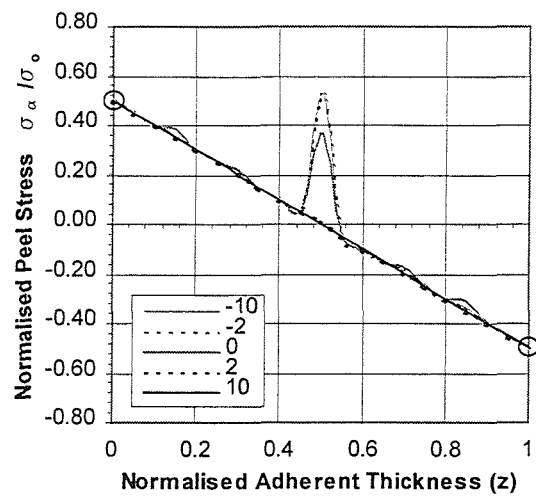
Fig. I.3b Composite 45° scarf

150
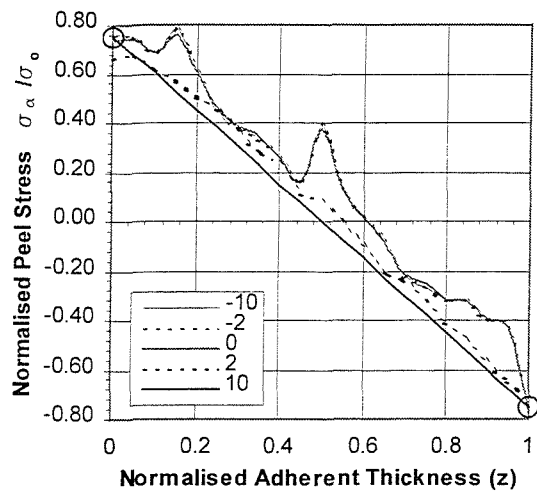
Fig. I.4a Aluminium 60° scarf
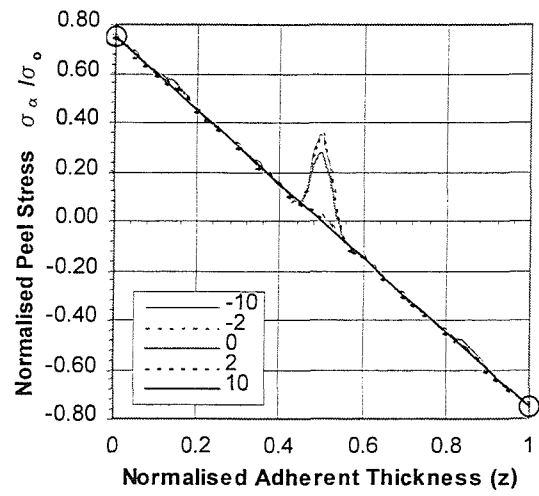
Fig. I.4b Composite 60° scarf
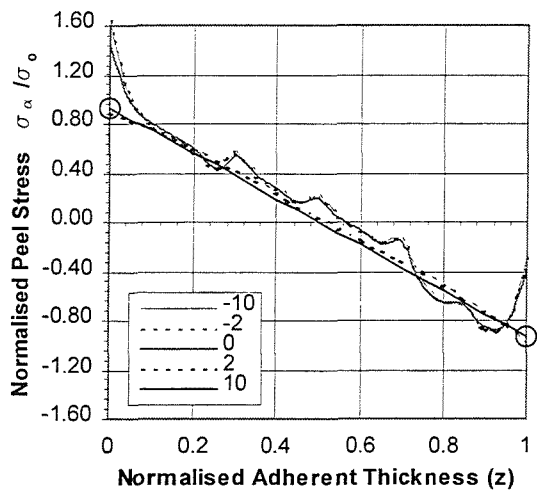
Fig. I.5a Aluminium 75° scarf
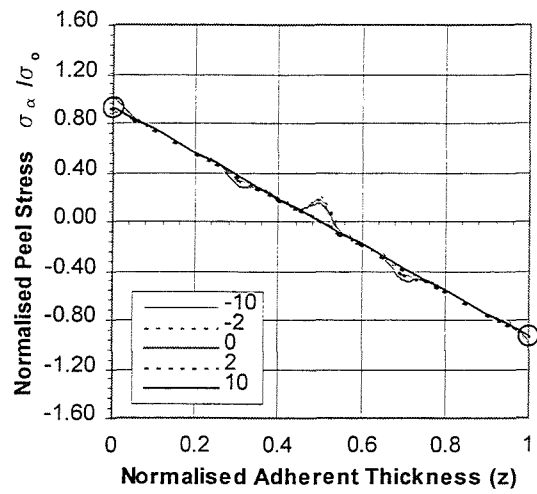
Fig. I.5b Composite 75° scarf
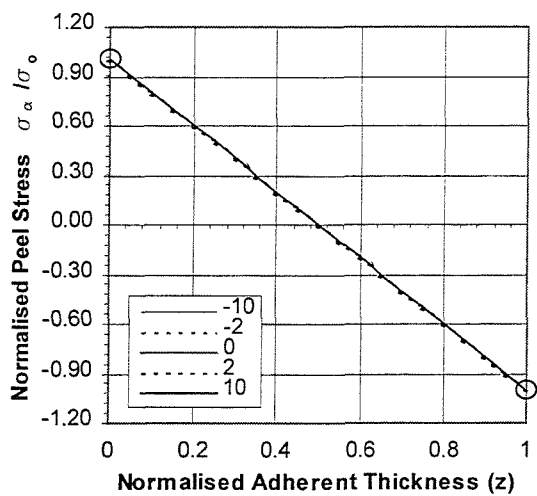
Fig. I.6a Aluminium 90° (butt) scarf
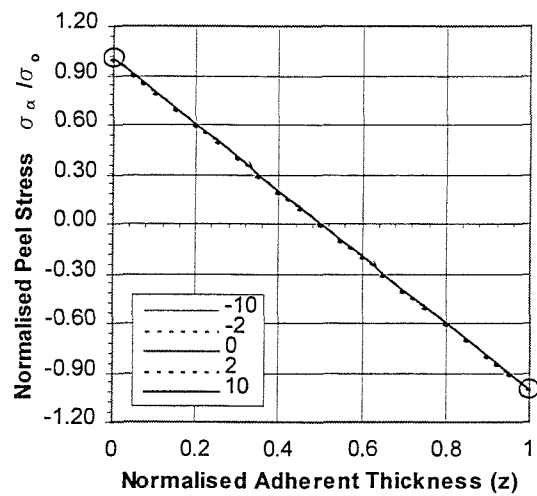
Fig. I.6b Composite 90° (butt) scarf

151
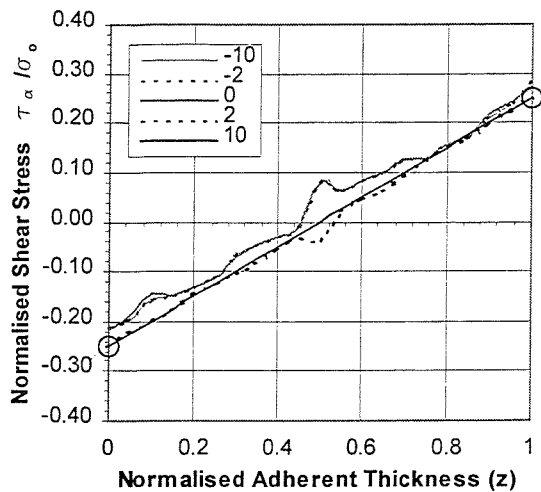
Fig. I.7a Aluminium 15° scarf
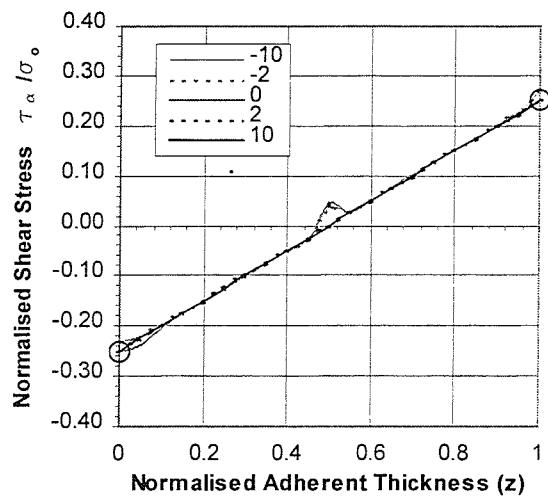
Fig. I.7b Composite 15° scarf
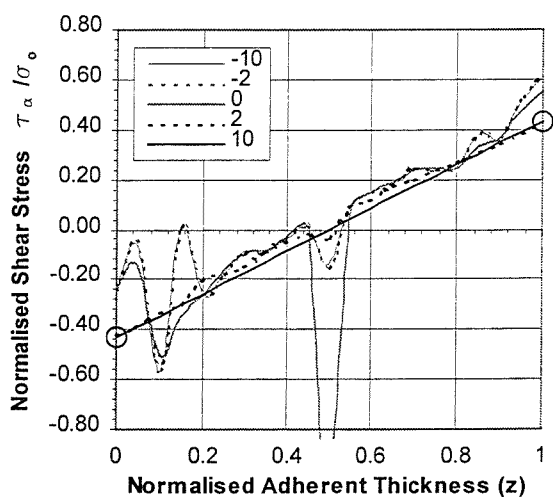
Fig. I.8a Aluminium 30° scarf
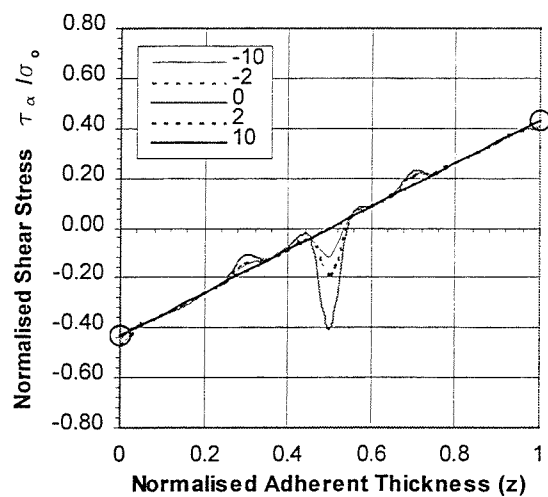
Fig. I.8b Composite 30° scarf
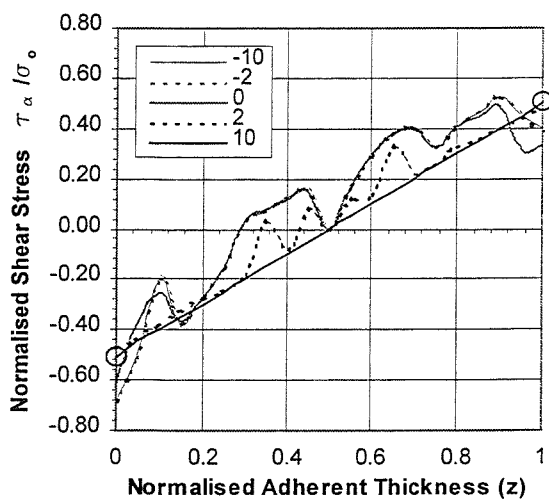
Fig. I.9a Aluminium 45° scarf
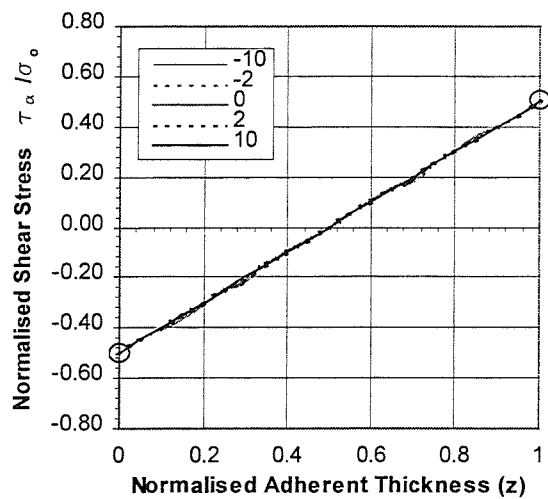
Fig. I.9b Composite 45° scarf

152
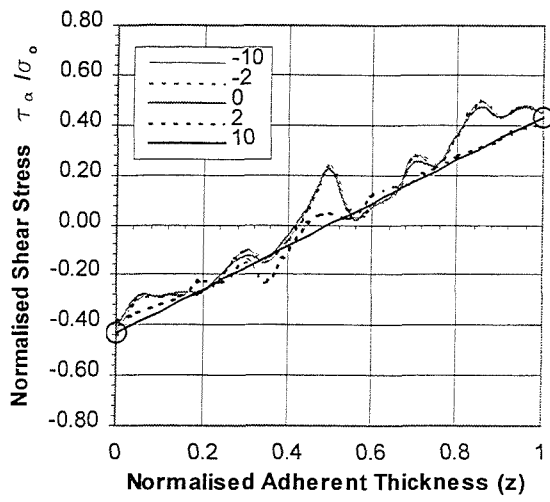
Fig. I.10a Aluminium 60° scarf
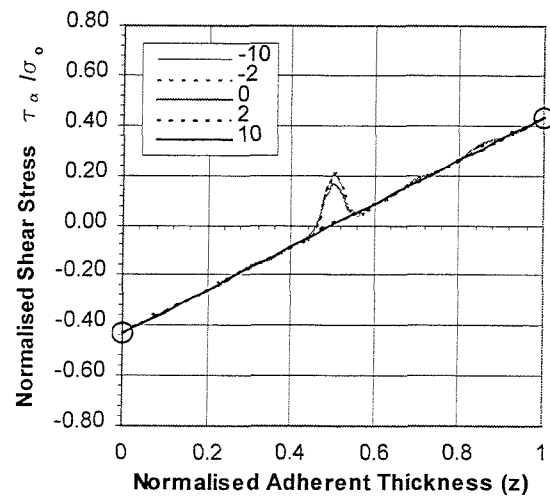
Fig. I.10b Composite 60° scarf
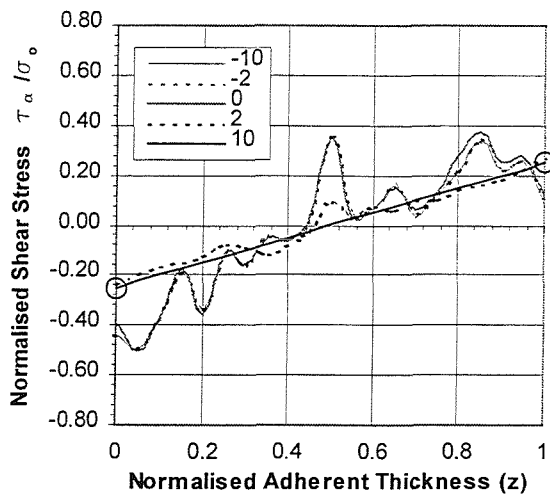
Fig. I.11a Aluminium 75° scarf
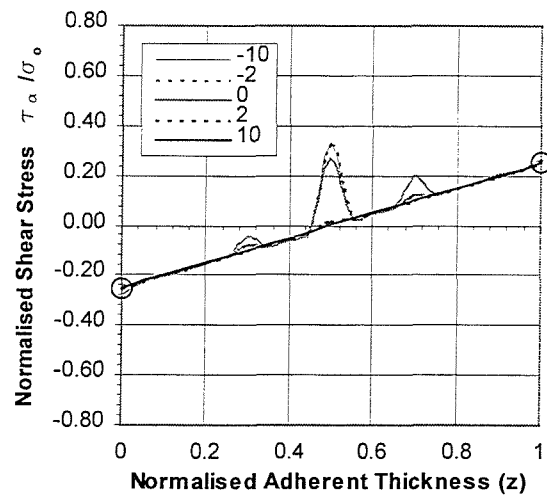
Fig. I.11b Composite 75° scarf
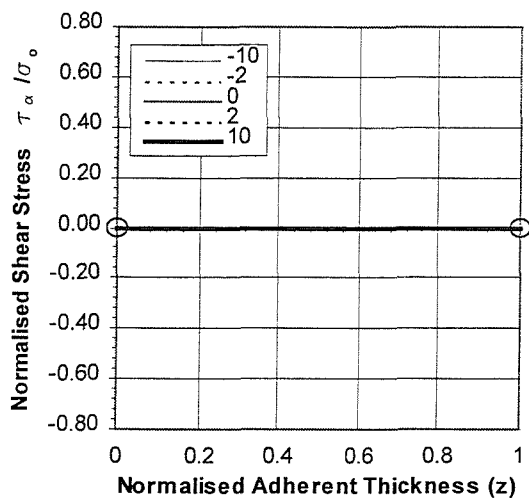
Fig. I.12a Aluminium 90° (butt) scarf
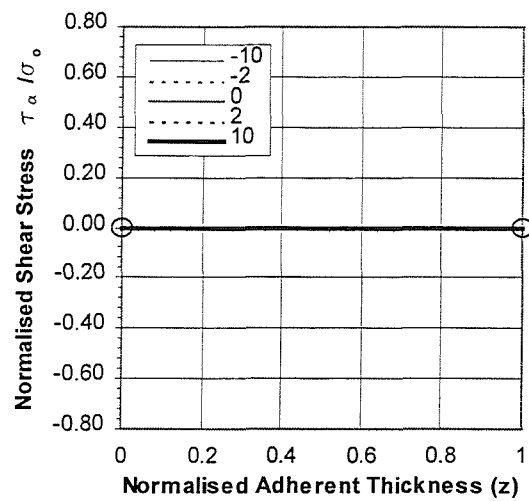
Fig. I.12b Composite 90° (butt) scarf

153
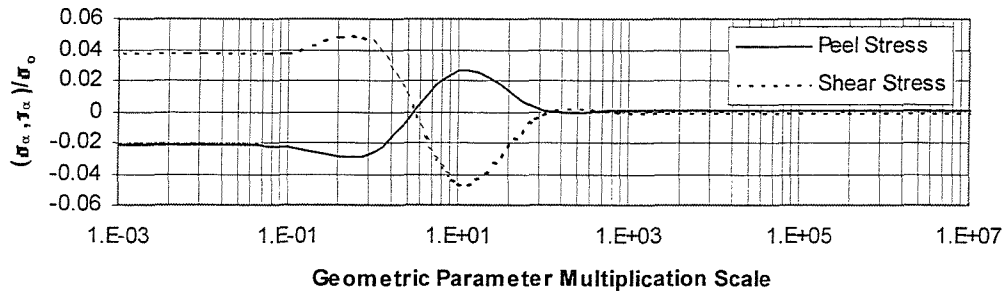
Figure I.13 Quasi-isotropic composite - centreline stress at varying geometric scales for $\alpha = 15°$.
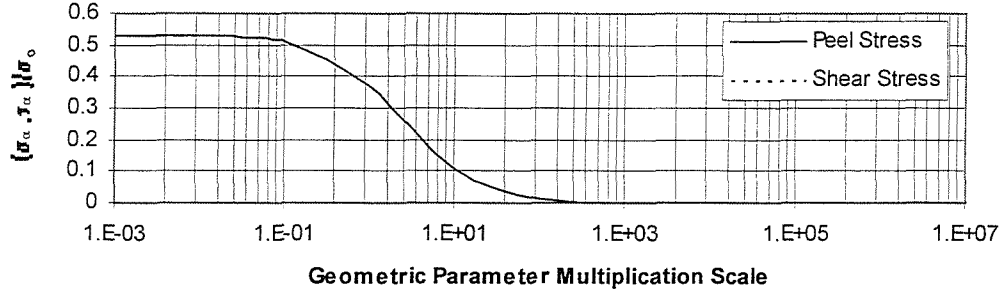
Figure I.14 Quasi-isotropic composite - centreline stress at varying geometric scales for $\alpha = 30°$.
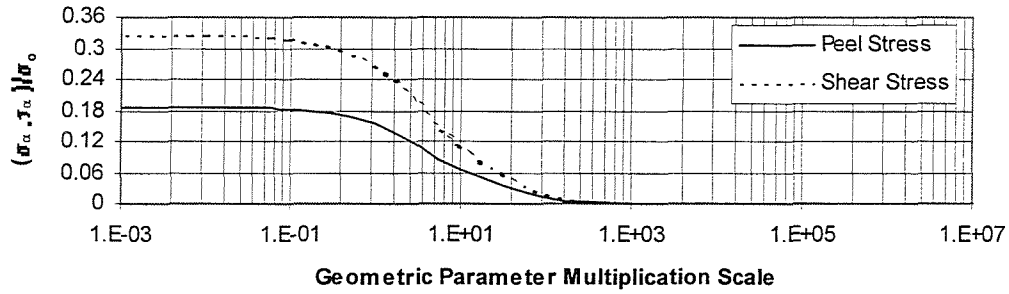
Figure I.15 Quasi-isotropic composite - centreline stress at varying geometric scales for $\alpha = 45°$.
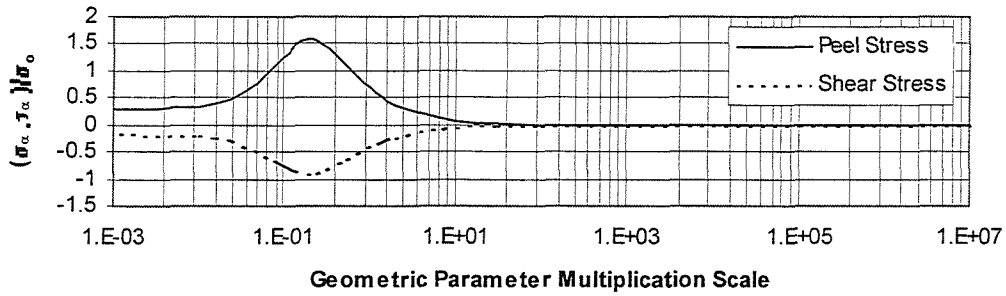
Figure I.16 Quasi-isotropic composite - centreline stress at varying geometric scales for $\alpha = 60°$.
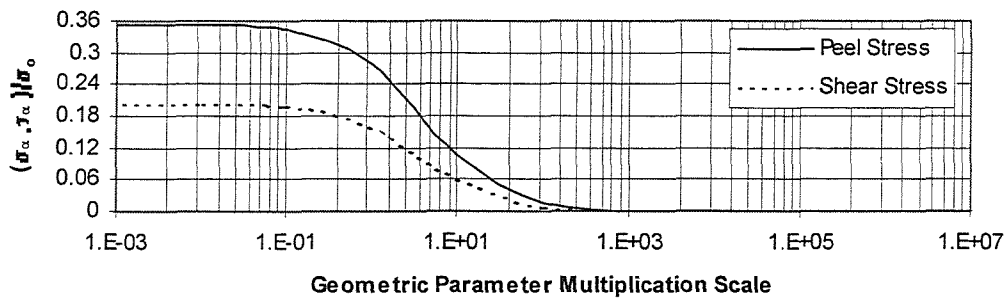
Figure I.17 Quasi-isotropic composite - centreline stress at varying geometric scales for $\alpha = 75°$.

154

APPENDIX J

Through Thickness Properties

Composite skins are traditionally made from multiple layers of individual plies, either unidirectional, or multi-axial depending on the final desired characteristics. The composite skins considered were biaxial (0/90) E-glass impregnated with an epoxy resin system. Whilst in-plane properties were readily available, through thickness details were not.

A simplification of the plied laminate was desired, as the analytical solutions were based on homogenous adherents. Similarly for the finite element analysis, stress variance was localised at the free edge and use of a simplified model was feasible. The basic laminate and constituent material information from which these property derivations are achieved is listed in tables J.1-2.

	Biaxial (0/90)[*]	Unidirectional (0)[*]
Fibre Volume Fraction	45%	45%
Fibre Weight Fraction	62%	62%
Composite Density	1.83 g/cm^3	1.83 g/cm^3
Longitudinal Modulus E	21370 MPa	34470 MPa
Transverse Modulus E	21370 MPa	8270 MPa
Shear Modulus G	4275 MPa	4275 MPa
Poisson's Ratio v	0.10	0.26
Longitudinal Tensile σ_t	359 MPa	703 MPa
Transverse Tensile σ_t	359 MPa	26.9 MPa
Longitudinal Compressive σ_c	379 MPa	614 MPa
Transverse Compressive σ_c	379 MPa	123 MPa
In-Plane Shear τ	43.4 MPa	43.4 MPa
Longitudinal Flexural σ_f	462 MPa	738 MPa
Transverse Flexural σ_f	462 MPa	26.9 MPa

[*]Compilation of experimental results from Johnston Industries (1997) and CET4149/1-5 (1995).

Table J.1. Mechanical properties of E-glass laminates.

	ADR240/ADH160 Epoxy[†]	E-Glass[‡]
Young's Modulus	$E_m = 3000$ MPa	$E_f = 72000$ MPa
Poisson's Ratio	$v_m = 0.368$	$v_f = 0.20$

Sources: [†] ATL Composites, [‡] Shenoi and Wellicome (1993)

Table J.2 Mechanical properties of laminate matrix and fibre.

J.1 Property Derivation

Through thickness G_{c31} is primarily resin dominated, therefore unidirectional shear modulus should prove appropriate. For E_{c3} the in-plane unidirectional transverse modulus provided a suitable approximation. Figure J.1 shows the three dimensional designations of material properties.
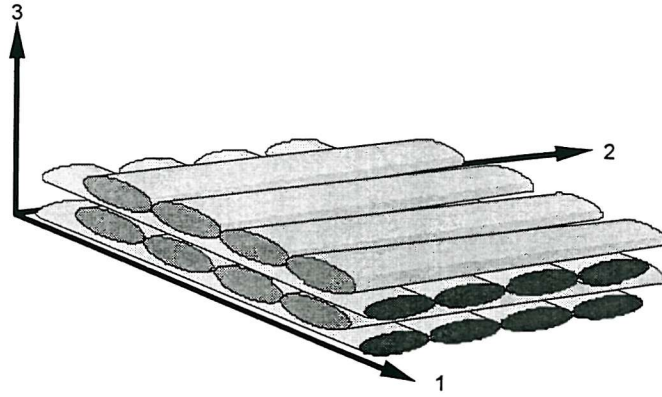
Figure J.1 Material property sign convention.

E_{c2} and v_{c31} were estimated using rule of mixtures based on the following equations

$$E_{c2} = E_1 V_1 + E_2 V_2 \qquad (J.1)$$

$$\frac{1}{v_{c31}} = \frac{V_m}{v_m} + \frac{V_f}{v_f} \qquad (J.2)$$

with shear modulus being estimated by

$$\frac{G_{c31}}{G_m} \approx \frac{E_{c3}}{E_m} \qquad (J.3)$$

where

E_1 = unidirectional longitudinal modulus E_2 = unidirectional transverse modulus

V_1 = 0 degree ply volume V_2 = 90 degree ply volume

v_{12} = unidirectional Poisson's ratio G_m = matrix shear modulus

V_m = matrix volume fraction (55%) V_f = fibre volume fraction (45%)

and as the laminate individual ply thicknesses are the same, $V_1 = V_2 = 0.5$. Material attributes of the composite can therefore be easily determined, and are listed in table J.3.

Longitudinal Modulus E_{c2}	21370 MPa	Transverse Modulus E_{c3}	8270 MPa
Shear Modulus G_{c31}	3020 MPa	Poisson's Ratio v_{c31}	0.267

Table J.3 Homogenised through thickness biaxial laminate properties.

J.2 Verification

Confidence in the mechanical properties was achieved through some simple checks, such as the equivalence of E_{c2} with E_2 of the biaxial laminate. A slightly more detailed calculation for G_{c31} and E_{c3} was performed using the Halpin and Tsai (1969) equations and coefficients as described by Shenoi (1993).

Halpin-Tsai transverse modulus

$$\frac{E_{c3}}{E_m} = \frac{1 + \xi \eta V_f}{1 - \eta V_f} \tag{J.4}$$

where

$$\eta = \frac{(E_f / E_m) - 1}{(E_f / E_m) + \xi}$$ and $\xi = 2$ for circular sectioned filaments.

Halpin-Tsai shear modulus

$$\frac{G_{c31}}{G_m} = \frac{1 + \xi \eta V_f}{1 - \eta V_f} \tag{J.5}$$

$$\eta = \frac{(G_f / G_m) - 1}{(G_f / G_m) + \xi}$$ and $\xi = 1$

As both matrix and fibre are essentially isotropic, shear modulus can be simply calculated via $G = E/[2(1+v)]$. Substitution into the above equations yields

$E_{c3} = 8950$ MPa, an 8% higher estimate, and
$G_{c31} = 2673$ MPa, a 12% lower estimate.

After correction for fibre volume fraction, E_{c3} and v_{c31} also compare favourably with that determined by Phillips (1997). The estimate of G_{c31} is however lower than expected, but can be accommodated by Nielsen's (1970) extension of the Halpin-Tsai equation.

Nielsen's modification offered a more accurate prediction of shear modulus by taking into consideration the maximum volumetric packing fraction $V_{fmax} = 0.83$, and is verified by excellent agreement with the finite difference representation of Adams and Doner (1967). The governing equations are

$$\frac{G_{c31}}{G_m} = \frac{1 + ABV_f}{1 - B\psi V_f} \tag{J.6}$$

where $A = 0.5$ based on a generalised Einstein coefficient from Nielsen (1974) and B is a constant for any given composite defined as

$$B = \frac{(G_f/G_m) - 1}{(G_f/G_m) + A}$$

with ψ determined by

$$\psi = 1 + \left[\frac{1 - V_{fmax}}{V_{fmax}^2}\right] V_f$$

The estimation of V_{fmax} is much lower than that achievable in an individually splayed fibre tow, and hence a value of 0.70; slightly less than that for cubic packing of fibres. This quantity takes into consideration the inevitable gap between tows in a knitted biaxial laminate, even at the highest consolidation pressures.

Substitution into Nielsen's equations produces

$G_{c31} = 2900$ MPa, a 4% lower estimate.

It therefore seems reasonable to assume that the values listed in table J.3 are a good approximation of through thickness properties for an E-glass knitted biaxial fabric in an epoxy matrix.

APPENDIX K

Finite Element Analysis - Bondline Stress Distributions

Stresses are read from 49 evenly spaced Gauss points along a given path i.e. adhesive interface or centreline.

Path and contour plots are based on the following sub-model geometry for homogenous and sandwich models in both tension and flexure.
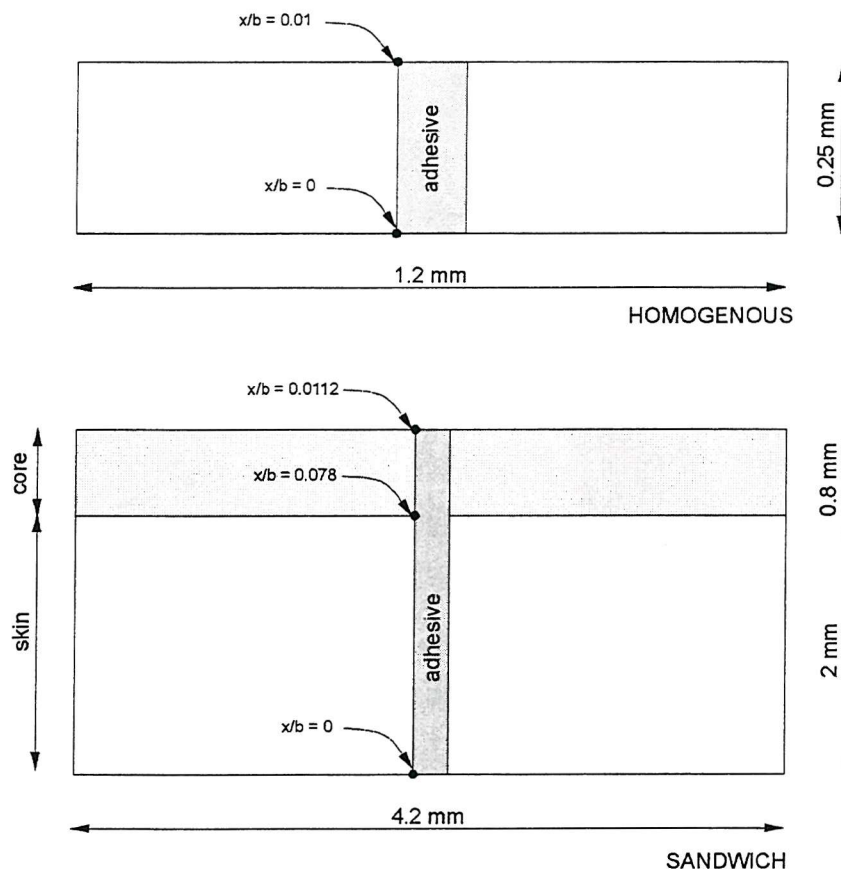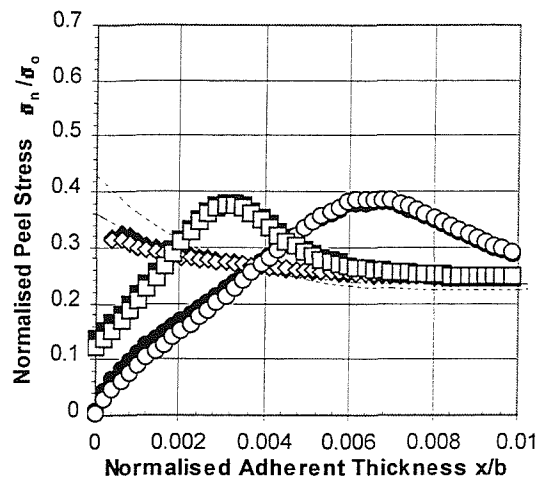
Fig. K.1a. Aluminium peel stress - 30° tension
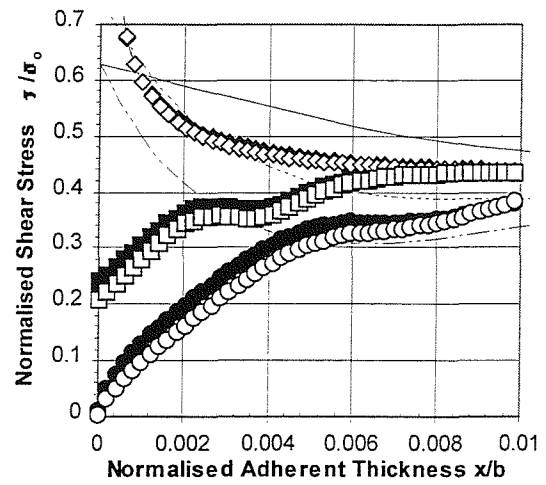
Fig. K.1b. Aluminium shear stress - 30° tension
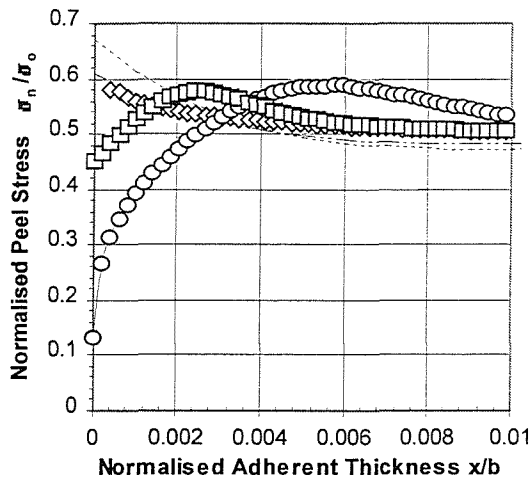
Fig. K.2a Aluminium peel stress - 45° tension
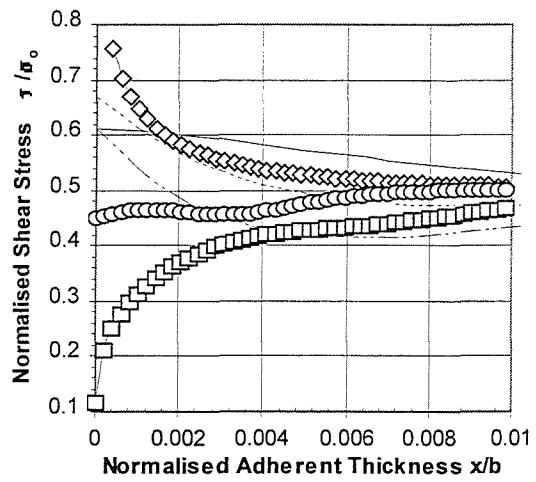
Fig. K.2b Aluminium shear stress - 45° tension
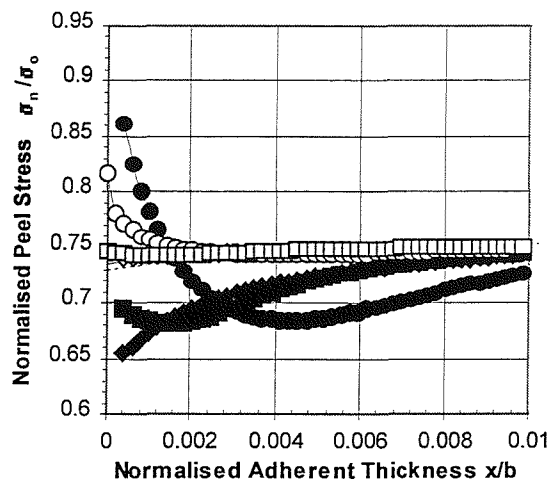
Fig. K.3a Aluminium peel stress - 60° tension
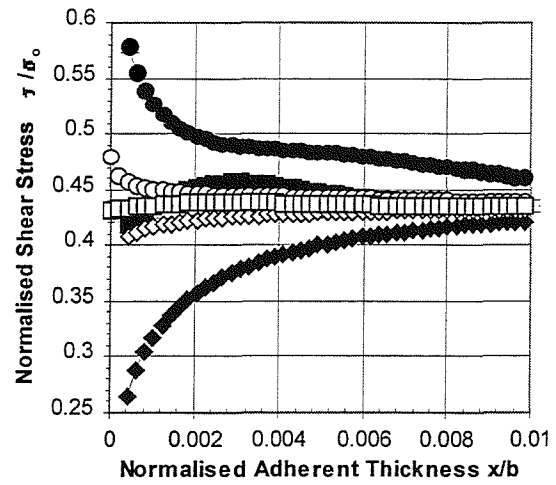
Fig. K.3b Aluminium shear stress - 60° tension

161
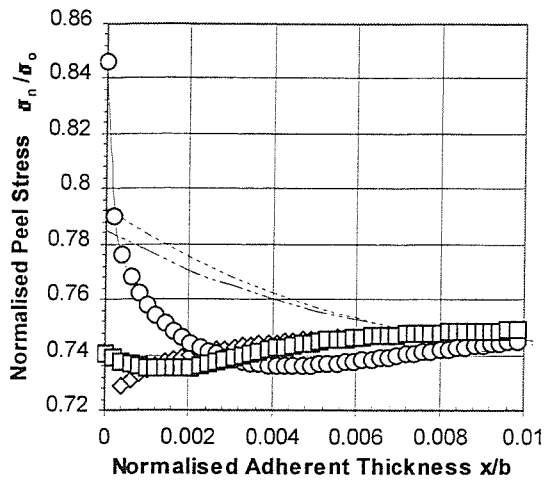
Fig. K.4a Composite peel stress - 60° tension
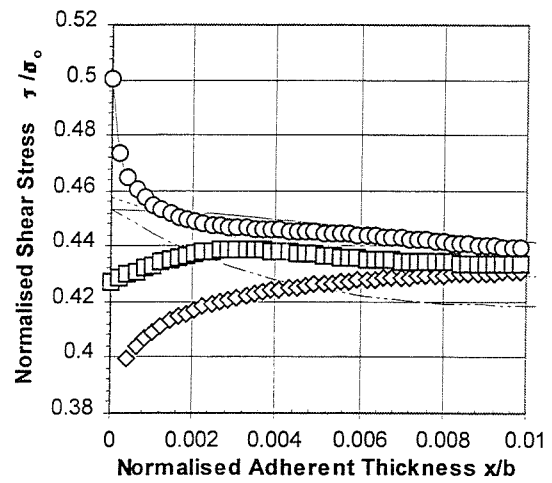
Fig. K.4b Composite shear stress - 60° tension
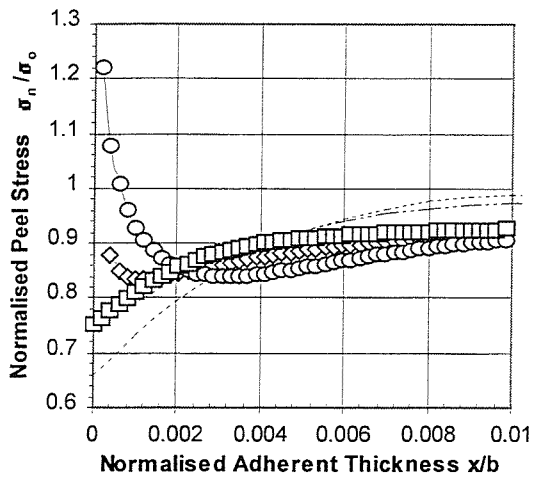
Fig. K.5a Aluminium peel stress - 75° tension
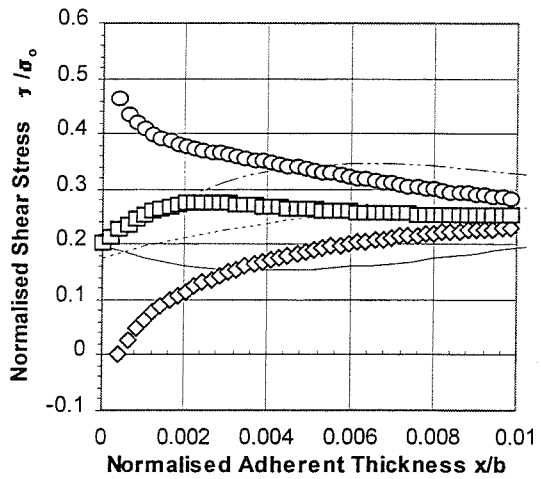
Fig. K.5b Aluminium shear stress - 75° tension
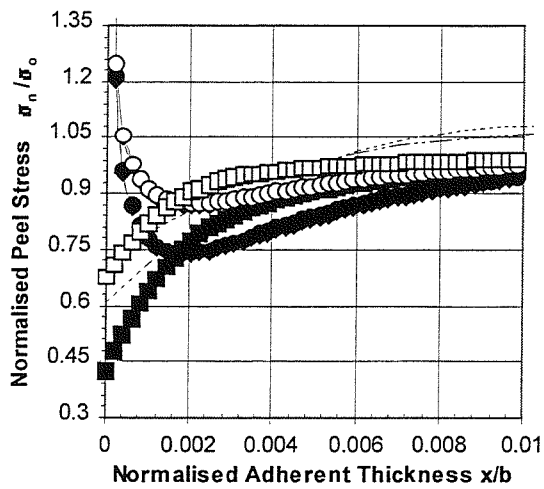
Fig. K.6a Aluminium peel stress - 90° tension
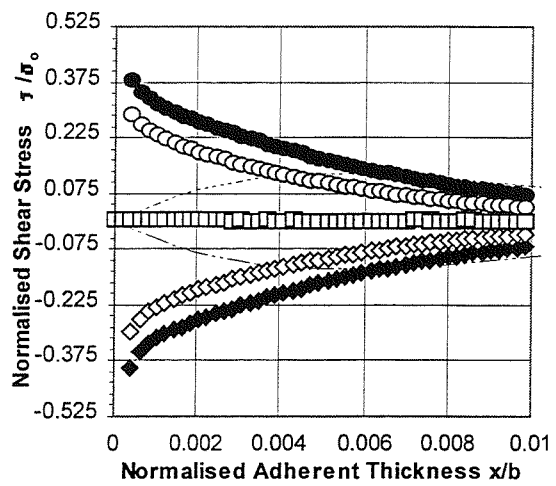
Fig. K.6b Aluminium shear stress - 90° tension

162
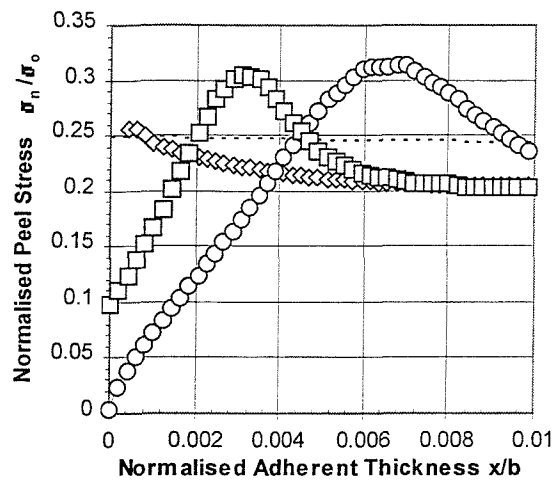
Fig. K.7a Composite peel stress - 30° flexure
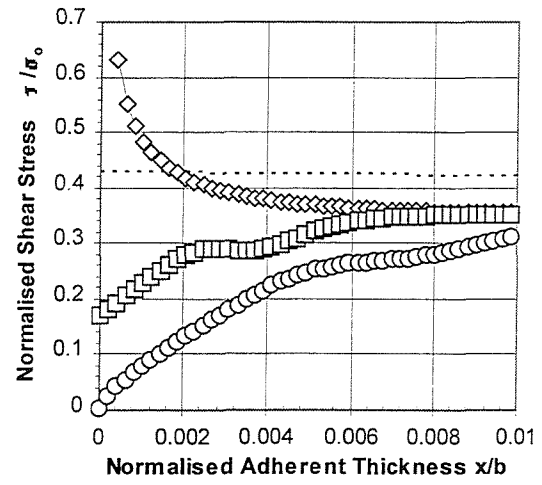
Fig. K.7b Composite shear stress - 30° flexure
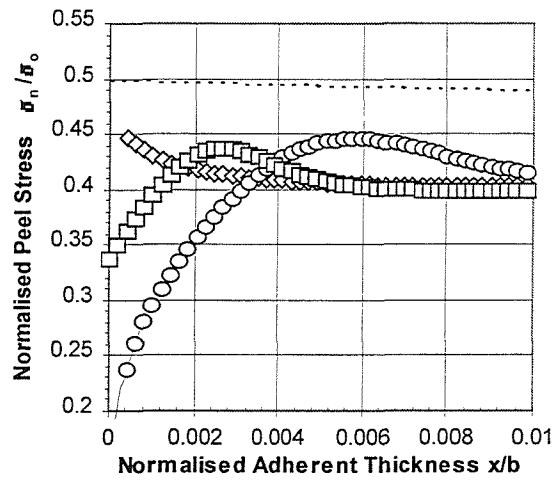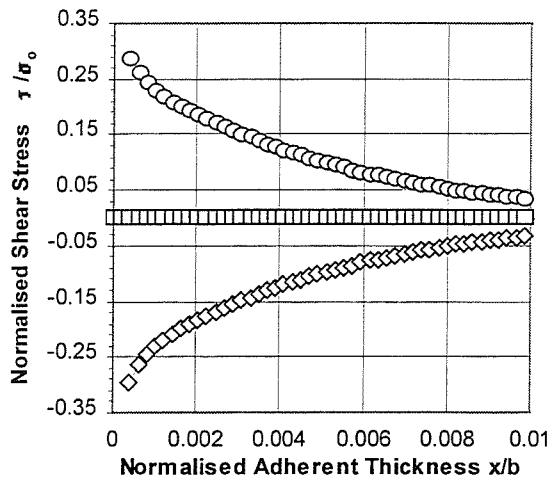

Fig. K.8a Composite peel stress - 45° flexure
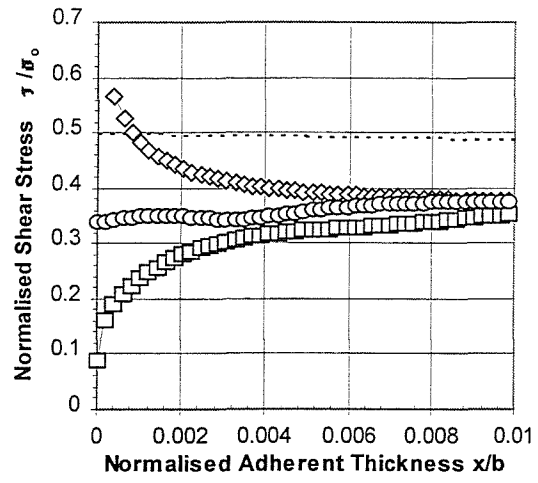
Fig. K.8b Composite shear stress - 45° flexure
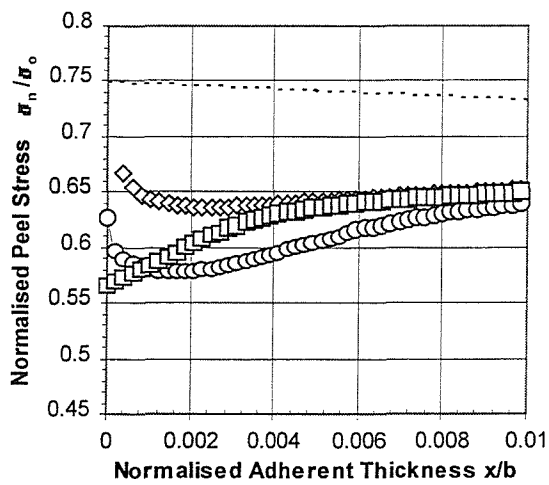
Fig. K.9a Composite peel stress - 60° flexure
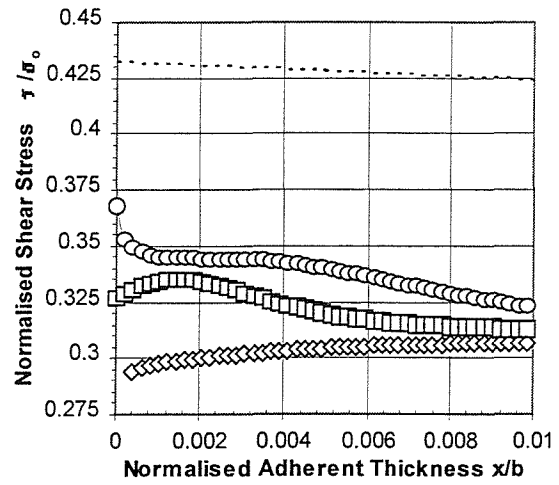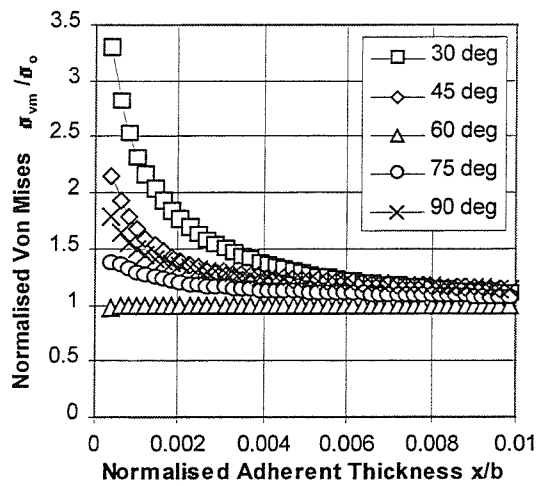

Fig. K.9b Composite shear stress - 60° flexure

163
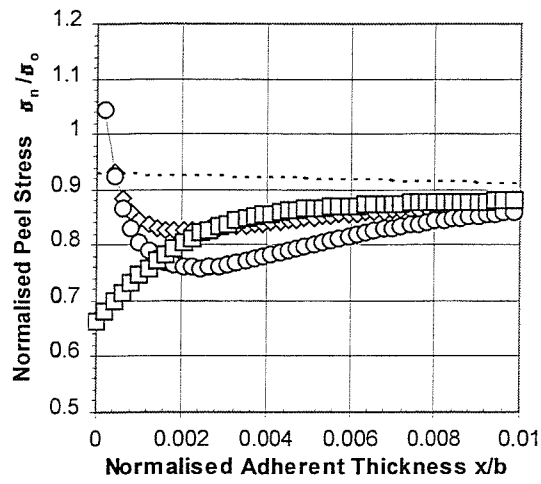
Fig. K.10a Composite peel stress - 75° flexure
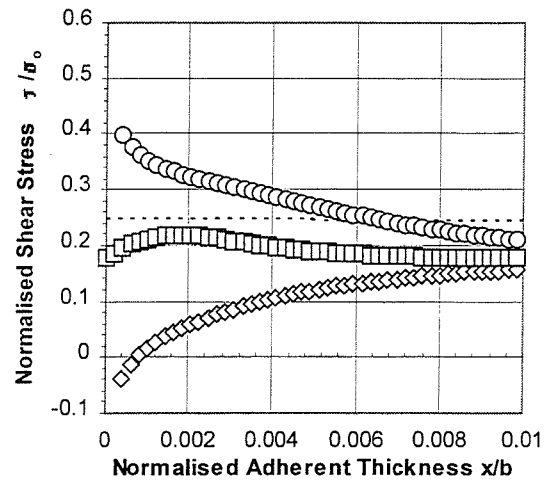
Fig. K.10b Composite shear stress - 75° flexure
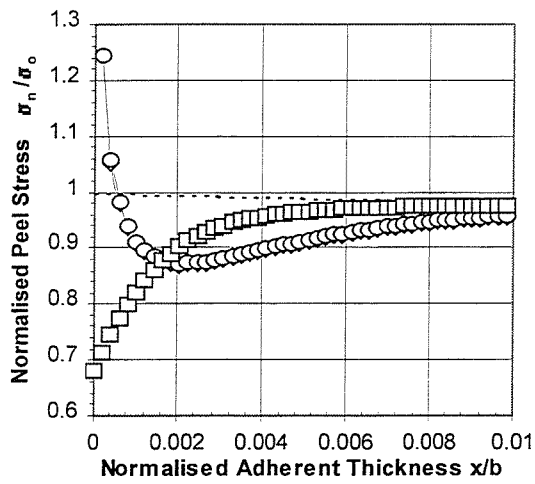
Fig. K.11a Composite peel stress - 90° flexure

Fig. K.11b Composite shear stress - 90° flexure

Fig. K.12a Aluminium Von Mises stress - tension
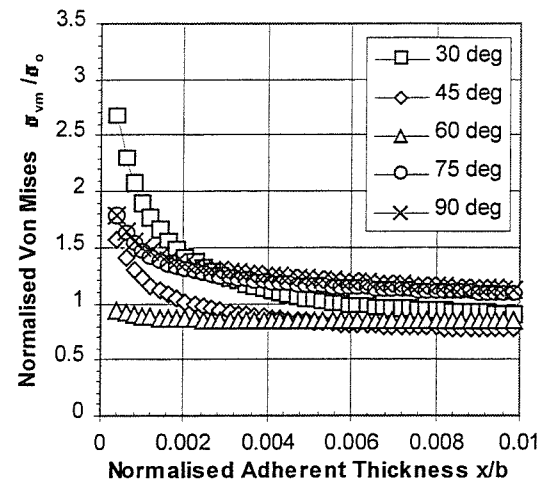
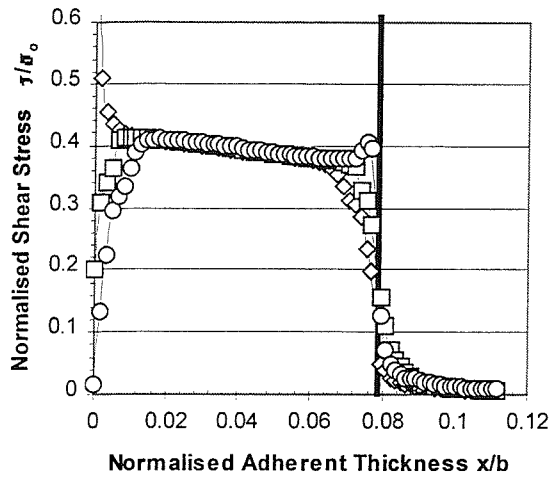Fig. K.12b Composite Von Mises stress - flexure
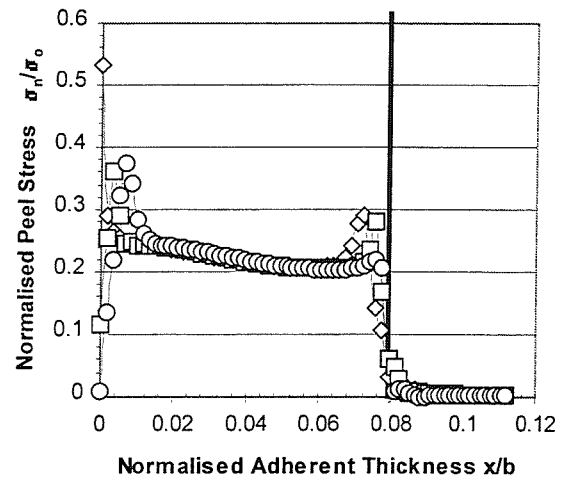
164

Fig. K.13a Shear stress – 2mm aluminium skin 30°

Fig. K.13b Peel stress – 2mm aluminium skin 30°

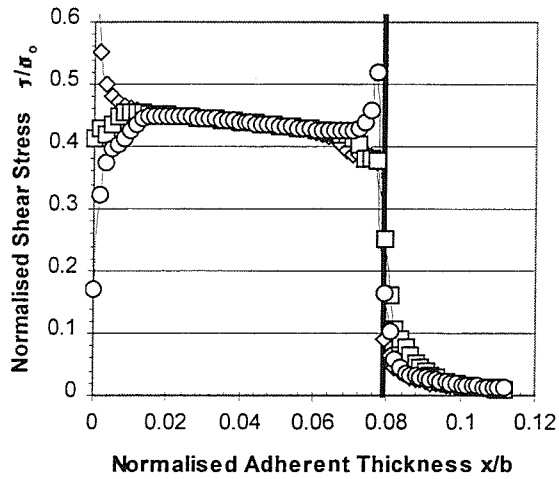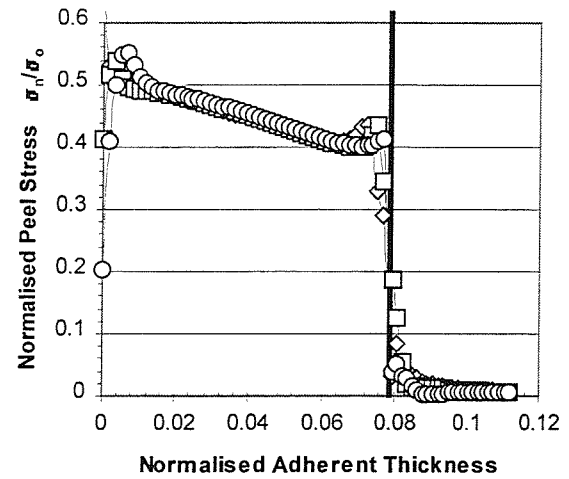Fig. K.14a Shear stress – 2mm aluminium skin 45°
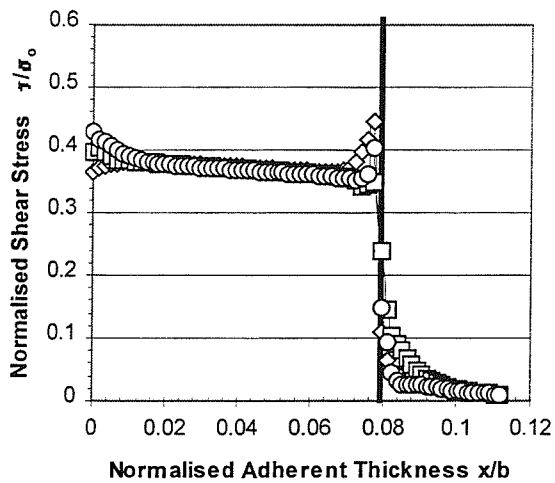

Fig. K.14b Peel stress – 2mm aluminium skin 45°

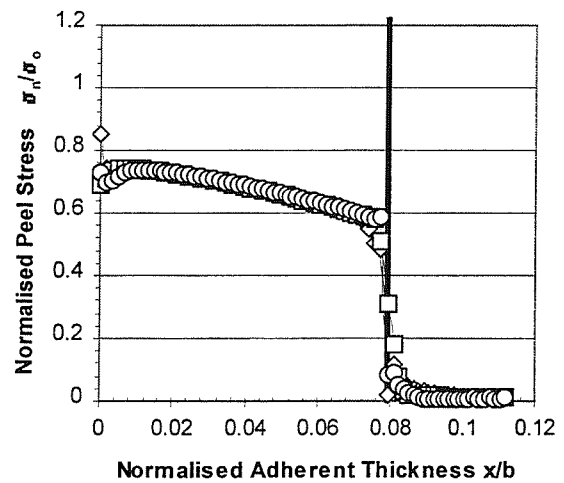Fig. K.15a Shear stress –2mm aluminium skin 60°

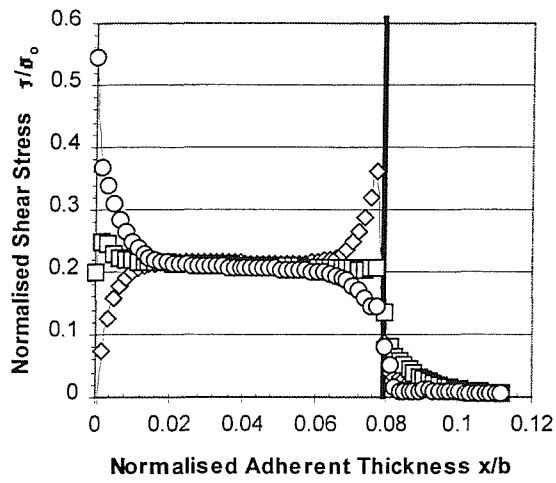Fig. K.15b Peel stress – 2mm aluminium skin 60°

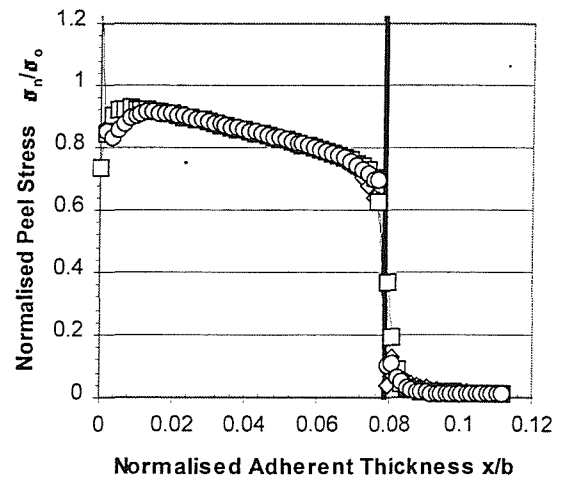Fig. K.16a Shear stress – 2mm aluminium skin 75°

Fig. K.16b Peel stress – 2mm aluminium skin 75°
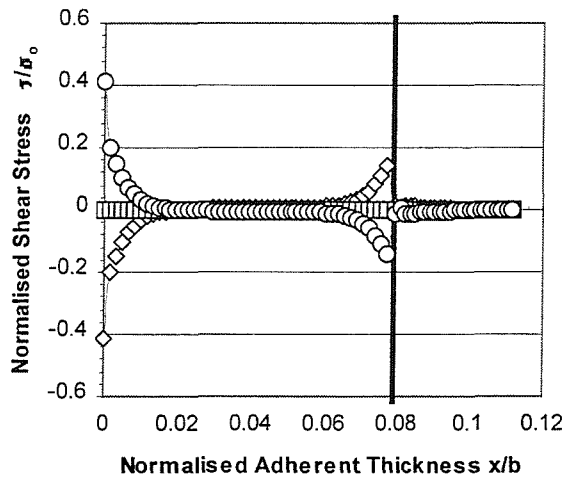

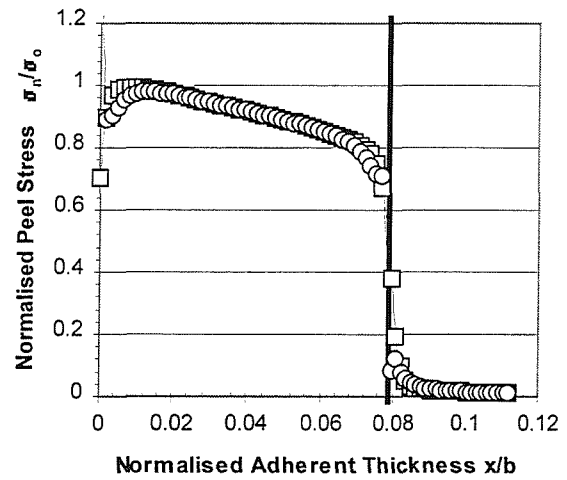Fig. K.17a Shear stress – 2mm aluminium skin 90°

Fig. K.17b. Peel stress – 2mm aluminium skin 90°

The following graphs demonstrate the variation of von Mises stress with scarf angle for use in joint failure prediction.

Fig K.18a Von Mises stress for 2mm aluminium sandwich skin and core transition - pure bending (α=30°).

166

Fig K.18b Von Mises stress for 2mm aluminium sandwich skin and core transition - pure bending (α=45°).
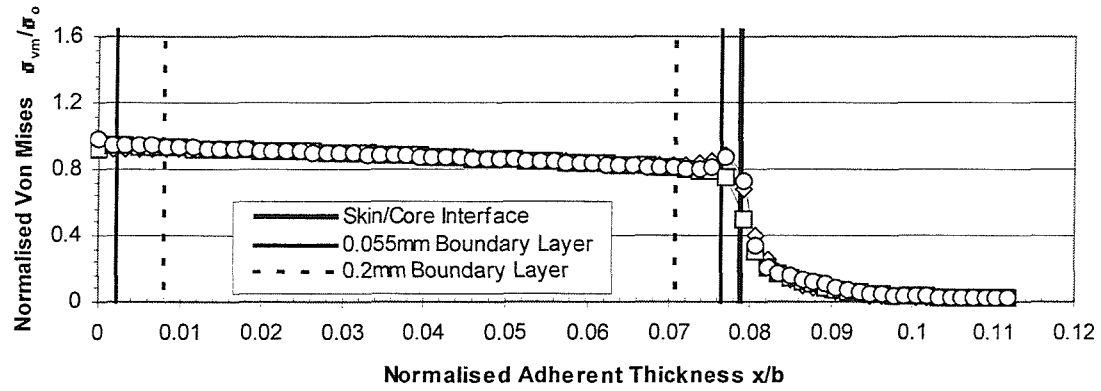
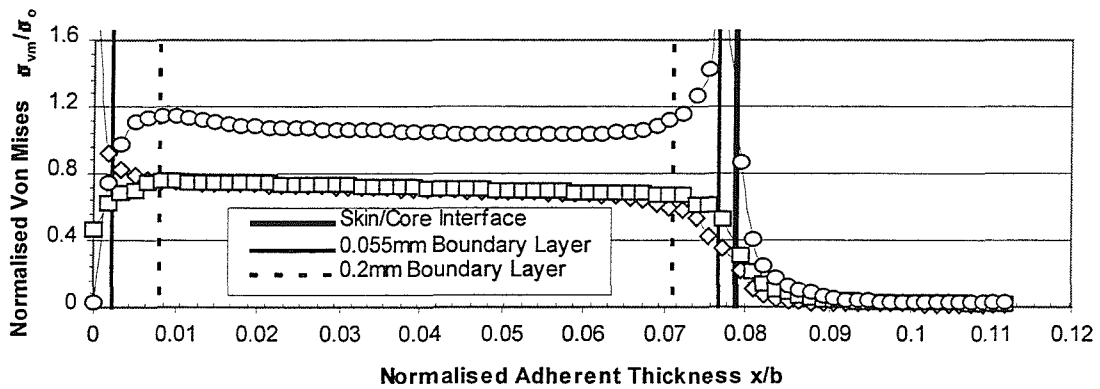Fig K.18c Von Mises stress for 2mm aluminium sandwich skin and core transition - pure bending (α=60°).

Fig K.18d Von Mises stress for 2mm aluminium sandwich skin and core transition - pure bending (α=75°).

Fig K.18e Von Mises stress for 2mm aluminium sandwich skin and core transition - pure bending (α=90°).

Fig. K.19a Shear stress – 2mm composite skin 30°
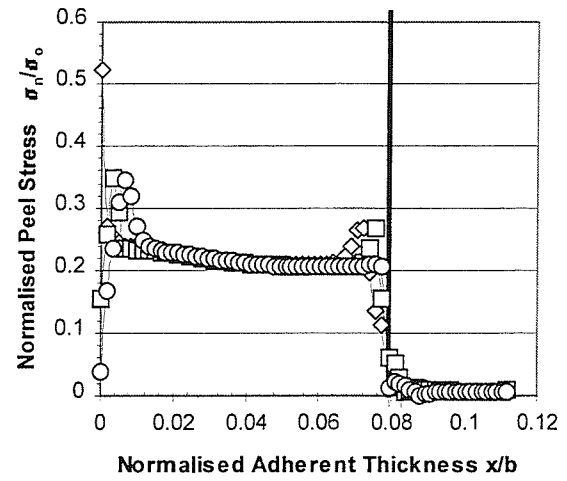
Fig. K.19b Peel stress – 2mm composite skin 30°
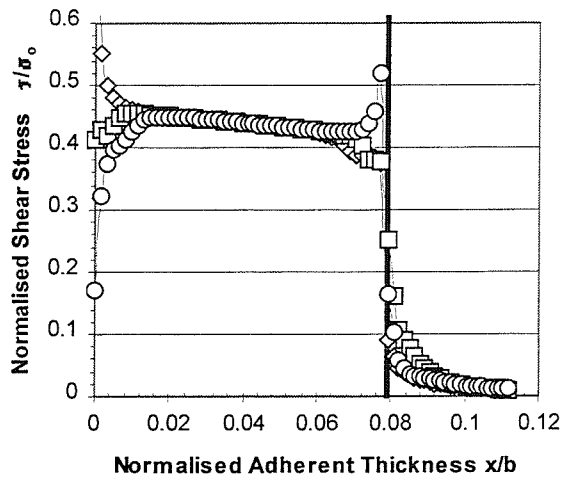
Fig. K.20a Shear stress – 2mm composite skin 45°
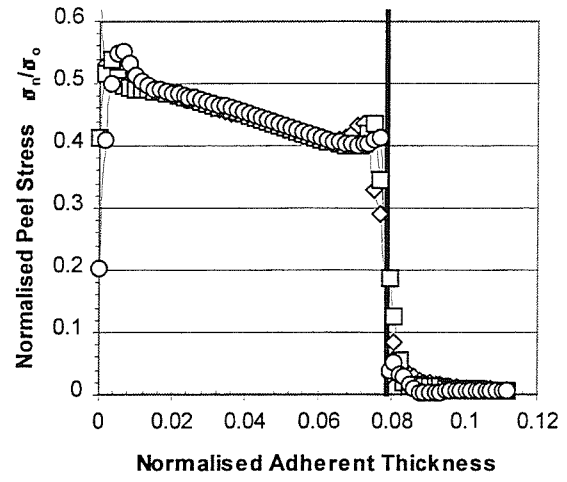
Fig. K.20b Peel stress – 2mm composite skin 45°
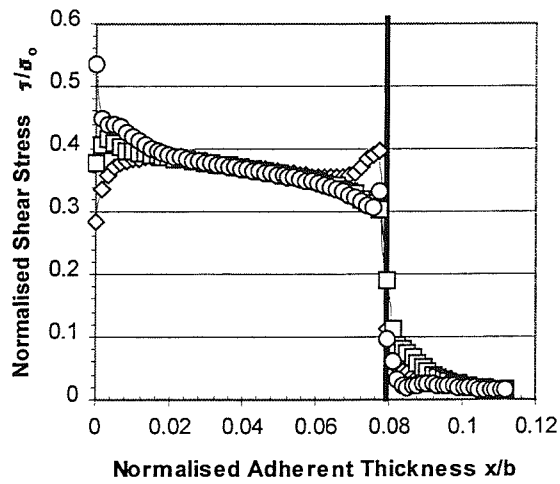
Fig. K.21a Shear stress –2mm composite skin 60°
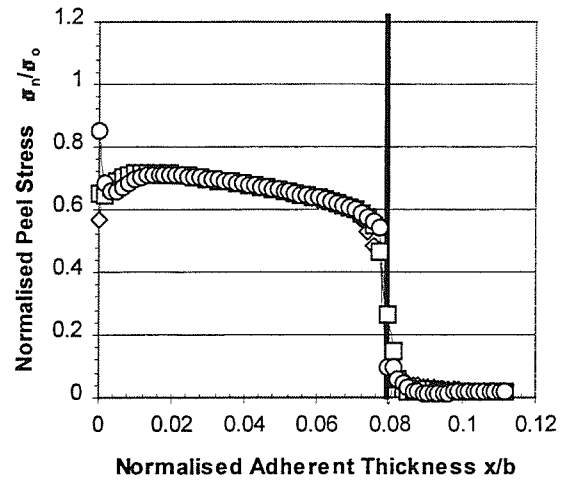
Fig. K.21b Peel stress – 2mm composite skin 60°

168
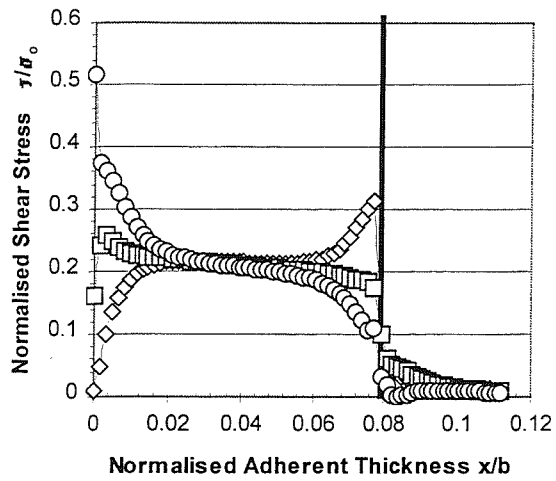
Fig. K.22a Shear stress – 2mm composite skin 75°   Fig. K.22b Peel stress – 2mm composite skin 75°
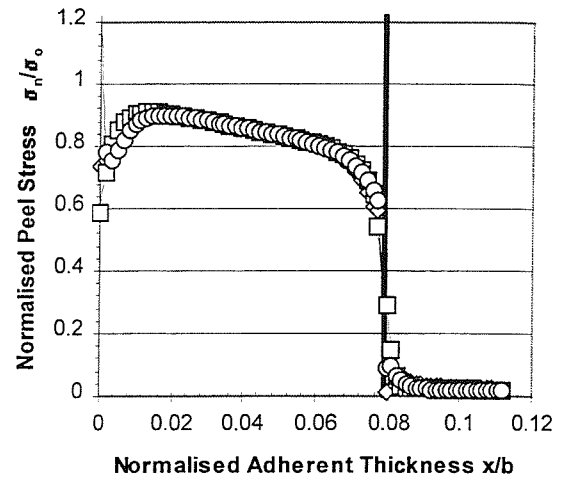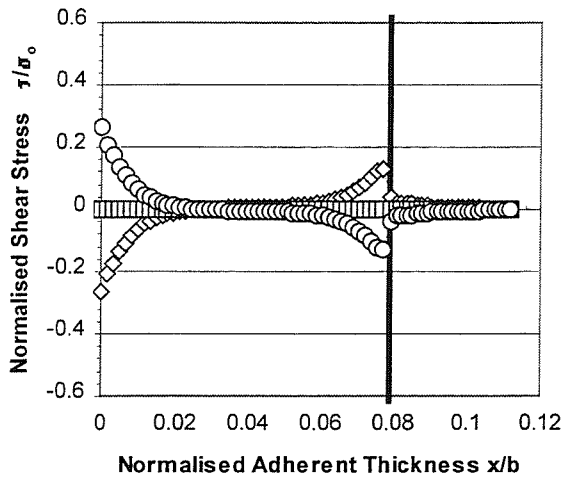
Fig. K.23a Shear stress – 2mm composite skin 90°   Fig. K.23b Peel stress – 2mm composite skin 90°
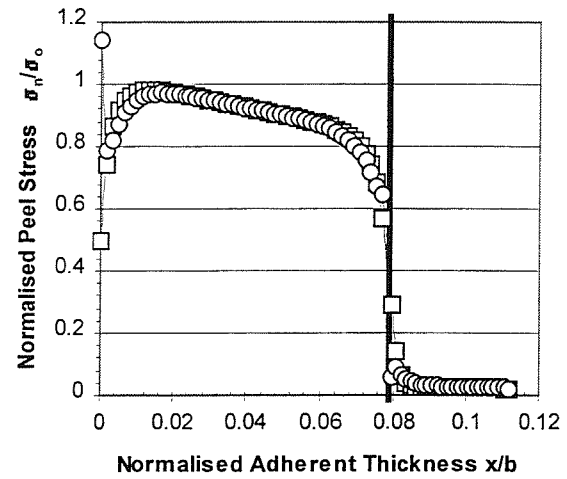
The following graphs demonstrate the variation of principle stress (σ_1) with scarf angle for use in joint failure prediction.
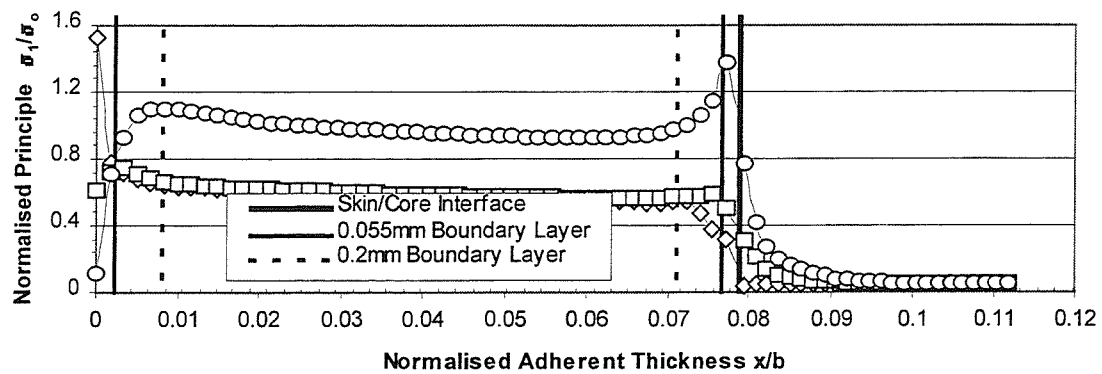
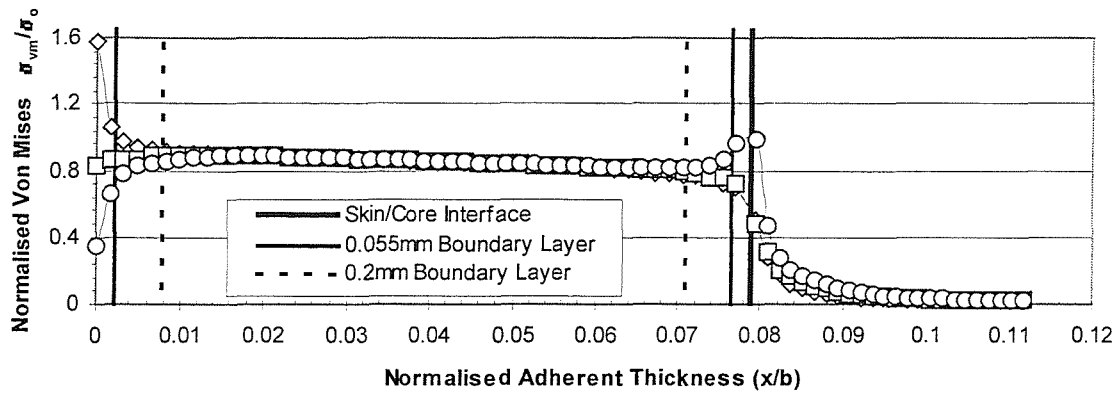Fig K.24a Principle stress for 2mm composite sandwich skin and core transition - pure bending ($\alpha=30°$).

169

Fig K.24b Principle stress for 2mm composite sandwich skin and core transition - pure bending ($\alpha=45^\circ$).

Fig K.24c Principle stress for 2mm composite sandwich skin and core transition - pure bending ($\alpha=60^\circ$).

Fig K.24d Principle stress for 2mm composite sandwich skin and core transition - pure bending ($\alpha=75^\circ$).
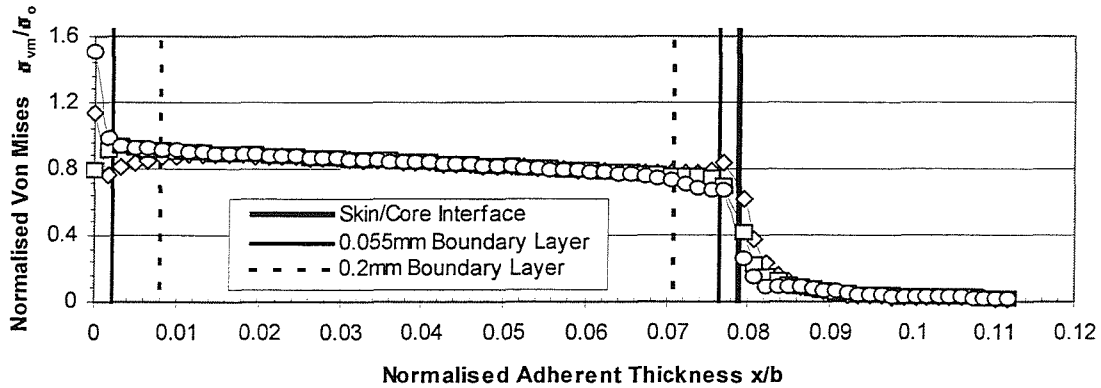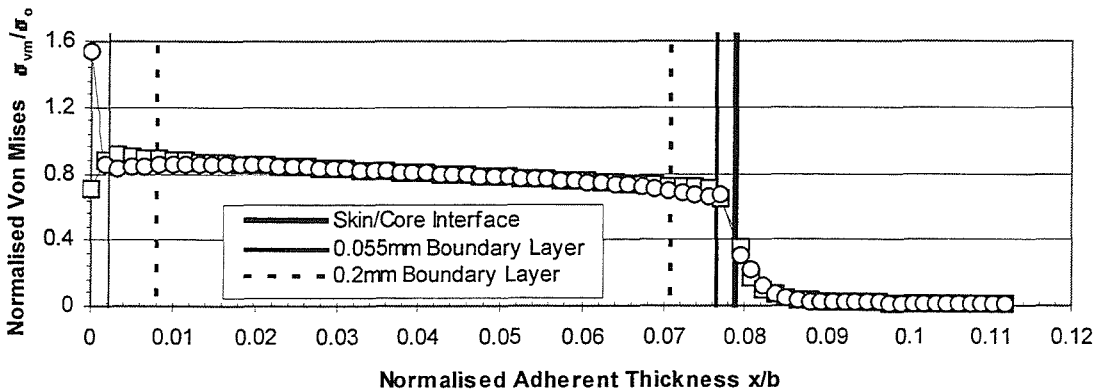

Fig K.24e Principle stress for 2mm composite sandwich skin and core transition - pure bending ($\alpha=90^\circ$).
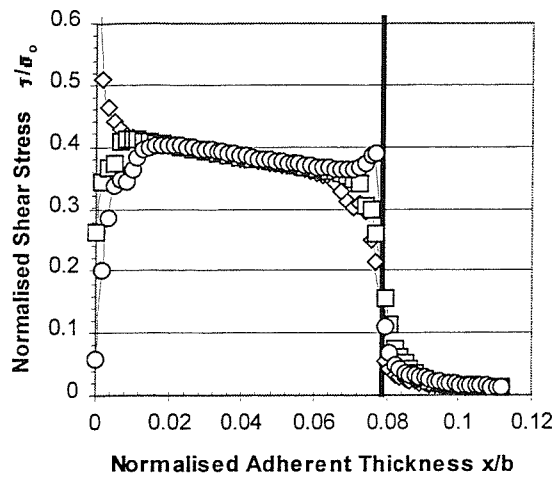
Ansys Input Deck for Scarfed Sandwich Joint

```
/prep7
/Title, Scarf30
ET,1,PLANE82
ET,2,BEAM3
R,1,10000,1000000,100,,,,

mp,ex,1,71000
mp,nuxy,1,0.334
mp,ex,2,2015
mp,nuxy,2,0.368
mp,ex,3,1000000
mp,nuxy,3,0.33
mp,ex,4,500
mp,nuxy,4,0.3

c***, BOTTOM POINTS
k,1,0,0,0
k,2,59.797045,0,0
k,3,61.797045,0,0
k,4,62.197045,0,0
k,5,64.197045,0,0
k,6,80,0,0,0

c***, SECOND ROW
k,7,0,2,0
k,8,56.332943,2,0
k,9,58.332943,2,0
k,10,58.732943,2,0
k,11,60.732943,2,0
k,12,80,2,0

C***, THRID ROW
k,13,0,23.4,0
k,14,19.267097,23.4,0
k,15,21.267097,23.4,0
k,16,21.667097,23.4,0
k,17,23.667097,23.4,0
k,18,80,23.4,0

C***, FOURTH ROW
k,19,0,25.4,0
k,20,15.802955,25.4,0
k,21,17.802955,25.4,0
k,22,18.202955,25.4,0
k,23,20.202955,25.4,0
k,24,80,25.4,0

c***, LINE REGIONS
1,1,2
lesize,1,,,15,,
1,2,3
lesize,2,,,10,,
1,3,4
lesize,3,,,2,,
1,4,5
lesize,4,,,10,,
1,5,6
lesize,5,,,15,,
1,7,8
lesize,6,,,15,,
1,8,9
lesize,7,,,10,,
1,9,10
lesize,8,,,2,,
1,10,11
lesize,9,,,10,,
1,11,12
lesize,10,,,15,,
1,13,14
lesize,11,,,15,,
1,14,15
lesize,12,,,10,,
1,15,16
lesize,13,,,2,,
1,16,17
lesize,14,,,10,,
1,17,18
lesize,15,,,15,,
1,19,20
lesize,16,,,15,,
1,20,21
lesize,17,,,10,,
1,21,22
lesize,18,,,2,,
1,22,23
lesize,19,,,10,,
1,23,24
lesize,20,,,15,,
1,1,7
lesize,21,,,10,,
1,2,8

lesize,22,,,10,,
1,3,9
lesize,23,,,10,,
1,4,10
lesize,24,,,10,,
1,5,11
lesize,25,,,10,,
1,6,12
lesize,26,,,10,,
1,7,13
lesize,27,,,40,,
1,8,14
lesize,28,,,40,5,
1,9,15
lesize,29,,,40,5,
1,10,16
lesize,30,,,40,5,
1,11,17
lesize,31,,,40,5,
1,12,18
lesize,32,,,40,,
1,13,19
lesize,33,,,10,,
1,14,20
lesize,34,,,10,,
1,15,21
lesize,35,,,10,,
1,16,22
lesize,36,,,10,,
1,17,23
lesize,37,,,10,,
1,18,24
lesize,38,,,10,,

c***, GLUE LINE
a,3,4,10,9
a,9,10,16,15
a,15,16,22,21

c***, CORE

a,7,8,14,13
a,8,9,15,14
a,10,11,17,16
a,11,12,18,17

aatt,4,1,1,0,

c***, ADHEREND
a,1,2,8,7
a,2,3,9,8
a,4,5,11,10
a,5,6,12,11
a,13,14,20,19
a,14,15,21,20
a,16,17,23,22
a,17,18,24,23

asel,s,area,,1,3,1,0
aatt,2,1,1,0
asel,all

aglue,all
eshape,2,0
amesh,1,3,1
amesh,12,15,1
amesh,4,7,1
amesh,8,11,1

c***, RIGID END
SUPPORTS

lsel,,loc,x,0
lsel,a,loc,x,80
latt,3,1,2,0,
lsel,all
lmesh,21,,
lmesh,26,,
lmesh,27,,
lmesh,32,,
lmesh,33,,
lmesh,38,,

c***, ----APPLYING
BOUNDARY CONDITIONS----

d,2235,ux
d,2235,uy
d,6355,ux
d,6355,uy

c***, ----APPLYING
LOADS----

f,537,fx,1000
f,9136,fx,1000
f,8086,fx,-1000
f,1636,fx,-1000

c***, ----ROTATED WORK
PLANE #11----

k,25,0,-5
k,26,1.732051,-6
k,27,1,-3.267949

cskp,11,0,25,26,27,1,1
,

/solu
antype,static,new
save
solve
finish

c***, ----CREATE
SUBMODEL----

/clear
/filname,sub30
/prep7
/Title, Scarf30Sub
ET,1,PLANE82

mp,ex,1,71000
mp,nuxy,1,0.334
mp,ex,2,2015
mp,nuxy,2,0.368
mp,ex,3,1000000
mp,nuxy,3,0.33
mp,ex,4,500
mp,nuxy,4,0.3

c***, BOTTOM POINTS
k,1,59.797045,0,0
k,2,61.797045,0,0
k,3,62.197045,0,0
k,4,64.197045,0,0

c***, SECOND ROW
k,5,58.06,1,0
k,6,60.06,1,0
k,7,60.46,1,0
k,8,62.46,1,0

c***, THIRD ROW
k,9,56.332943,2,0
k,10,58.332943,2,0
k,11,58.732943,2,0
k,12,60.732943,2,0

c***, FOURTH ROW
k,13,54.85,2.856,0
k,14,56.85,2.856,0
k,15,57.25,2.856,0
k,16,59.25,2.856,0

c***, LINE REGIONS
1,1,2
lesize,1,,,20,0.2,
1,2,3
lesize,2,,,10,,
1,3,4
lesize,3,,,20,5,
1,5,6
lesize,4,,,20,0.2,
1,6,7
lesize,5,,,10,,
1,7,8
lesize,6,,,20,5,
1,9,10
lesize,7,,,20,0.2,
1,10,11
lesize,8,,,10,,
1,11,12
lesize,9,,,20,5,
1,13,14
lesize,10,,,20,0.2,
1,14,15
lesize,11,,,10,,
1,15,16

lesize,12,,,20,5,
1,1,5
lesize,13,,,15,5,
1,2,6
lesize,14,,,15,5,
1,3,7
lesize,15,,,15,5,
1,4,8
lesize,16,,,15,5,
1,5,9
lesize,17,,,15,0.2,
1,6,10
lesize,18,,,15,0.2,
1,7,11
lesize,19,,,15,0.2,
1,8,12
lesize,20,,,15,0.2,
1,9,13
lesize,21,,,15,5,
1,10,14
lesize,22,,,15,5,
1,11,15
lesize,23,,,15,5,
1,12,16
lesize,24,,,15,5,

c***, GLUE LINE
a,2,3,7,6
a,6,7,11,10
a,10,11,15,14

c***, CORE
a,9,10,14,13
a,11,12,16,15

aatt,4,1,1,0

c***, ADHEREND
a,1,2,6,5
a,3,4,8,7
a,5,6,10,9
a,7,8,12,11

asel,s,area,,1,3,1,
0
aatt,2,1,1,0
asel,all

aglue,all
eshape,2,0
amesh,all

c***, ----ROTATED
WORK PLANE #11----

k,17,0,-5
k,18,1.732051,-6
k,19,1,-3.267949

cskp,11,0,17,18,19,
1,1,

c***, CUT BOUNDARY
SELECTION

lsel,s,line,10,10,1
3,1,0
lsel,a,line,16,16,1
7,1,0
lsel,a,line,20,20,2
1,1,0
lsel,a,line,24,24,,
,0
nsll,r,1
nwrite
allsel

save
finish

c***, COARSE MODEL
INTERPOLATION

resume,scarftest,db
/post1
file,scarftest,rst
set,1
cbdof,,,,,,,0,,
finish

c***, SUBMODEL
DOF & SOLUTION

resume
/solu
antype,static,new
/input,sub30,cbdo
solve
finish
/post1
rsys,11
lpath,1,532,1012
pdef,,s,x,noav
pdef,,s,y,noav
pdef,,s,xy,noav
pdef,,s,eqv,noav
pdef,,s,1,noav
/output,sda30fac,
dat,,,
prpath,sx,sy,sxy,
seqv,s1
/output,,
lpath,12,542,1022
pdef,,s,x,noav
pdef,,s,y,noav
pdef,,s,xy,noav
pdef,,s,eqv,noav
pdef,,s,1,noav
/output,sda30fad,
dat,,,
prpath,sx,sy,sxy,
seqv,s1
/output,,
lpath,2,502,982
pdef,,s,x,noav
pdef,,s,y,noav
pdef,,s,xy,noav
pdef,,s,eqv,noav
pdef,,s,1,noav
/output,sda30fob,
dat,,,
prpath,sx,sy,sxy,
seqv,s1
/output,,
plesol,s,eqv,0
```
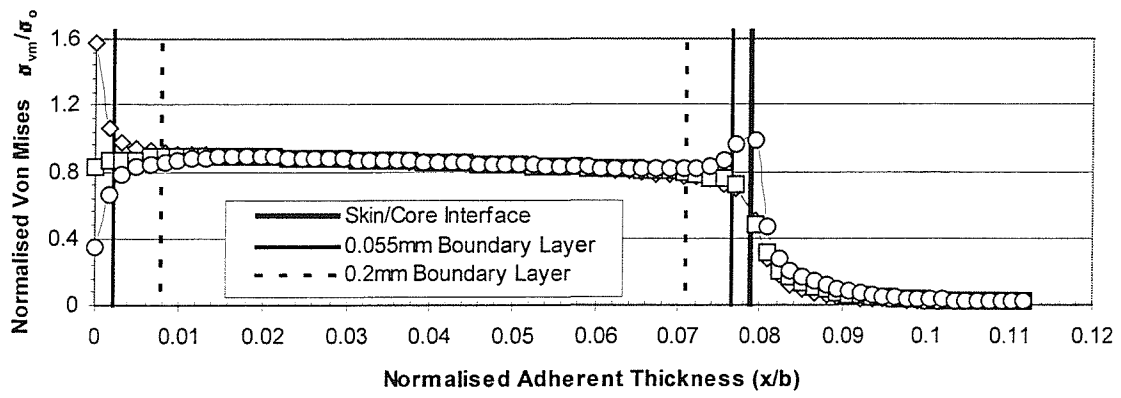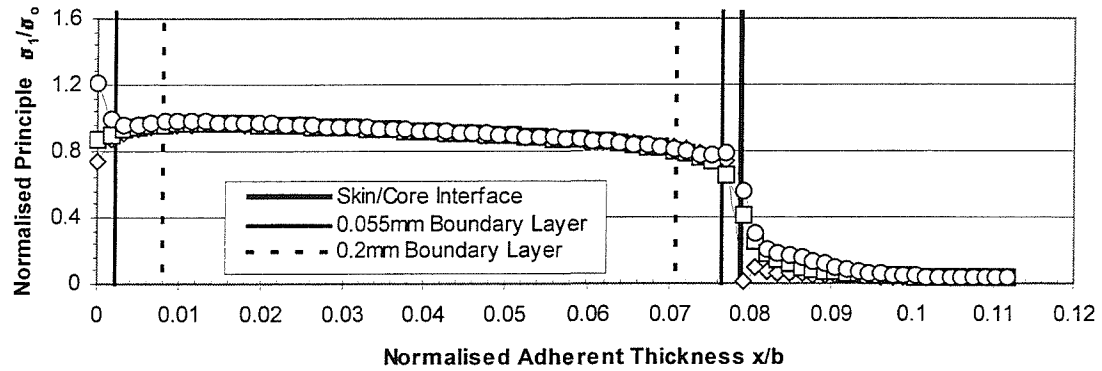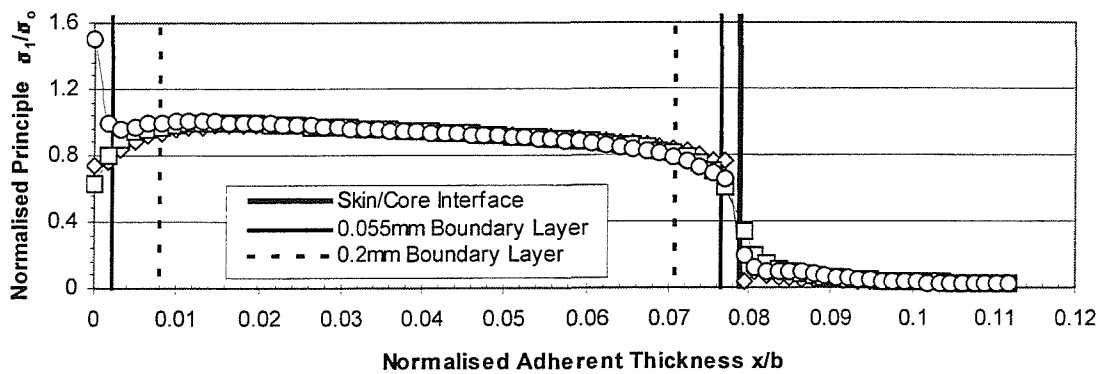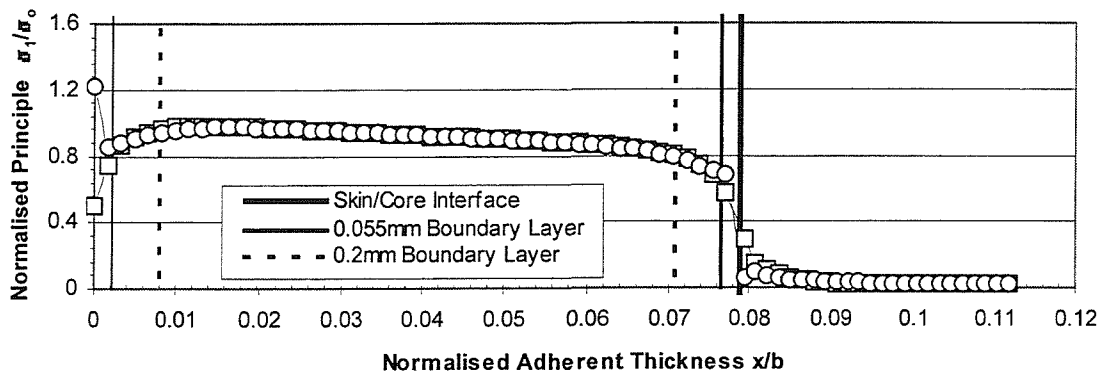
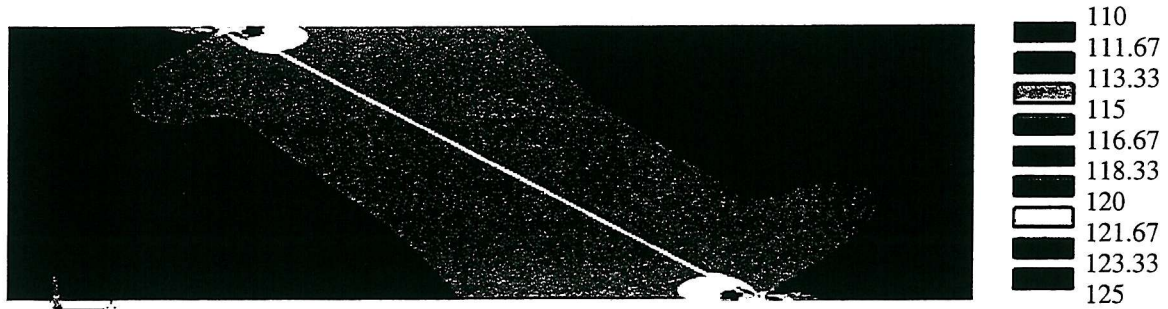**FEA – Contoured Stress Distributions (ref. Appendix K for dimensions)**

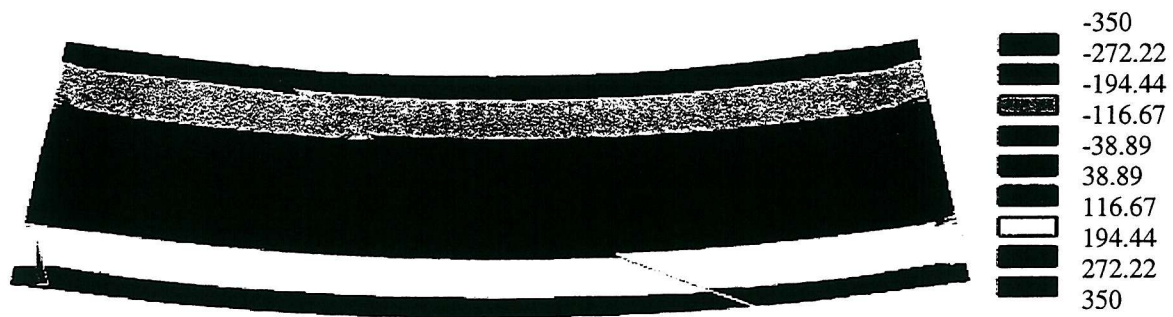Fig. M.1 σ_1 – Global homogeneous tension model (composite $\alpha = 30°$).

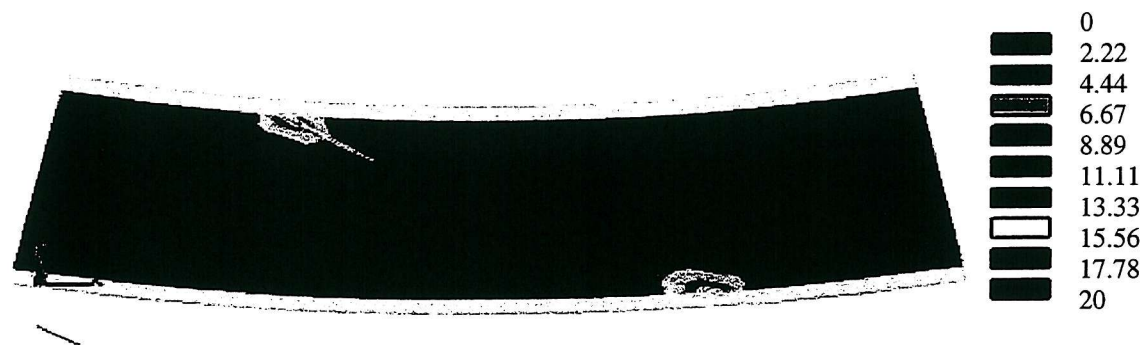Fig. M.2 σ_x – Global homogeneous flexural model (composite $\alpha = 30°$).

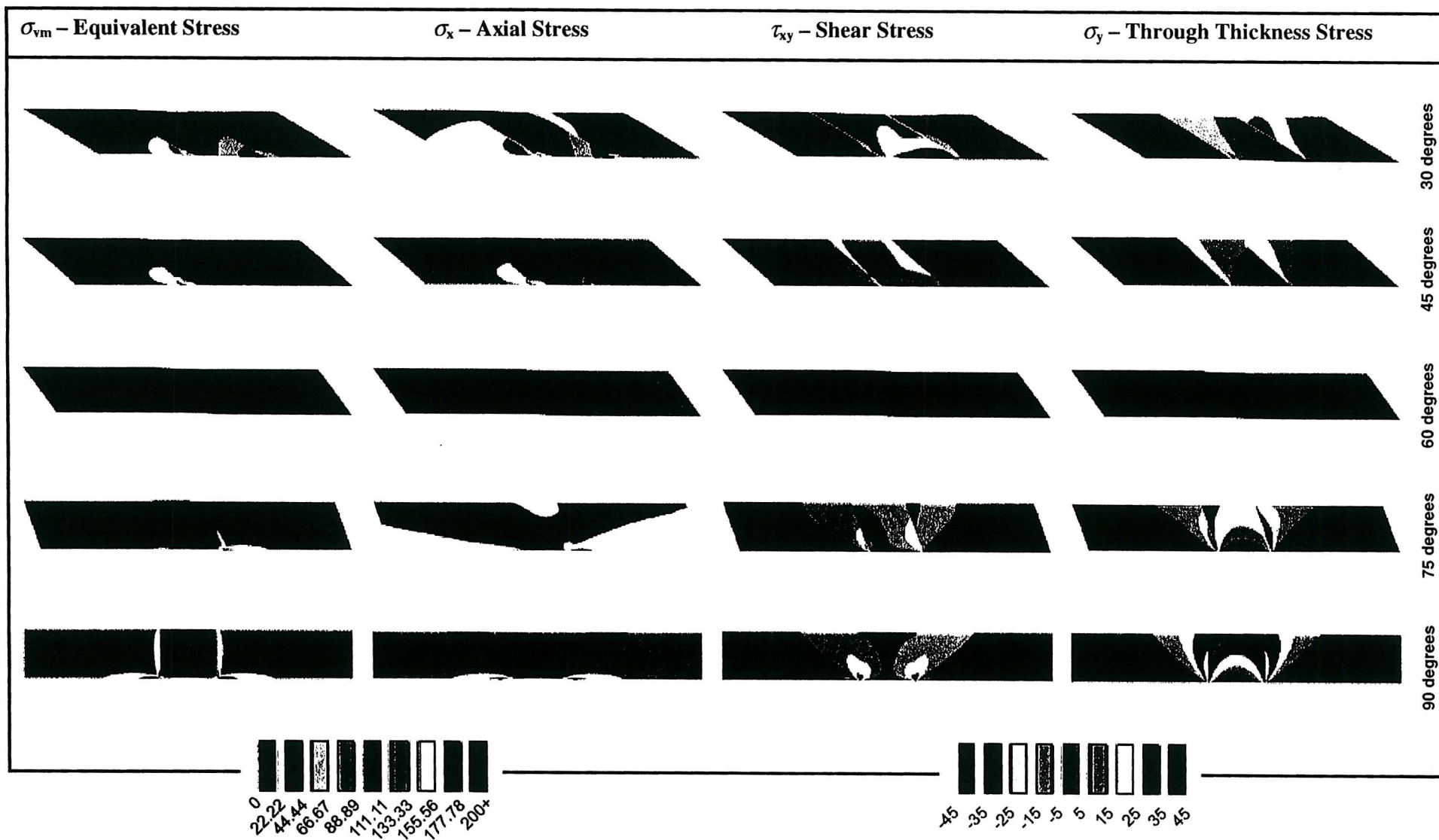Fig. M.3 σ_{vm} – Global sandwich flexural model showing foam core stress distribution ($\alpha = 30°$).

Figure M.4 Stress variation (MPa) in tension as a function of angle for homogenous aluminium adherents and epoxy adhesive – plane stress.

| σ_{vm} – Equivalent Stress | σ_x – Axial Stress | τ_{xy} – Shear Stress | σ_y – Through Thickness Stress |

30 degrees
45 degrees
60 degrees
75 degrees
90 degrees

174

0 22.22 44.44 66.67 88.89 111.11 133.33 155.56 177.78 200+

-45 -35 -25 -15 -5 5 15 25 35 45
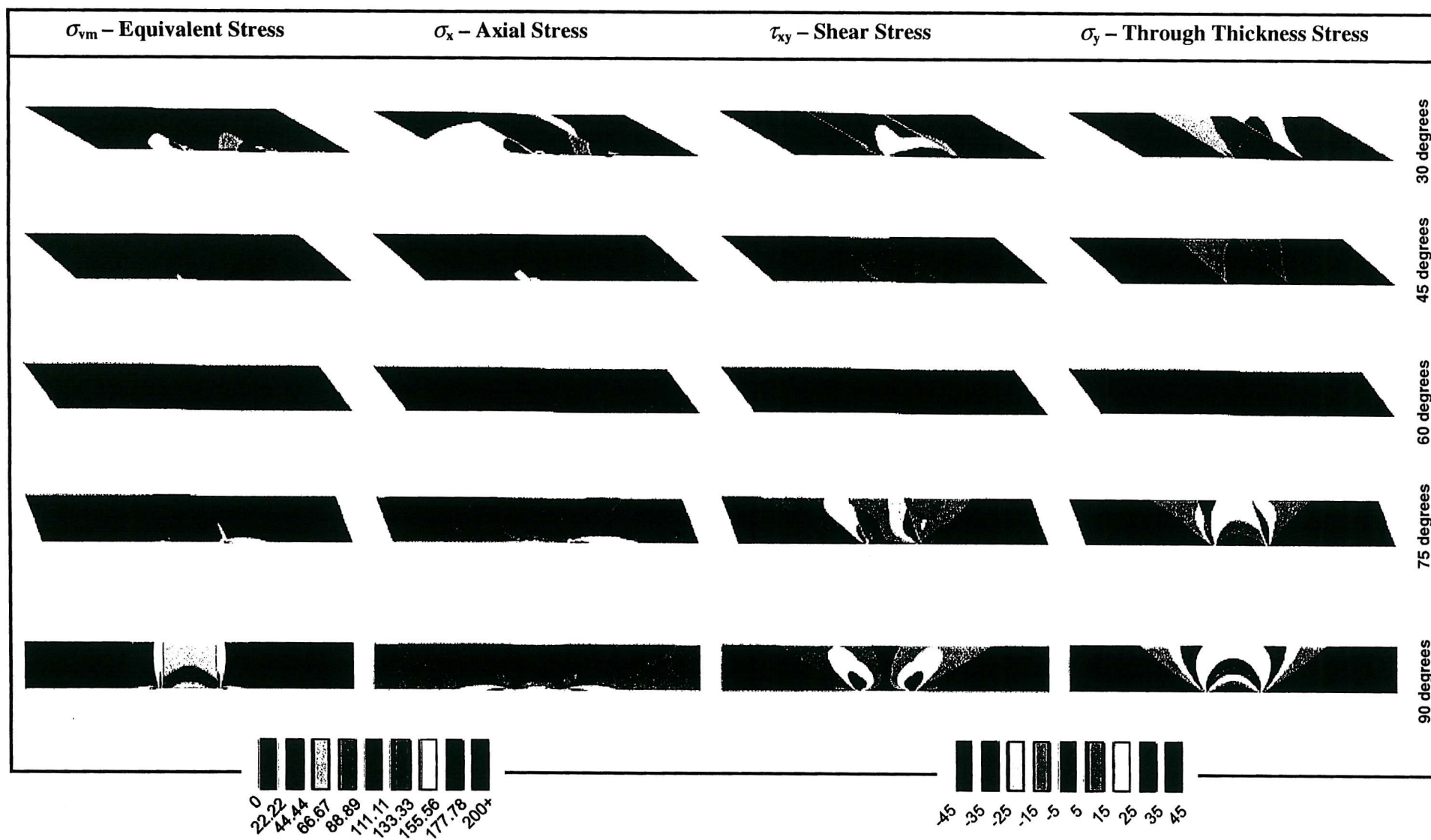
Figure M.5 Stress variation (MPa) in tension as a function of angle for homogenous aluminium adherents and epoxy adhesive – plane strain.
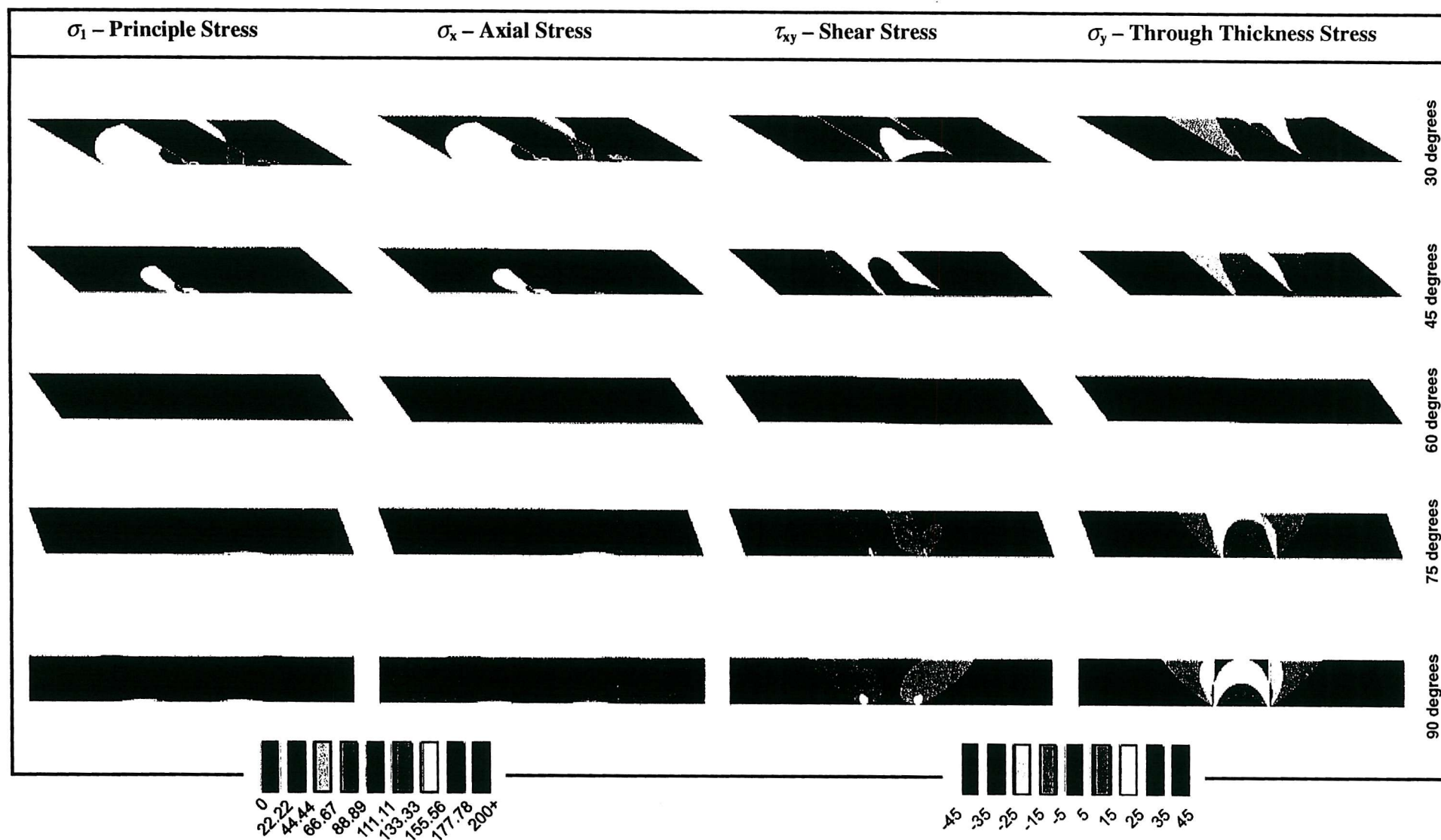
Figure M.6 Stress variation (MPa) in flexure as a function of angle for homogenous composite adherents and epoxy adhesive – plane stress.

175
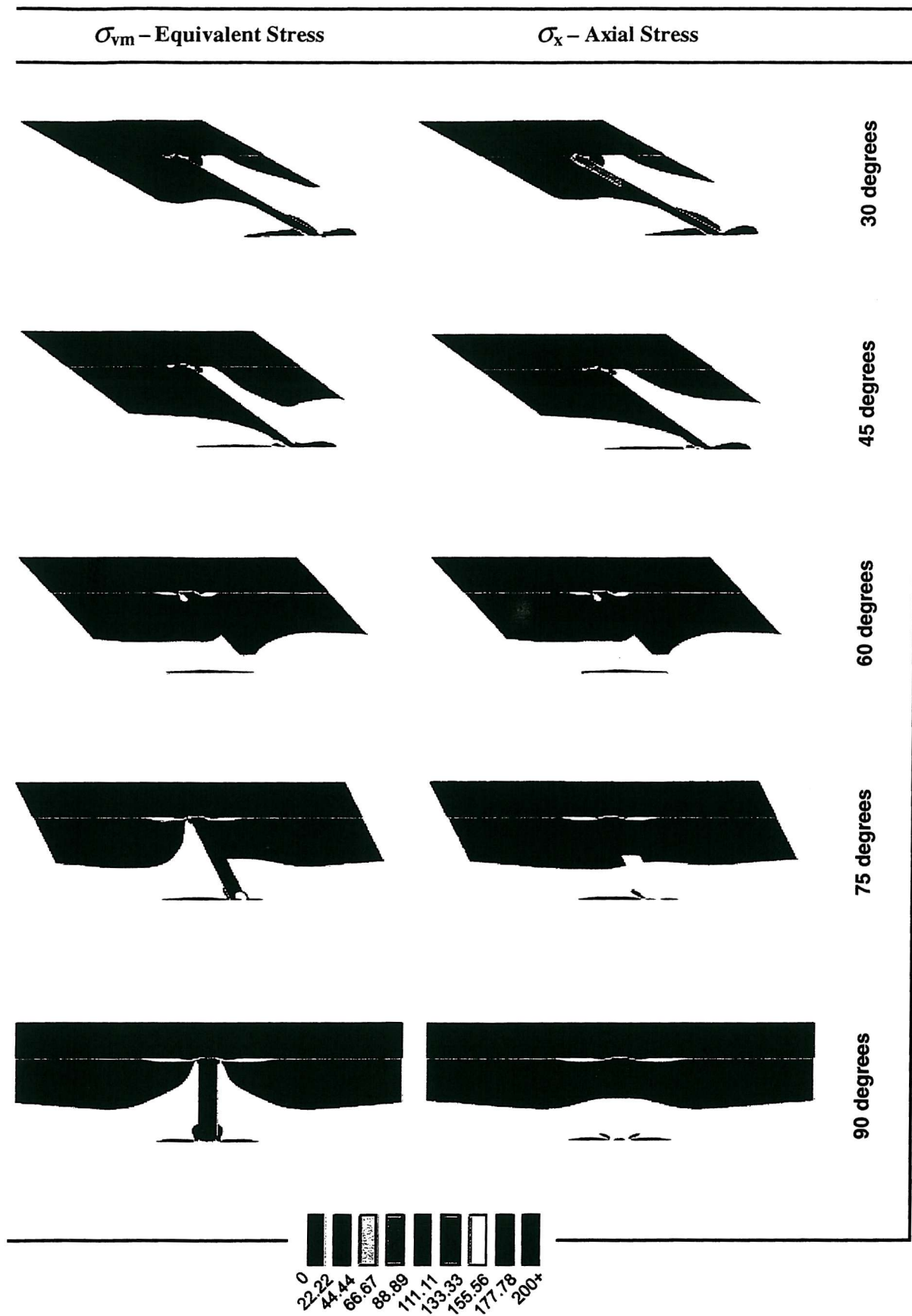
Figure M.7a Variation of Von Mises and axial stress (MPa) distribution in a scarfed sandwich joint with 2mm thick aluminium skins and foam core in flexure – plane strain.
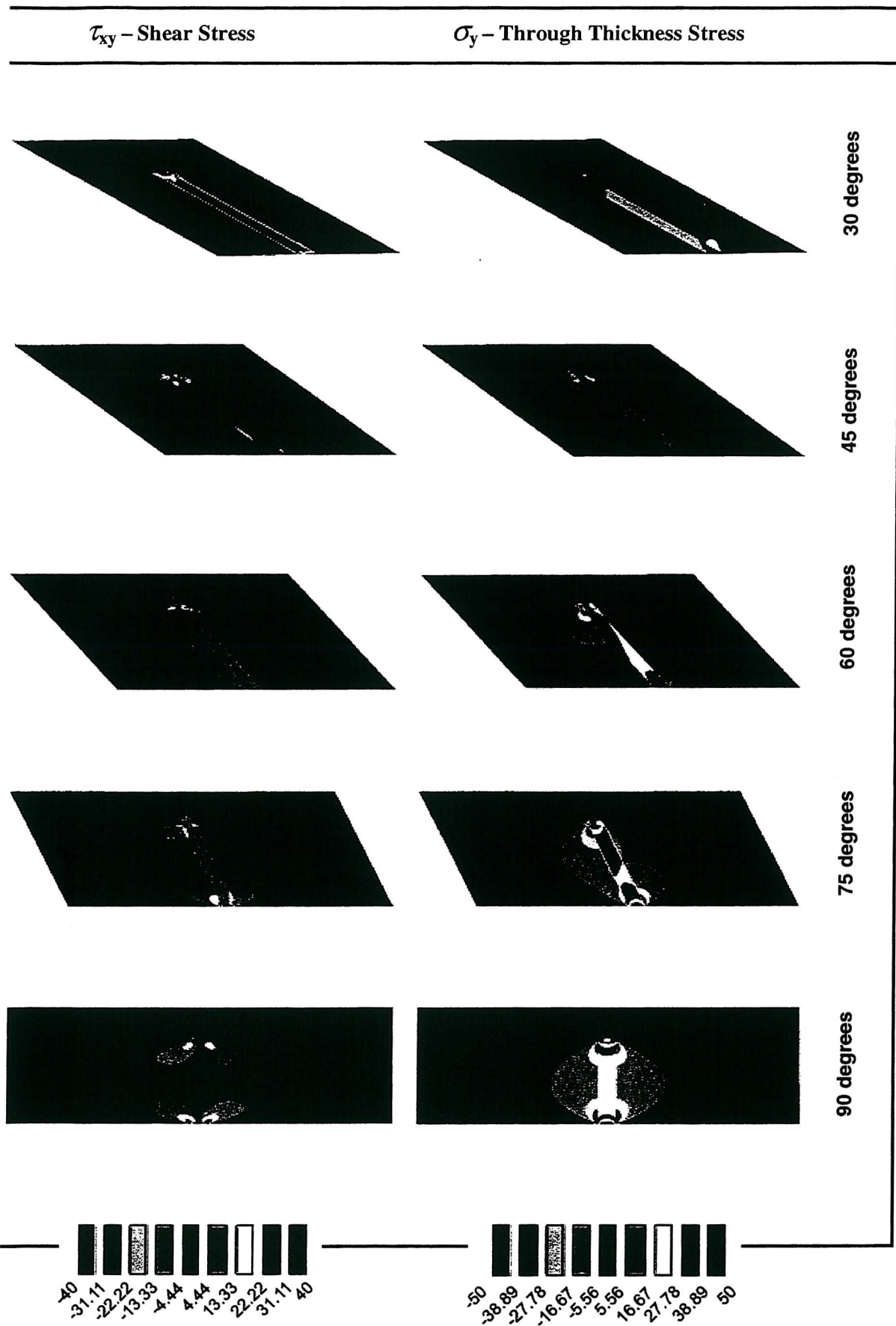
| τ_{xy} – Shear Stress | σ_y – Through Thickness Stress |

30 degrees

45 degrees

60 degrees

75 degrees

90 degrees

-40 -31.11 -22.22 -13.33 -4.44 4.44 13.33 22.22 31.11 40
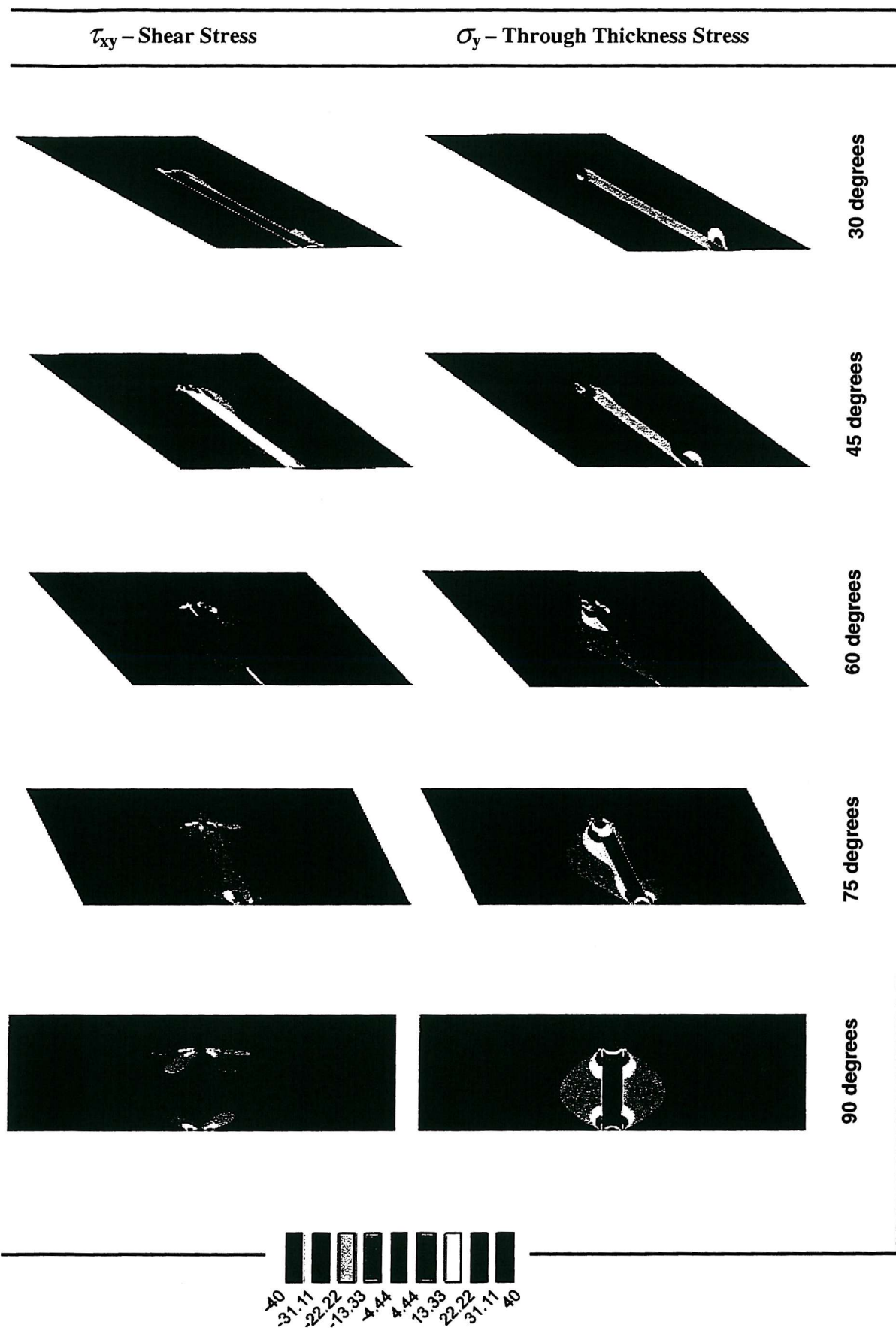
Figure M.7b Variation of shear and through thickness stress (MPa) in a scarfed sandwich joint
with 2mm thick aluminium skins and foam core in flexure – plane strain.

σ_1 – Principle Stress $\qquad$ σ_x – Axial Stress

30 degrees

45 degrees

60 degrees

75 degrees

90 degrees

0 22.22 44.44 66.67 88.89 111.11 133.33 155.56 177.78 200+
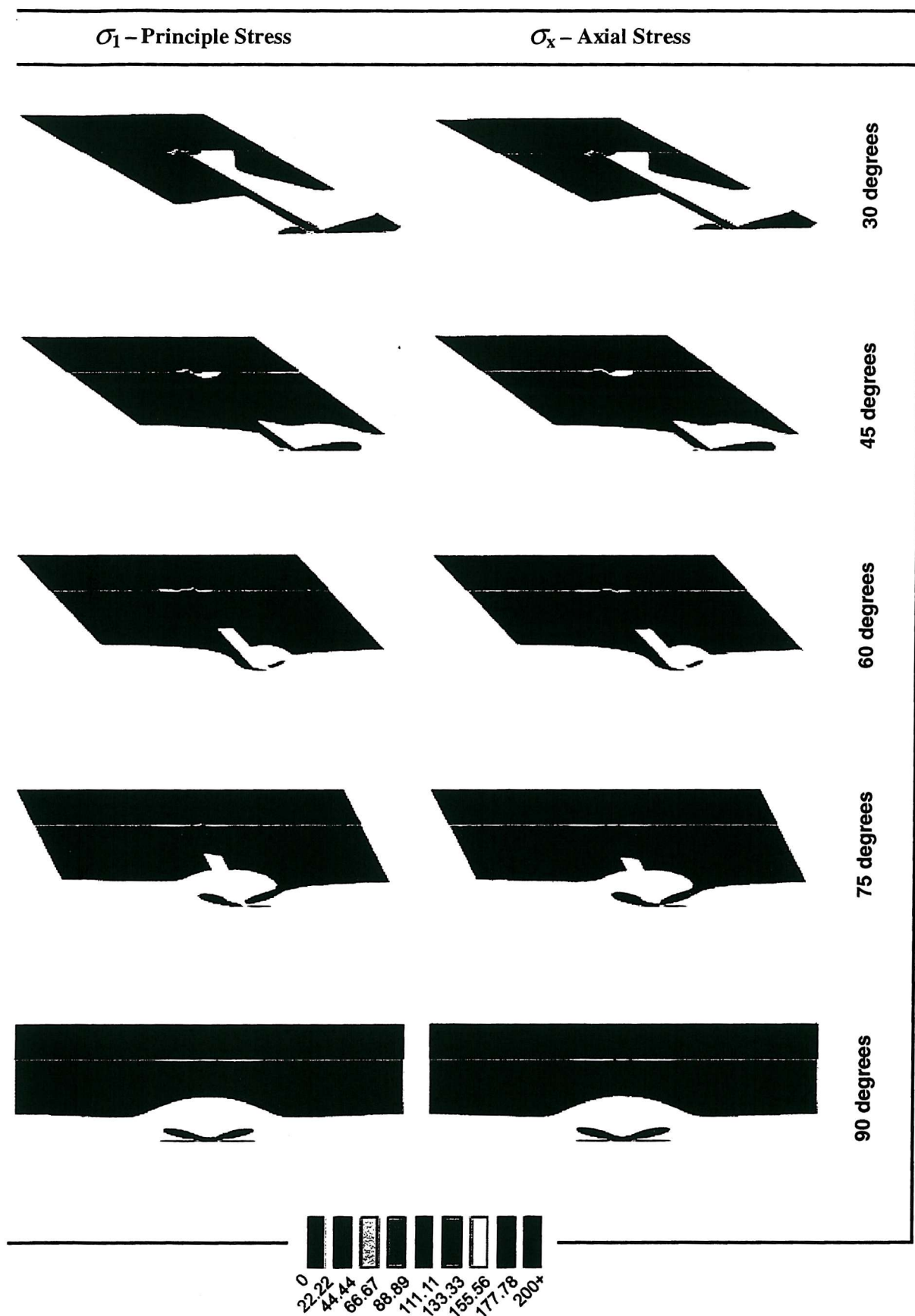
Figure M.8a Variation of principle and axial stress (MPa) distribution in a scarfed sandwich joint with 2mm thick composite skins and foam core in flexure – plane strain.

178

Figure M.8b Variation of shear and through thickness stress (MPa) in a scarfed sandwich joint with 2mm thick composite skins and foam core in flexure – plane strain.

Scarf Jointed Sandwich Construction
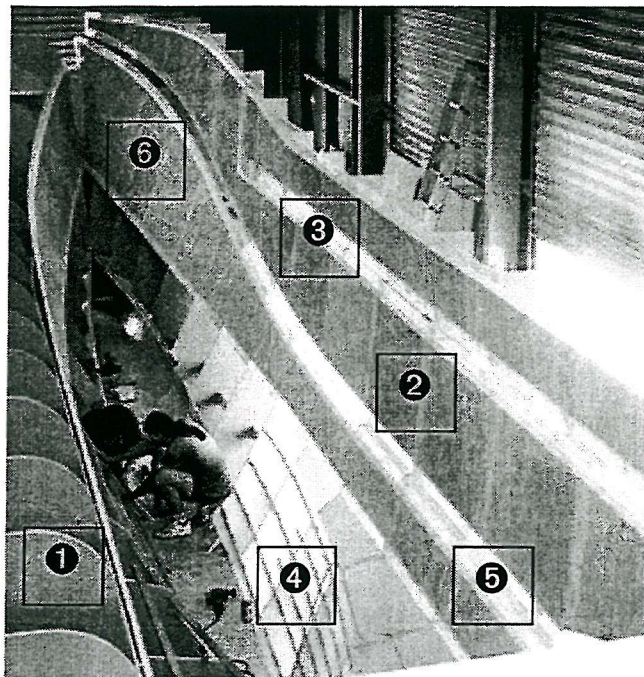
❶	MDF female mould
❷	Scarf joints positioned every 1200 mm
❸	Wet lay-up tape joined chines
❹	Moulded section - slat/ribbands for core
❺	Rebated core on panel edge for taping
❻	Pre-cut & developed sandwich panelling

Figure N.1 Starboard hull showing typical flat panel construction details on an 18m catamaran.
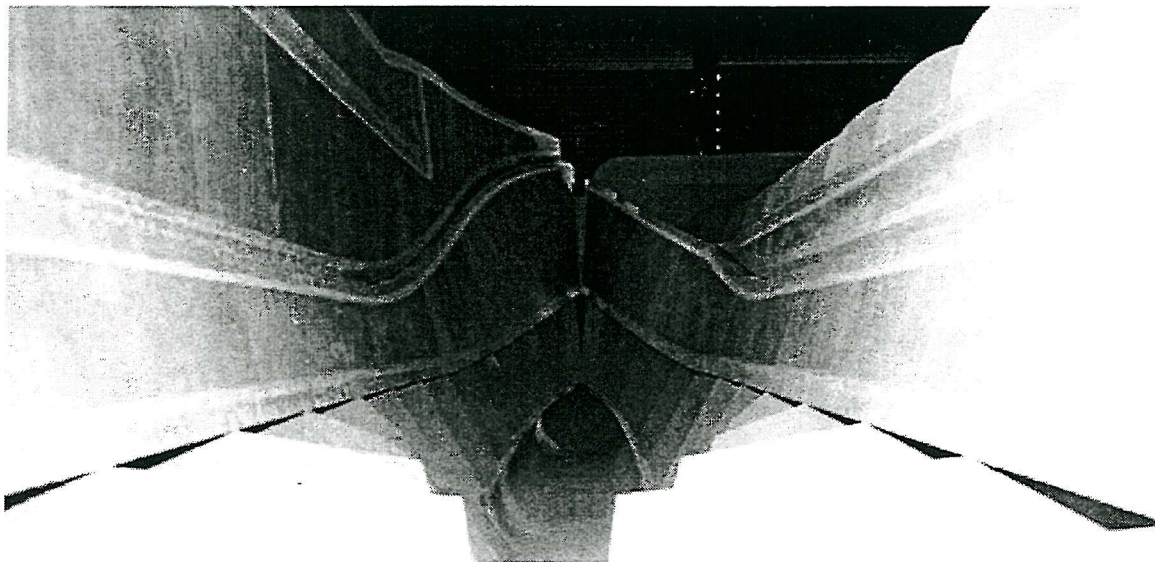
Figure N.2 Fast ferry port hull with high degree of single curvature to the first chine.
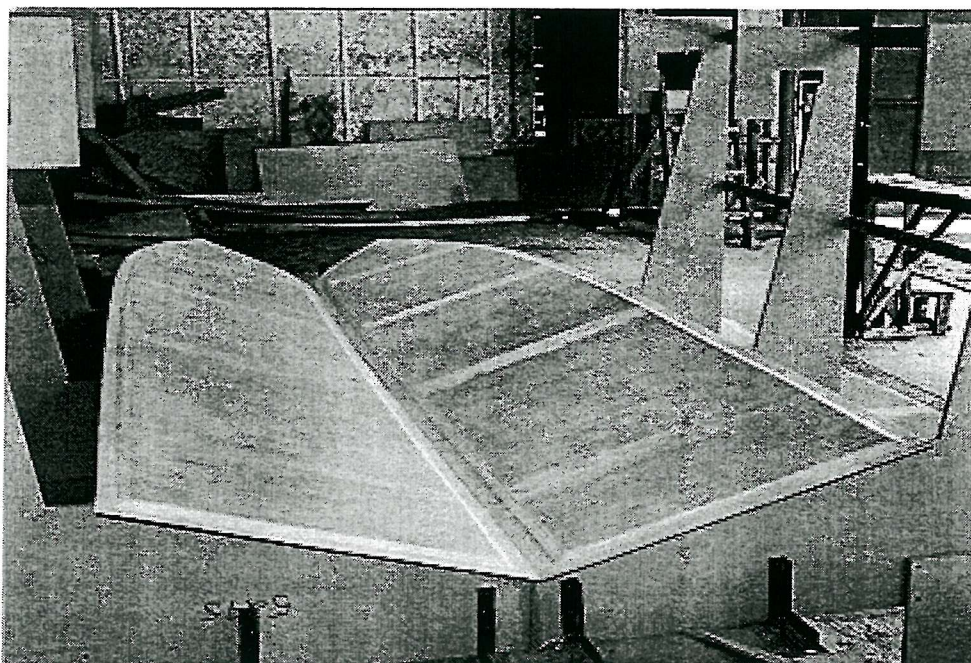
Fig. N.3 Bottom sandwich shell panels of small hard chined power boat prior to forming.
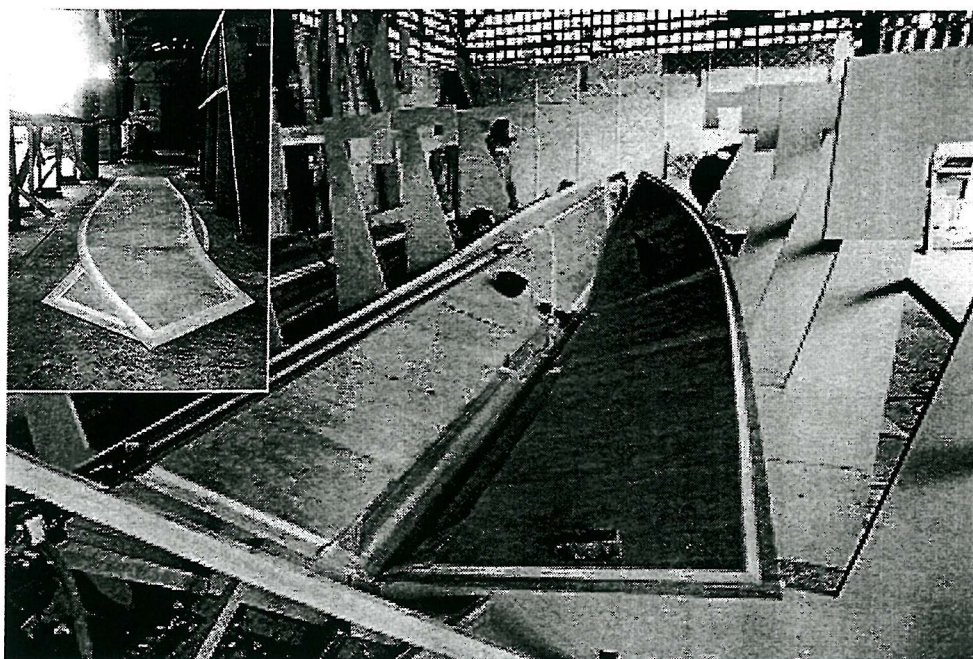
Fig,. N.4 Bottom shell forming at bow for stem joint using pulley system: side shell inset.
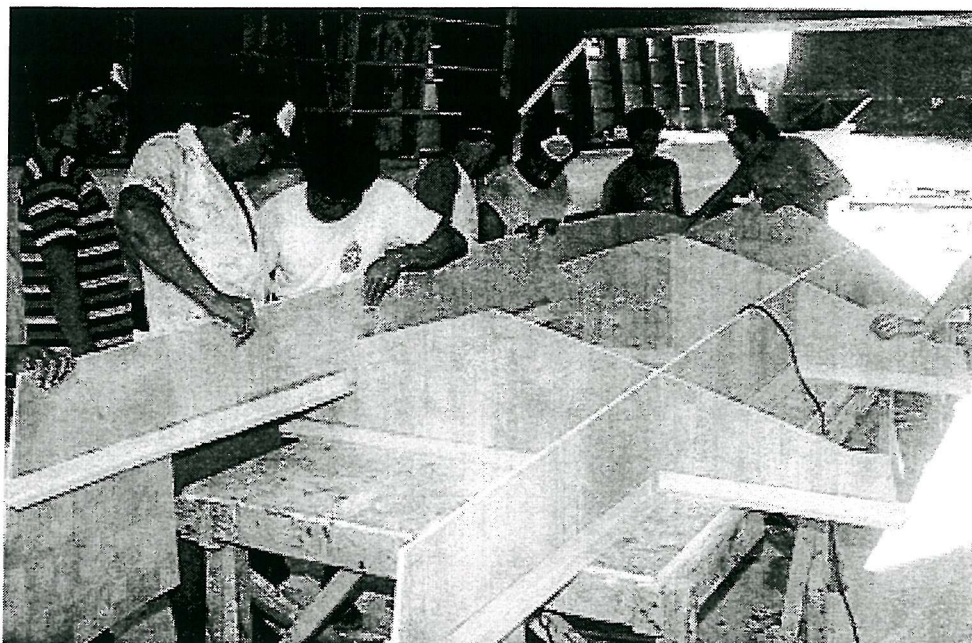
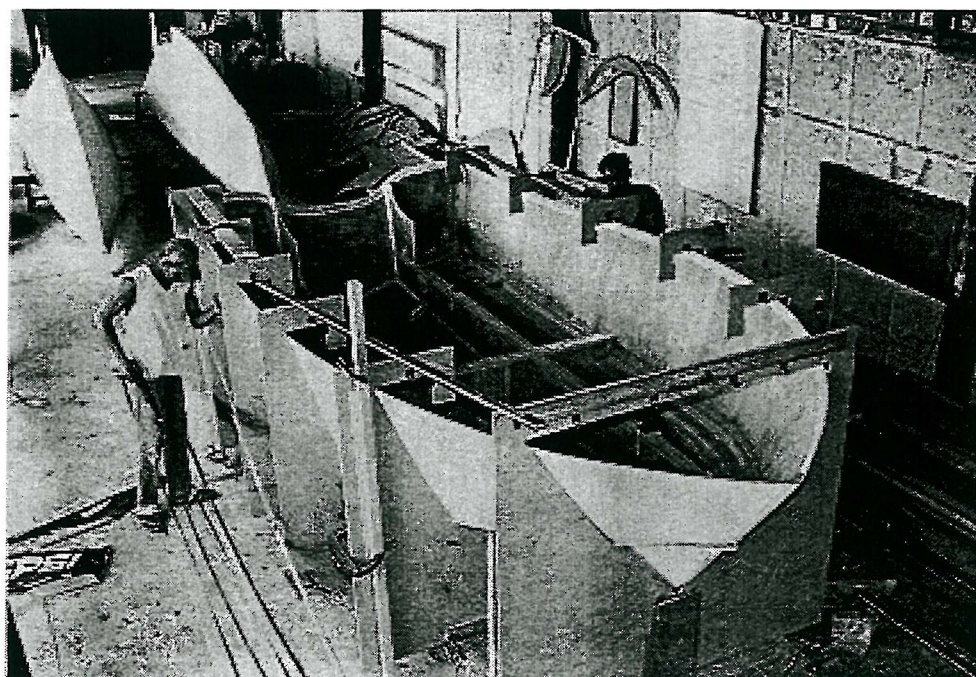Fig. N.5 Internal framework assembly using egg crating and composite bonding angles.

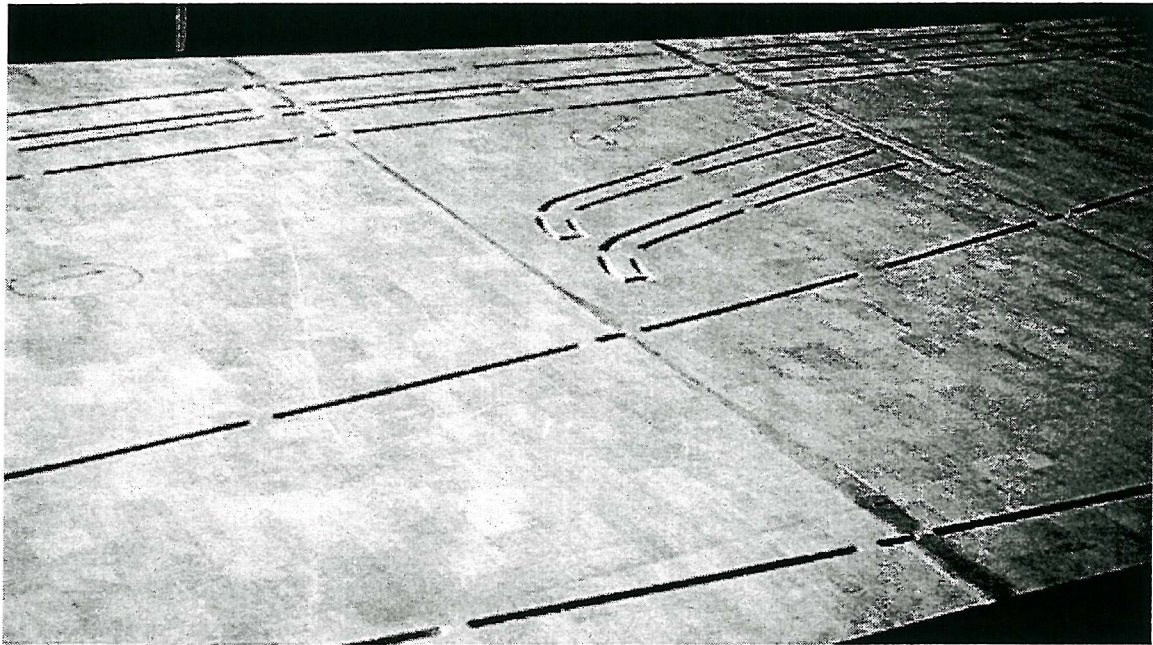Fig,. N.6 Assembled panel developed hull form including internal framing.

182

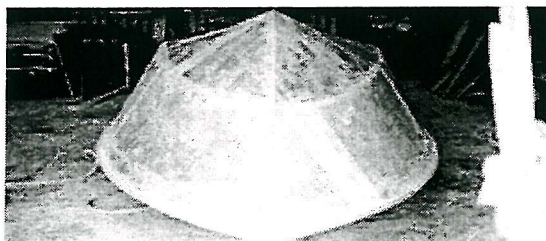Figure N.7 Pre-routed and joined 2400mm x 1200mm constituent panelling.

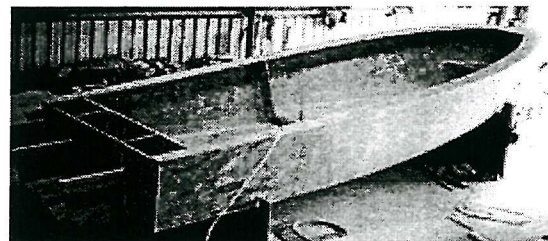Fig. N.8 Upturned hull with tight formation.

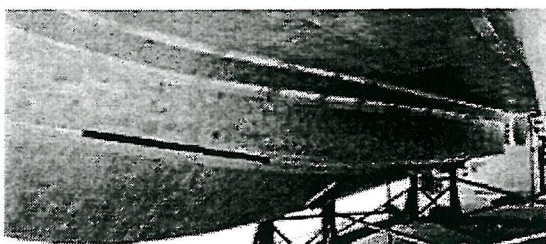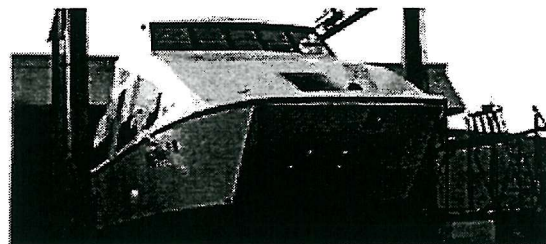Fig. N.9 Small sandwich hull form.

Fig. N.10 Underwing of sandwich hull.

Fig. N.11 Panel developed hard chined ferry.